Institute of Physical Chemistry, Polish Academy of Sciences

ul. Kasprzaka 44/52, 01-224 Warsaw

IChF

Volha Vetokhina

Spectroscopy, photophysics, conformational equilibria, and photoinduced tautomerization in selected bifunctional proton donor-acceptor azaaromatic molecules

Ph.D. dissertation written under the supervision of Prof. dr hab. Jerzy Herbich

Warsaw 2012

ACKNOWLEDGMENTS

To my family…

ABSTRACT

This work is devoted to a study of spectroscopic properties, photophysical processes and photochemical reactions in three series of trifunctional or bifunctional molecular systems having both a proton donor and acceptor centers. The aim of the work, *i.e.*, the qualitative and quantitative characterization of: (i) the photophysical parameters, (ii) the solvent-dependent rotamerization, and (iii) the ground and excited state tautomerization, was successfully realized with the use of steady-state and nanosecond and picosecond time-resolved UV-Vis spectroscopic methods, ^{1}H NMR spectrometry, and quantum chemical computations. In order to study the solvent effects, the investigations have been performed in solutions and under supersonic jet isolation conditions.

7-HQCs   **2-PPs**   **indole derivatives**
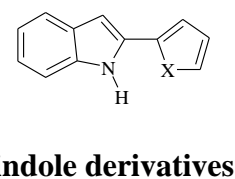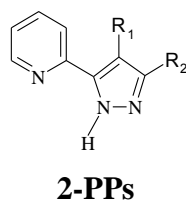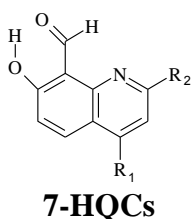
The first family of compounds, 7-hydroxyquinoline-8-carbaldehydes (**7-HQCs**), can exist in two tautomeric forms: **OH** (7-quinolinol) and **NH** (7(1*H*)-quinolinone). The compounds are composed of two moieties: a molecular "frame" (7-hydroxyquinolines, **7-HQs**) and a proton "crane" (carbaldehyde group), and have been proposed to serve as models of a reversible optically driven molecular switch. The comparative studies of the spectroscopy and photophysics of the series of **7-HQCs** and **7-HQs** and their prototropic reactions in a wide range of solvents allow us to explain the solvent-dependent mechanism of the ground and excited state long-range tautomerization.

The next two series of the studied compounds: (i) 2-(1*H*-pyrazol-5-yl)pyridines (**2-PPs**) and (ii) **indole derivatives** have the hydrogen bond donor and acceptor centers which are located in separate moieties, covalently linked by a single bond. The compounds can form *syn* (with the donor and the acceptor on the same side) and *anti* (with the two centers on the opposite sides) conformers *via* internal rotation around a single bond.

It is shown that **2-PPs** are a rare example of molecules that exhibit three types of excited state proton transfer (ESPT) reactions: (i) intramolecular (ESIPT) in the *syn* form; (ii) intermolecular (ESDPT) in the dimers in nonpolar media, and (iii) solvent-assisted ESDPT in H-bonded 1:1 complexes with protic partners. The excited state processes are manifested by the appearance of dual luminescence and a bimodal irreversible kinetic coupling of the two fluorescence bands. Ground state *syn-anti* equilibria are detected and discussed. The fraction of the higher energy *anti* form varies for different derivatives and is strongly dependent on solvent polarity and hydrogen bond donor or acceptor ability.

On the contrary, spectroscopy and photophysics of selected bifunctional **indole derivatives** containing thiophene, thiazole, and furan, do not depend on solvent properties − independent of solvent polarity and hydrogen bond donor ability the compounds show strongly allowed and very efficient fluorescence. Due to the fact that the *syn* rotamers of these compounds are able to form cyclic, doubly hydrogen bonded complexes with protic partners which upon excitation can be efficiently deactivated in S$_1$ *via* internal conversion and/or proton transfer, such finding was not expected. On the other hand, the luminescence of 3-pyridin-4-yl-1*H*-indole (**3-PI**) is strongly quenched in alcohols and water. The mechanism of the excited-state deactivation leading to fluorescence quenching is proposed.

STRESZCZENIE

Praca niniejsza poświęcona jest badaniu właściwości spektroskopowych, procesów fotofizycznych i reakcji fotochemicznych w trzech seriach dwufunkcyjnych lub trójfunkcyjnych układów molekularnych, posiadających zarówno donor jak akceptor wiązania wodorowego. Cel pracy, a mianowicie jakościowa i ilościowa charakterystyka: (i) parametrów fotofizycznych, (ii) zależnej od rozpuszczalnika rotameryzacji, oraz (iii) tautomeryzacji na poziomie stanu podstawowego i wzbudzonego, został pomyślnie zrealizowany dzięki zastosowaniu stacjonarnych i rozdzielczych w czasie (w zakresie nanosekund i pikosekund) metod spektroskopowych UV-VIS, spektrometrii ^{1}H NMR i obliczeń kwantowo chemicznych. W celu zbadania wpływu otoczenia, eksperymenty prowadzono w roztworach i w warunkach izolacji w naddźwiękowych wiązkach molekularnych.

7-hydroksychinolino-8-karbaldehydy (**7-HQCs,** patrz „abstract"**)** mogą występować w dwóch formach tautomerycznych: **OH** (7-chinolinol) i **NH** (7(1H)-chinolinon). Związki te są złożone z dwóch fragmentów: molekularnej "ramy" (7-hydroksychinoliny, **7-HQs**) i protonowego "dźwigu" (grupa karbaldehydowa), co sprawiło, że zaproponowano je jako model odwracalnego sterowanego optycznie przełącznika molekularnego. Badania porównawcze spektroskopii i fotofizyki serii **7-HQCs** i **7-HQs** i ich reakcji prototropowych w szerokim zakresie rozpuszczalników pozwoliły nam na wyjaśnienie mechanizmu zależnej od rozpuszczalnika dalekozasięgowej tautomeryzacji na poziomie stanu podstawowego S_0 i stanu wzbudzonego S_1.

Następne dwie serie badanych związków: (i) 2-(1H-pirazolo-5-yl)-pirydyny (**2-PPs**) i (ii) **pochodne indolu**, posiadają zarówno donor jak akceptor wiązania wodorowego, które znajdują się w różnych częściach cząsteczki połączonych wiązaniem pojedynczym. Związki te mogą tworzyć dwa konformery *syn* (donor i akceptor po tej samej stronie) i *anti* (oba centra po przeciwnych stronach) poprzez obrót wokół tego wiązania.

Wykazano, że **2-PPs** są rzadkim przykładem cząsteczek, które wykazują trzy rodzaje reakcji przeniesienia protonu w stanie wzbudzonym (ESPT): (i) wewnątrzcząsteczkowe przeniesienie protonu (ESIPT) w formie *syn*, (ii) międzycząsteczkowe przeniesienie dwóch protonów (ESDPT) w dimerach tworzonych w niepolarnym środowisku, oraz (iii) ESDPT w związanych wodorowo kompleksach o stechiometrii 1:1 z protycznymi „partnerami". Procesy w stanie wzbudzonym prowadzą do pojawienia się podwójnej luminescencji; oba pasma emisji są sprzężone kinetycznie w ramach modelu opisującego proces nieodwracalny. Wykryto i omówiono równowagi *syn-anti* w stanie S_0. Udział formy *anti* o wyższej energii różni się dla różnych pochodnych i jest silnie zależny od polarności rozpuszczalnika oraz jego zdolności do oddawania lub przyłączania protonu.

W odróżnieniu od **2-PPs**, spektroskopia i fotofizyka wybranych dwufunkcyjnych **pochodnych indolu**, zawierających tiofen, tiazol, i furan, nie zależy od właściwości rozpuszczalnika – niezależne od polarności i zdolności protycznych rozpuszczalnika, związki te charakteryzują się w pełni dozwoloną i wydajną fluorescencję. To odkrycie nie było oczekiwane ze względu na fakt, że rotamery *syn* tych związków mogą tworzyć cykliczne, podwójnie związane wodorowo kompleksy z protycznym „partnerem", które po wzbudzeniu elektronowym do stanu S_1 mogą być efektywnie depopulowane na drodze procesu konwersji wewnętrznej i/lub przeniesienia protonu. Z drugiej strony, luminescencja 3-pirydyn-4-yl-1H-indolu (**3-PI**) jest silnie wygaszana w alkoholach i w wodzie. Zaproponowano mechanizm dezaktywacji stanu wzbudzonego prowadzący do wygaszania fluorescencji.

PUBLICATIONS

Related to the PhD thesis:

1. V. Vetokhina, M. Kijak, G. Wiosna-Sałyga, R. P. Thummel, J. Herbich, J. Waluk, On the origin of fluorescence quenching of pyridylindoles by hydroxylic solvents, *Photochem. Photobiol. Sci.*, **2010**, *9*, 923-930.

2. V. Vetokhina, K. Dobek, M. Kijak, I. I. Kamińska, K. Muller, W. R. Thiel, , J. Waluk, J. Herbich, Three modes of proton transfer in one chromophore: photoinduced tautomerization in 2-(1*H*-pyrazol-5-yl)pyridines, their dimers and alcohol complexes, *ChemPhysChem.,* DOI: 10.1002/cphc.20120602.

3. V. Vetokhina, J. Nowacki, M. Pietrzak, M. F. Rode, A.L. Sobolewski, J. Waluk, J. Herbich, Ground and excited state long-range prototropic tautomerization of 7-hydroxyquinoline-8-carbaldehyde and its derivatives, *submitted.*

Other:

4. D. T. Gryko, J. Piechowska, V. Vetokhina, D. Wójcik, Fluorescent Dyes with 2-Amino-4,7-diazaindole Skeleton: Synthesis and Spectroscopy, *Bull. Chem. Soc. Jpn.*, **2009**, *82*, 1514-1519.

5. H. Dodziuk, V. Vetokhina, H. Hopf, R. Luboradzki, P. Gaweł, J. Waluk, Electronic states of cyclophanes with small bridges, *J. Chem. Phys.*, **2012**, *136*, 074201.

CONFERENCES

List of conference presentations (posters):

C1. V. Vetokhina, A. Zielińska, J. Herbich,
Photophysics and conformational equilibria of bifunctional azaaromatic molecules,
„Polish Photoscience Seminar", Lipnik, Poland, 11-12 June 2008.

C2. V. Vetokhina, A. Zielińska, P. Borowicz, T. Lipińska, R. P. Thummel, J. Waluk,
J. Herbich,
Photophysics and structure of selected bifunctional azaaromatic molecules,
"XXIV International Conference on Photochemistry", Toledo, Spain, 19-24 July 2009.

C3. M. Pietrzak, V. Vetokhina, J. Nowacki, J. Herbich, A. L. Sobolewski,
^{1}H NMR study on 7-hydroxy-4-methylquinoline-8-carbaldehyde in solution,
"V Symposium on Nuclear Magnetic Resonance in Chemistry, Physics and Biology",
Warszawa, Poland, 23-25 September 2009.

C4. V. Vetokhina, M. Kijak, I. Kamińska, A. Zielińska, W. R. Thiel, J. Waluk, J. Herbich,
*Spectroscopy, photophysics and photochemistry of 2-(1H-pyrazol-5-yl) pyridine (PPP)
and its derivatives,*
„Polish Photoscience Seminar", Krutyń, Poland, 8-11 June 2011

C5. V. Vetokhina, K. Dobek, M. Kijak, I. I. Kamińska, K. Muller, W.R. Thiel, , J. Waluk,
J. Herbich,
*Three modes of proton transfer in one chromophore: photoinduced tautomerization in 2-
(1H-pyrazol-5-yl)pyridines, their dimers and alcohol complexes,*
International Conference on „Reaction Kinetics in Condensed Media (RKCM)", Łochów
Palace, Poland, 11-16 September 2012.

TABLE OF CONTENTS

Chapter 1: Introduction

1.1. Hydrogen bond and proton transfer. Introduction

The importance of hydrogen bond is difficult to overestimate. It lays in the basis of unique properties of water such as ability of ice to float on the surface of the reservoir without freezing it to the bottom. It plays a key role in enzyme catalysis mechanism, DNA formation connecting its bases and composing proteins into 3D tertiary structures, and is responsible for mutations.[1-3] Even the human hair shape (curly hair, wavy hair, straight hair, etc.) depends on the hydrogen bonds involving the SH groups of cysteine (HO-CO-CH(NH_2)-CH_2-SH) which is a component of alpha-keratin.[4] These and many other factors make hydrogen bond one of the most important topics to be investigated since it determines and, moreover, makes possible the existence of all living creatures and life itself.

In spite of the importance and decades of thorough studies in all branches of chemistry, the nature of hydrogen bond is still an opened question. Moreover, proton or hydrogen atom transfer processes are of great interest. This reaction plays vital role in several physical, chemical, biological processes,[5-9] such as DNA chemical damage and repair[10], photostability of DNA base pairs and proteins,[11,12] cellular respiration[13,14] and photosynthesis.[15] Prototypical molecules have been extensively studied as simplified models of participants of all these processes, for example, of hydrogen-bonded pairs in DNA.

1.2. Ground and excited state proton transfer. A historical outlook

Ground and excited-state proton transfer reactions are one of the most important processes in chemistry. Transport of the proton is accompanied with mass and charge transfer between the reactants making it one of the simplest reactions where an actual displacement of a simple particle occurs.

Significant changes appear in the electronic structure of a molecule as an electron is promoted from the ground to the excited state.[7-9,16] The difference in electronic distribution in these two states provokes the difference in photophysical properties such as dipole moments and acid-base equilibria. A large variety of reactions have been observed in the excited state including isomerizations, and electron and proton transfers between spatially separated chromophores. Tautomerization, as a reaction between two (or more) structural isomers that can exist in equilibrium and are readily converted from one isomeric form to another due to a proton (or hydrogen atom) transfer, is one of the most widely studied processes within about last 50 years.

The driving force of the photoinduced proton transfer process comes from the drastic changes of acidity and basicity of the involved groups and moieties of the system under study. When these changes are energetically favourable, the reaction can occur providing that no steric or strain reasons prevent the reaction. In molecules such as phenols and naphthols excitation acts in the way that electron density shifts from the oxygen to the aromatic ring. As a result, acidity of excited state phenols and naphthols is much higher (typically orders of magnitude[17-19]) than in the ground state and may be deprotonated by solvent or other ground-state molecules. This process is referred to as excited state proton transfer (ESPT). Following proton transfer, the resulting anion can either react or relax back to the ground state where reprotonation will occur. On the other hand, 1,4 diazines containing a pyrazine ring (such as quinoxaline, phenazine, 1,4-diazatriphenylene, 1,4-diazaphenanthrene) reveal a dramatic increase of basicity.[20] It is a general rule in aromatic molecules that electron donating substituents become stronger donors in the excited state, while acceptors will attract the electrons more strongly.

Excited state proton transfer may result in two emissions in many cases. One of these emission bands originates from the excited state of the neutral molecule. The other one arises from the anion (deprotonated form) or cation (protonated species), which is produced in the photoexcited state. This second band has large Stokes shift relatively to the first one.[9] For the

first time the shift of an acid-base equilibrium was reported in 1931 by Weber.[21] It occurs when the energy difference between the ground state of neutral and protonated/deprotonated form is larger than the respective energy difference in the excited state. Later on, Förster[18,19] provided an explanation of this phenomenon, proposing the method for the calculation of the excited state change of pK_a of a molecule (now termed as "Förster cycle") based upon the observed electronic absorption and fluorescence (see also ref. [20]).

Weller[22-26] has prompted extensively a study of the proton transfer processes in the excited electronic states related both to the acid-base reactions[22,23] and isomerization in bifunctional molecules having both proton donor and acceptor linked by an internal hydrogen bond.[24] On example of methyl salicylate he assigned a strong red-shifted fluorescence to the phototautomer, formed *via* a proton transfer in the excited state and represented by a zwitterionic structure.

There are three possible proton transfer scenarios based on the change of acidity and basicity. Two of them are the result of enhanced acidity/basicity of a single moiety of the excited molecule (Fig. 1.1). A third type of ESPT occurs when a molecule contains both such moieties on the same chromophore. The enhancement in the acidity of one functional group and enhancement in the basicity of the other upon excitation results in a driving force for excited state proton transfer.
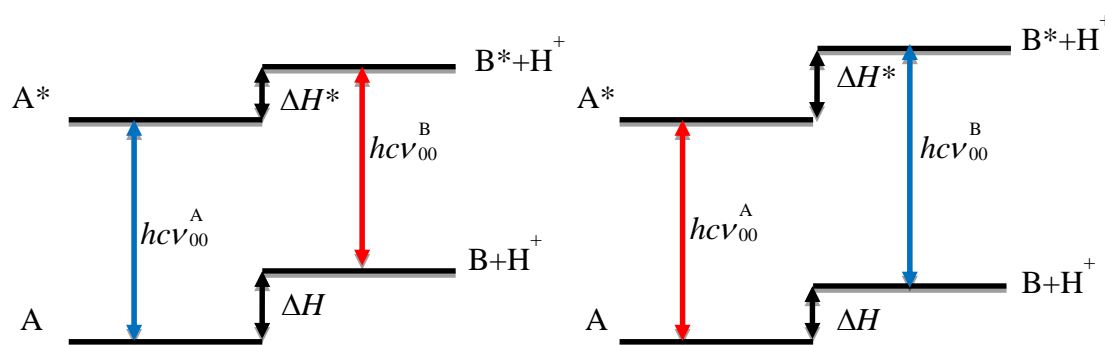
Figure 1.1. Principle of Förster cycle for the reaction A→B+H^{+}. The left part corresponds to the enhancement of acidity in the excited state, the right part – to the enhancement of basicity.

A formation of neutral phototautomer is another result of a proton transfer in the excited state. A favorable situation for this ESPT process occurs in the strongly hydrogen bonded species such as heteroaromatic bifunctional molecules that can simultaneously act as proton donors and acceptors and may reveal simultaneous enhancement of acidity and basicity upon electronic excitations, as well as in their dimers and complexes with protic partners. Such molecular systems can show dual luminescence from a "substrate" (a "normal"

emission from the primarily excited state) and a "product" (phototautomer) of the ESPT reaction. An observation of dual luminescence allows to determine kinetics of the reaction from a decay of the normal emission and a rise and decay of the tautomer fluorescence. These ESPT processes often proceed within picosecond time scale (to compete effectively with the other deactivation processes) and with a quite low barrier,[27-31] although the time range of a tautomer formation spans from femto- to microseconds and the barrier could be significant. Phototautomers relax quickly to the ground state and show a large red shifted emission. In many cases a short-wave fluorescence from the primarily excited state does not appear at all. On the other hand, the intensity of tautomeric emission could be negligibly small in comparison to that of the "normal" emission. A large Stokes shift of the latter emission is a manifestation of a large structural rearrangements and geometrical changes caused by proton transfer. The dynamics of ESPT process depends strongly on the conformation of the molecule, temperature, and the nature of the solvent, especially with respect to the ability of hydrogen bonds formation[5,32-34] and on hydrogen bond strength (geometry, inter alia, distances and angles between proton donating and accepting centers). In most cases, decay of the excited tautomer (radiative or radiationless) is accompanied by reverse isomerization in the ground state. Thus, the process is cyclic assuming photostability of the molecule.

The proton transfer reactions could be classified into two categories: (i) excited state intermolecular proton transfer appears in complexes of a compound with protic partners or in molecular clusters (for example, in dimers), (ii) excited state intramolecular proton transfer (ESIPT) takes place within one molecule. In intermolecular ESPT processes, a proton (one or more) is transferred from one molecule (proton donor) to another (proton acceptor). This type of reaction has been employed as a mechanistic tool in technological applications in pH and pOH jump experiments (rapid change of pH and pOH after excitation),[35,36] in the study of proton hydration dynamics[37,38] and as probes to study the microenvironment of the fluorophore in protein,[39-41] micelle,[42-44] reversed micelle[45-47] and cyclodextrin media.[48-50] Bifunctional molecules (such as 7-azaindole, 1*H*-pyrrolo[3,2-*h*] quinoline, dipyrido[2,3-*a*:3,2-*I*]carbazole) are in the center of attention of many recent publications. The compounds can form the cyclic hydrogen bonded complexes due to specific interactions with protic solvents or can form doubly hydrogen bonded dimers in which intermolecular excited state double proton transfer (ESDPT) can occur. In the case when the donor and acceptor centers are in close proximity and in a proper structural arrangement in a molecule, an intramolecular hydrogen bond can be formed and the ESIPT process can occur. Molecules which contain two such centers *ortho* to each other have been shown to undergo ESIPT. These basic processes,

4

as well as photochemical and physical applications relating to the use of such systems as probe molecules, sunblocks,[51-58] monomer and polymer stabilizers,[59,60] have been extensively reviewed. Intramolecular reactions have been applied in chemical lasers,[61,62] energy storage systems and information storage devices at a molecular level,[62] high-energy radiation detectors.[63]

The well-known classification of proton transfer reactions gave Kasha,[64] who was one of the pioneers in the field of excited state tautomerization processes. He distinguished four mechanistic classes: (i) intrinsic intramolecular transfer (hydrogen bond is linking directly the hydrogen atom of the donor group and the acceptor center), (ii) concerted solvent assisted biprotonic transfer (the proton is far away from the acceptor and requires a mediator), (iii) static and dynamic catalysis of proton transfer (cyclic complexes can be considered as examples of static catalysis, but a dynamic catalysis can also be involved if a singly attached H-bonded component must rearrange upon excitation to the cyclic doubly H-bonded complex), and (iv) proton relay transfer (in which the proton transfers are coupled through the inductive electronic effect in the cyclic complex). Later on, an extension of this classification has been presented by Heldt et al.[65]: *only the intrinsic process is a real ESIPT; all the others are combinations of excited state intermolecular proton transfer processes within the microsolvent clusters*.

Ab initio, semi-empirical, and DFT computations can provide information that complements experimental data. By way of a series of calculations (linking molecular structure and the resultant energy) one can generate the potential energy surfaces (PES) for the proton transfer processes in the ground and excited states. Using simplified one-coordinate description of PES one can distinguish three types of ESPT: (i) single minimum – a barrierless transition; (ii) two minima and asymmetric PES – tunneling through a low-energy barrier (~4 kJ/mol); (iii) two minima and symmetric PES – tunneling through high-energy barrier (Fig. 1.2).

In a barrierless transition, isomerization is simply encompassed in the vibrational redistribution and relaxation processes. The absence of energy barrier would lead to proton transfer rates in a subpicosecond range. Tunneling through a small barrier would also lead to similar results. In the extreme case potential energy curves of a single minimum may occur for both S_0 and S_1 states, and broad and structureless absorption and emission spectra should be observed.

PES

i   ii   iii
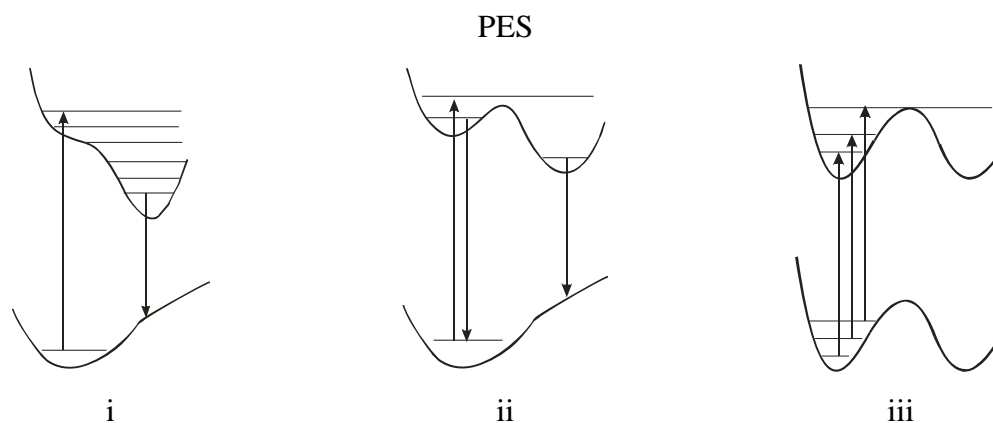
Figure 1.2. Scheme of potential energy surfaces in electronic ground and excited states: i – single minimum; ii – two minima and asymmetric PES; iii – two minima and symmetric PES.

Systems similar to 9-hydroxyphenalenone (**9-HP**) (Scheme 1.1), where ESIPT is characterized by a symmetric double well potential (iii in Fig. 1.2), are stable in two equivalent conformations.[66] In a case of the excited-state proton transfer system which is characterized by the potential surfaces with the asymmetric double well potential (ii), one should expect the dual fluorescence arising from the primary excited and the proton transferred forms. In many cases, the energy difference of the initially excited and tautomeric forms is large, the energy barrier to ESIPT is rather low and the proton is translocated very fast (i); under these conditions the fluorescence of the primary excited structure is undetectable and a large Stokes shifted emission arises exclusively from the final tautomeric form.
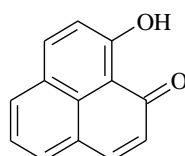
9-HP

Scheme 1.1. Formula and acronym of 9-hydroxyphenalenone.

Let us consider an ESIPT with double potential energy wells in both S_1 and S_0 states for a sample compound (Scheme 1.2). The excited phototautomer **2*** resulting from the ESIPT process is lower in energy than its excited state precursor **1*** (a substrate of ESIPT), while the ground-state tautomer **2** is higher in energy than **1**. As a result, fluorescence from the excited state tautomer **2*** is significantly red-shifted from that of **1*** (if the latter is observed). In order to prove the excited state reaction, the kinetic analysis of the both emitting bands should be performed. On the other hand, a lack of fluorescence from **1*** and the observation of the excitation spectrum of the tautomeric emission matching well the

6

absorption spectrum of **1** indicate reaction in the excited state. The ground-state tautomer **2** can either return to **1** through reverse proton transfer or react further. The former process predominates especially for PES (i) and (ii) in Fig. 1.2.
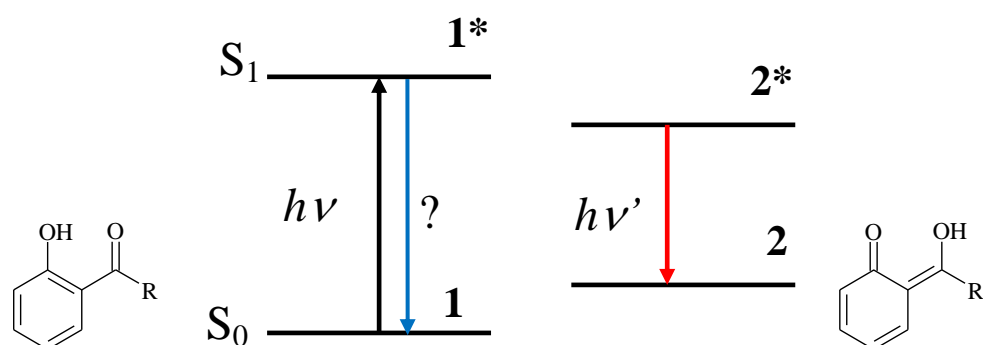
Scheme 1.2. Formulas and energy levels scheme of a sample compound.

1.3. Examples of ESIPT and ESDPT

Numerous publications on ESIPT were devoted to 3-hydroxyflavone, **3HF** (Scheme 1.3), which corresponds to the similar four-level scheme as shown above. The intrinsic ESIPT was observed in hydrocarbon solvents where green emission (centred at 520 nm), attributed to tautomer, appears. The proton transfer process was found to be very fast with a small energy barrier. The green emission is shifted to lower energy by 8400 cm^{-1} with respect to the absorption. The violet emission of the normal form (410 nm) can only be observed when ESIPT is suppressed due to external hydrogen bonds formation (*e.g.*, in alcohol solution). Both fluorescence bands are observed in methanol at room temperature. Studies in molecular jets[67] of isolated molecules confirmed a small energy barrier. Experiments with picosecond resolution reveal approximately 6 ps ESIPT in acetonitrile while tautomer lifetime in the same solvent is about 0.9 ns. This decay is considerably longer than the rate of tautomer formation, which makes this molecule the source of efficient amplified spontaneous emission.[68] Proton transfer in **3HF** was found to be extremely sensitive to hydrogen bonding impurities in hydrocarbon solvents.

3-HF
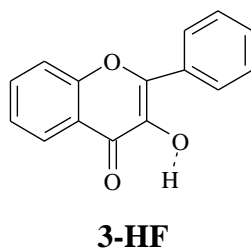
Scheme 1.3. Formula and acronym of 3-hydroxyflavone.

Substituted hydroxyl aldehydes, esters and acids of naphthalene or benzene molecules having intramolecular hydrogen bond make a wide class of molecules which are able to undergo ESPT reactions. Such molecules can exist as closed (intramolecularly hydrogen bonded), open, and intermolecularly hydrogen bonded conformers. 3-hydroxy-2-naphthaldehyde (**HN32**) (Scheme 1.4) belongs to the group of such compounds. Two absorption bands observed in nonpolar solvents were assigned to the ground-state open (~300 nm) and closed (~392 nm) conformers (Fig. 1.3).[69] In protic solvents, a new low energy band (~465 nm) arises, which corresponds to the intermolecularly hydrogen bonded species since the complex of the solute and solvent is created. In both protic and nonpolar solvents, **HN32** shows two emission bands. Upon low energy excitation in cyclohexane (~392 nm) dual luminescence is observed, the higher energy band (~450 nm) corresponds to the closed

8

conformer and the lower energy emission (~690 nm) was attributed to the keto tautomer resulting from the ESIPT process. Upon high energy excitation (300 nm), however, only one emission band (~350 nm) was observed corresponding to the open conformer. This band appears in both polar and nonpolar solvents. In protic medium an additional emission takes place in the region ~450-520 nm and corresponds to the solute intermolecularly hydrogen bonded with a solvent molecule(s).
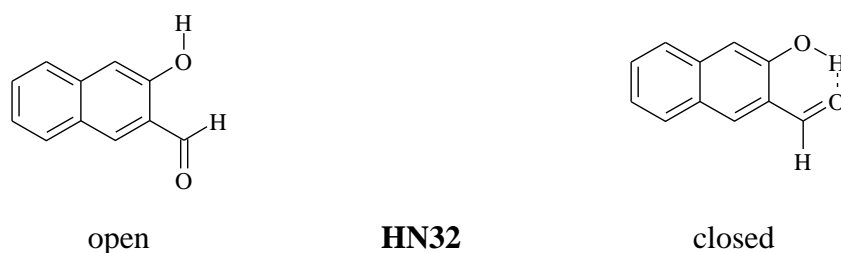
Scheme 1.4. Formulas and acronyms of two conformers of 3-hydroxy-2-naphthaldehyde.
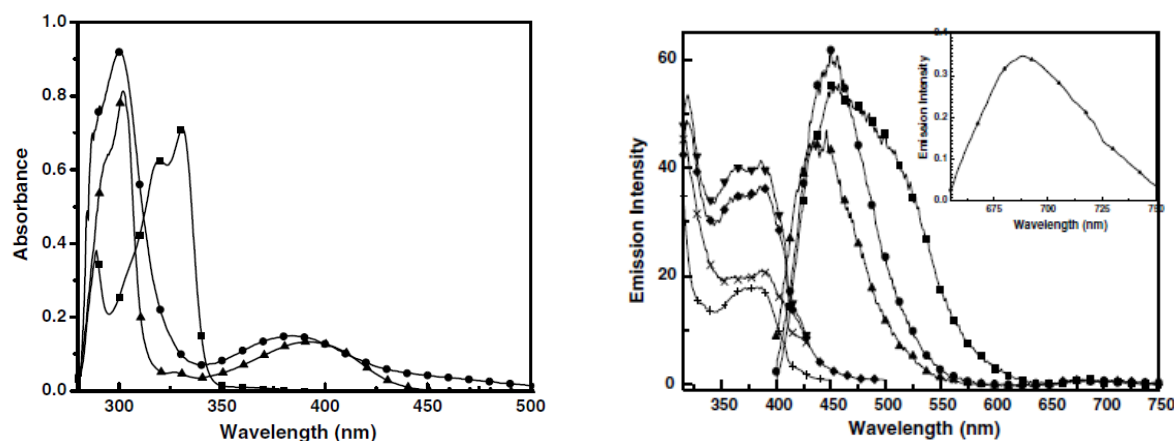
Figure 1.3. Absorption (left) and fluorescence and fluorescence excitation (right) spectra of **HN32** and 2-naphthol.[69] Absorption of **HN32** in cyclohexane is marked as -▲-, in MeOH as -●-; absorption of 2-naphthol in MeOH is marked as filled squares. Fluorescence of **HN32** in n-heptane is marked as -●-, in MeOH as filled squares, in ACN as -▲-; fluorescence excitation in n-heptane is marked as -▼- (λ_{em}= 450 nm), in MeOH as -×- (λ_{em}= 450 nm), in MeOH as -♦- (λ_{em}= 520 nm), in ACN as -+- (λ_{em}= 696 nm). Inset: fluorescence spectrum at 690 nm region.

One of the influencing factors for ESPT is the proximity of the $^1(\pi,\pi*)$ and $^1(n,\pi*)$ states. A small aromatic molecule o-hydroxybenzaldehyde (**OHBA**) (Scheme 1.5) with intramolecular hydrogen bond, which can undergo ESIPT and has protecting abilities from UV light, is an example of such effects. Hydrogen bonding may result in the reversal of the state ordering or lead to large changes in the strength of vibronic or spin-orbit coupling.[70] The potential energy surface (PES) is barrierless for the intramolecular proton transfer in the lowest $^1(\pi,\pi*)$ state of **OHBA**, while that in the $^1(n,\pi*)$ state has a significant barrier. For **OHBA** these two states are almost isoenergetic and this proximity may bring the system from

the PES of prepared $^1(\pi,\pi*)$ state to that of $^1(n,\pi*)$ state which is not reactive. A fast PES crossing of that type can compete with the proton transfer rate. This coupling may explain the slow proton transfer in **OHBA**.[71,72] Such crossings are associated with non-radiative process. Tautomer is initially produced with an excess energy and the new internal hydrogen bond in the tautomer is week and can be dissociated leading to a non-fluorescent state.[73] If the hydrogen bonding strength is not the same in the ground and excited states, different shapes and positions of the minima in the PES of the two states are possible. This, in turn, may activate rapid internal conversion from the S_1 state to the ground state S_0.

OHBA
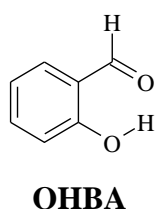
Scheme 1.5. Formula and acronym of o-hydroxybenzaldehyde.

A direct access to dynamics of fast proton transfer processes becomes possible with the discovery of pico- and femtosecond laser spectroscopy techniques. Some interesting examples are 2-(2'-hydroxyphenyl)benzothiazole (**HBT**), 2-(2'-hydroxyphenyl)benzoxazole (**HBO**) (Scheme 1.6) and mentioned above **OHBA**. In the ground state they exist in the enol form in which hydrogen is bound to the oxygen atom (Fig. 1.4). Upon excitation the keto form becomes more stable which is confirmed by a large Stokes shift[74-79] between absorption and fluorescence spectra. ESIPT in these molecules corresponds to a transfer of a proton to the basicity centers located at the benzoxazole (**HBO**) or benzothiazole (**HBT**) nitrogen atom, or at the carbaldehyde oxygen atom (**OHBA**).

HBO   **HBT**

Scheme 1.6. Formulas and acronyms of 2-(2'-hydroxyphenyl)benzoxazole and 2-(2'-hydroxyphenyl)benzothiazole.

The ESIPT process for **HBT** was confirmed by time-resolved IR spectroscopy investigations.[80,81] Femtosecond IR spectroscopy (UV-pump–mid-IR-probe measurements in tetrachloroethene, C_2Cl_4) showed a disappearance of the OH stretching vibration of the enol form and appearance of the NH and the C=O stretching vibrations on a time scale of 30-50 fs.

Ultrafast (with 30 fs time resolution) transient absorption measurements[75] give opportunity to examine these processes in real time. In the work of Lochbrunner *et. al.*[82] such investigations were made for **HBT**, **HBO**, and **OHBA**. They proposed the wavepacket model, according to which H-chelated ring is contracted by bending of the molecular skeleton. This reduces the proton donor-acceptor distance. The time-scale of the motion is determined by the inertia of the participating atoms. When the contraction is sufficient, *i.e.* when the OH distance is sufficiently shortened, the change in electronic configuration appears. It leads to the formation of a new bond between the hydrogen and the acceptor atom and the change of the strength of other bonds. It results in a new equilibrium geometry. Thus, caused by this contraction upon optical excitation, the created wavepacket is propagated in a ballistic fashion along the adiabatic PES of the S_1 state. The PES shape is determined by the coupling between the electronic *enol* and *keto* configurations. Therefore, it was shown that the proton is shifted from the donor to the acceptor center by the skeletal motion and tunneling has not to be considered.
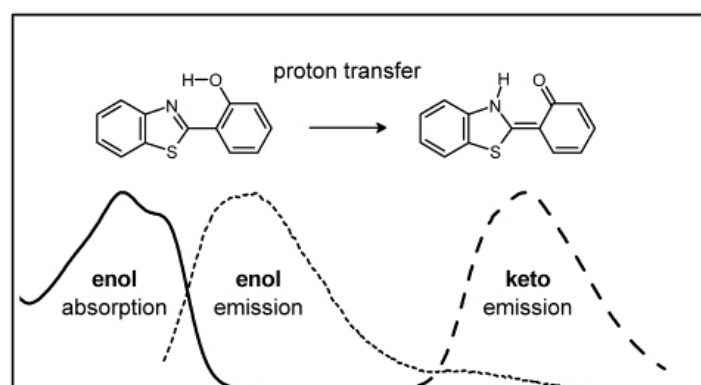
*Figure 1.4. Structure of the enol and keto forms of **HBT**. Absorption (straight line) and fluorescence spectra in cyclohexane (dashed line) and in ethanol (dotted line).*

The examples described so far show a photoreaction connected with an intramolecular transfer of one proton. Intramolecular double proton transfer (ESDPT), in which two protons are transferred, were investigated in specially synthesized molecular systems (Scheme 1.7), such as 2,2'-bipyridyl-diols,[83-90] "double" benzoxazoles (*e.g.*, bis-2,5-2(2-benzoxazolyl)hydroquinone) and related compounds.[31,91-96] The reactivity of the compounds was studied in three electronic states, in the ground state S_0 and in the excited singlet S_1 and triplet T_1 states. Steady-state and time-resolved UV-Vis and Raman studies have been performed in solutions and under supersonic jet isolation conditions in order to explain the mechanism of photoreactions.

BP(OH)₂   **BBHQ**
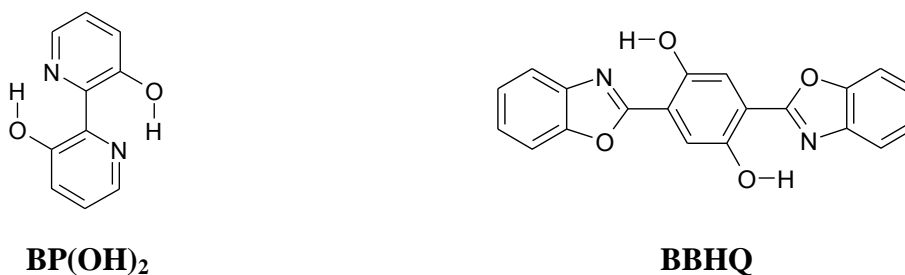
*Scheme 1.7. Formulas and acronyms of 2,2'-bipyridyl-3,3'-diol (**BP(OH)₂**) and bis-2,5-2(2-benzoxazolyl)hydroquinone (**BBHQ**).*

A lot of attention is paid to the intermolecular process of ESDPT due to its role in purine and pyrimidine base paring in nucleic acids[97]. ESDPT was observed for model systems such as dimers and alcohol complexes of some specific compounds, for example 7-azaindole (**7AI**)[97-101] and 1-azacarbazole (**1AC**),[102-105] and for heterodimers of **1AC** and **7AI**[106] (Scheme 1.8). ESDPT in these systems is manifested by double luminescence.

Two fluorescence bands were observed in alcohol solutions of **1AC**.[102-105] Each band was assigned to a certain individual ground-state species. The low-energy emission is given by the 1:1 complex with alcohol that can undergo ESDPT. The second band is due to the most stable ground-state species creating 1:2 complexes with alcohol which cannot tautomerize. It was found that **1AC** hydrogen-bonded dimers undergo photoinduced double proton transfer reaction in S_1 state. The photoreaction depends rather on viscosity of the surrounding medium than on temperature due to the comparatively large size of the dimer. The activation energy was concluded to be related to an internal rotation of the monomeric moieties toward flattening of their initially twisted geometry.

1AC···(ROH)   **7AI**···**7AI**

Scheme 1.8. Formulas and acronyms of the cyclic, doubly hydrogen-bonded complex of 1-azacarbazole with protic partner and dimer of 7-azaindole.

It has been shown that a barrierless intermolecular ESDPT process occurs in solid **1AC**, consisting of planar, doubly hydrogen bonded dimers.[102-105] Fluorescence spectra recorded at room temperature, at liquid nitrogen temperature, at 13 K, and at 1.5 K showed a

large Stokes shift of about 8000 cm^{-1} and were similar to the tautomeric fluorescence observed in solutions.

The most extensively studied molecule showing intermolecular ESDPT processes in dimers and complexes is **7AI**. The process, discovered by Kasha and co-workers[107] more than 50 years ago, is still attracting much attention.[108] **7AI** exhibits dual fluorescence in various solvents corresponding to the substrate and product of the excited state reaction. Room-temperature fluorescence spectra of **7AI** in 3-methylpentane (Fig. 1.5) consist of two bands centered at about 325 nm and 480 nm. The former is attributed to the normal fluorescence, the latter – to the fluorescence of the tautomeric form produced in the excited state of the dimer. A relative intensity of the bands strongly depends on temperature, concentration and excitation wavelength.[107,109,110] **7AI** dimers were theoretically and experimentally investigated in details[111,112] in order to understand the mechanism of the process, in particular the issue of stepwise versus concerted movement of the protons. The mechanism, however, is still under debate.
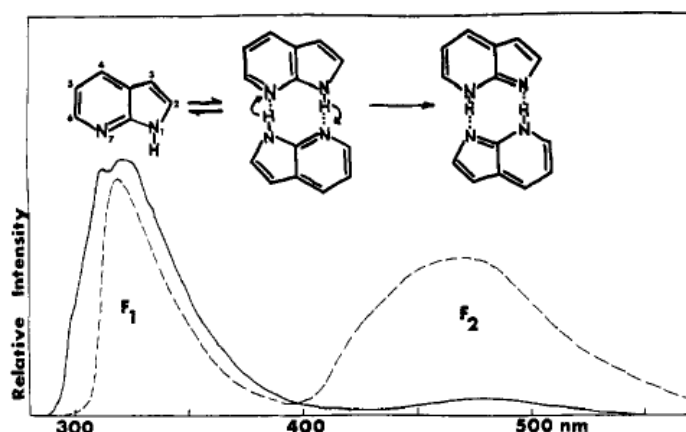
*Figure 1.5. Room temperature fluorescence of **7AI** in 3-methylpentane at 10^{-4} M (solid line) and 10^{-2} M (dashed line).*[109]

Numerous investigations of hydrated clusters were performed as well.[113-115] In pure water only a small fraction of **7AI** (20%) is correctly solvated to tautomerize, while the majority (80%) is in the polysolvated configuration that blocks tautomerization.[97,116,117] It was found that the photoreaction is strongly enhanced when water is diluted in other solvent, for example in ethyl ether. The latter breaks up the liquid water structure and permits **7AI** monohydrate to form.[107,118] Theoretical calculations of isolated compounds[119] show that the tautomer is ~20 kcal/mol more stable than the normal **7AI** in the lowest excited singlet state.[120] A significant reduction of the proton transfer barrier in 1:1 **7AI** water complexes in

13

comparison with individual **7AI** was also observed. Addition of more than one water molecule lowers the activation energy even more.[115,121]

In the case of **7AI** and **1AC**, the structure of the complexes appropriate for ESDPT is achieved mainly upon excitation; lowering of temperature leads to a disappearance of the tautomeric long-wave emission bands and to the recovery of the strong normal short-wave fluorescence. The situation is different for some structurally related molecules, such as 1*H*-pyrrolo[2,3-*h*]quinoline (**PQ**) and dipyrido[2,3-*a*:3',2'-*i*]carbazole (**DPC**) (Scheme 1.9), extensively studied in the Institute of Physical Chemistry PAS.[122-129] In this case the tautomeric emission is still observed in low-temperature rigid alcohol glasses. The process was identified for **PQ** and related compounds by comparing the long-wave fluorescence of the phototautomeric products with the emission of molecules synthesized to serve as chemical models of the tautomeric structures.[129] Interesting phenomenon is shown by **DPC** – in 1-propanol glass at 77 K three emission bands are observed: short-wave normal fluorescence, phosphorescence, and long-wave tautomeric fluorescence.[128]

PQ   **DPC**

Scheme 1.9. Formulas and acronyms of 1H-pyrrolo[2,3-h]quinoline and dipyrido[2,3-a:3',2'-i]carbazole.

It appeared that the rapid, barrierless excited-state reaction occurs in the alcohol and water complexes of ground-state prepared proper structure and stoichiometry.[128,129] If the precursor of the tautomer is not of such structure the reaction may occur through a barrier and deactivation *via* internal conversion must be taken into account. The structure of **PQ** complexes with methanol of 1:1 stoichiometry, which is difficult task for solution studies, has been determined with the use of supersonic beam techniques, combined with femtosecond laser spectroscopy and mass detection.[125,126]

A special class of bifunctional molecules consists of compounds for which the hydrogen bond donor and acceptor centers are located in separate moieties, connected by a single bond (for example, 2-(2'-pyridyl)indole (**2-PI**) and 2-(2'-pyridyl)pyrrole (**PP**), Scheme 1.10). This leads to an appearance of two rotameric forms, *syn* and *anti*, with the both centers on the same or on the opposite sides of the molecule, respectively. The two conformers may

14

reveal drastically different excited state properties. Only the *syn* form is able to form cyclic, hydrogen-bonded complexes with alcohol or water. Electronic excitation of such complexes of 1:1 stoichiometry can result in the ESDPT process. Moreover, in the *syn* form ESIPT process may occur if the flexibility of the molecular skeleton enables a close and proper approach of the both centers.

2-PI   **PP**

Scheme 1.10. Formulas and acronyms of the syn forms of 2-(2'-pyridyl)indole and 2-(2'-pyridyl)pyrrole.

2-PI emit a single, short-wave fluorescence band; the compound do not show any measurable long-wave emission.[130-133] Photophysical studies of **2-PI** reveal that in aprotic solvents fluorescence quantum yields are quite high and fluorescence lifetimes are monoexponential (*ca*. 1.3 ns). In alcohols quantum yields become significantly lower. In alcohol solutions, as well as in solutions containing a mixture of alcohols with both polar and nonpolar aprotic solvents, the fluorescence decay is biexponential. The value of the short decay component ($\tau < 0.5$ ns) was practically the same as that observed for bridged pyridyl-indoles (*e.g.*, 3,3'-tetramethylene-2-(2'-pyridyl)indole) and thus was assigned to the *syn* form. Therefore, the long component (*ca*. 3.3 ns) was attributed to the *anti* conformer. The co-existence of these two rotameric forms was also supported by NMR measurements and theoretical calculations (about 85% of the ground-state population in deuterated methanol is predicted to correspond to the *anti* rotamer).[133] Fluorescence decay studies performed in mixed solvents show that the fraction of the *anti* conformer increases upon adding alcohol to *n*-hexane solution (more than 90% in pure alcohol). The radiative rate constant k_f of the *anti* form was estimated to be about one order of magnitude smaller than that of the *syn* rotameric form (*ca*. 5×10^7 s^{-1} as compared to 5×10^8 s^{-1}).

For **PP**, contrary to **2-PI**, in *n*-hexane solution fluorescence quantum yield is lower than that in alcohols. This was explained[134] by the excited state intramolecular proton transfer, leading to a short-lived phototautomer. The presence of the latter is manifested by the appearance of a low-intensity low-energy fluorescence band (Fig. 1.6). The similar dual emission with a slight blue shift of the "normal" band is observed for jet-isolated **PP**.[135] Laser induced fluorescence (LIF) excitation and hole-burning UV/UV spectra demonstrated that all

the observed spectral features originate from the only one ground-state species. Interestingly, the studies of **PP** under supersonic jet isolation conditions revealed mode-selective ESIPT. The LIF excitation spectra have been recorded for both emission bands. The spectrum corresponding to the tautomeric fluorescence exhibits much fewer lines with respect to the rich pattern observed for the short-wave emission. The detailed analysis of the LIF excitation spectra and dispersed fluorescence (DF) spectra obtained for excitation into specific vibronic levels (SVLF) showed that all the vibrational modes that promote ESIPT are able to strengthen the intramolecular hydrogen bond.[135]
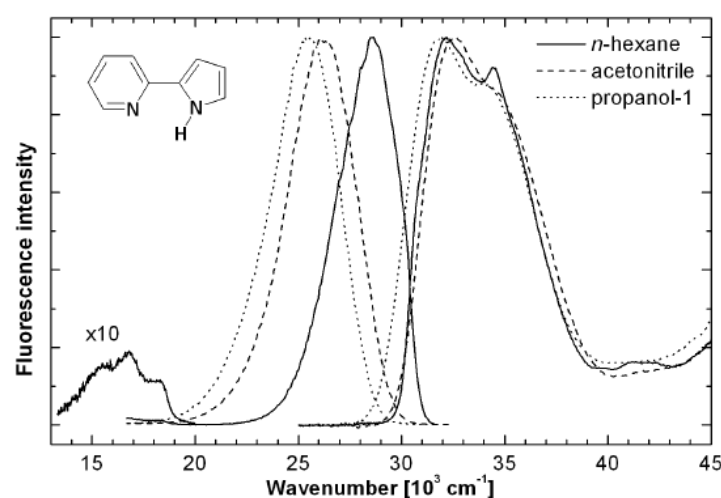
*Figure 1.6. Room-temperature absorption and fluorescence of **PP** in n-hexane, acetonitrile and 1-propanol.*

The general scheme showing the solvent-induced rotamerization and excited state deactivation channels in bifunctional heteroazaromatic molecules such as **2-PI** and **PP** has been proposed by Waluk and coworkers.[132,136] In nonpolar solvents only the *syn* species should be present (this rotamer predominantly exist in the gas phase in supersonic jets[137]). This form can undergo ESIPT process depending on the mutual arrangement of the proton donor and acceptor centers. A small fraction of the *anti* form can be expected in polar aprotic solvents, while in alcohols it becomes significant. Stabilization of the *anti* structure is due to a larger ground state dipole moment and stronger and more linear hydrogen bonds with hydroxylic partners than in the *syn* species.[134,138] In some cases (as for 2-(2'-pyridyl)indoles) the *anti* conformer can be more stable in alcohol solutions than the *syn* one because of a stabilization of the *anti* structure by two separate alcohol molecules connected to the opposite sides of a chromophore. In alcohols and water the excited state of the *syn* conformer is rapidly depopulated due to a formation of cyclic hydrogen-bonded complexes with protic partner. It may involve $S_1 \rightarrow S_0$ enhanced internal conversion and/or fast double proton transfer. The

latter process (ESDPT) occurs in 1:1 complexes on a time-scale of single picoseconds or faster, whereas the former involves complexes with two (or more) molecules of alcohol (1:n complex), and takes much longer (tens to hundreds of picoseconds).[139] The lack of tautomeric fluorescence in alcohols combined with fluorescence quenching indicates a domination of other complexes than that of cyclic structure and 1:1 stoichiometry.

1. 4. 7-hydroxyquinolines and molecular photoswitches

Studies of 7-hydroxyquinoline (**7-HQ**) started more than 50 years ago. This is one of the comprehensively examined compounds showing solvent-assisted excited-state long-range proton transfer. The distance between proton donating and proton accepting centers of **7-HQ** is too long to form intramolecular hydrogen bond, thus ESIPT can not occur. The only way phototautomerization can appear is *via* multiple proton transfer in alcohol or water complexes.

For the first time absorption spectra of **7-HQ** were presented in 1946[140] showing bathochromic shifts in both acidic and basic solutions. Later,[141-144] UV-Vis and IR spectroscopic and photophysical parameters were reported. In 1968 Mason[145] explained prototropic equilibria in the ground state S_0 and in the lowest excited singlet state S_1 between four neutral and ionic species of **7-HQ** appearing in water solutions: a normal molecule (7-quinolinol, abbreviated as the **OH** tautomeric form), a deprotonated anion (**A**), a protonated cation (**C**) and a zwitterion (**Z**) (Scheme 1.11). The resonance hybrid of the zwitterionic form is the **NH** tautomer (7(1H)-quinolinone). In the literature the **OH** and **NH** forms are frequently termed as "enol" and "keto" forms, respectively.
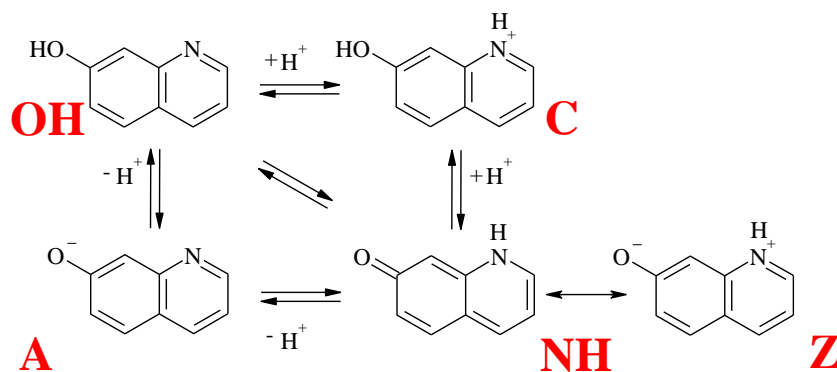
*Scheme 1.11. Formulas of the neutral and ionic forms of **7-HQ** (**OH** – 7-quinolinol, **A** – deprotonated anion, **C** – protonated cation, **Z** – zwitterion, **NH** – 7(1H)-quinolinone).*

It was found that the spectral positions of the lowest absorption bands and fluorescence spectra of the neutral and ionic forms are located at wavelength in the order: $Z \leftrightarrow NH > A > C > OH$ (Fig. 1.7).
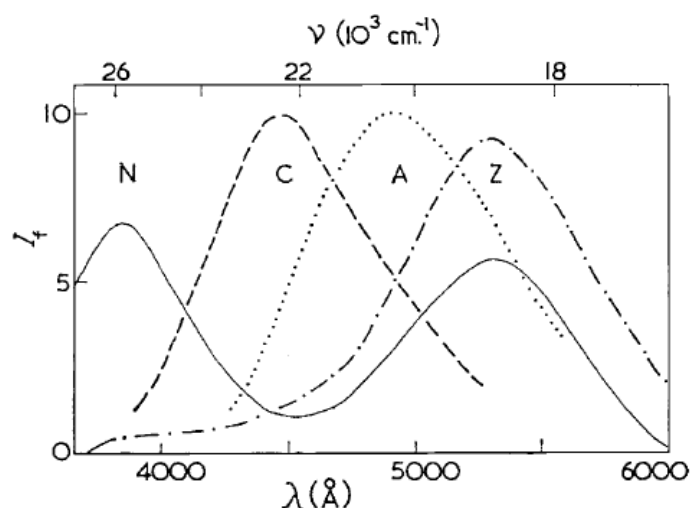
*Figure 1.7. The fluorescence spectra of **7-HQ** in ethanol (straight line), in water at pH 7 (dash-dotted line), in 10M-perchloric acid (dashed line), and in 8M-sodium hydroxide (dotted line).[145] N labels the normal (i.e. **OH**) form.*

On the basis of these experimental results and using the Förster cycle, the pK_a values describing the prototropic equilibria between the neutral and ionic forms in the both states S_0 and S_1 were determined.[145,146] It was observed that upon excitation to the S_1 state the phenolic group of **7-HQ** becomes more acidic, and the quinoline nitrogen atom is more basic than those in the ground state. This finding suggests a shift of the **OH**, **C**, and **A** forms towards the **NH** form upon excitation. In the case where two groups with opposite pK_a tendencies in excited states exist in a molecule a photon may initiate protonation and deprotonation to yield a zwitterion **Z**. Due to that the fluorescence of **C** and **A** is observed in strong acids (pH < 1) or bases (pH > 13), respectively. In aqueous solutions in the range of pH from 2 to 13, only emission of the neutral forms of **7-HQ** (the dominant band corresponds to the **NH** form) is observed (Fig. 1.8), although the absorption spectra show the existence of the ionic forms in the ground state. The ground-state fractions of the various forms of **7-HQ** in aqueous solution at pH = 7 estimated from the respective pK_a values are: 67% (**OH**), 29% (**NH**), 3% (cation) and 1% (anion).[147]
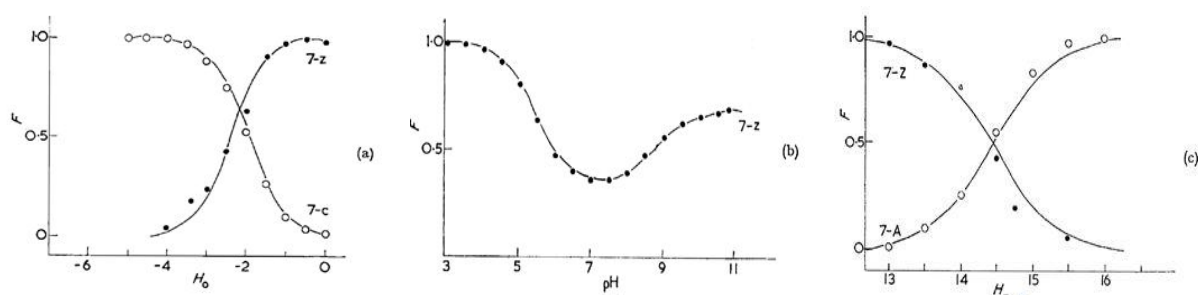
*Figure 1.8. The relations between fractional concentrations F of the excited ionic forms of **7-HQ** and the acidity of the medium over: (a) the H_0 scale, (b) the pH range, and (c) the H. region.[145]*

The similar results were recently reported[148] for two **7-HQ** derivatives: 7-hydroxy-4-methylquinoline (**H4MQ**) and 7-hydroxy-2,4-dimethylquinoline, **HDMQ** (Scheme 1.12).

H4MQ   **HDMQ**

Scheme 1.12. Formulas and acronyms of 7-hydroxy-4-methylquinoline and 7-hydroxy-2,4-dimethylquinoline.

Two absorption bands of all the three compounds in aqueous solution at pH = 7 peaking around 330 and 400 nm were assigned to the lowest electronic transitions of the **OH** and **NH** forms, respectively (Fig. 1.9). In emission, a single band at around 500 nm assigned to the **NH** form appears. Introduction of methyl groups leads to the increase of the fluorescence quantum yield of 3-4 times. The changes of absorption spectra observed in the range of pH from 2 to 12 prove the ground-state formation of cations and anions, whereas fluorescence spectra as well as fluorescence quantum yields remain the same as at pH = 7. These facts indicate the excited-state deprotonation of cations and protonation of anions to yield the **Z ↔ NH** form.
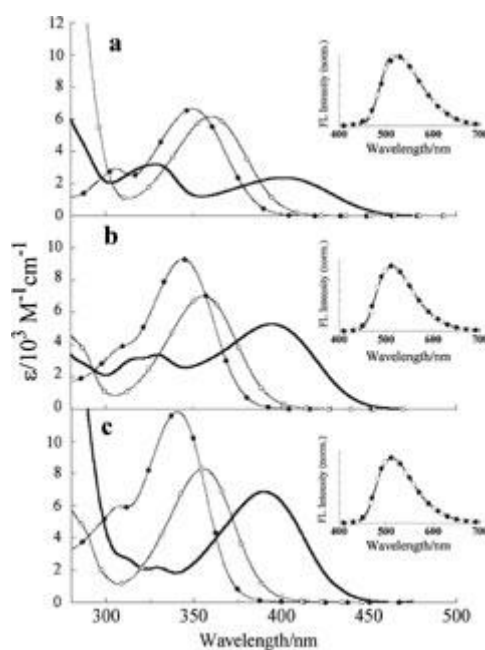
*Figure 1.9. Absorption spectra of **7-HQ** (a), **H4MQ** (b), and **HDMQ** (c) at pH 2.0 (closed circle), pH 7.0 (solid line), and pH 12.0 (opened circle), respectively. Inset of each figure shows the normalized fluorescence spectra at this pH range.[148]*

Time-resolved measurements determining reaction rates were conducted since 1982.[149-152] It was found[147] that after excitation of the **OH** species in aqueous solution, the emission decay of the cation and anion are in a good agreement with the rise of the **NH** form. The **OH** fluorescence decay at 430 nm is described by three components: 30 ps (92%), 230 ps (7%), and 2.6 ns (1%). The kinetic profile of the **NH** fluorescence at 520 nm shows two rise components of 30 ps (90%) and 200 ps (10%) and 2.6 ns decay. The observed 30 ps decay and rise times at neutral pH were ascribed to the **OH** deprotonation of the cation while 200 ps decay and rise times – to quinoline nitrogen atom protonation of the anion (Fig. 1.10). It was suggested that the excited state **OH** species undergoes within 10 ps protonation to the nitrogen atom to form an excited cation intermediate or deprotonation from the OH group to form an excited anion intermediate. The lowest excited singlet state of the photochemically produced **NH** form is depopulated in 2.6 ns. Using time-resolved transient absorption spectroscopy, ground state relaxation of the prototropic equilibrium perturbation was estimated to be about 20 μs.
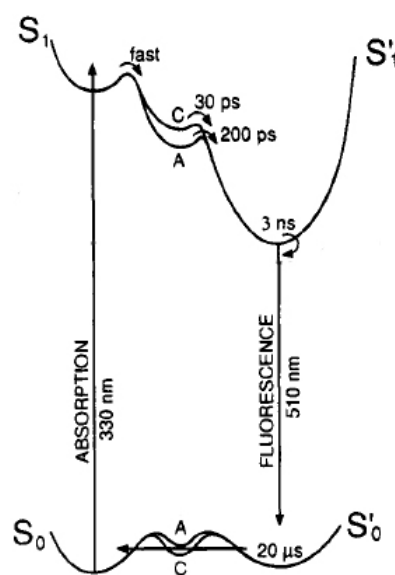
*Figure 1.10. Schematic interpretation of the mechanism and observations of the proton transfer cycle in neutral aqueous **7-HQ** solution. S and S' describe the **OH** and **NH** species, respectively.*[147]

Investigations of the formation of complexes of **7-HQ** with protic partners (methanol and water mostly) gave interesting results. Transient absorption studies[153] of **7-HQ** in mixed *n*-hexane-methanol solvents reveal two ground-state complexes of 1:1 and 1:2 stoichiometry. In pure *n*-hexane there is only one fluorescence band at 350-400 nm which is a mirror image of the absorption and then can be attributed to the **OH** form. An addition of methanol to the solution leads to the appearance of the second band centred at 530 nm. Its intensity increases

with the increase of methanol concentration. The long-wave fluorescence was attributed to the tautomer formed *via* a triple proton transfer in the 1:2 cyclic complex of **7-HQ** with methanol molecules (Scheme 1.13).[154]

Laser induced fluorescence (LIF) excitation and dispersed emission (DF) spectroscopy experiments under supersonic jet isolation conditions[155] revealed 1:1 and 1:3 water-chain clusters of **7-HQ** with unusually large spectral shift for the latter. But no significant excited-state proton transfer was found. Supersonic jet investigations combined with mass-selected resonant two-photon ionisation (R2PI MS) technique[156] show existence of water-chain complexes of various structures and stoichiometry: **7-HQ**·(H$_2$O)$_n$ with n = 1-4 water molecules.

Potential energy profiles of the multiproton transfer in the ground state were computed using different methods.[157] The calculations predict a formation of clusters **7-HQ**·(H$_2$O)$_n$ with n = 1-3. The global minimum corresponds to the 1:1 complex with water molecule attached to the oxygen atom. From among 1:2 and 1:3 complexes, the preferential are those of cyclic structures. The potential energy barriers of the tautomerization from the **OH** to the **NH** form were found to be 12.6 and 8.5 kcal/mol for 1:2 and 1:3 clusters, respectively, while the barrier heights of the reverse reaction were much smaller. This suggests instability of the **NH** form.
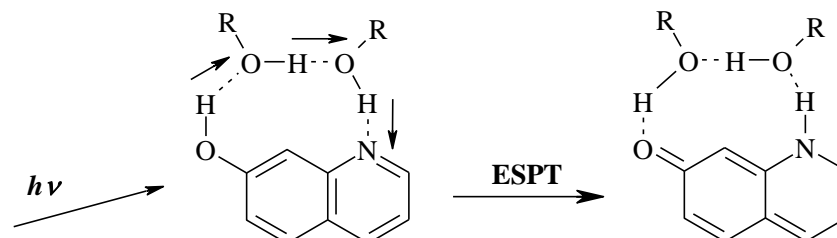
*Scheme 1.13. Scheme of excited state triple proton transfer in 1:2 complexes of **7-HQ** with protic solvent molecules.*[158]

The solvent-assisted ESPT of **7-HQ** in neutral aqueous solution,[147] as well as in 1:1 complexes with glycerol and ethylene glycol,[159] was described as a stepwise process; as a process incorporating rotational diffusion dynamics of the protic solvent within 1:1 complexes with acetic acid;[160] as a two-step process in neat alcohols;[154,161] and as a multiple proton transfer in cyclic 1:2 and 1:3 complexes with water and methanol,[157,162] and with other alcohols (such as ethanol, 2-propanol).[158]

The derivatives of **7-HQ** that can undergo ESIPT (such as 7-hydroxy-(8-oxazine-2-one)quinoline, 2-hydroxy-1-(N-piperidinomethyl)naphthalene and 7-hydroxy-4-methyl-quinoline-8-carbaldehyde) have been proposed as optically driven reversible molecular

switches.[163-166] Molecular switch is a molecule that has two or more stable states and can be switched between them under precise and controlled conditions, for example, by changing pH or temperature of the surrounding medium or simply by irradiating it with light of different specific wavelengths. One of the most important roles molecular switches could play is a replacement of a current generation of transistors, thus it will be possible to fit more than a trillion switches onto a centimetre-square chip. A molecule that can exhibit two different phases when subjected to electric fields can work as a molecular switch: one phase is the "zero" and the other is the "one", which form the foundation of digital electronics.[167] Reversible switching between different conductance states and many different mechanisms of its operation have been studied. For example, reversible redox reactions in catenane and rotaxane molecules triggered by voltage pulses,[168] STM employment[169] or photoinduced hydrogen transfer[170] have been proposed. Another application lies in biology and medicine. For example, molecular switch controls interspecific prion disease transmission[171] or the switch that might prevent cancer cells from metastasizing from a primary tumour to other organs.[172] They also could be used in more "down to earth" applications, such as skin protection from cancer-causing UV sun radiation by activating the sun-tan process.[173] This type of photostabilization is in widespread technical use for the protection of the organic polymers against degradation by UV light.[174,175] The proposed model for the functioning of photostabilizers involves barrierless (2-(2'-hydroxyphenyl)benzothiazole[176]) or with a very low barrier (salicylic acid[177]) enol-to-keto proton (or hydrogen) transfer in the electronically excited S_1 state, ultrafast (ca. 100 fs) radiationless decay of the excited (S_1') **NH** form, and barrierless proton backtransfer to the electronic ground state S_0, thus closing the photocycle.[178]

The mechanism of the ESIPT process in 7-hydroxy-8-(N-morpholinomethyl)quinoline (**7HMMQ**) was proposed by Varma *et al.*.[163] A fluorescence behavior of **7HMMQ** was compared with that of 2-hydroxy-1-(N-morpholinomethyl)naphthalene (**2HMMN**) and **7-HQ** (Fig. 1.11). In polar solvents **7HMMQ** shows, contrary to the other compounds, three fluorescence bands. Two bands, at the short- and long-wave sides of the spectrum, are also observed in the fluorescence spectrum of **7-HQ** in alcohols. These two bands are assigned to emission from the excited initial tautomeric form (**OH**) and from the adiabatically produced excited **NH** form, respectively. The third band originates from an excited transient species (when the proton is located at the N atom of the morpholine moiety). The proposed mechanism of the excited-state long-range intramolecular phototautomerization of **7HMMQ** is as follows: one part of the molecule (**7-HQ**) having both proton donor and acceptor groups

23

acts as a molecular "frame", while the side group (morpholinomethyl) – as a proton "crane". The latter has a single proton accepting site. It picks up the proton from the initial point on the one side (OH group) of the "frame" moiety and deposits it at the final point (nitrogen atom) on opposite side. The twisting mechanism was confirmed by the time-resolved fluorescence investigations in solvents of various viscosity.[163]
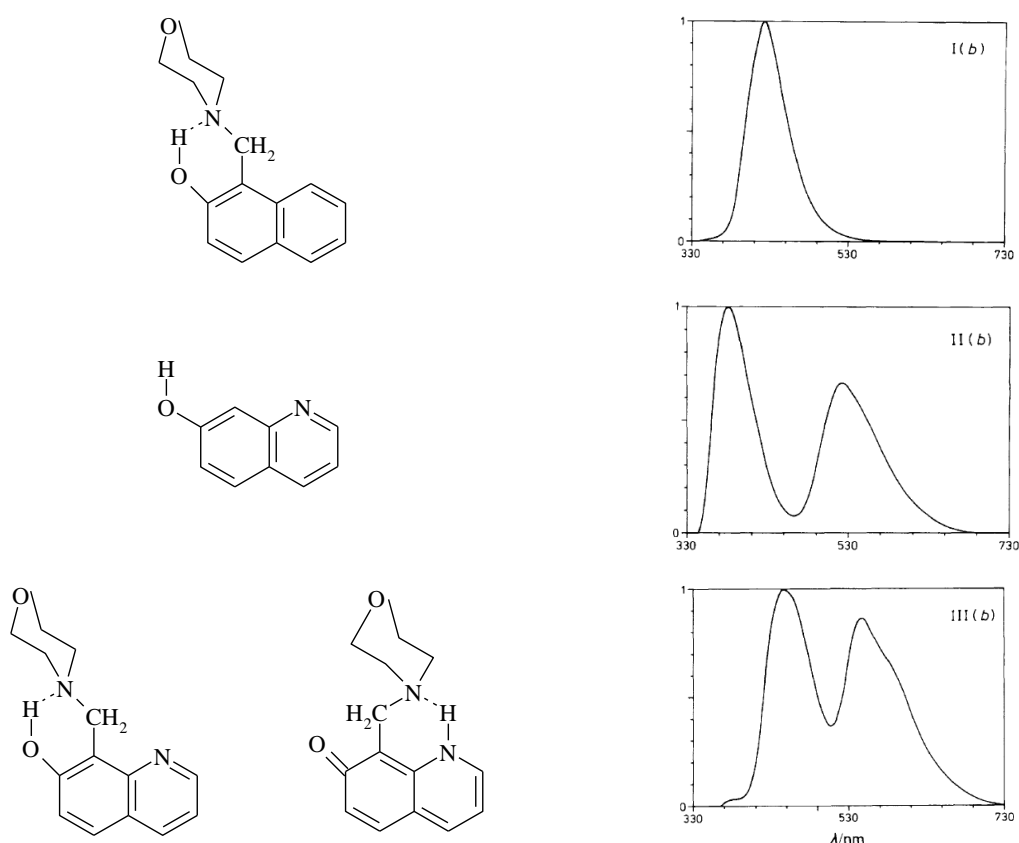
Figure 1.11. Molecular structures and emission spectra of 2-hydroxy-1-(N-morpholinomethyl)naphthalene in acetonitrile (top), 7-hydroxyquinoline in methanol (middle) and 7-hydroxy-8-(N-morpholinomethyl)quinoline in acetonitrile (bottom) at room temperature (λ_{exc}= 300 nm).[163]

Computational studies of similar molecules as promising candidates for future optical switching applications were provided recently.[164-166] Sobolewski *et al.* proposed to use smaller groups as a rotating proton "crane" (*e.g.*, carbaldehyde group) and developed an idea of a photo-switch system based on the, postulated by Varma, mechanism of the ESIPT process (Fig. 1.12).
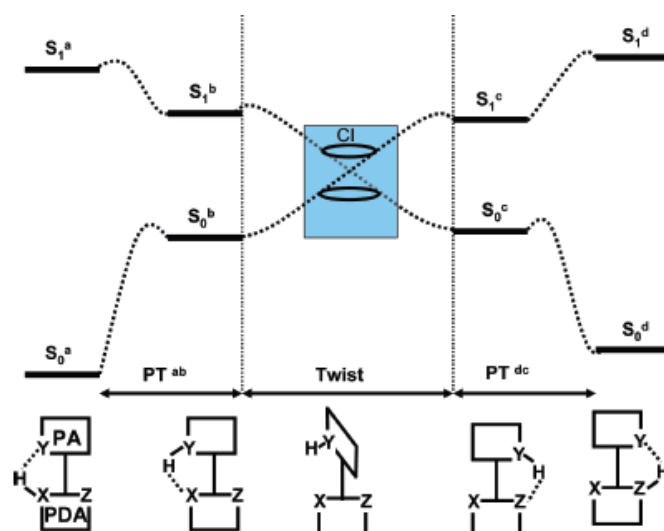
Figure 1.12. Potential energy diagram illustrating the photophysics of an optical molecular switch driven by the ESIPT process.[166]

The molecular "frame" (PDA) has two proton-donating/accepting atoms, X and Z, whereas the proton "crane" (PA) has only a single proton-accepting site (Y). The left part of the picture shows the proton transfer (PT^{ab}) from X to Y site. It connects two tautomeric forms of the switch "a" and "b". The right panel describes the same reactions between Z and Y sites (PT^{dc}) and links another pair of tautomers "d" with "c". The $S_0^a \rightarrow S_1^a$ optical excitation induces the $S_1^a \rightarrow S_1^b$ proton transfer (PT^{ab}) reaction. The torsion (the central panel) breaks X-H$\cdots$Y intramolecular hydrogen bond and thus the system evolves to the S_0-S_1 conical intersection (CI). Since the "crane" moiety can be quite small, its torsional motion can be relatively fast (sub-picoseconds). There are two possibilities for the system to evolve after the $S_1 \rightarrow S_0$ nonadiabatic transition at the CI. The S_0^b form can be populated or the system can continue the torsional motion. This motion leads to the formation of the Y-H$\cdots$Z hydrogen bond (form S_0^c). The S_0^b and S_0^c structures are not expected to be stable. Thus, the proton initially attached to the atom Y spontaneously transfers to X (or Z) atom. In this way, either the system restores the structure S_0^a or creates the new one – S_0^d. Therefore, the net effect is a transfer of the hydrogen atom from atom X to atom Z *via* an intramolecular proton "crane". By choosing the proper excitation wavelength, one can switch the system between two well-defined tautomeric forms within some sub-picoseconds. Such a molecule may represent an elementary memory unit.

A similar scheme can be applied to photostabilizers without Z atom in their structure.[164-166] Here opened "d" conformer is undesired. In good stabilizers the barrier of the ground-state process from the open-**NH** to the closed-**OH** tautomer is extremely low, so the system has no chance to find itself in the opened form. Organic photostabilizer were not

found to be exposed to the photo-induced degradation. The same postulate can be employed to the molecular switches as far as they operate under the same principle.

A molecular switch described in Fig. 1.12 must have some unique properties. Its rotameric/tautomeric forms must represent only two minima on the PES of the ground state. These minima must be well-defined and separated from each other by a sufficient energy barrier. Two forms of the system should absorb light at different wavelengths and these bands should be separated in the spectrum by a "window". Both conformers should have the possibility of barrierless transition from S_1 to conical intersection of S_0 and S_1; CI itself should occur in nearly perpendicular mutual conformation of "frame" and "crane" with a global minimum on the S_1 PES.

7-hydroxy-4-methyl-quinoline-8-carbaldehyde, **H4MQC** (Scheme 1.14) has been very recently proposed as a reversible bistable molecular switch driven by photoinduced hydrogen atom transfer.[165,166] The compound can exist in three tautomeric structures; moreover, one of them can appear in two rotameric forms.
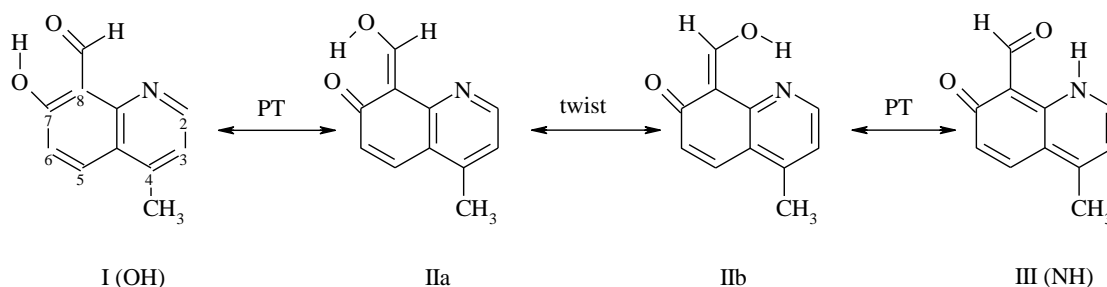
Scheme 1.14. Structures of isomeric forms of **H4MQC** and photoprocesses taking place in the system.

The theoretical *ab initio* study of **H4MQC** (Fig. 1.13) has indicated that the **OH** and **NH** forms are stable on the ground-state PES; the value of the separating barrier is of the order of 2 eV. Thus, these tautomers should be thermochemically and kinetically stable. The **OH**-to-**NH** phototautomerization for this compound was numerically found to be reversible due to the nonadiabatic transition at the S_0-S_1 conical intersection (contrary to the mentioned earlier **7HMMQ** which show in alcohols and nitriles at room temperature the irreversible, adiabatic formation of the tautomeric form in the excited singlet state). Two crucial obstacles are predicted by computations. The first one is that for all the forms involved in the excited-state reaction the $^1(n,\pi^*)$ states were found to be lower in energy than the corresponding "reactive" $^1(\pi,\pi^*)$ states. The second one is the essential barrier for the ESPT process from the S_1 state of the **NH** tautomer to the S_1 state of the **IIb** form.
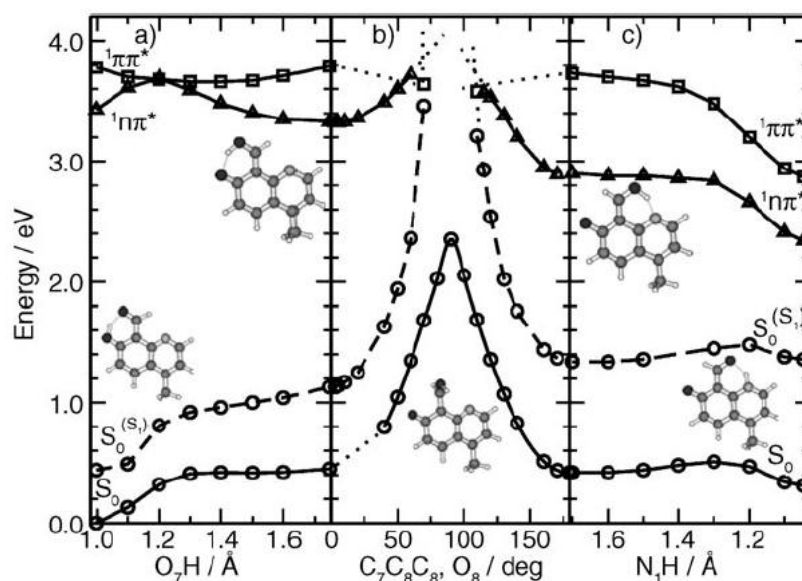
*Figure 1.13. Energy profiles of **H4MQC** in the S_0 state (circles) and in the lowest $^1(n,\pi^*)$ (triangles) and $^1(\pi,\pi^*)$ state (squares), and in the, determined at the CC2/def-SV(P) level along the minimum-energy path (solid) for hydrogen transfer from structure I, for carbaldehyde-ring torsion (b), and for hydrogen transfer from structure III (c). $S_0^{(S1)}$ denotes the energy of the S_0 state, calculated along the minimum-energy path of the S_1 $^1(n,\pi^*)$ state (dashed curves). Dotted lines denotes interpolations in regions where CC2 optimization was not possible, due to collapse to a lower-lying excited state or degeneracy with the ground state.[165]*

In spite of these predicted obstacles, the experimental confirmation of the reversible ESIPT process was obtained by irradiating the monomer of **H4MQC**, isolated in low-temperature Ar matrix, with UV light of proper wavelengths (Fig. 1.14).[165] The IR spectra, recorded just after deposition of the matrix (b) and after 1.5 h irradiation with UV light of $\lambda > 295$ nm (c), showed that after irradiation the intensity of lines decreased, and, at the same time, new IR lines appeared. That points on some photoproduct which replaces the initial isomer in some extent. Further irradiation of the matrix did not result in any additional changes. This demonstrates that the observed UV-induced process leads to a final, photostationary state of a product. When immediately after UV irradiation of $\lambda > 295$ nm, the matrix was additionally irradiated by UV light of longer wavelength $\lambda > 360$ nm, the population of the photoproduct decreased, whereas the initial form was regenerated in some extent. This fact proves a photoreversibility of the studied transformation process.
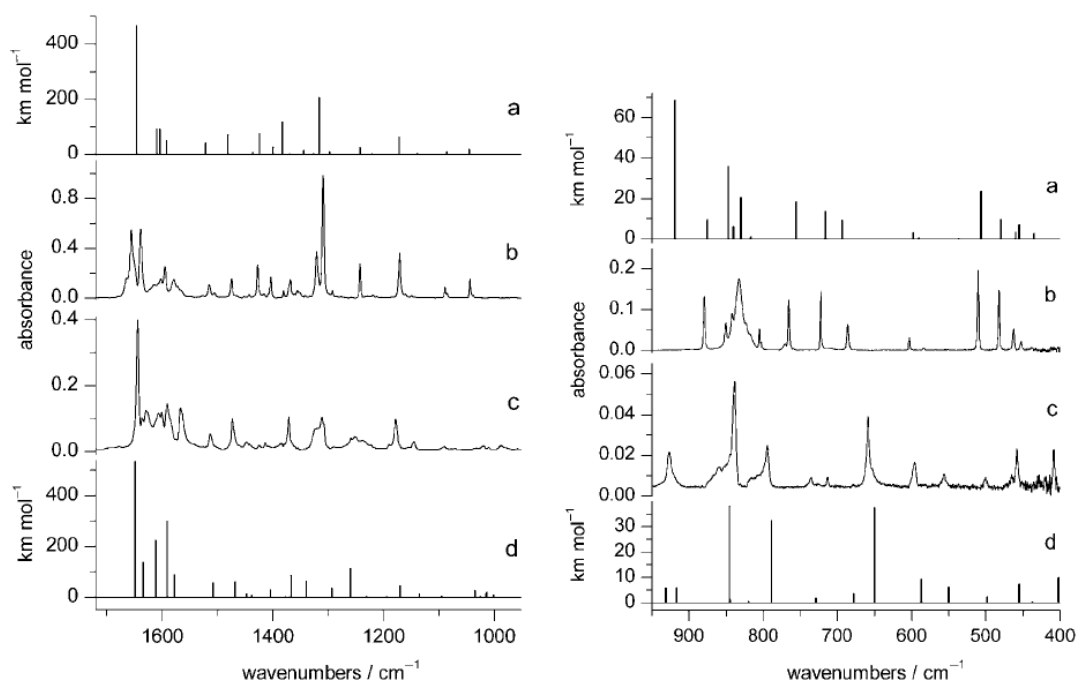
*Figure 1.14. a)-d) IR spectra of **H4MQC** monomers in higher (left panel) and lower (right panel) wavenumber range. The experimental spectrum recorded after deposition of the matrix (b) and the extracted spectrum (c) of the photoproduct generated on UV ($\lambda > 295$ nm) irradiation, are compared with the theoretical spectra predicted for structure I (a) and structure III (d). Spectrum (c) of the photoproduct is obtained by subtraction of spectrum (b), multiplied by 0.43, from the spectrum recorded after UV ($\lambda > 295$ nm) irradiation. The theoretical spectra were calculated at the DFT/B3LYP/aug-cc-pVDZ level. The computed wavenumbers were scaled by a factor of 0.98.*[165]

The identification of the forms responsible for the presented IR spectra was provided by a comparison with theoretical computations at the DFT/B3LYP/aug-cc-pVDZ level (Fig. 1.14). These theoretically predicted IR spectra of the **OH** (a) and **NH** (d) tautomeric forms are in a good agreement with the experimentally obtained data. The calculations confirm the idea of the reversible **OH** $\leftrightarrow$ **NH** transformation upon selective electronic excitation. No signs of transient forms **IIa** and **IIb** were experimentally observed in agreement with the theoretical computations predicting that these forms do not correspond to stable minima on the PES of the ground state. Moreover, it was claimed that no signs of any other photoproducts were detected in low temperature Ar matrices.

1.5 Goals

The aim of this work is to study spectroscopic properties, photophysical processes and photochemical reactions in three series of bifunctional and trifunctional molecular systems having both proton donor and acceptor centers in solutions and under supersonic jet isolation conditions by means of the steady-state and time-resolved UV-Vis spectroscopic methods and quantum chemical calculations. The goal is to study the influence of solvent properties (including polarity and hydrogen bond donor and acceptor ability) on the photophysical processes and photochemical reactions such as ground and excited state proton transfer and rotamerization in selected molecules. Quantum chemical computations are provided to characterize ground and excited state geometry and dipole moments, and calculate the energies of electronic absorption and emission transitions. The chosen compounds, solvents selected to cover a wide range of the static permittivity values ε[179] and that of index α[179,180] describing the solvent hydrogen bond donor ability, instrumentation and experimental procedures as well as computational details are described in Chapter 2. The work is divided into three parts:

1. Chapter 3 describes stationary and time-resolved UV-Vis spectroscopic studies and ^{1}H NMR investigations performed in order to understand the mechanism of the ground and excited-state long-range prototropic tautomerization of 7-hydroxyquinoline-8-carbaldehydes (**7-HQCs**) in various media. The compounds represent trifunctional proton donor-acceptor systems composed of two moieties: a molecular "frame" (7-hydroxyquinolines, **7-HQs**) and a proton "crane" (carbaldehyde group), and were proposed[165] to serve as models of a bistable molecular switch driven by photoinduced hydrogen atom transfer. In order to identify the individuals responsible for the absorption and multiple fluorescence bands, the spectroscopy and photophysics of **7-HQCs** are compared to those of their **7-HQs** precursors (Scheme 3.2). The effects of polarity and hydrogen bond donor ability of the surrounding media on the photophysical and photochemical properties of the compounds as well as prototropic equilibria in acidic and basic solutions are examined and discussed.

2. Chapter 4 is devoted to rotamerization and photoinduced tautomerization in the series of 2-(1*H*-pyrazol-5-yl)pyridines (**2-PPs**). The use of steady-state and time-resolved spectroscopic techniques and quantum chemical computations leads to the understanding of ESIPT and ESDPT processes and conformational equilibria of the

variety of possible rotameric and tautomeric forms.[181] The group of compounds (Scheme 4.1) was specially synthesized to study the effects of withdrawing (bromine atom, nitrogen dioxide group) or electron donating (methyl group) substituents on the spectroscopy, photophysics, and photochemistry of **2-PPs**.

3. Spectroscopy and photophysics of a series of selected bifunctional indole derivatives is considered in the last part of the work (Chapter 5). The hydrogen bond donor (the indole NH group) and acceptor centers (such as oxygen, nitrogen, or sulphur atoms) are located in separate moieties of the molecules, covalently linked by a single bond. The goal is to compare the properties of molecules which can form two rotameric forms, *syn* and *anti*, with the compounds which either unable to rotamerize due to the topology (*i.e.* 3-pyridyn-4-yl-1*H*-indole, **3-PI**) or does not have any acceptor center as 2-(1*H*-pyrrol-2-yl)-1*H*-indole (Scheme 5.1). The former compounds containing thiophene, thiazole, and furan were expected to show solvent dependent photophysics. Contrary to our expectation, the compounds reveal very efficient fluorescence independent of solvent polarity and hydrogen bond donor and acceptor ability. Laser spectroscopic studies combined with supersonic jet technique and quantum chemical computations have been performed in order to identify their rotameric forms and to gain more insight into the changes of the molecular structure accompanying electronic excitation. Contrary to the other members of the series, the luminescence of **3-PI** appeared to be strongly quenched in protic solvents. The experimental investigations, combined with calculations allow us to explain the mechanism of the efficient excited state deactivation.[182]

Chapter 2: Experimental

2.1. Materials

2.1.1. Compounds

Two series of bifunctional proton donor-acceptor compounds, for which the proton donor and acceptor are located in separate moieties linked by a single bond, namely 2-(1*H*-pyrazol-5-yl)pyridines, **2-PPs** (Scheme 2.1) and indole derivatives (Schemes 2.2 and 2.3), and a third series of 7-hydroxyquinoline-8-carbaldehydes, **7-HQCs** (Schemes 2.4 and 3.1) representing trifunctional proton donating/accepting systems, have been chosen and synthesised to study their spectroscopy, photophysics, conformational equilibria and phototautomerization processes in solutions. The selected indole derivatives have been studied also under supersonic jet isolation conditions. The former two series of molecules, except 3-pyridin-4-yl-1*H*-indole (**3-PI**), similarly to 2-(2'-pyridyl)indoles[132,133,183,184] and 2-(2'-pyridyl)pyrroles,[134,135,185,186] can exist in various rotameric forms, the *syn* form, with the proton donor and the acceptor on the same side, and the *anti* rotamer, with the two centers on the opposite sides.

The first family of compounds, especially designed to probe the conformational equilibria as well as excited state proton transfer (ESPT) processes (Chapter 4), was synthesised in the group of Prof. W. R. Thiel (Anorganisch-Chemisches Institut, Technische Universität München).[187] The parent molecule 2-(1*H*-pyrazol-5-yl)pyridine (**PPP**) and its three derivatives: 2-(3-methyl-1*H*-pyrazol-5-yl)pyridine (**MPP**), 2-(4-bromo-1*H*-pyrazol-5-yl)pyridine (**BPP**) and 2-(4-nitro-1*H*-pyrazol-5-yl)pyridine (**NPP**) can formally exist in six isomeric forms. Pyrazole, having two nitrogen atoms, can create two *syn* and two *anti* forms, and in addition, two tautomeric forms are possible (Scheme 4.2). The compounds allow us to study the possible role of substitution at different positions in the pyrazole ring by electron acceptors (Br atom and NO_2 group) or electron donor (CH_3 group).

PPP   **MPP**   **BPP**   **NPP**
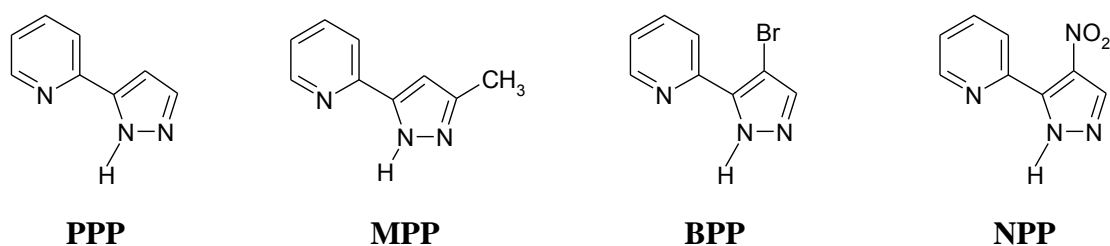
Scheme 2.1. Formulas and acronyms of investigated 2-(1H-pyrazol-5-yl)pyridines.

31

The second series of compounds was synthesised by Prof. T. M. Lipińska (Institute of Chemistry, University of Podlasie)[188,189] and Prof. R. P. H. Thummel (Department of Chemistry, University of Houston). The four indole derivatives: 2-thiophen-2-yl-1*H*-indole (**THOIN**), 2-thiazol-2-yl-1*H*-indole (**THAIN**), 2-furan-2-yl-1*H*-indole (**FURIN**) and 2-(1*H*-pyrrol-2-yl)-1*H*-indole (**PYRIN**) have a possibility to exist in the *syn* and *anti* rotameric forms. Only the *syn* conformers (except **PYRIN**) are able to form cyclic, doubly hydrogen bonded complexes with protic partners. Thus, it was expected that these molecules, similarly to 2-(2'-pyridyl)indoles,[132,133] should show solvent dependent photophysics. Contrary to our expectation, the compounds do not undergo any efficient fluorescence quenching due to internal conversion (**THOIN**, **THAIN**, and **FURIN**) and ESPT (**THAIN**) processes (Chapter 5).

THOIN   **THAIN**   **FURIN**   **PYRIN**
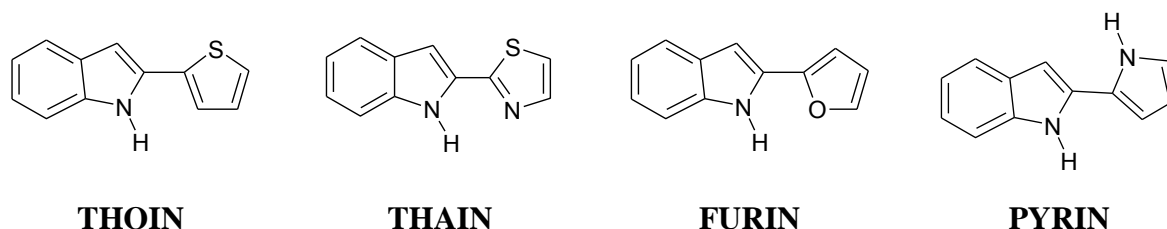
Scheme 2.2. Formulas and acronyms of investigated indole derivatives.

3-pyridyn-4-yl-1*H*-indole (**3-PI**), synthesised in the group of Prof. R. P. H. Thummel,[190] was chosen to serve as an example of a compound in which neither rotamerization no tautomerization can occur.[182]

3-PI
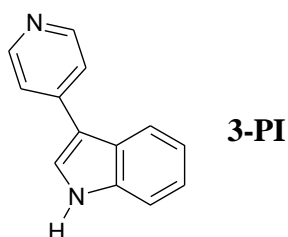
Scheme 2.3. Formula and acronym of 3-pyridin-4-yl-1H-indole.

The third series of compounds, synthesised by Dr. Jacek Nowacki (Department of Chemistry, Warsaw University),[191] is constituted by 7-hydroxyquinoline-8-carbaldehyde (**HQC**) and its six derivatives substituted at the positions 4 and/or 2 of 7-hydroxyquinoline moiety by methyl, methoxy, and phenyl groups. The representatives of the series: 7-hydroxy-4-methylquinoline-8-carbaldehyde (**H4MQC**), 7-hydroxy-2-methoxy-4-methylquinoline-8-carbaldehyde (**HMMQC**), and 7-hydroxy-2-phenylquinoline-8-carbaldehyde (**HPQC**), are shown in Scheme 2.4 (the whole **7-HQCs** family, together with their synthetic precursors, 7-

hydroxyquinolines (**7-HQs**), is presented in Schemes 3.2 and S.3.1). The compounds can exist in two tautomeric forms, **OH** (7-quinolinol) and **NH** (7(1H)-quinolinone) (Scheme 3.1) and have been proposed very recently[165] to serve as models of a reversible optically driven molecular switch. Being inspired by this hypothesis, we studied the solvent and temperature effects on the ground and excited-state long-range tautomerization of **7-HQCs**, as well as their prototropic reactions in aqueous solutions. The results of photostationary and time-resolved UV-Vis spectroscopic investigations, ^{1}H NMR studies, and quantum chemical computations are described in Chapter 3.

HQC   **H4MQC**   **HMMQC**   **HPQC**
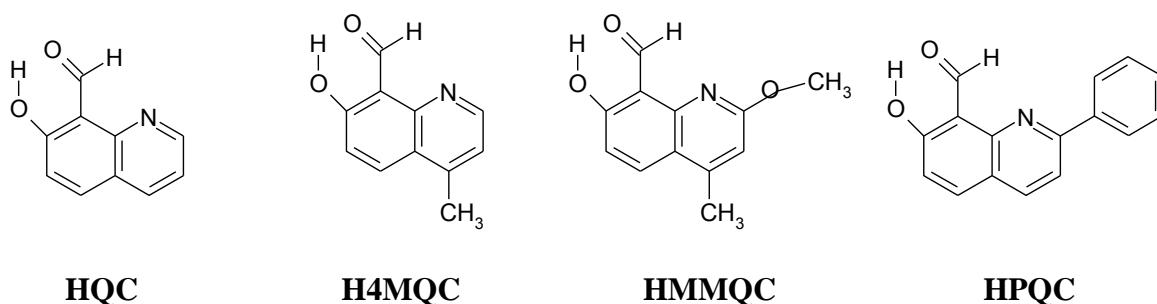
*Scheme 2.3. Formulas and acronyms of representatives of 7-hydroxy-4-methylquinoline-8-carbaldehydes (**7-HQCs**). All the compounds under study are shown in Scheme 3.2.*

2.1.2. Solvents.

The solvents (Table 2.1) used for our studies: *n*-hexane (HEX), butyl ether (BE), ethyl ether (EE), butyl acetate (BA), ethyl acetate (EA), tetrahydrofuran (THF), dichloromethane (DCM), 1,2-dichloroethane (DCE), dimethyl sulfoxide (DMSO), acetonitrile (ACN), methanol (MeOH), ethanol (EtOH), 1-propanol (1-PrOH), 1-butanol (1-BuOH), and 1,1,1,3,3,3-hexafluoro-2-propanol (HFP) were of spectroscopic or fluorescence grade (Aldrich or Merck). Butyronitrile, BN (Merck, for synthesis) was distilled successively over $KMnO_4 + K_2CO_3$, P_2O_5, and CaH_2. Water was used after four distillations over $KMnO_4$ in a quartz apparatus. The solvents have been selected to cover a wide range of the static permittivity values ε (HEX, BE, EE, BA, EA, THF, DCM, DCE, BN, DMSO, ACN)[179] as well as that of the index α describing the solvent hydrogen bond donor ability of bulk water and alcohols.[180] Perchloric acid $HClO_4$ (60%, for analysis, Merck, p.a.) was used to obtain protonated cations, and sodium hydroxide NaOH (Merck, p.a.) was used to obtain deprotonated anions. All solvents were checked for the presence of fluorescing impurities. NMR studies were performed in the following deuterium substituted solvents of 99.8% purity

(ARMAR Chemicals and Cambridge Isotope Laboratories, Inc.): perdeuterated cyclohexane, dichloromethane (CD_2Cl_2), chloroform ($CDCl_3$), acetonitrile (CD_3CN), and methanol (CD_3OD).

Table 2.1. List of used solvents and comparison of their refractive indices (n), dielectric constants (ε) and hydrogen bond donor abilities (α).[179,180]

Solvent	acronym	n	ε	α
n-hexane	HEX	1.37894	1.89	0
Butyl ether	BE	1.3989	3.88	0
Ethyl ether	EE	1.3524	4.34	0
butyl acetate	BA	1.394	5.0	0
ethyl acetate	EA	1.3724	6.02	0
tetrahydrofuran	THF	1.4072	7.58	0
dichloromethane	DCM	1.4242	8.93	0.3
1,2-dichloroethane	DCE	1.4448	10.36	0
butyronitrile	BN	1.3842	24.6	0
acetonitrile	ACN	1.3441	37.5	0.19
dimethyl sulfoxide	DMSO	1.4783	46.68	0
1-butanol	1-BuOH	1.3993	17.5	0.79
1-propanol	1-PrOH	1.3866	20.3	0.78
ethanol	EtOH	1.3614	24.55	0.83
methanol	MeOH	1.3284	32.7	0.93
water		1.3371	78.3	1.17
1,1,1,3,3,3-hexafluoro-2-propanol	HFP	1.277	16.62	1.96

2.2. Instrumentation and procedures

2.2.1. Investigations in solutions

2.2.1.1. Electronic absorption and fluorescence

Electronic absorption spectra were measured on Shimadzu UV 3100 spectrophotometer equipped with variable-temperature chambers, allowing temperature control between 88 K and 333 K, with accuracy of ±1 K. Stationary fluorescence and fluorescence excitation spectra were recorded on an Edinburgh FS 900 CDT fluorometer and corrected for the sensitivity of the instrument. Fluorescence spectra were multiplied by the factor λ^2 in order to convert counts per wavelength into counts per wavenumber. This recalculation takes into account the differences in spectral width of the monochromator slit in various spectral regions in these two scales. Excitation spectra were measured for optical densities not exceeding 0.1 in the maxima of absorption bands in order to avoid nonlinear effects. Low-temperature fluorescence measurements were held on a Jasny spectrofluorometer.[192]

2.2.1.2. Radiative and radiationless rate constants

Fluorescence quantum yields Φ_f of the studied compounds were determined using comparative method with quinine sulphate in 0.1 N H_2SO_4 (Φ=0.51[193]) and DMAP in ACN (Φ=0.017[194]) as the standards. The emission quantum yields of **MPP** and **BPP** were obtained in comparison with **PPP** in the respective solvent. Recording of fluorescence spectra on the Edinburgh SF 900 CDT fluorometer of the solution of the compound under study and of the solution of the standard, both excited at the wavelength of identical absorbance, allow us to determine the values of Φ_f from the simple relation[195-198]

$$\Phi_f = \Phi_0 \frac{S}{S_0}\left(\frac{n}{n_0}\right)^2, \tag{2.1}$$

where Φ_0 denotes the quantum yield of the standard; S and S_0 − areas under the fluorescence spectra of the studied compound and the standard, respectively; n and n_0 are refractive indices of the studied and standard solutions, respectively.

Fluorescence lifetimes in the nanosecond range were obtained on an Edinburgh FL 900 CDT time-resolved spectrofluorometer with the use of single photon counting technique.

An estimated time resolution was about 500 ps. Time-resolved fluorescence investigations in the picosecond range were performed at the Centre for Ultrafast Laser Spectroscopy at the Adam Mickiewicz University in Poznań. Experimental setup,[181,199] in short, includes an argon-ion laser (Millennia Prime, Spectra Physics). It was a source of pump for the picosecond titanium-sapphire laser (Tsunami, Spectra Physics) with repetition frequency ~4 MHz which was reduced with help of pulse selector (Model 3985, Spectra Physics). The excitation wavelength was the 3rd harmonic of the fundamental frequency. In the emission pathway there was a polariser set at magic angle to vertical polarisation of the excited beam. Electronic detection pathway enclosed an upgraded quad constant fraction discriminator CFD TC 454 (Tennelec), a time-to amplitude convertor TAC-TC 864 (Tennelec), a multichannel analyser Noland 5000 MCA and proximity type (6 μm) microchannel plate MCP-PMT R3809U-05 (Hamamatsu). The TAC worked in the reverse mode. Picosecond decays were analysed by home-made software,[199] which allowed the use of the Levenberg-Marquardt[200] or simplex[201,202] optimization algorithms. The instrument response function (IRF) was determined by scattering method. The full width at half maximum (FWHM) of the IRF was ~35 ps. The χ^2 test and the distribution of weighted residuals were the main criteria in the evaluation of the fit quality.

The experimental determination of fluorescence quantum yields (Φ_f) and fluorescence lifetimes (τ) allow us to obtain radiative (k_f) and nonradiative (k_{nr}) rate constants. The Φ_f value corresponding to the emission from the lowest, primary excited state (see Fig. 4.10) is simply related to the rate constants[203-207]

$$\Phi_f = k_f /(k_f + k_{nr}), \tag{2.2}$$

where k_{nr} is a sum of all rate constants of nonradiative processes depopulating the fluorescent state (*e.g.*, internal conversion to the ground state k_{IC}, intersystem crossing to the triplet manifold k_{ISC}, and the irreversible photoreaction $\vec{k}$, see Fig. 4.10.)

$$k_{nr} = k_{IC} + k_{ISC} + \vec{k} \tag{2.3}$$

and

$$\tau = 1/(k_f + k_{nr}) \tag{2.4}$$

Thus, the fluorescence rate constant k_f are given by

$$k_f = \Phi_f / \tau \tag{2.5}$$

and the sum of the rate constants k_{nr} of nonradiative depopulation processes

$$k_{nr} = (1 - \Phi_f)/\tau . \tag{2.6}$$

More information about the nature of the radiative transitions one can obtain from the analysis of the electronic transition dipole moments in absorption (M_{abs}) and fluorescence (M_{fl}). These values are the best quantitative measure of the transition probability. In the electric dipole approximation, the M_{abs} and M_{fl} values could be determined

$$\left|\vec{M}_{abs}\right|^2 = \frac{3\ln 10 \, hc}{8\pi^3 N_A n \tilde{\nu}_{abs}} \int \varepsilon(\tilde{\nu}) \mathrm{d}\tilde{\nu} \qquad \text{and} \qquad k_f = \frac{64\pi^4}{3h}\left(n\tilde{\nu}_f\right)^3 \left|\vec{M}_{fl}\right|^2, \qquad (2.7)$$

which can be simplified (the M_{abs} and M_{fl} values in debyes, D) as

$$M_{abs} \approx 0.09582 \sqrt{\frac{\varepsilon \Delta\tilde{\nu}}{n\tilde{\nu}_{abs}}} \qquad \text{and} \qquad M_{fl} \approx 0.1786 \sqrt{\frac{k_f}{n^3 \tilde{\nu}_f^3}}, \qquad (2.8)$$

where N_A – is the Avogadro number, ε is the molar absorption coefficient at wavenumber $\tilde{\nu}_{abs}$ (in cm^{-1}) corresponding to the absorption band maximum, $\Delta\tilde{\nu}$ (in cm^{-1}) is a half-width (full width at half maximum, FWHM) of the absorption band, and $\tilde{\nu}_f$ (in cm^{-1}) denotes the spectral position of the maximum of the fluorescence band.

2.2.1.3. Spectrophotometric titration

The investigations in protic solvents showed the formation of hydrogen-bonded complexes. Ground-state complexation of the studied compounds was monitored by absorption and emission experiments in mixed solvents. Spectrophotometric titration of solutions of the studied compounds in a nonpolar solvent with alcohol (in concentration low enough to prevent the formation of alcohol oligomers), accompanied by changes in the absorption showing an isosbestic points, leads to the determination of the stoichiometry of the complex and respective equilibrium constant.[132,208] For a reaction involving one chromophore molecule X and *n* alcohol molecules Y

$$\mathrm{X} + n\mathrm{Y} = \mathrm{XY}_n \qquad (2.9)$$

the equilibrium constant, K_{1n}, may be expressed as

$$K_{1n} = \frac{[\mathrm{XY}_n]}{[\mathrm{X}][\mathrm{Y}]^n} \qquad\qquad K_{1n} = \frac{A - A_0}{(A_\infty - A)[Q]^n}, \qquad (2.10)$$

where A_0 and A_∞ denote the absorbance measured when only the bare or complexed forms are present, respectively, and A is the absorbance measured at an alcohol concentration $[Q]$. From the plot of $\ln[(A-A_0)/(A_\infty-A)]$ vs. $\ln[Q]$ one may obtain *n*, the number of alcohol molecules in the complex. For 1:1 stoichiometry, one can calculate equilibrium constant K_{11} using relation

$$\frac{\left(1 - \dfrac{A_0}{A}\right)}{[Q]} = -K_{11} + \frac{\varepsilon_{11}}{\varepsilon_0} K_{11} \frac{A_0}{A} \, , \tag{2.11}$$

where ε_{11} and ε_0 are extinction coefficients of complexed and uncomplexed molecule, respectively. The intercept of the plot of $(1 - A_0/A)/[Q]$ vs. A_0/A should yield the value of K_{11}.

2.2.1.4. Acid-base equilibria

The 'driving force' for the excited state photon transfer is the electron density redistribution occurring upon excitation. This redistribution in molecules capable of NH/N phototautomerization leads to an increase in the excited state pK_a value of the proton acceptor and decrease in the excited-state pK_a value of the proton donor. Assuming that the entropy changes are the same in the ground state and the excited state, the change of pK_a upon electronic excitation can be obtained from the 'Förster cycle',[18,20,209] employing the formula

$$\Delta pK_a = pK_a^* - pK_a^G \approx -0.00207 \left(\tilde{\nu}_{00}^{BH+} - \tilde{\nu}_{00}^{B} \right), \tag{2.12}$$

where pK_a^* and pK_a^G denote the values in the excited and ground state, respectively, $\tilde{\nu}_{00}^{BH+}$ and $\tilde{\nu}_{00}^{B}$ (in cm^{-1}) are the electronic transition energies in an acid and base forms, correspondingly. These energies can be estimated from the absorption and fluorescence maxima $\tilde{\nu}_{00} = 0.5 \left(\tilde{\nu}_{abs} + \tilde{\nu}_{flu} \right)$ determined at room temperature.[20]

2.2.1.5. Excited-state dipole moments

Excited-state dipole moments can be estimated by the solvatochromic shift method, under Lippert and Mataga assumptions.[210-214] Approximating a solute molecule as a point dipole situated in the center of the spherical cavity and neglecting the solute polarizability in the states involved in the transition, the linear plot of the absorption and solvent equilibrated fluorescence maxima, vs. solvent polarity function, $f(\varepsilon,n)$, relates the measured quantities to the ground (μ_g) and excited (μ_e) state dipole moments of the solute:

$$hc\tilde{\nu}_{abs} \cong hc\tilde{\nu}_{abs}^{vac} - \frac{2\vec{\mu}_g \left(\vec{\mu}_e - \vec{\mu}_g \right)}{a_0^3} f(\varepsilon,n), \tag{2.13}$$

$$hc\tilde{\nu}_{flu} \cong hc\tilde{\nu}_{flu}^{vac} - \frac{2\vec{\mu}_e \left(\vec{\mu}_e - \vec{\mu}_g \right)}{a_0^3} f(\varepsilon,n), \tag{2.14}$$

where

38

$$f(\varepsilon,n) = \frac{\varepsilon-1}{2\varepsilon+1} - \frac{1}{2}\frac{n^2-1}{2n^2+1}. \tag{2.15}$$

$hc\,\tilde{\nu}_{abs}$, $hc\,\tilde{\nu}_{flu}$, $hc\,\tilde{\nu}_{abs}^{vac}$, and $hc\,\tilde{\nu}_{flu}^{vac}$ are the energies corresponding to the absorption and fluorescence maxima in solutions and to the values extrapolated to the gas phase respectively; a_0 is the effective radius of the Onsager's cavity,[212] ε is the static dielectric constant, n is the refractive index of the solvent.

The linear correlation between $hc\,\tilde{\nu}_{abs}$ and $hc\,\tilde{\nu}_{flu}$, and the solvent polarity function allows one to determine directly the values of $\vec{\mu}_g(\vec{\mu}_e - \vec{\mu}_g)/a_0^3$ and $\vec{\mu}_e(\vec{\mu}_e - \vec{\mu}_g)/a_0^3$ respectively. The estimated value of excited state dipole moment depends on the evaluated value of a_0.

Under assumption that the nature of the fluorescent state and the Franck-Condon state reached directly upon excitation is the same, the μ_e values could be obtained from the solvatochromic plots related to the Stokes shifts according to:

$$\frac{1}{2}\left(hc\,\tilde{\nu}_{abs} - hc\,\tilde{\nu}_{flu}\right) = \frac{1}{2}\left(hc\,\tilde{\nu}_{abs}^{vac} - hc\,\tilde{\nu}_{flu}^{vac}\right) - \frac{(\vec{\mu}_e - \vec{\mu}_g)^2}{a_0^3}\left(\frac{\varepsilon-1}{2\varepsilon+1} - \frac{n^2-1}{2n^2+1}\right) \tag{2.16}$$

and from the solvatochromic plots related to the sum of the CT absorption and fluorescence maxima according to:

$$\frac{1}{2}\left(hc\,\tilde{\nu}_{abs} + hc\,\tilde{\nu}_{flu}\right) = \frac{1}{2}\left(hc\,\tilde{\nu}_{abs}^{vac} + hc\,\tilde{\nu}_{flu}^{vac}\right) - \frac{(\vec{\mu}_e^2 - \vec{\mu}_g^2)}{a_0^3}\left(\frac{\varepsilon-1}{2\varepsilon+1} - \frac{n^2-1}{2n^2+1}\right). \tag{2.17}$$

2.2.2. Laser spectroscopy in a supersonic molecular beam

The challenging problem concerning the structure of the most stable rotameric forms of selected compounds as well as of their hydrogen bonded complexes with protic partners can be hardly resolved from solutions studies. In order to gain more insight into this problem a supersonic jet technique combined with laser spectroscopy has been applied. This technique allows us to study the structure and photoinduced conformational changes of well-defined individuals under isolated conditions due to the possibility of their selection created by a strong simplification (in comparison with molecular UV-VIS spectroscopy in solutions) and high resolution of the vibrational structure of dispersed fluorescence (DF) and laser induced fluorescence (LIF) excitation spectra.

The molecular beam is formed by a supersonic expansion of the molecules of interest, seeded in an inert gas (known as a carrier gas). The sample is heated to increase its vapour pressure and with a help of a carrier gas it is provided from a high-pressure (p_0) reservoir into the vacuum chamber through an orifice of a small diameter. The expansion in the supersonic beam proceeds with the speed near to $M = 1$, where the Mach number M is defined as the ratio of the local flow velocity and the local speed of sound. The simplified scheme of the experimental set-up is presented in Figure 2.1.
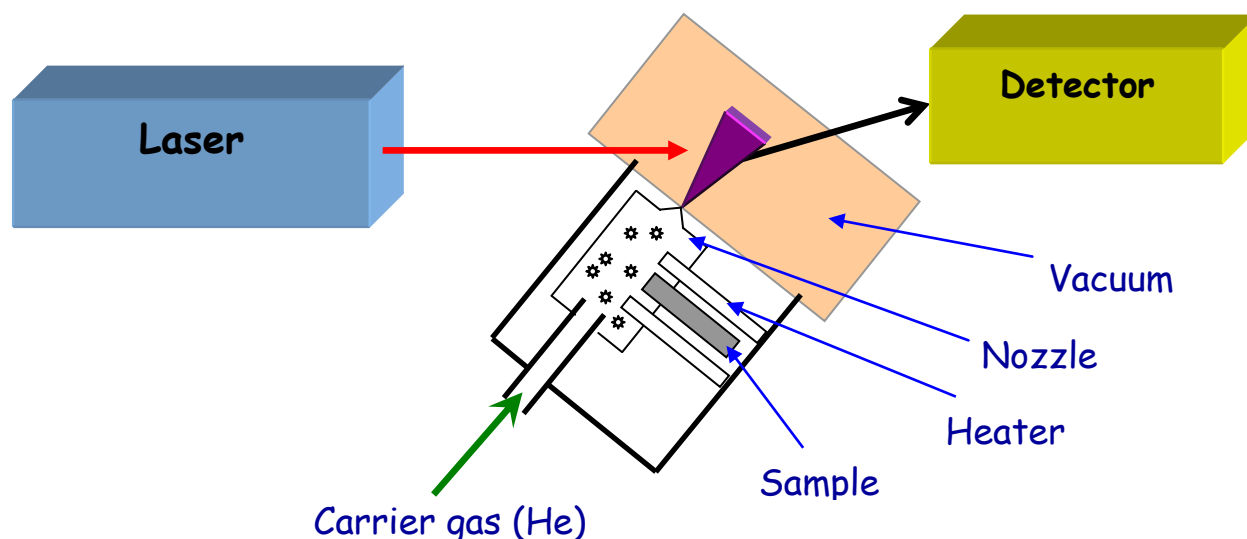
Figure 2.1. Schematic of experimental setup.

In the orifice, at densities where the collision probability is high, the thermal energy of the molecules, which is composed of translational, rotational and vibrational energy, is partly transferred into kinetic energy of the beam. The random molecules motion turns into the directed one in a vacuum chamber. As a result, the molecule finds itself in collision-free

conditions and its internal energy is adiabatically 'cooled'. Whereas at thermodynamic equilibrium in the reservoir all degrees of freedom have the same energy $kT/2$, after adiabatic expansion the typical values (in nonequilibrium conditions) for translational, rotational (T_r) and vibrational (T_v) temperatures in a supersonic beam at $p_0 = 1\text{-}3$ bar are as low as 0.5-10 K, 1-50 K, 10-100 K, respectively. The translational cooling reduces the Doppler broadening of the spectral lines. At low values of T_r and T_v only the lowest vibrational energy levels of the ground electronic state are populated. Using a narrow-band laser as an excitation source leads to a population of only a few vibrational levels of the excited electronic state and a dramatic reduction of the observed absorption transitions. Similar situation is observed for emission: it occurs from a single vibrational level of the excited state to a limited number of vibrational levels of the ground state. Moreover, collision-free conditions in a supersonic beam imply also a considerable decrease of the inhomogeneous broadening of the energy levels. Thus, instead of the broad absorption and emission bands (as it is in solution spectroscopy) one can obtain narrow lines of limited number.

The experimental results presented in this work (Chapter 5) are based on utilizing the following methods:

(i) Laser-induced fluorescence (LIF) excitation. The LIF excitation spectrum represents a number of photons emitted by molecules as a function of laser frequency that is used to excite the system under study. Thus, in a fluorescence excitation measurement a tunable, narrow-band excitation laser is scanned across the electronic absorption region and the monitored fluorescence wavelength is fixed. The obtained spectrum contains information on the excited states of the molecule.

(ii) Dispersed fluorescence (DS). The DS spectrum which represents a number of emitted photons as a function of their frequency is recorded upon laser excitation that is fixed at a particular wavelength. This technique, contrary to LIF excitation, provides information about the ground electronic state of the molecule and its vibrational structure.
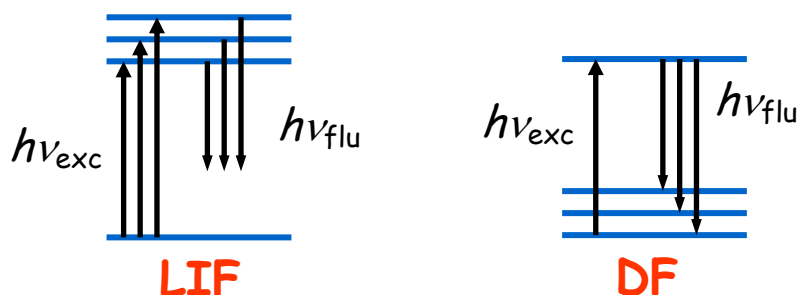
Figure 2.2. Energy schemes of LIF excitation and DF spectroscopy.

The home-made spectrometer used for obtaining LIF and dispersed fluorescence (DF) spectra has been described previously.[95,215,216] Excitation was provided *via* two different systems. One of them is the system of tunable dye lasers pumped by the second harmonic of the Nd:YAG laser (Sureline I-10). All dyes were provided by Exciton and their concentrations were chosen in accordance with information bulletins.[217] The first dye-laser has a prism beam expander in the resonator. Its laser linewidth is about 0.4 cm^{-1} and the average pulse energy, obtained from the oscillator, is about ~0.5 mJ. The second one is a grazing incidence dye laser with intracavity etalon. It provides the bandwidth of about 0.1 cm^{-1} and energy of about ~0.5 mJ/pulse. The other excitation source was commercial SunliteEX (Continuum) optical parametric oscillator (OPO) that was pumped by the third harmonic of a Nd:YAG laser (Powerlite 8000 Precision). It covers 445-1750 nm spectral range and its typical linewidth is < 0.1 cm^{-1}. KDP or BBO nonlinear crystals work as frequency doublers and allow us to make measurement in appropriate wavelength range. The beam is provided into the vacuum chamber where excites the studied molecules. In the chamber vacuum is obtained with help of two pumps: turbomolecular (650 1/s) and Roots ones. The sample is heated (up to 300 °C) and transported in pulsed portions (pulsed valve: modified General Valve Series 9) into the chamber by carrier gas (helium) through an orifice (0.5 and 0.2 mm in diameter). Laser beam crosses the free jet 5-8 mm downstream from the nozzle. LIF excitation spectra are detected by Hamamatsu R2949 photomultiplier tube, processed by digital oscilloscope (YOKOGAWA DL9140) and put into final form by a homemade computer program. For DF measurements fluorescence was collected and directed to a spectrograph (SCIENCETECH, model 9040) and CCD camera (ANDOR iDus type DV-401A-BRD). In order to prevent formation of complexes with water, helium was passed through a copper cooler immersed in liquid nitrogen.

The wavelength calibration was done by the spectrograph constructed by Dr. J. Jasny.

2.2.3. NMR investigations

NMR spectra were recorded on a Bruker Avance II 300 spectrometer operating at 300.17 MHz for ^{1}H with a BVT-3200 variable temperature unit. The temperature ^{1}H NMR studies were performed in three solvents: acetonitrile-d_3, $CDCl_3$ and CD_2Cl_2 at the range of temperatures from 298 K down to 213 K (in the case of acetonitrile down to 233 K). Concentration of the NMR samples was 7mM. They were prepared either in a dry-box from fresh deuterated solvents (acetonitrile, CD_2Cl_2) or by distillation in a vacuum line ($CDCl_3$ dried with CaH_2). 5 mm glass NMR tubes were sealed under argon in order to avoid condensation of water from air. Experiments, in which samples were irradiated with UV light prior to recording NMR spectra, were carried out on 2mM solution in CD_3CN and 7mM solution in $CDCl_3$. The UV-irradiation was performed outside the spectrometer, directly in sealed NMR tubes through glass walls with a Hg-lamp emitting light at wavelengths above 365 nm.

2.3. Computational details[218]

Quantum chemical calculations were performed using Gaussian 03[219] and Gaussian 09[220] suites of programs. First, an attempt to predict equilibrium structures of molecular systems was made *via* locating global minima on the potential energy surface (PES). Different minima correspond to different conformations or structural isomers of a single molecule. The optimization is based on step by step calculation of the energy at sequential points of the PES and determination of the gradient at these points. The optimization is finished when the forces are zero (gradient is negative) and the next step is very small – it has converged. The second step was to check if the geometry corresponds to the global energy minimum or to a saddle point. This can be done by frequencies calculation for all found stationary points. If there are no imaginary frequencies the optimized structure is a minimum, but if there is at least one imaginary frequency the structure is a saddle point (a transition state if there is only one). These calculations were carried out using harmonic approximation. This procedure was used for both ground and excited state modelling.

Two methods were used in this work. The first one was Density Functional Theory (DFT) – an approach that is based on a strategy of modelling electron correlation *via* general functionals (a function whose definition is itself a function) of the electronic density. It was chosen because of its quite balanced accuracy-to-cost correlation for medium-sized molecules. This method was applied for ground state geometry optimisation and vibrational transitions predictions. For selected compounds it was also used for excited state calculations (due to the fact that this method is time-consuming in excited state vibrational transitions predictions). Vertical transition excitation energies and frequencies were calculated within Time-Dependent DFT.[221]

The second method was Configuration Interaction Singles (CIS) – an *ab initio* method widely used for modelling excited states and predicting their properties. It is inexpensive and qualitatively accurate. CIS is based on replacement of occupied orbitals by virtual ones. This is equivalent to exciting an electron to higher energy orbitals. At its first step this model uses the ground state optimized geometry and models excited states as combinations of single excitations from the ground one. Only the lowest electronically excited states were optimised in this work.

B3LYP (Becke, Lee, Yang and Parr three-parameter)[222-224] hybrid functional with 6-31+G(d,p) basis set were applied in both cases. This is a split-valence basis set (allowing

orbitals to change size) with addition of polarization functions to both heavy atoms and hydrogens, and with diffuse functions added to heavy atoms (important for the excited states). This functional with such a basis set is again quite commonly used in the study of related molecules.

For vibrational frequency assignment, a scaling coefficient of 0.9648 (DFT) and 0.92 (CIS) was used to correct the computed values[225,226]. Estimated errors in the determination of energies of optimized structures were ~1 kcal/mol; errors in frequency assignments were *ca.* 3-6 cm^{-1} (ground state) and *ca.* 17 cm^{-1} (excited state). The simulated IR spectra were derived from Gaussian convolutions (FWHM = 15 cm^{-1} and resolution 3 cm^{-1} for emission spectra, and FWHM = 1 cm^{-1} and resolution 0.25 cm^{-1} for absorption ones) of the stick spectra associated with the harmonic vibrational frequencies and linear absorption intensities.

Chapter 3: Spectroscopy, photophysics, and photochemistry of trifunctional proton donating/accepting systems

3.1. Introduction. Compounds and their tautomeric forms

The ground and excited state long-range prototropic tautomerization of 7-hydroxyquinoline-8-carbaldehydes (**7-HQCs**) is considered in this chapter. The compounds are composed of two moieties: a molecular "frame" (7-hydroxyquinolines, **7-HQs**) and a proton "crane" (carbaldehyde group).[165] 7-hydroxyquinoline moiety has both hydrogen bond (HB) donating (a hydroxyl group) and HB accepting (a nitrogen atom) centers. These compounds can exist in two tautomeric forms: **OH** (7-quinolinol) and **NH** (7(1H)-quinolinone) (Scheme 3.1). The addition of carbaldehyde "crane" makes these molecules a possible model of a reversible optically driven molecular switch, as it has been proposed by Sobolewski *et al.*,[165] with a photoinduced hydrogen atom transfer proceeding *via* transient forms **IIa** and **IIb** (see Chapter 1.4).

I (OH)   **IIa**   **IIb**   **III (NH)**
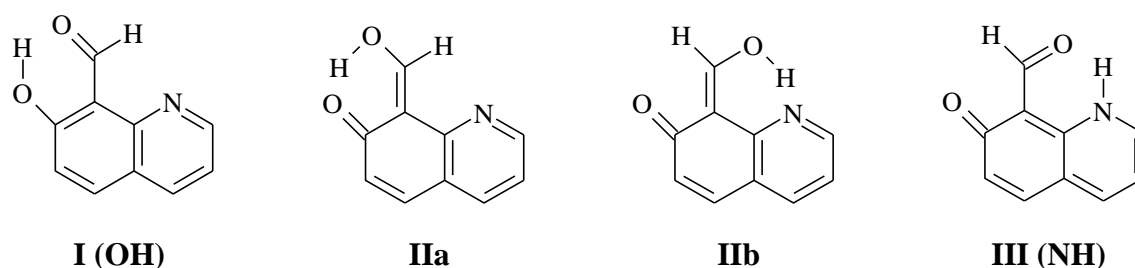
*Scheme 3.1. Structures of tautomeric/rotameric forms of **HQC**.*

The series of compounds contains 7-hydroxyquinoline-8-carbaldehyde (**HQC**) and its derivatives substituted at the positions 4 and/or 2 of 7-hydroxyquinoline moiety by methyl, methoxy, and phenyl groups. The spectroscopy and photophysics of **7-HQCs** are compared to those of their 7-hydroxyquinoline precursors (**7-HQs**). All the compounds are presented in Scheme 3.2 (full names can be found in Scheme S.3.1 Chapter 7: Supporting information) in corresponding pairs having the same substituent: 4-methyl (**H4MQC** and **H4MQ**), 2-methyl (**H2MQC** and **H2MQ**), 2,4-dimethyl (**HDMQC** and **HDMQ**), 2-phenyl (**HPQC** and **HPQ**), 2-2'-methylphenyl (**HMPQC** and **HMPQ**) and 2-methoxy-4-methyl (**HMMQC** and **HMMQ**).

The chapter shows the results of solvent and temperature effects on the UV-Vis spectroscopy and photophysics of the compounds as well as quantum chemical computations.

The effects of polarity and hydrogen-bond donor ability of the surrounding media on the room-temperature and low-temperature electronic absorption and fluorescence spectra, as well as the prototropic reactions in aqueous solutions are examined. Time-resolved experiments performed with a nanosecond and subnanosecond resolution are presented and discussed.
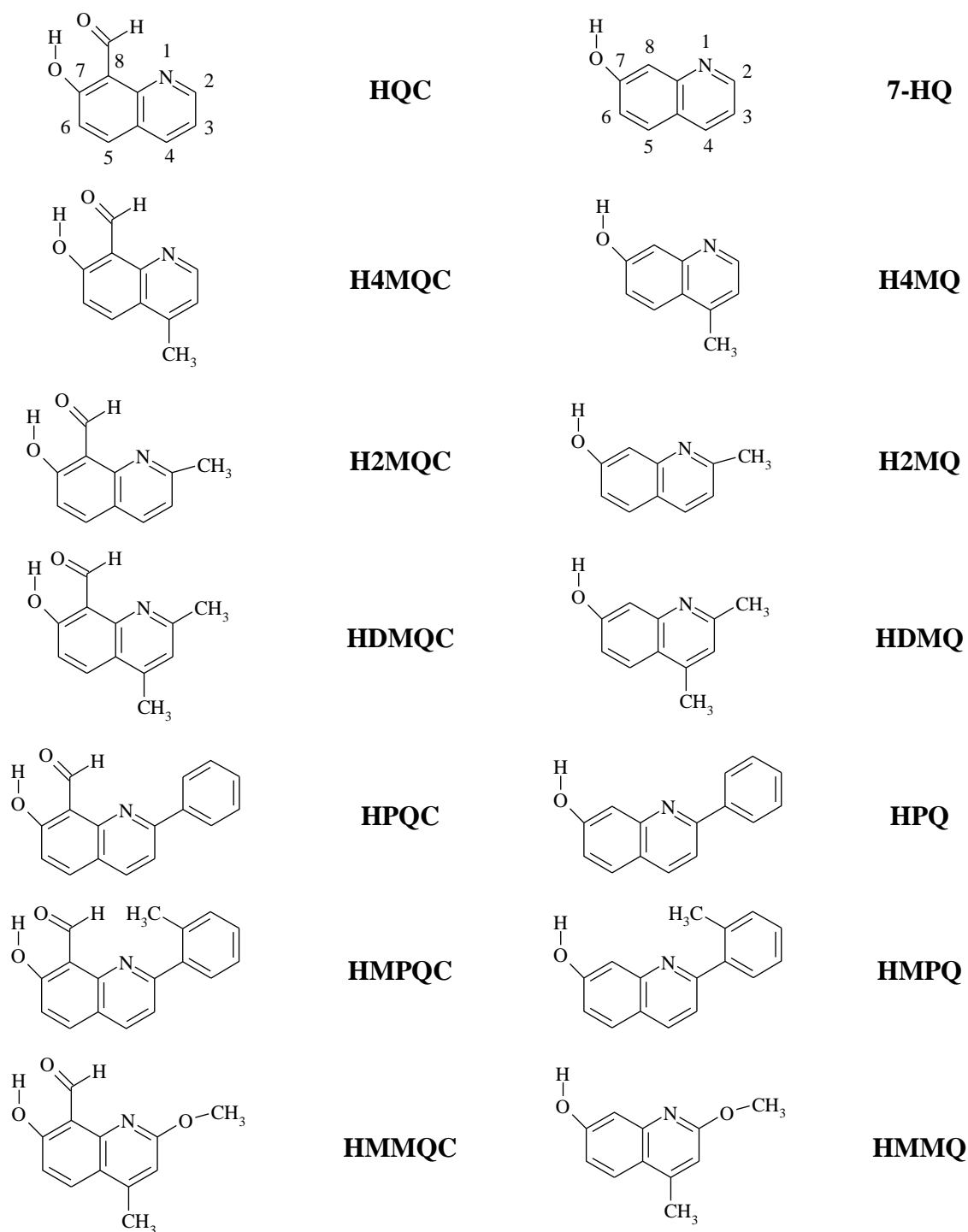
Scheme 3.2. *Formulas, labeling of atoms, and acronyms of investigated compounds. Full names can be found in Scheme S.3.1 Chapter 7: Supporting information.*

47

3.2. Ground state tautomerization: electronic absorption and NMR studies, and theoretical computations

The room temperature electronic absorption spectra of **7-HQCs** and **7-HQs** were recorded in nonpolar (*n*-hexane), medium polar aprotic (ethyl acetate), strongly polar aprotic (acetonitrile), and polar protic (1-propanol, methanol, water) solutions. The near-UV absorption spectrum (Fig. 3.1) of **HQC** in *n*-hexane shows three bands centered at ~345 nm, 299 nm, and 287 nm (~29000 cm^{-1}, ~33450 cm^{-1}, and ~34850 cm^{-1}, respectively). These bands do not reveal any significant shift with increasing solvent polarity. On the other hand, the increase of solvent polarity and its hydrogen-bonding ability leads to the appearance of a low-energy band at *ca*. 400 nm (~25000 cm^{-1}). This long-wave band is particularly intense in strongly polar and protic environment, such as methanol and water (see Chapter 3.4). The dependence of the intensity of the low-energy absorption band on solvent properties suggests the co-existence of two tautomeric forms of **HQC** in the ground state.
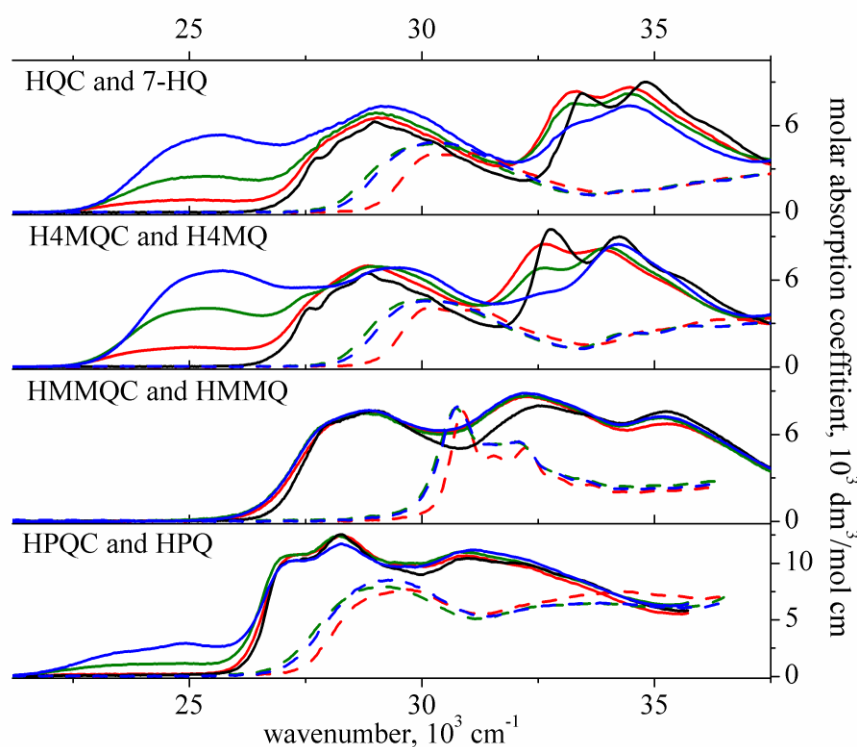
*Figure 3.1. Comparison of the room temperature absorption spectra of **7-HQCs** and corresponding **7-HQs**. Black – n-hexane, red – acetonitrile, green – 1-propanol, blue – methanol; solid lines – **7-HQCs**, dashed lines – **7-HQs**. The spectra of **H2MQC** and **HDMQC** are similar to those of **H4MQC**; and that of **HMPQC** to **HPQC**. The solubility of **7-HQs** in n-hexane is too low to determine the molar absorption coefficients.*

*Table 3.1. Solvent effects on the spectral position of the room temperature electronic absorption (λ_{abs}, nm),[a] molar absorption coefficients (ε, in $dm^3/mol\ cm$), and electronic transition dipole moments (M_{abs}, in D,[b] eq. 2.8) assigned to the **OH** and **NH** tautomeric forms of **7-HQCs** and **7-HQs** (see text for explanation).*

Compound	Solvent	7-HQCs					7-HQs[c]			
		λ_{abs} **OH**	ε	λ_{abs} **NH**	ε	M_{abs} **OH**	λ_{abs} **OH**	ε	λ_{abs} **NH**	M_{abs} **OH**
HQC /7-HQ	HEX	345	6500			2.2				
	EA	345	6120			2.1	331	4100		1.7
	ACN	344	6530	400	~9700		331	4000		1.7
	1-PrOH	345	6980	395			331	4700		1.9
	MeOH	343	7360	390	~10500		331	4800		1.9
H4MQC / H4MQ	HEX	347	6350			2.1				
	EA	347	6100			2.0	333	3900		1.7
	ACN	347	6990	400	~9000		333	4100		1.7
	1-PrOH	345	6890	395			333	4600		1.8
	MeOH	340	7170	390	~10800		333	4550		1.9
H2MQC / H2MQ	HEX	344	5700				327			
	EA	344	6390				330	4900		1.9
	ACN	344	6740	400			328	5100		1.9
	1-PrOH	345	7190	400			330	5800		2.0
	MeOH	345	9120				330	5650		2.1
HDMQC / HDMQ	HEX	348	~7300							
	EA	345	7290				330	6300		2.0
	ACN	348	7720	395			330	6750		2.1
	1-PrOH	346	8210	385			330	7800		2.4
	MeOH	345	8470	390	~12900		330	7300	~400	2.3
HPQC / HPQ	HEX	354	12530			3.1	333			
	EA	354	12920			3.2	338	7500		2.3
	ACN	354	12430	420		3.1	338	7700		2.4
	1-PrOH	354	12420	420			342	7900		2.3
	MeOH	354	11720	400			342	8500		2.5
HMPQC / HMPQ	HEX	350	9300							
	EA	350	10000				332	6900		2.1
	ACN	350	9650				332	6200		2.0
	1-PrOH	350	9600	410			337	11100		2.6
	MeOH	350	9220	400			335	7100		2.1
HMMQC / HMMQ	HEX	346	7690			2.4	323			
	EA	346	7570			2.4	324.5	8200		1.9
	ACN	346	7560			2.4	323.5	7600		1.8
	1-PrOH	346	7630			2.4	325.5	7800		1.9
	MeOH	346	7660			2.5	325	7900		2.0

[a] Scatter of results: ± 2.0 nm. [b] Error is about 10%. [c] The solubility of **HQC**, **H4MQC**, **HDMQC**, and **HMPQC** in *n*-hexane is too low to measure the absorption spectra.

Similar solvent effects on the absorption spectra are observed for the other **7-HQCs** under study, except **HMMQC**. Interestingly, the intensity of the low-energy band observed for **HPQC** is lower than that of **HQC** and its methyl substituted derivatives. According to the results of the experimental investigations of **H4MQC** in the low-temperature matrices[165] and theoretical calculations[164,166] we suppose that both forms, **OH** and **NH**, are present already in the ground state. The *ab initio* computations of **7-HQCs**[164,166,191] predict that the vertical excitation energies to the lowest $^1(\pi,\pi^*)$ states of the forms **NH** are about 25000 cm^{-1} (for **HQC** and its methylated derivatives), 23250 cm^{-1} (**HPQC**), and 27000 cm^{-1} (**HMMQC**) under vacuum conditions (Table 3.2). These spectral positions for the studied **7-HQCs** (except **HMMQC**) are lower of about 7000 cm^{-1} and 5400 cm^{-1} than those predicted for the **OH** and **IIb** forms, respectively (the structure **IIa** is generally not stable in the ground electronic state as it relaxes spontaneously towards the form **OH**). The TD-DFT computations show similar results (the calculated values are lower than those of CC2/cc-pVDZ method and are in better agreement with experimental data). Thus, the long-wave absorption band can be assigned to the **NH** tautomer. The computed values of dipole moments support this assignment. The dipole moments of the **NH** tautomers of all the **7-HQCs** under study are about two times higher than that of the **OH** forms (Table 3.3). This should favor the stabilization of the **NH** form in polar solvents, which is indeed observed as the appearance and growth of the low-energy band in absorption. In protic solvents another factor that can change the relative energies of the **OH** and **NH** forms is the influence of intermolecular hydrogen bonds on their stabilization energies. The MP2/aug-cc-pVDZ simulations of the solvent effect (with the use of the Polarizable Continuum Model)[227,228] on the relative energies of the tautomeric forms of **HQC** and **HMMQC** do not show, however, any significant differences between acetonitrile and water.[191]

*Table 3.2. Comparison between vertical ab initio CC2/cc-pVDZ ($\tilde{v}_{CC2}$, in 10^3 cm^{-1})[191] and TD-DFT B3LYP/6-31+G(d,p) ($\tilde{v}_{TDDFT}$) excitation energies of the low-lying $^1(\pi,\pi^*) \leftarrow S_0$ transitions and oscillator strengths (f_{CC2}, f_{TDDFT}) for various forms (Scheme 3.1) of **HQC**, **H4MQC**, **HPQC**, and **HMMQC** and the locations of the experimental absorption maxima ($\tilde{v}_{exp}$, scatter of results: ± 150 cm^{-1}) in n-hexane. Only transitions of significant intensity are shown (f > 0.02). * - $\tilde{v}_{exp}$ obtained from the excitation spectra in acetonitrile (Figs. 3.5 and 3.7).*

Compound	Tautomer	Excited state	$\tilde{\nu}_{CC2}$	f_{CC2}	Excited state	$\tilde{\nu}_{TDDFT}$	f_{TDDFT}	$\tilde{\nu}_{exp}$
	I (**OH**)	S_2	32.10	0.117	S_2	30.75	0.103	~29.0
		S_3	38.23	0.093	S_4	34.21	0.075	33.45
		S_4	40.33	0.056	S_5	37.00	0.098	34.85
	III (**NH**)	S_2	25.25	0.130	S_2	24.61	0.100	25.00
HQC		S_3	31.05	0.192	S_4	30.22	0.115	
		S_4	38.80	0.034	S_7	35.13	0.073	
	IIb	S_2	30.57	0.179	S_2	28.29	0.131	
		S_3	33.63	0.082	S_3	31.33	0.027	
		S_4	40.97	0.243	S_6	36.98	0.265	
	I (**OH**)	S_2	31.86	0.114	S_2	30.46	0.103	~28.8
		S_3	37.75	0.132	S_3	33.51	0.117	32.8
		S_4	40.65	0.032	S_5	37.25	0.059	34.28
	III (**NH**)	S_2	24.68	0.120	S_2	24.24	0.094	25.33
H4MQC		S_3	30.97	0.194	S_4	30.25	0.108	28.6*
		S_4	38.39	0.062	S_6	35.13	0.107	
	IIb	S_2	30.00	0.174	S_2	27.87	0.129	
		S_3	33.72	0.065	S_6	36.52	0.318	
		S_4	40.17	0.301	S_8	41.16	0.053	
	I (**OH**)	S_2	30.65	0.221	S_2	28.47	0.304	~27.1
		S_3	34.92	0.239	S_3	30.55	0.070	28.23
		S_4	38.15	0.020	S_5	33.68	0.019	31.0
	III (**NH**)	S_2	23.23	0.223	S_2	22.77	0.111	23.74
HPQC		S_3	30.41	0.157	S_4	29.49	0.087	28.3*
		S_4	35.01	0.277	S_6	31.95	0.221	
	IIb	S_2	29.20	0.317	S_2	26.90	0.262	
		S_3	32.02	0.066	S_3	29.61	0.021	
		S_4	36.30	0.436	S_4	33.06	0.293	
	I (**OH**)	S_2	31.86	0.159	S_2	29.63	0.114	~29.0
		S_3	36.46	0.123	S_3	32.76	0.114	~32.6
		S_4	39.85	0.089	S_4	37.12	0.125	~35.25
	III (**NH**)	S_2	26.94	0.231	S_2	26.49	0.174	
HMMQC		S_3	29.36	0.169	S_3	28.65	0.099	
		S_4	39.20	0.058	S_6	36.04	0.091	
	IIb	S_2	29.44	0.188	S_2	26.66	0.112	
		S_3	33.31	0.130	S_3	31.68	0.088	
		S_4	38.64	0.278	S_5	35.99	0.302	

51

The assignment of the absorption bands centered at about 29000 cm^{-1} and 31000-34000 cm^{-1} (Fig. 3.1) is more ambiguous due to the fact that the close lying electronic transitions in this spectral region are computed for the forms **OH**, **NH,** and **IIb**. Theoretical calculations predict that the **OH** form should be dominant in the ground state for all the studied molecules under vacuum conditions (Table 3.3). The energy gap ΔE between **OH** and **NH** forms is predicted to be of about 6 kcal/mol (DFT calculations) and 11 kcal/mol (CC2) for all the **7-HQCs**, except **HMMQC** (ΔE = 12.2 kcal/mol and 17.3 kcal/mol, correspondingly). Noticeably, the predicted relative energies of the **IIb** forms (Scheme 3.1) are very similar to those of the **NH** tautomers. Thus, it is difficult to predict which tautomeric forms contribute to the experimental absorption spectrum. The evidence that only the **OH** and **NH** tautomers exist in the ground state is provided by the results of NMR investigations.

The electronic absorption spectra of **7-HQs** are significantly blue-shifted in comparison to the spectra of the corresponding 7-**HQCs** (Fig. 3.1, Table 3.1). The spectral positions of the lowest energy band of all the **7-HQs** do not depend on solvent properties and are centred at about 30000 cm^{-1}. The compounds (except **HDMQ** in methanol solutions) do not show any trace of the low-energy band. This finding indicate that the studied **7-HQs**, similarly to **7-HQ**,[140] in nonpolar and polar aprotic media as well as in alcohols exist in the ground state as the **OH** (7-quinolinol) form.

*Table 3.3. Ground state CC2/cc-pVDZ (ΔE_{CC2})[191] and DFT/B3LYP/6-31+G(d,p) (ΔE_{DFT}) relative energies (in kcal/mol) of the **OH**, **NH**, and **IIb** forms (Scheme 3.1) of **HQC**, **H4MQC**, **HPQC**, and **HMMQC** and corresponding dipole moments (μ, D).*

		I (**OH**)		III (**NH**)		**IIb**	
		CC2	DFT	CC2	DFT	CC2	DFT
HQC	ΔE	-	-	11.3	6.2	9.9	7.8
	μ	3.5	5.0	6.6	8.0	4.7	5.8
H4MQC	ΔE		-	11.5	6.2	10.1	7.7
	μ	4.0	5.6	7.1	8.7	5.1	6.4
HPQC	ΔE	-	-	10.8	5.9	9.7	7.8
	μ	3.3	4.9	7.2	8.7	5	6.2
HMMQC	ΔE	-	-	17.3	12.2	12.7	10.7
	μ	3	4.4	6.8	8.1	4.7	5.7

The ^{1}H NMR investigations of **7-HQCs** were performed in order to identify the tautomeric forms which exist in the ground state.[191] The spectra exhibit – in most cases – two set of signals that can be ascribed to two forms of the same compound that are in slow-

exchange equilibrium. The bridging protons are deshielded and exhibit NMR signals in the range of 12-16 ppm. The chemical shifts of CHO protons that are in the range 10-12 ppm are characteristic for aldehydes. Thus, the observed chemical shifts strongly suggest the co-existence of the **OH** and **NH** tautomers for **HQC** and its derivatives in a moderately polar (such as CDCl$_3$), polar (CD$_3$CN), and protic (CD$_3$OD) solvents. The evidence that one of the signals correspond to the **NH** form is provided by a lineshape analysis. For **H4MQC** in CDCl$_3$, as an example, the signal at 15.2 ppm is broadened and exhibits two shoulders (Fig. 3.4).[191] This is clearly caused by the coupling to the ^{14}N nuclei in the quinoline ring. The large value obtained for the coupling ^1J (^{1}H-^{14}N) ≈ 54 Hz is possible only for the direct H-N coupling through one bond. This fact excludes the origin of the line from the proton which is hydrogen-bonded to the N quinoline atom as in the **IIb** structure (Scheme 3.1). Moreover, a 2D NMR COSY experiment shows a cross peak between H2 and HN protons and the coupling constant is 6.3 Hz. This is again a typical value for the ^3J (^{1}H-^{1}H) in an aromatic ring which gives the next argument for the origin of this line from the **NH** form. These findings prove that the **NH** tautomer exists in solutions.
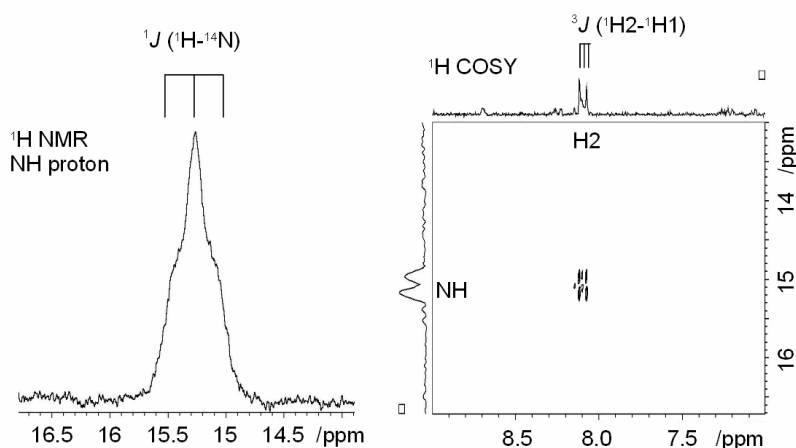
Figure 3.4. ^{1}H NMR signal of NH proton of H4MQC in CD$_3$CN showing coupling to the ^{14}N nuclei (left) and a cross-peak between NH and H2 proton signals of H4MQC (right). ^1J (^{1}H-^{14}N) ≈ 54 Hz, ^3J (^{1}H2-^{1}HN) = 6.3 Hz. [191,229]

The estimated fractions of the **OH** and **NH** forms (Table 3.4) confirm the assignment of the electronic absorption bands. In a nonpolar solvent (perdeuterated cyclohexane) the NMR spectra of **H4MQC** indicate the lack of the **NH** form. Thus, the absorption band in *n*-hexane centered at 347 nm (~28820 cm^{-1}) corresponds to the **OH** tautomer. In moderately polar solvents the recorded trace of the long-wave absorption band (in EA) of the all **7-HQCs** (except **HMMQC**) clearly corresponds to the appearance of the **NH** form observed in NMR experiments (in CDCl$_3$). Moreover, the increase of the intensity of the long-wave absorption

band centered at about 400 nm (~25000 cm^{-1}) in acetonitrile and alcohols is related to the significant growth of the fraction of the **NH** form in strongly polar (CD$_3$CN) and protic (CD$_3$OD) media. Thus, there is no doubt that the long-wave absorption band corresponds to the **NH** tautomer.

*Table 3.4. Ground-state fractions of the **OH** (7-quinolinol)) and **NH** (7(1H)-quinolinone) tautomeric forms of **7-HQCs** obtained from the room-temperature ^{1}H NMR spectra.*

	cyclohexane	CDCl$_3$	CD$_3$CN	methanol-d_4
HQC		**OH** - dominant, **NH** - trace	**OH** : **NH** ≈ 10:1 * 91% : 9%	**OH** : **NH** ≈ 1:1 * 50% : 50%
H4MQC	100% **OH** (no **NH**)	**OH** : **NH** ≈ 10:1 91% : 9%	**OH** : **NH** ≈ 5.5:1 85% : 15%	**OH** : **NH** ≈ 1:1.6 38.5% : 61.5%
H2MQC		**OH** : **NH** ≈ 8:1 89% : 11%		
HDMQC		**OH** : **NH** ≈ 3:1 75% : 25%		**OH** : **NH** ≈ 1:2.7 27% : 73%
HPQC		**OH** - dominant, **NH** – trace	**OH** : **NH** ≈ 100:1 99% : 1%	**OH** : **NH** ≈ 7:1 87.5% : 12.5%
HMPQC		**OH** - dominant, **NH** - trace	**OH** : **NH** ≈ 5:1 83% : 17%	
HMMQC	100% **OH** (no **NH**)	**OH** : **NH** ≈ 20:1 * 95.5% : 4.5%	**OH** : **NH** ≈ 17:1 * 94.5% : 5.5%

* estimated from broad lines indicating faster exchange between two forms

Contrary to the other **7-HQCs** under study, the electronic absorption spectra of **HMMQC** do not show any trace of the long-wave band centered at about 400 nm even in acetonitrile and alcohols (Fig. 3.1). On the other hand, the relatively small increase of the intensity is observed at the red corner of the lowest absorption band with the increase of polarity and hydrogen bond donor and acceptor ability of the environment. This finding is in agreement with: (i) the results of NMR investigations, *i.e.* the very small fraction of about 5% of the **NH** tautomer in strongly polar and protic media (noticeably, the computed ground-state destabilization energy of the **NH** tautomer of **HMMQC** (0.75 eV) is considerably higher than that of the other **7-HQCs** (~0.4-0.5 eV) and (ii) the predicted vertical excitation energy of *ca.*

27000 cm^{-1} to the lowest $^1(\pi,\pi^*)$ state of the **NH** form of **HMMQC** which is about 2000 cm^{-1} higher than that computed for **HQC** and its methylated derivatives and about 3700 cm^{-1} higher than that for **HPQC** (Table 3.3).

It should be stressed that **HMMQC** seems to be a good model to study the excited state tautomerization process due to the fact that the **OH** tautomer (which is a substrate of the photoreaction) is a major form of the compound in the ground state.

3.3. Excited-state long-range prototropic tautomerization: emission, excitation, and spectrophotometric titration.

3.3.1. Room-temperature studies of 7-hydroxyquinoline-8-carbaldehydes (7-HQCs)

The room temperature fluorescence spectra of **HQC, H4MQC, H2MQC**, and **HMMQC** are presented in Figure 3.5. **HQC** and its methyl derivatives in acetonitrile and in alcohols show a single broad fluorescence band with a maximum centred at about 20500 cm^{-1} and at about 21000 cm^{-1}, respectively. The fluorescence excitation spectra (monitored in various parts of the fluorescence spectrum) show that luminescence is preferentially excited from the low-energy absorption band. The shape and spectral position of fluorescence, however, recorded upon direct excitation of the **NH** form at 25000 cm^{-1} and upon excitation at the second absorption band at 28570 cm^{-1} are very similar. Therefore, it is natural to propose that fluorescence in sufficiently polar media originates from the **NH** tautomer.
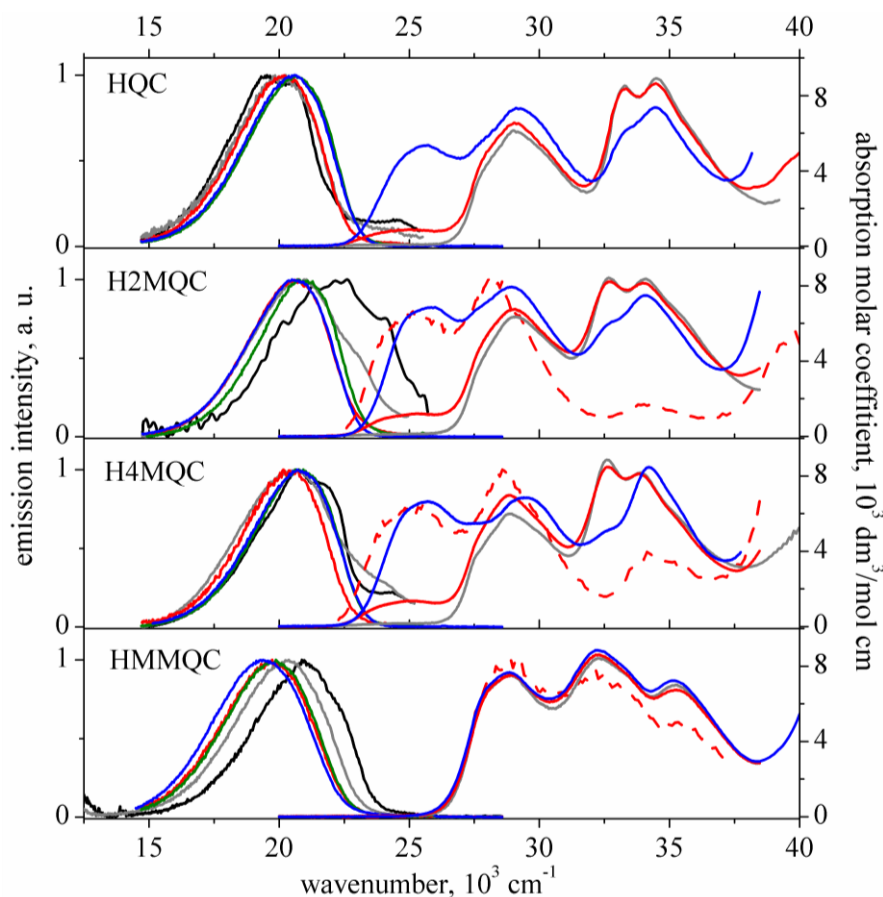
*Figure 3.5. Solid lines – room temperature absorption and corrected and normalized fluorescence spectra (black – n-hexane, grey – ethyl acetate, red – acetonitrile, green – 1-propanol, blue – methanol) of **HQC**, **H2MQC**, **H4MQC**, and **HMMQC** (the emission spectra of **HDMQC** are similar to those of **H4MQC**). Concentrations of the compounds were in the range 10^{-5}-10^{-4} mol dm^{-3}. Dashed lines – fluorescence excitation spectra in acetonitrile monitored at the emission maximum.*

56

In the contrary, the emission spectra of **HQC**, **H2MQC**, and **H4MQC** in *n*-hexane and in ethyl acetate exhibit two bands: a dominant band at about 21000 cm^{-1} and a second one of lower intensity at 24000-24500 cm^{-1}. The spectra of **HDMQC** (not shown) are considerably wider than those in the highly polar and protic media. These interesting spectral features suggest that emission in nonpolar and medium polarity solvents originates from at least two different species. The spectral position of the long-wave fluorescence is similar to that observed in acetonitrile and in alcohols. Thus, this emission is assigned to the **NH** tautomer. The assignment of the short-wave emission is more ambiguous. Most probably, the **OH** tautomeric form (which dominates in the ground state) is responsible for the emission observed at ~24500 cm^{-1}. Interestingly enough, the shape of the fluorescence spectra of **H4MQC** (and **H2MQC**) suggests the third emission centered at 22100 ($\pm$ 500) cm^{-1}. This emission, similarly to 7-hydroxy-8-(N-morpholinomethyl)quinoline (7HMMQ),[163,230] can be attributed to the transient intermediate structure **IIa** or **IIb** (Scheme 1.14). This interesting finding suggests that the **NH** tautomer, which exists already in the ground state for **HQC** and its methylated derivatives, is formed in part in the excited state *via* intramolecular proton transfer (ESIPT) processes.

The absorption, fluorescence, and excitation spectra of **HMMQC** suggest that the excited-state long-range irreversible 7-quinolinol $\rightarrow$ 7(1H)-quinolinone (**OH** $\rightarrow$ **NH**) tautomerization is observed for this compound. The ^{1}H NMR investigations and electronic absorption spectra prove that the **OH** form is dominant in the ground state. On the other hand, the spectral position and shape of the single emission band of **HMMQC** suggests that both in polar and nonpolar media the luminescence corresponds to only one excited-state species, being responsible in **HQC** for the long-wave emission (*i.e.* the **NH** form). The increase of solvent polarity and its hydrogen-bond donor and acceptor ability leads to a red shift of the emission from 20930 cm^{-1} in *n*-hexane to 19400 cm^{-1} in methanol. The corresponding Stokes shift is as large as 8000 cm^{-1} in *n*-hexane and about 9200 cm^{-1} in polar and protic solvents with respect to the lowest absorption band assigned to the **OH** tautomer. There is no doubt that this fluorescence is related to the other form of the molecule. Thus, although in the ground state we either do not observe the **NH** tautomer (in low polarity media) or its fraction is negligibly small (in acetonitrile and in alcohols), this tautomer is created *via* an excited state proton transfer (ESPT) processes and is responsible for the observed emission. This conclusion is in agreement with the finding that the excitation spectra monitored in various parts of the fluorescence spectrum match well the corresponding absorption spectra.

Table 3.6. Solvent effects on the spectral position of the room temperature fluorescence maxima ($\tilde{\nu}_{fl}$, in cm^{-1}), quantum yields (Φ_f) determined for various excitations (λ_{exc}, in nm), lifetimes (τ, in ns) and resulting radiationless (k_{nr}, in $10^8 s^{-1}$) and radiative (k_f, in $10^7 s^{-1}$) rate constants and electronic transition dipole moments corresponding to fluorescence (M_{fl}, in D) of 7-HQCs.

Compound	Solvent	λ_{exc}[b]	Φ[a]	$\tilde{\nu}_{fl}$[c]	τ[a]	k_{nr}	k_f	M_{fl}
HQC	HEX	345	0.005	19500/20500				
				ca. 24400				
	EA	345	0.006	20100				
				ca. 24000				
	ACN	356	0.01	20200				
		380	0.04					
	1-PrOH	345	0.018	20700				
	MeOH	343	0.035	20700				
H2MQC	HEX	346	0.002	19900/20900				
				ca. 22600	< 0.4			
				ca. 24000				
	EA	346	0.005	20900	< 0.4			
				ca. 23000				
	ACN	346	0.01	20600				
		380	0.045		0.9	10.6	5.0	2.7
	1-PrOH	346	0.02	20900				
		380	0.064		0.9	10.4	7.1	3.1
	MeOH	346	0.045	20600				
HPQC	HEX	350	0.003	18100/19200	4.0			
				ca. 20500				
				ca. 24000	2.2			
	EA	350	0.005	*ca.* 20000	5.7(d) and ~0.8			
				21500	< 0.5(d) and 4.4			
				23300				
	ACN	350	0.013	19600				
				21500	4.0			
				ca. 23500	< 0.05(d) and 2.7			
	1-PrOH	350	0.022	19500	3.9(d) and < 0.3			
				22600				
	MeOH	350		19100				
HMMQC	HEX	346	0.039	21000	1.5	6.4	2.6	1.9
	EA	346	0.037	20300	1.4	6.9	2.6	2.0
	ACN	346	0.035	19700	1.6	6.0	2.2	1.9
	1-PrOH	346	0.04	19700	1.8	5.3	2.2	1.9
	MeOH	346	0.023	19400				

[a] Error is about 10%. Thus, the maximum error is about 20% for the rate constants k_{nr} and k_f and about 10% for the transition moment M_{fl}. [b] Scatter of results: ± 2.0 nm. [c] Scatter of results: ± 150 cm^{-1}. (d) Dominant contribution.

The analysis of the solvent effects on the fluorescence quantum yield (Φ_f) and decay times (τ) of **HMMQC** (Table 3.6) supports the conclusion that fluorescence corresponds to only one excited-state species. The values of Φ_f of 3-4% and lifetimes τ = ~1.6 ns (τ values do not depend on the monitored emission wavelengths) are similar for the whole range of solvents (Table 3.6). Fluorescence transition dipole moments $M_f \cong 1.9$ (± 0.2) D of **HMMQC** are slightly smaller than those estimated for the absorption of the **OH** tautomeric form (being about 2.5 D). This parameter as well as the radiative rate constants $k_f \approx 2.4 \cdot 10^7$ s^{-1} proves the allowed character of the absorption and luminescence transitions. Without any doubt the observed absorption and emission spectra correspond to the excited $^1(\pi,\pi^*)$ states.

The fluorescence data for the representatives of **7-HQCs** are collected in Table 3.6 (all the obtained data are presented in Table S.3.1, Chapter 7: Supporting information). The fluorescence quantum yields of **HQC**, **H2MQC**, and **H4MQC** were measured upon excitation at the two absorption bands corresponding: (i) mainly to the **OH** tautomer (~350 nm) and (ii) to the **NH** tautomer (~380 nm). The direct excitation of the **NH** tautomer of **H2MQC** results in the quantum yield values about 3-5 times higher than those obtained upon higher energy excitation. This interesting result seems to support a strong nonradiative decay of the transient intermediates **IIa** and **IIb** which was theoretically predicted in the excited-state route of a formation of the **NH** form (Figure 1.12),[164-166] Fluorescence lifetimes in the nanosecond range were measured monitoring different parts of the emission spectrum. The decay times for **H2MQC** in low polarity media are too short to be measured correctly, in ACN and in 1-PrOH the lifetimes of the fluorescent state are about 0.9 ns. The resulting values of the radiative rate constants $k_f \approx 5-7 \cdot 10^7$ s^{-1} and of the fluorescence transition dipole moments $M_f \approx 2.7-3.0$ D prove the $^1(\pi,\pi^*)$ nature of the fluorescent state.

The room-temperature absorption spectra of **HPQC** (Fig. 3.1) and **HMPQC** (Fig. 3.6) in acetonitrile and in alcohols, similarly to **HQC** and its methylated derivatives, show the low-energy absorption bands centered at about 400-420 nm which indicate the formation of the **NH** tautomer already in the ground state. The shape and spectral position of the fluorescence spectra of **HPQC** and **HMPQC** (Fig. 3.6), contrary to the other **7-HQCs** under study, depend on excitation. The direct excitation of the **NH** tautomeric form of **HPQC** in polar media at 410 nm (~24400 cm^{-1}) results in a single emission band centered at 18700 cm^{-1} (in ACN), 18800 cm^{-1} (in MeOH) and 19100 cm^{-1} (in 1-PrOH). The spectral position of this fluorescence is similar to that recorded for the other compounds under study. It is noticeable that in highly protic methanol solutions, even upon high-energy excitation, only low-energy

emission assigned to the **NH** tautomer is observed. On the other hand, two (or even three) emissions of **HPQC** are observed upon excitation at 325 nm (~30770 cm^{-1}, not shown) and 355 nm (~28170 cm^{-1}) in nonpolar and polar aprotic solvents as well as in 1-PrOH. The dominant band in acetonitrile, which is centred at 19700 cm^{-1}, originates from the **NH** tautomer. The shoulder recorded at *ca*. 21400 cm^{-1} is probably due to the emission from the form **IIa** or **IIb** (Figure 1.12), being a transient product of the ESIPT reaction, and the long blue tail (a distinct emission band centered at ~24000 cm^{-1} is observed upon excitation at 325 nm) seems to correspond to the **OH** form (similarly to the Varma's[163,230] interpretation of the triple emission of 7HMMQ). The fluorescence excitation spectra of **HPQC** in ACN are in agreement with this assignment (Fig. 3.7). The fluorescence monitored between 18000-20000 cm^{-1} is preferentially excited from the long-wave absorption band. On the other hand, the emission monitored at about 21500-23500 cm^{-1} is excited from the high-energy absorption bands. The similar effects are observed for **HMPQC**. The direct excitation of the **NH** tautomer at 24400 cm^{-1} leads to the single emission band centered at 19300 cm^{-1} (in ACN), 19600 cm^{-1} (in 1-PrOH) and 19700 cm^{-1} (in MeOH). The shape of the fluorescence spectra recorded upon excitation at 28570 cm^{-1} suggests the presence of two emissions which most probably correspond to the **OH** (the shoulder at ~23600 cm^{-1}) and the **NH** (the dominant band centered at about 19600 cm^{-1}) tautomeric forms.
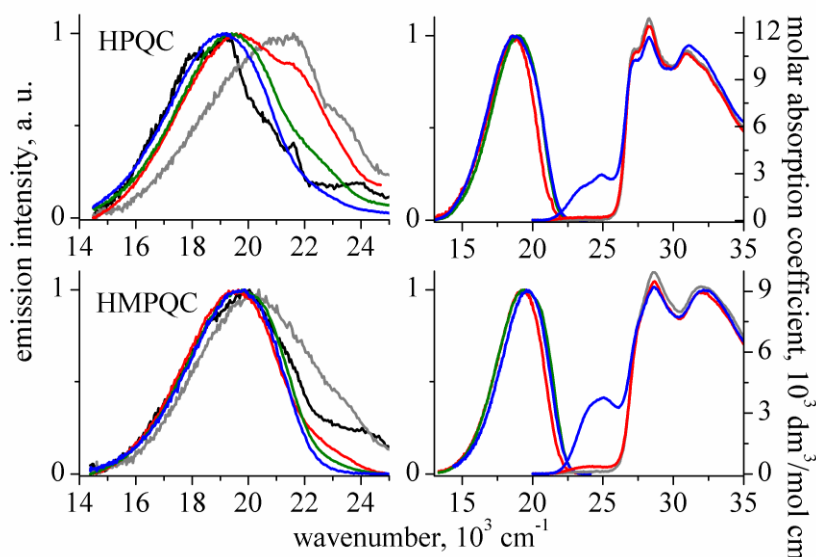
*Figure 3.6. Room temperature absorption and corrected and normalized fluorescence spectra (black – n-hexane, grey – ethyl acetate, red – acetonitrile, green – 1-propanol, blue – methanol) of **HPQC** and **HMPQC**. Left: fluorescence spectra upon excitation at ca. 28170 cm^{-1}; right: absorption and fluorescence spectra upon excitation at ca. 25000 cm^{-1}. Concentrations of the compounds were in the range from 10^{-5} to 10^{-4} mol dm^{-3}.*

The fluorescence spectrum of **HPQC** in *n*-hexane, in addition to the low energy fluorescence from the **NH** form, shows a clear high energy emission band of low intensity at about 24000 cm^{-1} which can be attributed to the **OH** tautomer. The spectral position and shape of the fluorescence spectrum in ethyl acetate indicate three emissions. Most probably, the **OH** and **NH** tautomers are responsible for the shoulders observed at about 23500 cm^{-1} and 20000 cm^{-1}, respectively. The maximum of the emission spectrum centered at ~21500 cm^{-1} is assigned to the intermediate product **IIa** or **IIb** of the ESIPT reaction (Scheme 1.14). This finding, which is similar to the luminescence properties of 7HMMQ,[163,230] manifests that the **NH** tautomer, which in part exists in the ground state, is formed also in the excited state *via* ESIPT reaction.

The time-resolved fluorescence investigations in the nanosecond range are in agreement with this interpretation (Table 3.6). Fluorescence decays in EA can be satisfactorily fitted to a sum of two exponentials. By varying the detection wavenumber from ~19500 cm^{-1} to ~21700 cm^{-1} the contribution of the long component decreases and that of the short-lived component increases. The decay in ACN show also the long and short (too short to be determined with subnanosecond resolution) components. Measurements in *n*-hexane exhibit different results: the decay of the long-wave and the short-wave parts of the fluorescence spectrum is monoexponential but the lifetimes are of 4 ns and 2.2 ns, respectively.
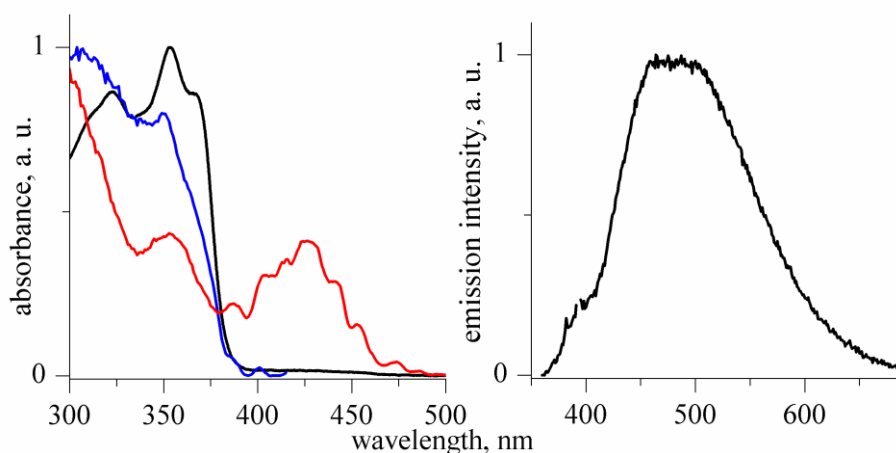
Figure 3.7. Room temperature emission (right panel), and absorption (black) and fluorescence excitation spectra of HPQC in acetonitrile monitored at the short-wave, i.e. between 425 nm and 465 nm, (blue) and at long-wave (between 500 nm and 555 nm, red) parts of the emission band (left panel). See text for explanation.

3.3.2. Low-temperature investigations of 7-HQCs

The temperature effects on the absorption spectra of **H4MQC** in 1-propanol (Fig. 3.8) show an increase of intensity of the long-wave absorption band with the decrease of temperature. The similar effects are observed in acetonitrile. The stabilization of the **NH** tautomeric form with lowering of temperature is most probably due to the increase of the solvent polarity; the dielectric constants of 1-PrOH[231] and ACN[232] increase with lowering of temperature. The interesting spectral changes are observed for the higher energy bands: the spectral positions of the both bands shift to the higher energy, for example the maximum of the band centred at 28900 cm^{-1} at room temperature shifts to 30030 cm^{-1} at 133 K, and the band observed at 32570 cm^{-1} at 298 K disappears at 133 K. This finding indicates that, in agreement with theoretical *ab initio* and TD-DFT computations (Table 3.2), the electronic transitions related to the various tautomeric forms of the molecule lay closely in this spectral region. The temperature dependence of the NMR spectra of **H4MQC** in CD_2Cl_2, $CDCl_3$, CD_3CN, and CD_3OD, which do not show any signals from the **IIa** or **IIb** forms, prove the origin of these bands from the **OH** and **NH** forms.
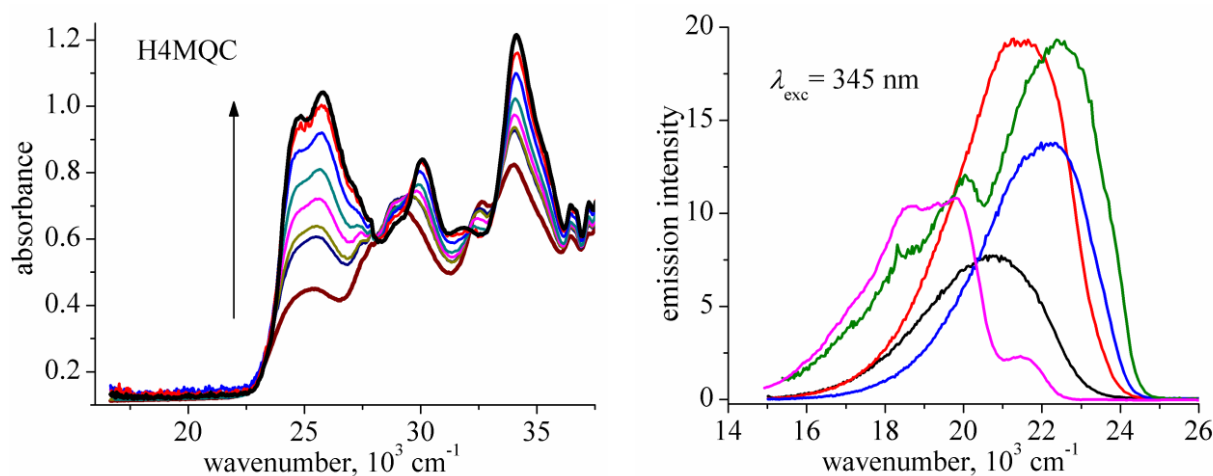
Figure 3.8. Temperature effects on the absorption (left panel, the spectra are recorded between 298 K and 133 K, the arrow shows the decrease of temperature) and emission (right panel) spectra of **H4MQC** *in 1-propanol. Right: room-temperature (black) and low-temperature (red – T=173 K, and blue – T=133 K) fluorescence spectra as well as total luminescence (green) and phosphorescence (pink) in a glass at 77 K; concentrations of the solute are about $4 \cdot 10^{-5}$ mol dm^{-3}.*

The temperature effects on the fluorescence of **H4MQC** in 1-propanol solutions show that, in addition to the increase of the fluorescence intensity with lowering of temperature, the fluorescence maximum shifts from 20800 cm^{-1} at room temperature to 22200 cm^{-1} in a strongly viscous solution at -140 ^{o}C. Notably, the total luminescence spectrum in rigid glass

at 77 K shows two distinct bands centred at 22500 cm^{-1} and 20000 cm^{-1}, and a shoulder at about 18500 cm^{-1}. The latter two transitions correspond to phosphorescence.

The temperature dependence of the fluorescence of **HPQC** in 1-PrOH solutions (Fig. 3.9) recorded upon direct excitation of the **NH** form shows similar effects to those observed for **H4MQC**. The fluorescence maximum shifts from 19100 cm^{-1} at room temperature to ~20900 cm^{-1} in a strongly viscous solution at 133 K and to about 21300 cm^{-1} at 77 K. This spectral shift can hardly be explained by the fluorescence of the other forms than the **NH** tautomer. On the other hand, the temperature effects on the fluorescence of **HPQC** in 1-PrOH observed upon excitation at 355 nm are in agreement with a hypothesis of the multiple fluorescence. In addition to the shift of the fluorescence maximum from ~19500 cm^{-1} at room temperature to ~21200 cm^{-1} in a strongly viscous solution at -140°C, the low temperature spectrum shows two shoulders at ~23200 cm^{-1} and ~25300 cm^{-1}. The latter spectral features can be assigned to the **OH** tautomeric forms of **HPQC** and **HPQ** (as an impurity, see next chapter), respectively.
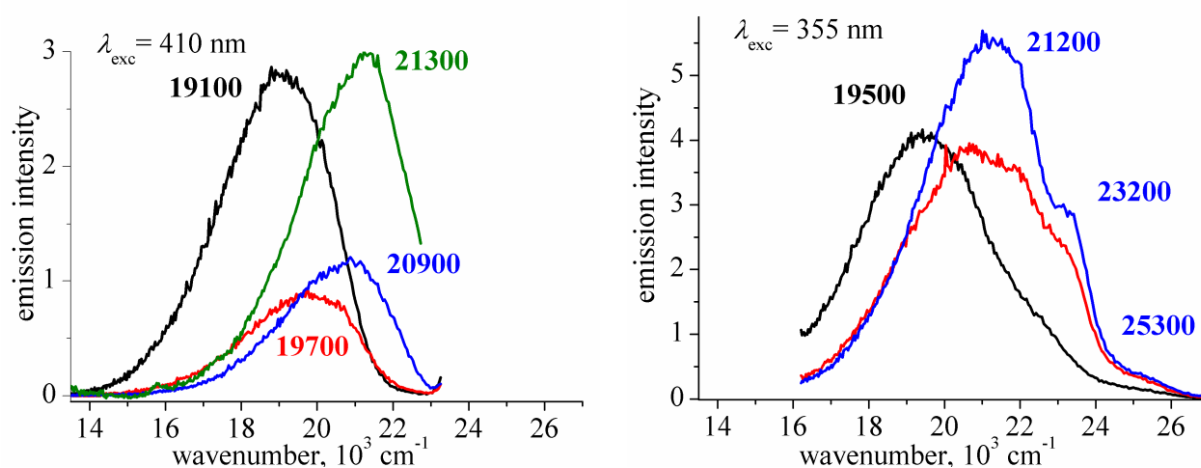
*Figure 3.9. Room-temperature (black) and low-temperature (red – T=173 K, and blue – T=133 K) fluorescence, and total luminescence at 77 K (green) spectra of **HPQC** in 1-propanol upon various excitations. Left: direct excitation of the **NH** tautomeric form (λ_{exc}= 400 nm); right: excitation of the **OH** and **NH** forms (λ_{exc}= 355 nm). Concentrations of the solute are about 4·10^{-5} mol dm^{-3}.*

3.3.3. Investigations of 7-hydroxyquinolines (7-HQs)

The above analysis of the fluorescence spectra of the studied **7-HQCs** is performed under the assignment that the observed spectral features do not correspond to the **7-HQs** (Scheme 3.2), the synthetic precursors of the former compounds. In order to prove the postulated origin of the emission bands discussed in Chapters 3.3.1 and 3.3.2, the spectra of the representatives of

7-**HQCs** are compared with those of the corresponding **7-HQs** in Figure 3.10. The spectral locations of the absorption and fluorescence bands of **7-HQs** are similar to those previously observed for 7-hydroxyquinoline (**7-HQ**).[140] Therefore, it is natural to assign these bands to the same tautomeric species; the studied **7-HQs** exist in the ground state as the **OH** form (7-quinolinol) and upon excitation show single fluorescence band in nonpolar and polar aprotic media (which is assigned to the **OH** tautomer) and dual luminescence phenomenon in alcohols (the long-wave band corresponds to the 7(1H)-quinolinone (**NH**) form).[149-154,158]
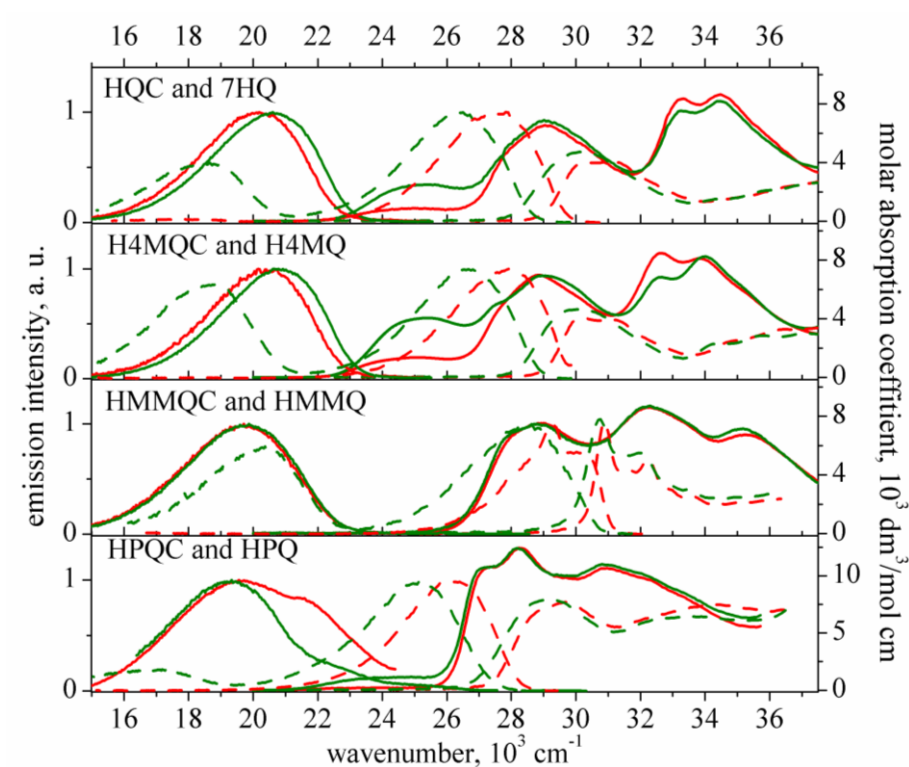
*Figure 3.10. Comparison of the room temperature absorption and corrected and normalized fluorescence spectra (green – 1-propanol, red – acetonitrile) of the representatives of **7-HQCs** (solid lines) and corresponding **7-HQs** (dashed lines). Concentrations of the compounds are in the range from 10^{-5} to 10^{-4} mol dm^{-3}.*

The short-wave fluorescence bands of **7-HQ**, its methylated derivatives, and **HMMQ** in *n*-hexane and ethyl acetate (not shown) as well as in ACN and alcohols are centered about 26300-28200 cm^{-1}. The bands for **HPQ** and **HMPQ** are red shifted of about 1000 cm^{-1} and observed between 25100 cm^{-1} and 27000 cm^{-1} for **HPQ** in methanol or *n*-hexane, respectively (Table S.3.2 Chapter 7: Supporting information).

In **7-HQ** the acidic hydroxyl group and the basic nitrogen atom in the ring are too far apart to form an intramolecular hydrogen bond. Thus, the phototautomerization of **7-HQ** is observed only in protic solvents (*e.g.*, alcohols). The long-wave band of **7-HQ** in alcohols was previously attributed to the **NH** form created by the excited-state triple proton transfer in

the cyclic hydrogen-bonded complexes of 1:2 stoichiometry.[149-154,158,163] These bands for all the **7-HQs** except for **HMMQ** are markedly red shifted with respect to the fluorescence of **7-HQCs**. The excited-state reorganization of the geometry of the majority of complexes to make it suitable for the ESPT process (Scheme 1.13) and the resulting ground-state destabilization energies can be the reason for this significant red shift.[154,158] On the contrary, the long-wave fluorescence band of **HMMQ** is slightly shifted to the blue with respect to the fluorescence of **HMMQC**. Most probably, the tautomerization of **HMMQ** is restricted to a particular complex of a cyclic geometry which is formed already in the ground state. In order to gain more insight into the ground-state formation of the complexes between **7-HQs** and an alcohol partner the titration experiments of **HMMQ** and **HPQ** in *n*-hexane solution with 1-butanol were performed (the solubility of the other **7-HQs** in *n*-hexane is too low to measure the changes in the absorption and fluorescence spectra). **HMMQ**, contrary to **HPQ**, shows the isosbestic point in the absorption spectra. The experiments indicate the formation of 1:2 complexes (Fig. 3.11). The appearance of these complexes is followed by dual luminescence: the decrease of the intensity of the short-wave fluorescence is accompanied by the appearance and growth of the low-energy band. This finding supports our interpretation: **HMMQ** shows the ground-state formation of the complex which is prepared for the excited-state proton transfer process.
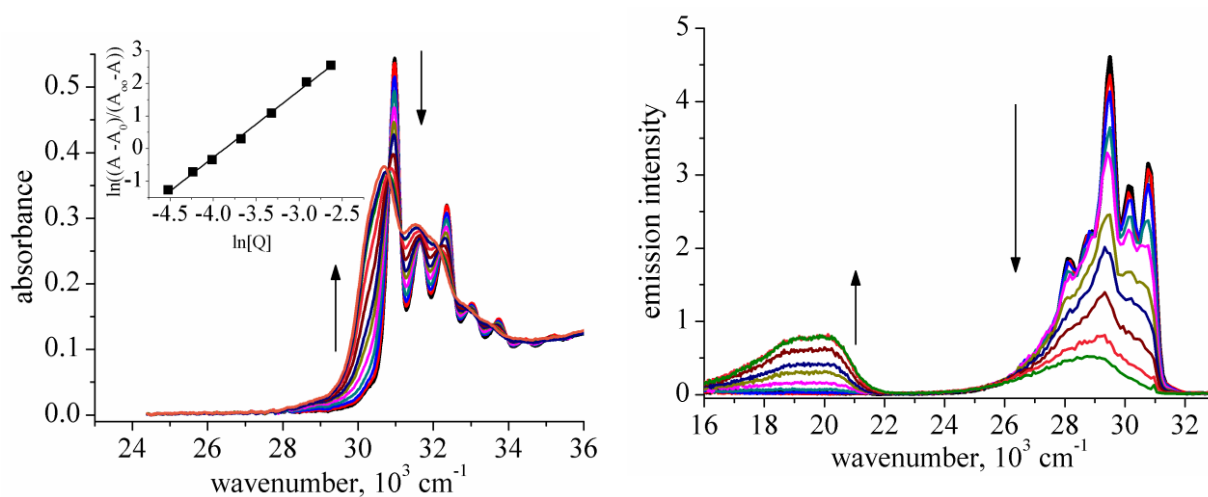
*Figure 3.11. Titration of **HMMQ** solution in n-hexane with 1-butanol at 293 K. Left: changes in absorption; right: evolution of both fluorescence bands. The arrows show spectral changes accompanying the addition of alcohol. The alcohol concentration varied from 0.0018 to 0.18 mol/dm³. The inset in the absorption part shows the determination of the stoichiometry of the complex (eq. 2.10) from the absorption data recorded at 30300 cm⁻¹; A_0 and A_∞ denote the optical density measured when only the bare or complexed forms are present, and A is the optical density measured at an alcohol concentration [Q].*

3.4. Ionic forms of 7-HQs and 7-HQCs

The comparative investigations of the photophysical properties of the ionic forms of the studied **7-HQCs** and **7-HQs** were performed in acidic (by adding aqueous solution of perchloric acid, $HClO_4$) and basic (by adding aqueous solution of sodium hydroxide, NaOH) solutions in acetonitrile and water. The investigations were provided in the wide range of acid (from 10^{-3} to 9.1 mol/dm^3) and base (between $3 \cdot 10^{-3}$ to 8.6 mol/dm^3) concentrations to track the evolution of the electronic absorption and emission spectra and to observe the spectra of the protonated cations (**C**) and deprotonated anions (**A**).

The previous intensive studies[140-147,149-154,158] of prototropic equilibria of 7-hydroxyquinoline (**7-HQ**) have shown that four ground-state prototropic species of **7-HQ** are present in a neutral aqueous solution at pH=7: **7-HQ** exists mostly as the **OH** (67%) and **NH** (29%) tautomers with minor fractions of the protonated cation **C** (3%) and deprotonated anion **A** (1%).[147] Mason *et al.*[145] concluded that in the excited state the hydroxyl group is more acidic and the quinoline nitrogen atom more basic than in the ground state. This indicates a shift towards the **Z ↔ NH** form on excitation (Chapter 1.4). Due to that the fluorescence of **C** and **A** is observed in strong acids or bases, respectively; the dominant emission band of the **NH** tautomeric form of **7-HQ** (and a trace of the **OH** emission) was observed in aqueous solutions in the range of pH between 2 and 13.[145] **H2MQ** and **HDMQ** in aqueous solutions at this pH range show the fluorescence originating only from the **NH** form due to the effects of the electron donating substituents.[148]

The room temperature electronic absorption and fluorescence spectra of **H4MQ**, **HMMQ**, and **HPQ** in neutral, acidic and basic aqueous solutions are presented in Figure 3.12. The corresponding data in water solutions of the studied **7-HQs** are collected in Table 3.7 (the data obtained in acetonitrile solutions are presented in Table S.3.3, Chapter 7: Supporting information). The absorption spectra of **7-HQs**, except **HMMQ**, show in water at pH = 7 the long-wave absorption band at about 390-410 nm, which was not observed in aprotic solvents and in alcohols (Fig. 3.10). This finding is a manifestation of the appearance of the **NH** tautomeric form.[145,148] The intensity of the long-wave band is relatively high for methylated derivatives of **7-HQ**, significantly lower for **HPQ** and **HMPQ**, and negligibly low for **HMMQ**. The ground state protonation and deprotonation was monitored by the changes in absorption. The formation of the cations was achieved by adding about 10^{-3}-10^{-1} mol/dm^3 of $HClO_4$ to the acetonitrile or water solutions as it was evidenced by the disappearance of the long-wave band and the formation of a new band at *ca.* 340-350 nm (~28600-29400 cm^{-1}) for

7-HQ and its methylated derivatives, 334 nm (~29900 cm^{-1}) for **HMMQ**, and 365 nm (~27400 cm^{-1}) for **HPQ**. The absorption spectra of the protonated cations do not show any changes up to the concentration of HClO$_4$ as large as 9.1 mol/dm^3. Similarly, the ground state deprotonation was achieved by adding about $3 \cdot 10^{-1}$ mol/dm^3 of NaOH to the aqueous solutions; the absorption spectra show a new band which is shifted to the red of about 1000 cm^{-1} with respect to that of the corresponding cation. Contrary to the absorption, the fluorescence spectra in aqueous solutions in a wide range of pH from 1 to 13 correspond to the **Z ↔ NH** forms of **7-HQs**. The driving force for the excited state transformation of the **C** and **A** forms into the **NH** form (*via* ESIPT process) is the increase of acidity of the hydroxyl group and the increase of basicity of the quinoline nitrogen atom (Table 3.8). The fluorescence of the ionic forms (with some exceptions) is observed in strongly acidic (in 60% HClO$_4$) and basic (c(NaOH) = 8.6 mol/dm^3) solutions.
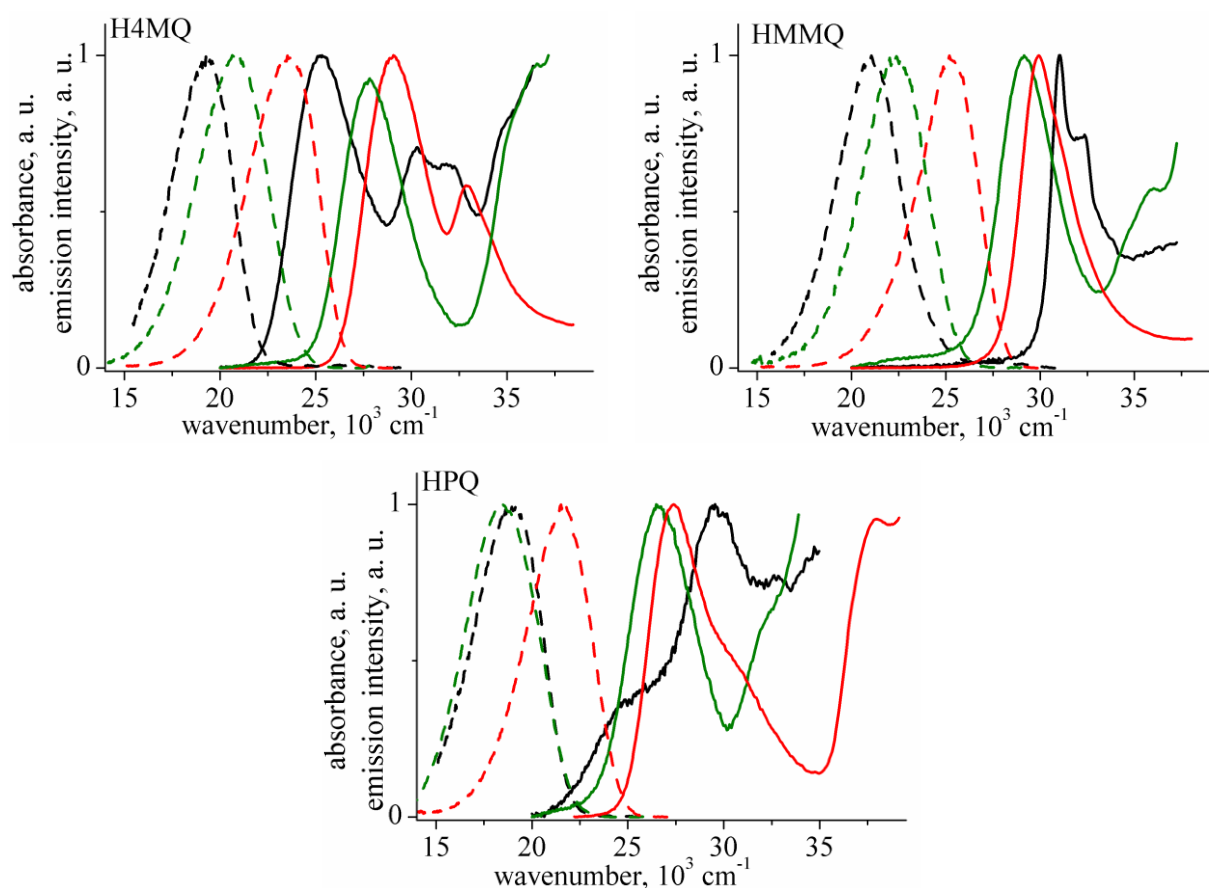
*Figure 3.12. Comparison of the room temperature normalized absorption spectra (full lines) and corrected and normalized fluorescence spectra (dashed lines) of **H4MQ** (left top panel), **HMMQ** (right top panel), and **HPQ** (bottom panel) in neutral water at pH = 7 (in black) with those recorded in strongly acidic (in 60% HClO$_4$ solution, in red) and basic (by adding about 8.6 mol/dm^3 NaOH, in green) aqueous solutions. Concentrations of the compounds are in the range from 10^{-5} to 10^{-4} mol dm^{-3}.*

*Table 3.7. Spectral positions of the room temperature absorption (abs) and fluorescence (em) maxima (in cm^{-1}) of **7-HQs** in neutral aqueous solutions and under acidic and basic conditions. **OH**, **NH**, **C**, and **A** denote the assignment of the bands to the tautomeric forms of neutral molecules, protonated cations, and deprotonated anions, respectively.*

| | +HClO$_4$ | | | | pH $\cong$ 7 | | +NaOH | |
| | c $\cong$9.1 mol/dm^3 | | pH $\cong$ 1 | | | | c $\cong$8.6 mol/dm^3 | |
	abs (**C**)	em (**C**)	abs (**C**)	em (**NH**)	abs	em	abs (**A**)	em (**A**)
7-HQ [b]			28900		30500(**OH**)	≈18800(**NH**) ≈25000(**OH**)	27600	≈20500
H2MQ[c]					25400(**NH**) 30300(**OH**)	≈19700(**NH**)		
H4MQ	29100	23500	29100	19300	25300(**NH**) 30200(**OH**)	19300(**NH**)	27900	20900
HDMQ[c]					25700(**NH**) 30300(**OH**)	≈19800(**NH**)		
HMMQ	29900	25300	29900	21100	31100(**OH**)	21100(**NH**)	29100	22300
HPQ	27400	21600	27400	19300	24800(**NH**) 29600(**OH**)	19000(**NH**)	26600	18500(**NH**)
HMPQ					24200(**NH**) 30400(**OH**)			

[a] Scatter of results: ± 150 cm^{-1}. [b] refs. [146,149]. [c] our results are similar to those published in ref. [149].

*Table 3.8. The changes of pK$_a$ ($\Delta pK_a = pK_a^* - pK_a^G$) upon $S_1 \leftarrow S_0$ excitation (estimated from eq. (2.12) with the use of Förster cycle and the data collected in Table 3.7) of the equilibria between various neutral (**NH** $\leftrightarrow$ **Z** and **OH**) tautomeric forms and protonated cations (**C**) and deprotonated anions (**A**) of the representatives of **7-HQs** (see text for explanation). Concentrations of the compounds were in the range of 10^{-5}-10^{-4} mol/dm^3.*

Solvent	Equilibrium	**7-HQ**[d]	**H4MQ**	**HDMQ**[e]	**HMMQ**	**HPQ**	**HMPQ**
ACN [a]	**C** $\rightleftharpoons$ **OH** + H$^+$	7.4	6.6	5.6	6.2	7.7	7.6
H$_2$O [b]	**C** $\rightleftharpoons$ **Z** + H$^+$	≈ -7- -8[145]	-8.3	-		-5.4	-
H$_2$O [c]	**Z** $\rightleftharpoons$ **A** + H$^+$	≈5.4[145,148]	4.3	-			-

[a] Protonation was achieved by adding about 0.9 mol dm^{-3} of HClO$_4$.
[b] The pK$_a$ changes are estimated for the 0-0 electronic transitions estimated from the absorption and fluorescence maxima in water at pH = 7 and in strongly acidic aqueous solutions obtained by adding 9.1 mol/dm^3 of HClO$_4$.
[c] The changes of pK$_a$ are estimated for the 0-0 electronic transitions in water at pH = 7 and in strongly basic aqueous solutions obtained by adding 8.6 mol/dm^3 of NaOH.
[d] The values of pK$_a^G$ for the quinoline nitrogen and 7-hydroxy group are 5.6 and 9.8 (ref. [149]).
[e] The values of pK$_a^G$ for the quinoline nitrogen and 7-hydroxy group are 6.5 and 10.1 (ref. [149]).

*Table 3.9. Spectral positions[a] of absorption (abs) and fluorescence (em) maxima (in cm^{-1}) of **7-HQCs** in neutral ACN and aqueous solutions and under strongly acidic and basic conditions. **OH**, **NH**, **C**, and **A** denote the assignment of the bands to the tautomeric forms of neutral molecules, protonated cations, and deprotonated anions, respectively.*

| | H₂O | | | | | | | | ACN | | | |
| | +HClO₄ 9.1 mol/dm³ C................? | | +HClO₄ 3 mol/dm³ C……….NH | | pH = 7 NH | | +NaOH 8.6 mol/dm³ A[b] ………?[b] | | | | +HClO₄ 3 mol/dm³ C | |
	abs	em	abs	em	abs	em	abs	em	abs	em	abs	em
HQC									25000 (**NH**) 29000 (**OH**)	20200 (**NH**)	28900	22900
H2MQC			29000	22500	26600	21800	26600	19200	25000 (**NH**) 29100 (**OH**)	20800 (**NH**)	28700	24200
H4MQC	28900	23550 (**C**)	28800	21600	26300	21600	26300	20500	25000 (**NH**) 28800 (**OH**)	20500 (**NH**) ≈24500(**OH**)	29000	23300
HDMQC			28800	22800	25800	22300	26400	19700	25000 (**NH**) 28800 (**OH**)	21100 (**NH**)	28400	24000
HPQC	26300	17500(??)	26400	19800	24900	19600	25700	18700 21400[c]	23700 (**NH**) 28300 (**OH**)	19300 (**NH**) ~24000(**OH**)	26500	18800[d] 23500
HMPQC									24500 (**NH**) 28600 (**OH**)	19500 (**NH**)	26900	22700
HMMQC	28500	18900(**NH**)	28570	18300	≈25900[c]	19600	26600	21900	28900 (**OH**)	19700 (**NH**)	28570	18800[d]

[a] Scatter of results: ± 150 cm^{-1}. [b] see text for the assignment. [c] shoulder. [d] assigned to the **NH** form.

The ground and excited-state prototropic reactions of the **OH** and **NH** tautomeric forms of the studied **7-HQCs**, due to the presence of carbaldehyde group, reveal some peculiarities with respect to those of the corresponding **7-HQs**. The spectral positions of the absorption and fluorescence maxima of the neutral **OH** and **NH** ↔ **Z** forms of **7-HQCs** and protonated cations (**C**) and deprotonated anions (**A**) are collected in Table 3.9. The room-temperature absorption and fluorescence spectra of **H4MQC**, **HMMQC**, and **HPQC** (as the representatives of **7-HQCs**) in neutral and acidic acetonitrile solutions as well as in neutral, acidic and basic aqueous solutions are presented in Figures 3.13, 3.14, and 3.15, respectively.

H4MQC in water at pH = 7 shows (Fig. 3.13) the relative increase of the intensity of the long-wave absorption band with respect to the second absorption band (the bands are centred at about 26300 cm^{-1} and 30000 cm^{-1}, respectively) in comparison with acetonitrile and alcohol solutions (Figs. 3.1 and 3.5). This finding indicates the increase of the ground-state fraction of the **NH** tautomer with respect to that of the **OH** tautomer. The spectral position and shape of the single fluorescence band do not depend on excitation. There is no doubt that this emission centred at 21600 cm^{-1} corresponds to the **NH** tautomer. The absorption spectra recorded in acidic acetonitrile and water solutions, which are located at about 28800-29000 cm^{-1}, are assigned to the protonated cation (**C**). The cations in acidic acetonitrile solutions emit fluorescence centred at 23300 cm^{-1} (the emission does not depend on the concentration of perchloric acid from 0.1 to 4.5 mol/dm^3). On the other hand, the emission spectrum of **H4MQC** in water in the wide range of pH from 0 to 7 (and even for the concentration of HClO$_4$ as large as 3 mol/dm^3) originates from the **Z** ↔ **NH** form. Thus, similarly to **7-HQs**, the electronic excitation leads to the deprotonation of the cations to yield a zwitterion. The fluorescence of the cations is observed in very strong acidic aqueous solutions (*e.g.,* in 60% HClO$_4$). An interesting result is provided by the very similar shape and spectral position of the absorption and fluorescence spectra of the cations of **H4MQC** and **H4MQ**. The NMR spectra of **H4MQC** in strongly acidic solutions do not show any sign of the creation of **H4MQ**. These findings suggest that: (i) the protonation center in both cations is the quinoline ring nitrogen atom and (ii) the π-electronic decoupling of the carbaldehyde group and a quinoline ring is achieved in the cation of **H4MQC** most probably due to the intramolecular twist to a mutually perpendicular conformation. The similar effects are observed for **HQC**, **H2MQC**, and **HDMQC**.

*Figure 3.13. Comparison of the room temperature normalized absorption spectra and corrected and normalized fluorescence spectra of **H4MQC** in neutral (in black) acetonitrile (a) and water at pH = 7 (b) with those recorded in strongly acidic (by adding HClO$_4$, in red) and basic (by adding about 8.6 mol/dm^3 NaOH, in green) acetonitrile and aqueous solutions. Black dotted curves correspond to the absorption and emission of **H4MQ** upon adding an amount of about 10^{-1} mol/dm^3 of HClO$_4$ to ACN. The concentrations of HClO$_4$ added to ACN and water are ~4.5 mol/dm^3 and ~9.1 mol/dm^3, respectively. Concentrations of the compound are in the range from 10^{-5} to 10^{-4} mol dm^{-3}.*

The assignment of the electronic absorption and emission spectra recorded in basic aqueous solutions of methylated **HQC** derivatives is not obvious. The shape and relative intensity of the three lowest absorption bands of **H4MQC** in water are changed with the increase of pH from 7 to 13. The intensity of the second absorption band located at 30000 cm^{-1} decreases and the band disappears at pH = 13.5. The positions of the bands centered at 26300 cm^{-1} and 34300 cm^{-1} do not depend on the further increase of concentration of NaOH up to 8.6 mol/dm^3. Interestingly enough the lowest absorption band is shifted to the red of about 1600 cm^{-1} with respect to that of **H4MQ**. The decrease of the intensity of the absorption band at 30000 cm^{-1} is accompanied by an efficient quenching of the **NH** fluorescence (Fig. S.3.1, Chapter 7: Supporting information). At pH = 13.5 a new emission band appears. The

71

further increase of the concentration of NaOH causes the changes of the shape and the increase of intensity of this fluorescence. The similar effects are observed for **H2MQC** and **HDMQC** in basic aqueous and acetonitrile solutions. Most probably, the emission spectra in strongly basic aqueous solutions correspond to a product of a photoreaction (or a ground-state reaction) connected with the carbaldehyde group. The absorption spectra seem to be related to the anions (**A**) of the compounds (see below).

*Figure 3.14. Comparison of the room temperature normalized absorption spectra and corrected and normalized fluorescence spectra of **HMMQC** in neutral (in black) acetonitrile (c) and water at pH = 7 (d) with those recorded in strongly acidic (by adding HClO$_4$, in red) and basic (by adding about 8.6 mol/dm^3 NaOH, in green) acetonitrile and aqueous solutions. Black dotted curves correspond to the absorption and emission of **HMMQ** upon adding an amount of about 10^{-2} mol/dm^3 of HClO$_4$ to ACN. The concentrations of HClO$_4$ added to ACN and water are ~3.0 mol/dm^3 and ~9.1 mol/dm^3, respectively. Concentrations of the compounds are in the range from 10^{-5} to 10^{-4} mol dm^{-3}.*

The absorption spectrum of **HMMQC** in neutral aqueous solution at pH = 7 presented in Figure 3.14 is noisy due to a very low solubility of this compound in water. In spite of that, the appearance of the long-wave shoulder at about 25900 cm^{-1} clearly indicates the ground-state formation of the **NH** form. The single fluorescence band in water, similarly to that in

other solvents (Fig. 3.5), corresponds to the **NH** tautomer. The spectral positions of the absorption spectra of **HMMQC** in acidic solutions are similar to those of methyl derivatives of **HQC** (Table 3.9). Thus, the spectra are attributed to the protonated cations. The emission, however, both in strongly acidic acetonitrile and water solutions shows a huge Stokes shift of about 9600-9800 cm^{-1} and is assigned to the neutral **NH ↔ Z** form (even in such strong acidic medium as 60% HClO$_4$ solution in water). Noticeably, the absorption and emission spectra of **HMMQC** in acidic media, contrary to the similar absorption and emission spectra of the cations of **H4MQC** and **H4MQ**, differ from those of **HMMQ**. The location of the lowest absorption band of **HMMQC** in basic aqueous solutions at 26600 cm^{-1} is similar to that of the methyl derivatives of **HQC**. On the other hand, the emission spectrum of **HMMQC**, centered at 21900 cm^{-1}, is shifted to the blue of about 1400-2700 cm^{-1} with respect to those for the latter compounds. The spectral position of this low intense emission does not depend on the concentration of NaOH and is similar to that of the emission spectrum of the anion of **HMMQ**. Most probably, the absorption and emission spectra of **HMMQC** in basic aqueous solutions at pH varying from 11.5 to 14 correspond to the deprotonated anion (**A**).

The room temperature electronic absorption and fluorescence spectra of **HPQC** in various neutral, acidic and basic media are shown in Figure 3.15. In aqueous solutions at pH = 7 the dominant absorption band is situated at 24900 cm^{-1} and corresponds to the **NH** form. The single fluorescence band in water at 19600 cm^{-1} does not depend on excitation and originates from this tautomer. Although the absorption spectra of the cations and anions in aqueous solutions at pH $\cong$ 1-3 and at pH $\cong$ 12-14, respectively, are similar to those in acidic and basic (not shown) acetonitrile solutions, the different fluorescence spectra are observed in these media. Two luminescence bands (centered at 18800 cm^{-1} and about 23500 cm^{-1}) are observed in acidic acetonitrile solutions. Noticeably, the former band is located in the same spectral region as the **NH** fluorescence bands of **HPQC** in neutral acetonitrile and of **HMMQC** in aqueous solutions (Fig. 3.14), and the latter − in the emission region of the protonated cations (**C**) of **HQC** and its methylated derivatives (Fig. 3.13, Table 3.9). The mutual intensity of both bands strongly depends on the amount of 60% perchloric acid aqueous solution added to acetonitrile, at low concentration of water solution of HClO$_4$ the short-wave band is about 3 times more intense than the long-wave band (Fig. S.3.2, Chapter 7: Supporting information). On the other hand, **HPQC** in aqueous solutions at pH from 0 to 7 shows a single fluorescence band centered at about 19600-19800 cm^{-1}. Thus, similarly to **HMMQC**, this emission is attributed to the **NH ↔ Z** tautomer. Unexpectedly, the spectral

position of this emission shifts to 17500 cm^{-1} in 60% HClO$_4$ aqueous solution (Table 3.9). The spectral location of the second emission band at 23500 cm^{-1} in acidic acetonitrile solutions suggests its origin from the protonated cations (**C**).
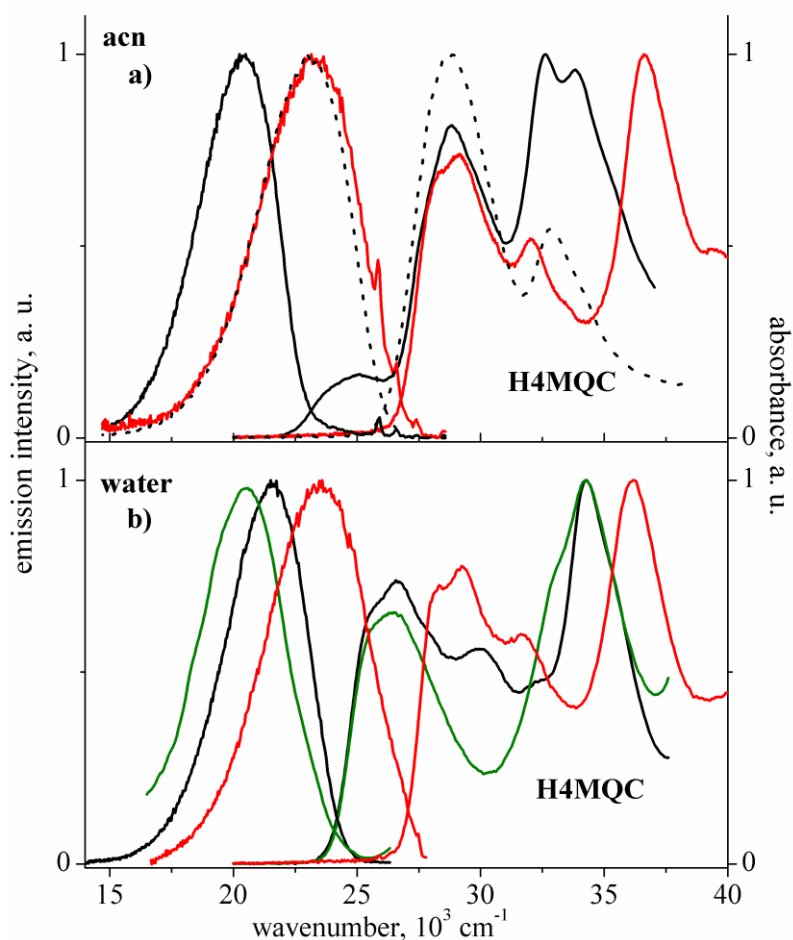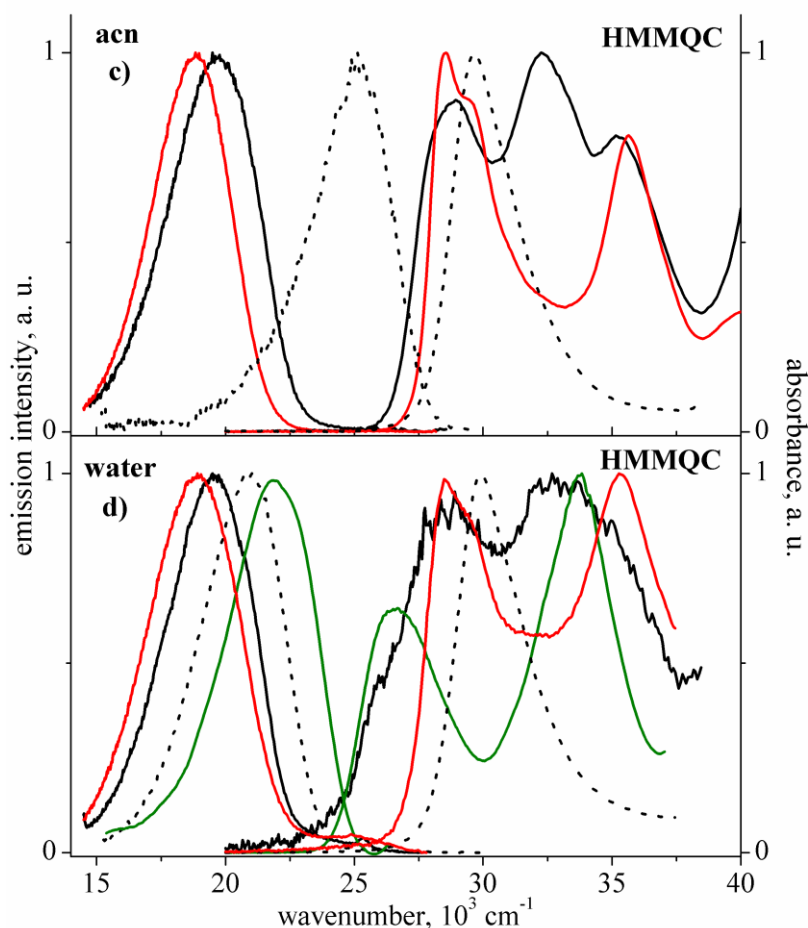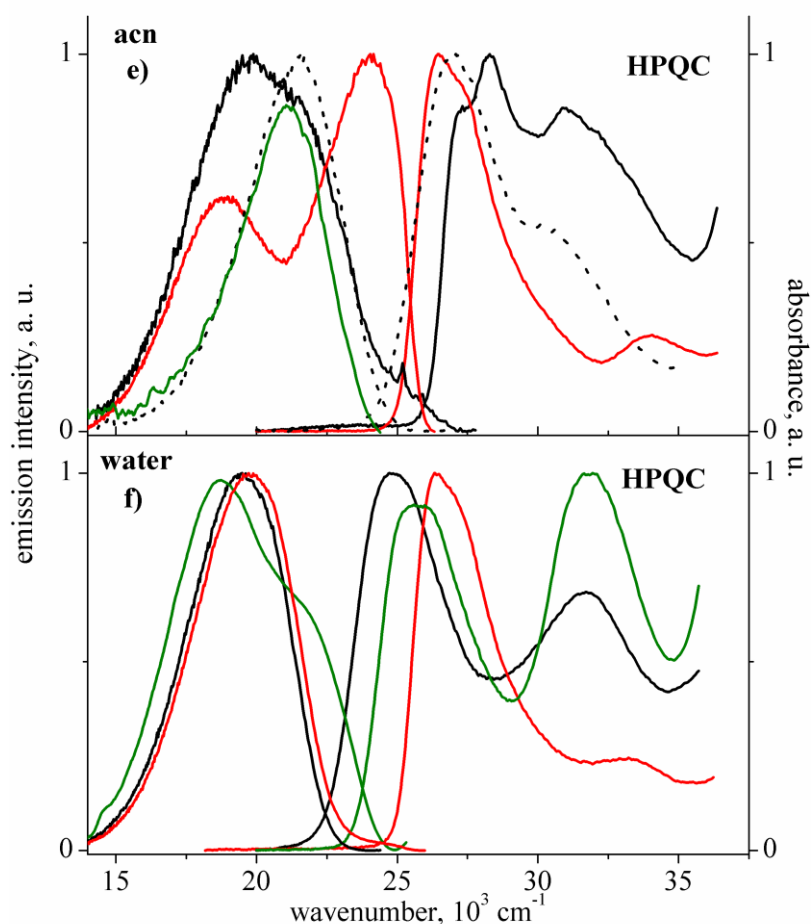

*Figure 3.15. Comparison of the room temperature normalized absorption spectra and corrected and normalized fluorescence spectra of **HPQC** in neutral (in black) acetonitrile (e) and water at pH = 7 (f) with those recorded in strongly acidic (by adding HClO$_4$, in red) and basic (by adding NaOH, in green) acetonitrile and aqueous solutions. Black dotted curves correspond to the absorption and emission of **HPQ** upon adding an amount of about 10^{-2} mol/dm^3 of HClO$_4$ to ACN. The concentrations of HClO$_4$ added to ACN and water are ~4.5 mol/dm^3 and ~3 mol/dm^3, respectively. The concentrations of NaOH added to ACN and water are ~0.03 mol/dm^3 and 8.6 mol/dm^3, respectively. Concentrations of the compounds are in the range from 10^{-5} to 10^{-4} mol dm^{-3}.*

The absorption spectra of **HPQC** in basic aqueous and acetonitrile (not presented) solutions show two bands located at 25700 cm^{-1} and 31800 cm^{-1} and are similar to those of the methyl derivatives of **HQC** and **HMMQC**. The spectra are attributed to the deprotonated anions (**A**). The very low intense emission centered at about 21100 cm^{-1} is observed in basic acetonitrile solutions containing NaOH ($c \approx 0.03$ mol/dm^3). The luminescence spectrum of **HPQC** in basic aqueous solutions depends on the concentration of NaOH. The single fluorescence band of the **NH** form is strongly quenched with the increase of the pH value up

to about 12. At pH $\cong$ 14 the new broad emission appears with the maximum centered at about 21400 cm^{-1}. Further increase of the concentration of NaOH up to 8.6 mol/dm^3, similarly to **H4MQC** (Fig. 3.13) and other methyl derivatives of **HQC** (Table 3.9), results in the appearance and growth of a new emission band located at about 18700 cm^{-1}. Most probably, the former emission, which is similar in basic acetonitrile and aqueous solutions, corresponds to the deprotonated anion (**A**) of **HPQC** and the latter to the product of a photoreaction (or a ground state reaction) connected with the carbaldehyde group.

The assignment of the absorption and emission spectra to the **OH** and **NH** forms of **H4MQC**, **HMMQC**, and **HPQC** as well as to their protonated cations (**C**) and deprotonated anions (**A**) allow us to determine the changes of pK_a values in the fluorescent state with the use of the "Förster cycle".[18,20] The estimated ΔpK_a values for various acid-base equilibria are collected in Table 3.10. The representatives of **7-HQCs**, similarly to **7-HQs**, show the increase of basicity of the quinoline nitrogen atom and the increase of acidity of the hydroxyl group upon excitation to the fluorescent state. The ratios of the concentrations of the neutral and ionic forms [**C**]/[**OH**], [**NH**]/[**C**], and [**NH**]/[**A**] increase upon excitation. This indicates the increase of the fraction of **NH** $\leftrightarrow$ **Z** tautomer in the excited state with respect to that in the ground state, what is indeed observed.

Table 3.10. The changes of pK_a (Δp$K_a = pK_a^* - pK_a^G$) upon $S_1 \leftarrow S_0$ excitation (estimated from eq. (2.12) with the use of the Förster cycle and the data collected in Table 3.9) of the equilibria between various neutral (NH $\leftrightarrow$ Z and OH) tautomeric forms and protonated cations (C) and deprotonated anions (A) of the representatives of 7-HQCs (see text for explanation). Concentrations of the compounds were in the range of 10^{-5}-10^{-4} mol/dm^3.

Solvent	Equilibrium	Ratio [a]	**H4MQC**	**HPQC**	**HMMQC**
ACN [b]	**C** $\rightleftharpoons$ **OH** + H$^+$	[OH]/[C] = K_a/[H$^+$]	1.0	$\geq$2.9 [e]	-
ACN [b]	**C** $\rightleftharpoons$ **Z** + H$^+$	[NH$\leftrightarrow$Z]/[C] = K_a/[H$^+$]	-7.0	-7.2	-
H$_2$O [c]	**C** $\rightleftharpoons$ **Z** + H$^+$	[NH$\leftrightarrow$Z]/[C] = K_a/[H$^+$]	-4.7	-	-
H$_2$O [d]	**Z** $\rightleftharpoons$ **A** + H$^+$	[NH$\leftrightarrow$Z]/[A] = [H$^+$]/K_a	-	~2.0	~3.1

[a] The ratio of the concentrations of the neutral and ionic forms.
[b] Protonation was achieved by adding about 0.1-3 mol/dm^3 of HClO$_4$.
[c] The pK_a changes are estimated for the 0-0 electronic transitions estimated from the absorption and fluorescence maxima in water at pH = 7 and in strongly acidic aqueous solutions obtained by adding 9 mol/dm^3 of HClO$_4$.
[d] The changes of pK_a are estimated for the 0-0 electronic transitions in water at pH = 7 and in strongly basic aqueous solutions obtained by adding 8.6 mol/dm^3 of NaOH.
[e] The value is estimated under the assumption that the maximum of the emission of the protonated cation is centered at 23500 cm^{-1} (Table 3.9).

3.5. Summary

The comparative studies of the spectroscopy and photophysics of the series of 7-hydroxyquinoline-8-carbaldehydes (**7-HQCs**) and 7-hydroxyquinolines (**7-HQs**), and their prototropic reactions allow us to understand the solvent dependent mechanism of the ground and excited-state long-range prototropic tautomerization.

The 7-quinolinol (**OH**) forms of all the studied 7-hydroquinolines (**7-HQs**), similarly to **7-HQ**, are dominant in the ground state in aprotic solvents and in alcohols. The compounds upon excitation show a single short-wave fluorescence band in aprotic solvents and two emission bands in alcohols. The long-wave band corresponds to the 7(1H)-quinolinone (**NH**) tautomer (its resonance hybrid is a zwitterionic species **Z**) created by the excited-state triple proton transfer in the hydrogen-bonded complexes of 1:2 stoichiometry. The appearance of the low-energy electronic absorption band located about 25000 cm^{-1} in aqueous solutions at pH = 7 prove the ground-state existence of the **NH** form for all the **7-HQs**, except for **HMMQ**. The investigations of the prototropic reactions in acidic and basic acetonitrile and water solutions show the ground-state formation of the protonated cations (**C**) and deprotonated anions (**A**). On the contrary, the fluorescence of the **C** and **A** ionic forms of the studied derivatives of **7-HQ** is observed only in very strong acids (60% HClO$_4$) or bases (c_{NaOH} = 8.6 mol/dm^3); in the range of pH between 1 and 13 only the emission of the **NH** form is observed. The electronic excitation leads to the deprotonation of the cations and protonation of the anions to yield a **Z** $\leftrightarrow$ **NH** form (Scheme 3.3).
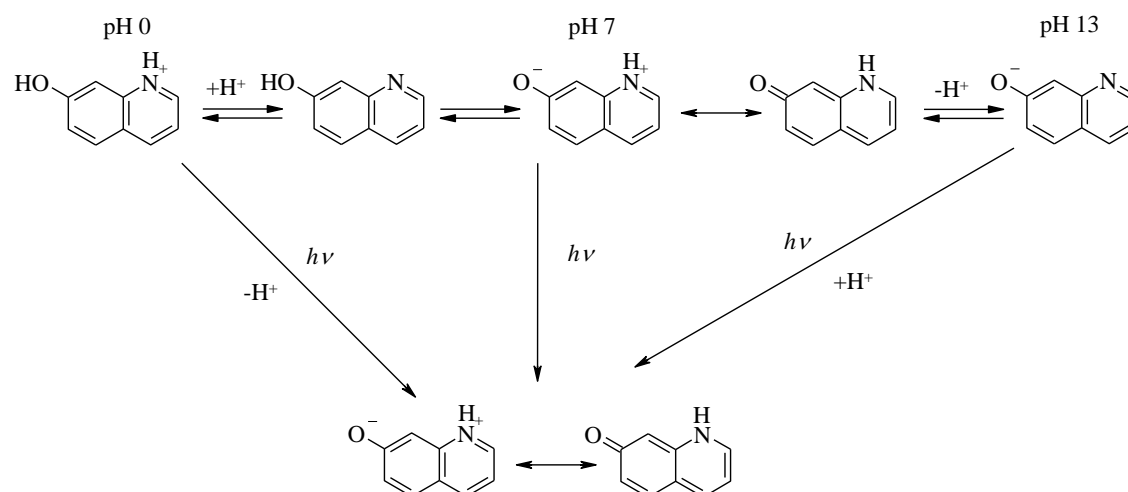
*Scheme 3.3. Neutral and ionic forms of **7-HQs** in the ground state (top) and upon excitation (bottom) in the range of pH from 0 to 13.*

The NMR and electronic absorption investigations prove the presence of the **OH** and **NH** tautomers in the ground state for all the studied **7-HQCs**, except for **HMMQC**. The fraction of the **NH** form increases with the increase of polarity and hydrogen bond donor ability of the surrounding environment. The comparison of the dependence of the electronic absorption spectra on the solvent properties with the results of NMR investigations allows us to assign the long-wave band at about 25000 cm^{-1} to the **NH** tautomer. **HMMQC** does not show any trace of this band (except aqueous solutions) and exists in the ground state nearly exclusively as the **OH** tautomer.

For all the studied **7-HQCs**, except for **HPQC**, the dominant fluorescence in aprotic media and in alcohols can be attributed to the $^1(\pi,\pi^*)$ excited state of the **NH** tautomer. This is confirmed by direct excitation of this tautomer and by the comparison with the emission of the protonated cations and deprotonated anions. The multiple, solvent and excitation dependent, fluorescence of **HPQC** most probably originate from: (i) the **OH** tautomer (~23300-23600 cm^{-1}), (ii) the intermediate transient product **IIa** or **IIb** (Scheme 1.14) of the excited state intramolecular proton transfer, ESIPT (~21500 cm^{-1}), and (iii) the **NH** tautomer (~19200-19700 cm^{-1}) which in part originates from the ground state and in part is formed in the excited state *via* ESIPT processes. The fluorescence of **HQC** and its methyl derivatives, **H2MQC**, **H4MQC** and **HDMQC**, in nonpolar and low polarity media show two emission bands assigned to the **OH** tautomer (~24000-24500 cm^{-1}) and to the **NH** tautomer (~20500-21000 cm^{-1}). The single emission band of **HMMQC**, observed about 19800-20900 cm^{-1} is attributed to the **NH** tautomer which is formed *via* ESIPT process. The different luminescent properties of **HMMQC** with respect to **HPQC** (and the other **7-HQCs**) are probably due to the smaller height of the energy barrier on the excited state path from the **OH** tautomer to the **NH** tautomer in the former and the resulting faster ESIPT process with respect to the latter. **HMMQC** seems to be a good model to study dynamics and kinetics of the excited state tautomerization process due to the fact that the **OH** tautomer (which is a substrate of the photoreaction) is a major form of the compound in the ground state.

The mechanism of the excited state tautomerization of **7-HQCs** in aprotic media seems to involve two irreversible adiabatic proton transfer processes connected with a twist of a proton "crane", as proposed by Varma and coworkers.[163] The electronic excitation of the form **OH** induces proton transfer along the hydrogen bond resulting in the structure **IIa** (Scheme 1.14).[164] The next step, which involves twisting around a single covalent bond connecting the 7-hydroxyquinoline moiety with carbaldehyde group, leads to the form **IIb**. The second PT process results in the tautomeric form **NH**. The intermediate structures **IIa** and

IIb are not stable in the ground state. This interpretation is corroborated by the results of the excitation dependence of the quantum yield investigations of **H2MQC**. However, the time-resolved nano- and picosecond[233] fluorescence investigations of **HMMQC** in such a strongly viscous medium as paraffin do not show any measurable rise of the **NH** fluorescence. Most probably, the excited state process is too short to be measured with the resolution of about 10-15 ps. The very efficient radiationless depopulation of the fluorescent states of **7-HQCs** is in agreement with the theoretical *ab initio* computations predicting the conical intersection on the route of the ESIPT process under vacuum conditions.[164-166]

In water and alcohol solutions, however, the mechanism of ESIPT reaction in **7-HQCs** seems to involve the additional reactions producing various hydrates (Scheme 3.4) or hemiacetals, respectively, which are in dynamic equilibria with the **OH** and **NH** tautomers. In such excited supermolecules the water or alcohol molecules may act as a proton-relay system which can efficiently transform the **OH** tautomer into the **NH** tautomer. The driving force for the ESIPT reaction is the increase of acidity of the hydroxyl group and the increase of basicity of the quinoline nitrogen atom upon electronic excitation. The results of our investigations of the prototropic reactions in acidic and basic acetonitrile and water solutions of **7-HQCs** indicate, similarly to **7-HQs** (Scheme 3.3), a shift towards the **NH** form upon excitation and prove the opposite pK_a tendencies of the acidic and basic centers of the compounds.
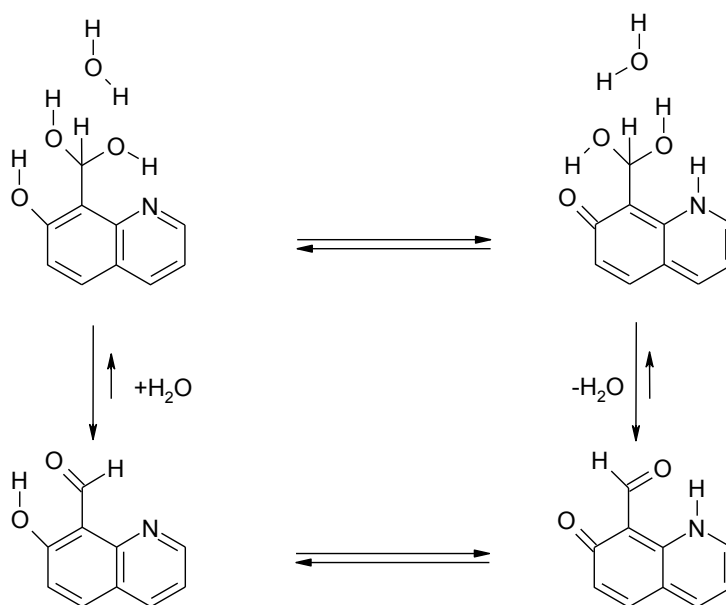
*Scheme 3.4. Hypothetical dynamic equilibria between 7-quinolinol (**OH**) and 7(1H)-quinolinone (**NH**) tautomers of **HQC** and respective hydrates in aqueous solutions.*

Finally, it should be stressed that the studied **7-HQCs**, except **HMMQC**, are not photostable. The UV irradiation of these compounds results in the photoproducts which emit short-wave fluorescence. One of the possible reactions, similarly to benzaldehyde,[234,235] is a decomposition of the particular **7-HQC** compound into respective **7-HQ** molecule and carbon monoxide. The preliminary NMR investigations of **HPQC** in CD$_3$CN, however, do not show any trace of **HPQ** upon intensive irradiation at 254 nm. On the other hand, the disappearance of the absorption and fluorescence bands of **HPQC** in acetonitrile under the same irradiation conditions is followed by the appearance of the bands characteristic for **HPQ**.

Chapter 4: Rotamerization and photoinduced tautomerization in 2-(1H-pyrazol-5-yl)pyridines (2-PPs)

4.1. Introduction. Rotameric/tautomeric forms of 2-PPs

This chapter presents the results of quantum chemical computations and stationary and time resolved UV-Vis spectroscopic investigations of solvent-dependent rotamerization and photoinduced tautomerization in 2-(1*H*-pyrazol-5-yl)pyridines (**2-PPs**). These interesting compounds are composed of pyrazole and pyridine moieties linked by a single bond (Scheme 4.1). The series contains a parent compound 2-(1*H*-pyrazol-5-yl)-pyridine (**PPP**) and three its derivatives: 2-(3-methyl-1*H*-pyrazol-5-yl)-pyridine (**MPP**), 2-(4-bromo-1*H*-pyrazol-5-yl)-pyridine (**BPP**), and 2-(4-nitro-1*H*-pyrazol-5-yl)-pyridine (**NPP**). This group of compounds was especially synthesized to study the effects of withdrawing (Br, -NO$_2$) or electron donating (-CH$_3$) substituents on the spectroscopy, photophysics, and photochemistry of **2-PPs**.
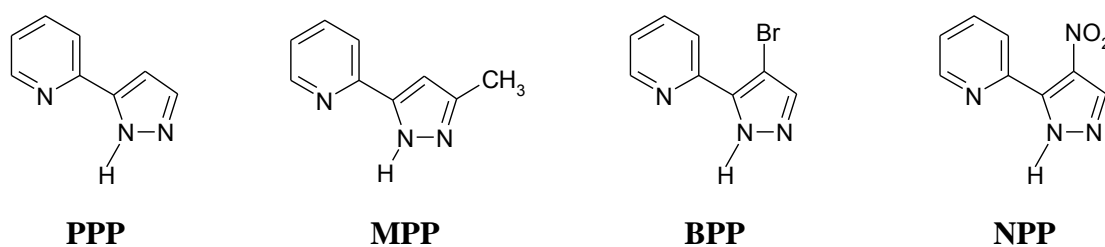
Scheme 4.1. Formulas and acronyms of investigated 2-(1H-pyrazol-5-yl)pyridines.

These molecules contain both a hydrogen bond (HB) donor (the pyrazole NH group) and a HB acceptor (the pyridine nitrogen atom) in separate moieties which can undergo an internal rotation around a single bond to form various rotameric structures. The hydrogen bonding centers of the pyrazole-pyridine family can be located either on the same or on the opposite sides of the molecule. These positions correspond to the *syn* and *anti* conformers, respectively. Moreover, a presence of the second nitrogen atom in the pyrazolic ring makes possible the existence of two other rotameric forms (*syn1* and *anti1*). Taking into account two tautomeric structures, *taut* and *taut1*, there are six different isomeric forms of each compound under study. As an example, DFT/B3LYP/6-31+G(d,p) optimized ground-state geometries of these forms of **PPP** are presented in Scheme 4.2.

syn   *syn1*

anti   *anti1*

taut   *taut1*
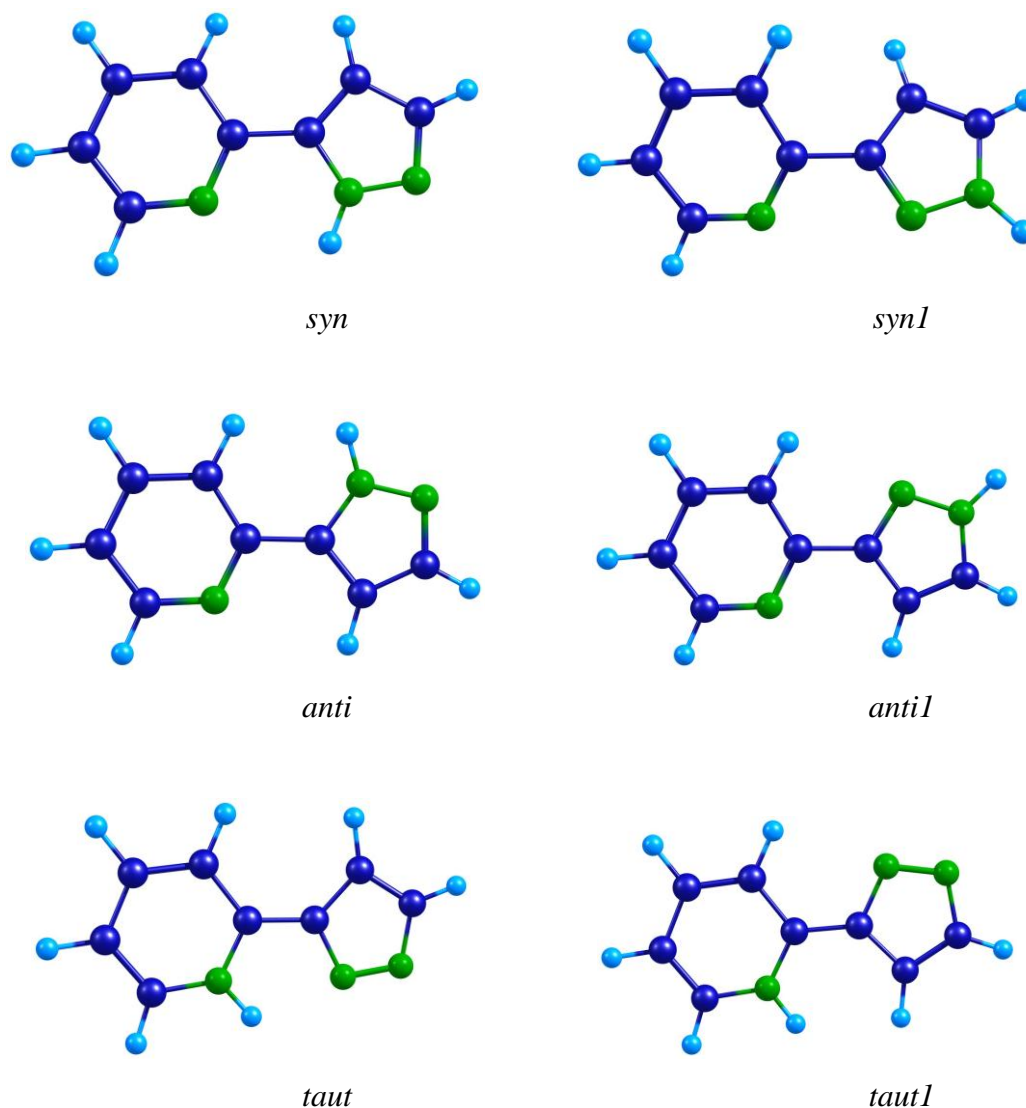
*Scheme 4.2. DFT/B3LYP/6-31+G(d,p) computed ground-state molecular structures of **PPP**.*

According to previous theoretical and experimental NMR and IR investigations in solutions, the *syn* form is the major form in the ground state of **PPP**, **MPP**, **BPP**, and **NPP**.[187] IR experiments in dichloromethane show only one N-H absorption band at about 3400 cm^{-1} for all the compounds (except for **MPP** which reveals also the second band at 3511 cm^{-1}) assigned to the *syn* form. Our DFT calculations, performed in order to estimate the relative stability of possible structures, support this hypothesis. The dominant species under vacuum isolation conditions corresponds to the planar *syn* form with hydrogen attached to the nitrogen atom of the pyridine ring. Relative energies of the ground and first excited electronic states are presented in Fig. 4.1. The stabilization of the *syn* rotamer is significant (*ca*. 5 kcal/mol) for **BPP** and **NPP** derivatives, whereas for **PPP** and **MPP** this isomer is separated by about 1.5 kcal/mol from the next, energetically higher one, which is the *anti1* form.

81
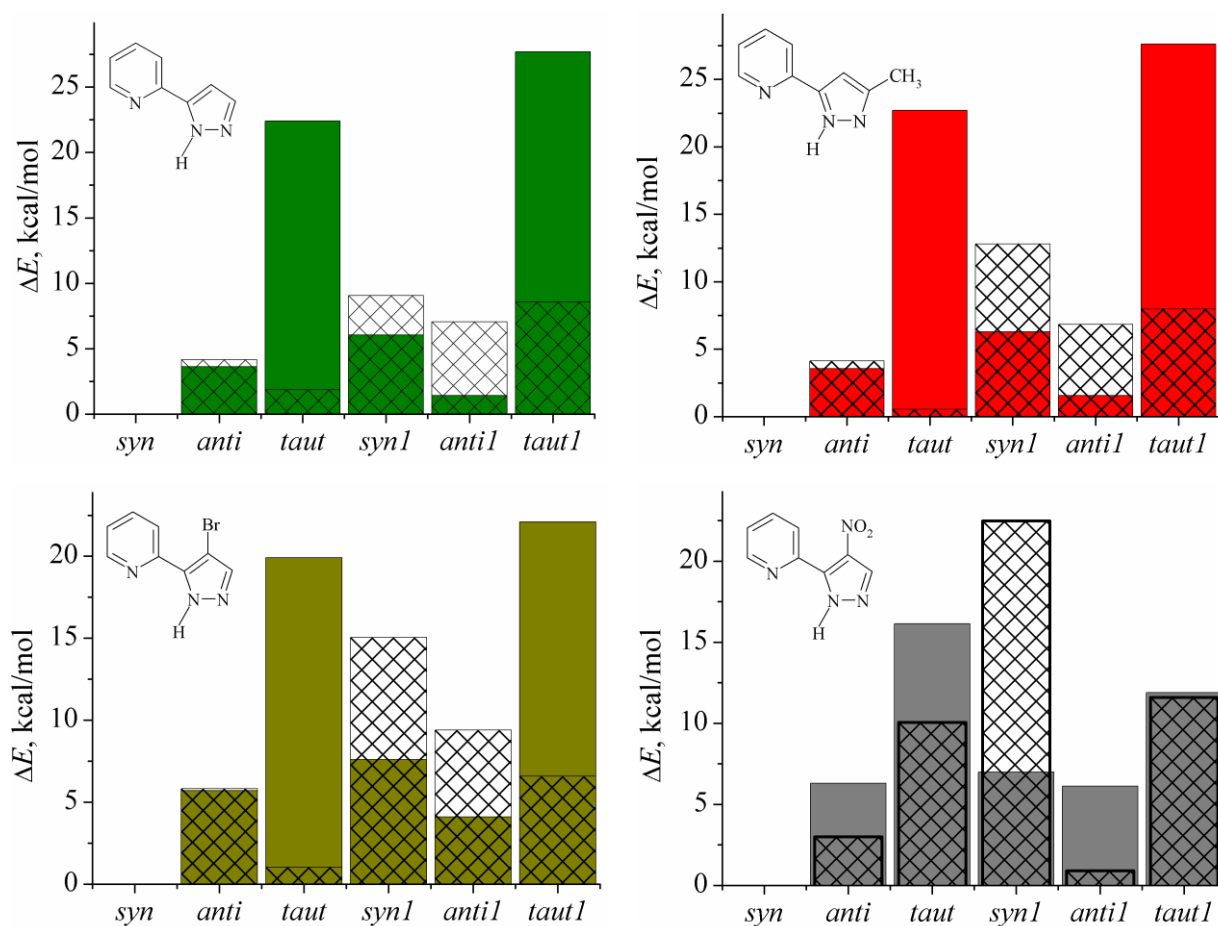
Figure 4.1. DFT/B3LYP/6-31+G(d,p) and CIS/B3LYP/6-31+G(d,p) computed relative energies of
***PPP** (green), **MPP** (red), **BPP** (yellow), and **NPP** (grey) isomers in the ground (colored) and first*
excited (patterned) states at the equilibrium geometries.

The CIS computations predict a significant stabilization of the *taut* form for **PPP**, **MPP**, and
BPP upon electronic excitation. The energy gap between the *syn* and *taut* forms in the S_1 state
of the $^1(\pi,\pi^*)$ nature lowers to 0.5 kcal/mol for **MPP**, 1 kcal/mol for **BPP**, and 1.9 kcal/mol
for **PPP**. On the contrary, the *anti1* form of **NPP** is markedly stabilized in the S_1 state.

*Table 4.1. Ground-state dipole moments (in Debyes) of the isomeric forms of **PPP, MPP, BPP**, and*
***NPP** at the equilibrium geometry calculated with the DFT/B3LYP/6-31+G(d,p) method.*

Compound	*syn*	*syn1*	*anti*	*anti1*	*taut*	*taut1*
PPP	4.1	2.9	3.7	1.6	8.5	9.6
MPP	3.7	3.5	3.2	2.0	7.8	8.9
BPP	3.7	1.7	4.5	2.6	8.6	9.0
NPP	5.5	3.4	6.8	5.2	10.3	9.2

The DFT calculated ground-state dipole moments μ_G are collected in Table 4.1. The
values of μ_G of both tautomeric forms of all the compounds under study as well as of the *anti*

forms of **BPP** and **NPP** are higher with respect to those of the *syn* forms. Thus, the former forms are expected to be stabilized in polar solvent. On the other hand, the μ_G values of the *anti1* forms are markedly lower than those of the *syn* ones. In spite of this fact, the *anti1* rotamer is relatively stabilized in a highly polar environment (*e.g.*, in acetonitrile) and its ground-state fraction significantly increases from 0.09 to 0.26 for **PPP**, from 0.07 to 0.37 for **MPP**, and from 0.00 to 0.07 for **BPP** (Table 4.2). The calculations predict for these compounds at room temperature only a small fraction of about 1-4% of the other ground state rotameric forms in aprotic polar media due to the relatively high energies of the *syn1* and *anti* forms. For **NPP**, however, the increase of the solvent polarity leads to significant fractions of *anti*, *anti1*, and *syn1* forms: 0.16, 0.14, and 0.11, respectively.

*Table 4.2. B3LYP/6-31G(d,p)/ZPE relative energies (in kcal/mol) and estimated fractions (f_{est})[a] of the various forms of **PPP, MPP, BPP,** and **NPP,** either under vacuum isolation conditions or in acetonitrile, ACN.[b] [181]*

Compound		*syn*		*syn1*		*anti*		*anti1*	
		energy	f_{est}	energy	f_{est}	energy	f_{est}	energy	f_{est}
PPP	vacuum	0.00	0.91	6.05	0.00	3.58	0.00	1.37	0.09
	ACN	0.00	0.68	2.11[a]	0.02	1.63[a]	0.04	0.57[a]	0.26
MPP	vacuum	0.00	0.93	6.27	0.00	3.55	0.00	1.56	0.07
	ACN	0.00	0.57	1.79[a]	0.03	1.57[a]	0.04	0.26[a]	0.37
BPP	vacuum	0.00	1.00	7.60	0.00	5.70	0.00	4.01	0.00
	ACN	0.00	0.92	2.86[a]	0.01	2.70[a]	0.01	1.56[a]	0.07
NPP	vacuum	0.00	1.00	7.00	0.00	6.30	0.00	6.12	0.00
	ACN	0.00	0.59	1.00[a]	0.11	0.79[a]	0.16	0.86[a]	0.14

[a] According to the Boltzmann distribution. [b] The Polarizable Continuum Model (PCM) is used.[227,228]

The vertical excitation energies ($\tilde{\nu}$, in cm^{-1}), oscillator strengths (*f*), and main electronic configurations (MEC) corresponding to the three lowest transitions for the *syn* rotameric forms of **PPP** and **NPP** (as representatives for the series) are presented in Table 4.3. The shapes of molecular orbitals involved in the low-lying vertical transitions at the equilibrium geometry of **PPP** are shown in Fig. 4.2 (the molecular orbitals of **MPP** and **BPP** are very similar to those of **PPP**). The order of the computed transitions (the lowest one corresponds to HOMO − LUMO excitation, the second transition to HOMO - LUMO+1, and the third one to HOMO-2 − LUMO) and the $\tilde{\nu}$ values are very similar for **PPP**, **MPP**, and

BPP. The first two transitions of the $^1(\pi,\pi*)$ nature carry high oscillator strength. The calculations predict a very close proximity of $^1(\pi,\pi*)$ and $^1(n,\pi*)$ states for all the **2-PPs** (**NPP** was not simulated) (Fig.4.3). Noticeably, the computed lowest-energy transitions for *syn* and *anti1* forms of **NPP** are markedly shifted to lower energy. Due to the lack of the planar structure of the *anti1*, *syn1*, and *anti* forms of **NPP** the strict distinction between $^1(\pi,\pi*)$ states and $^1(n,\pi*)$ states is not possible.

HOMO
LUMO

HOMO
LUMO+1

HOMO-2
LUMO

*Figure 4.2. Shapes of molecular orbitals of the syn rotameric form of **PPP** involved in low-lying transitions.*

*Table 4.3. TD-DFT/B3LYP/6-31+G(d,p) calculated energies ($\tilde{\nu}$), oscillator strengths (f) and main electronic configurations (MEC) corresponding to transitions to the low-lying excited singlet states of the syn forms of **PPP** and **NPP**.*

Compound	State	$\tilde{\nu}$, cm^{-1}	f	MEC	
PPP	S$_1$	35690	0.277	HOMO – LUMO	$\pi\pi^*$
	S$_2$	37940	0.220	HOMO – LUMO+1	$\pi\pi^*$
	S$_3$	38530	0.002	HOMO-2 – LUMO	$n\pi^*$
NPP	S$_1$	29760	0.000	HOMO-3 – LUMO HOMO-1 – LUMO	$n\pi^*$
	S$_2$	30930	0.224	HOMO – LUMO	$\pi\pi^*$
	S$_3$	34460	0.001	HOMO-1 – LUMO	$n\pi^*$
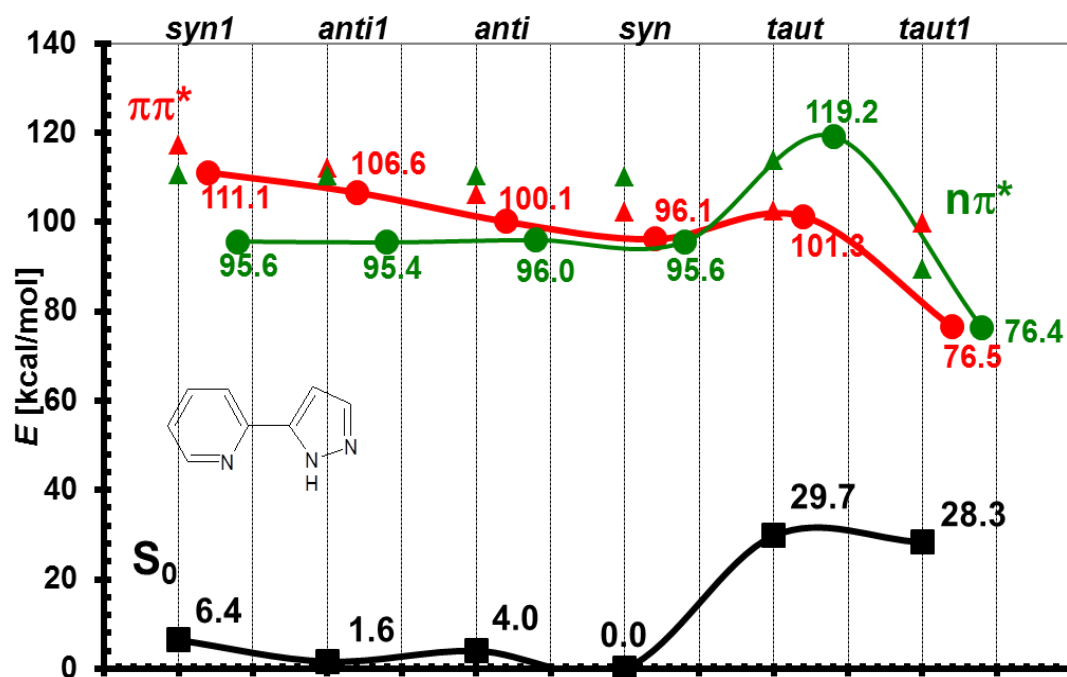
*Figure 4.3. TD-DFT/B3LYP/6-31+G(d,p) computed energies of the ground (black squares) and the lowest excited $^1(\pi,\pi^*)$ (red) and $^1(n,\pi^*)$ (green) states of the isomeric forms of **PPP**. Big circles connected with the lines correspond to the excited states of optimized geometry, small triangles – to vertical transitions.*

4.2. Electronic absorption. Experiments and calculations

Room-temperature electronic absorption spectra of the compounds under study recorded in nonpolar (*n*-hexane), polar aprotic (acetonitrile) and polar protic (1-propanol) solutions are presented in Fig. 4.4. The spectra for **PPP**, **MPP**, and **BPP** are similar and contain two bands between 30000 cm^{-1} and 50000 cm^{-1}. The two lowest energy absorption band maxima in *n*-hexane are located at 34780 cm^{-1} and 39060 cm^{-1}, 34600 cm^{-1} and 38540 cm^{-1}, 34660 cm^{-1} and 39140 cm^{-1} for **PPP**, **MPP**, and **BPP**, respectively, while for **NPP** they are approximately 1500 cm^{-1} red-shifted (Table 4.4). Moreover, in this spectral region **NPP** shows a third band at 44050 cm^{-1}.
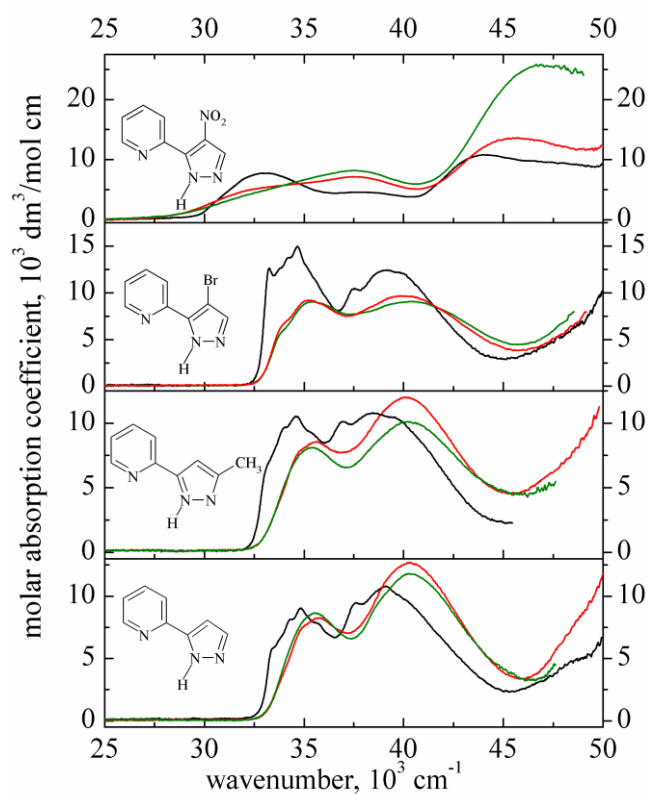
Figure 4.4. Absorption spectra in n-hexane (black), acetonitrile (red) and 1-propanol (green).

*Table 4.4. Comparison between vertical TD-DFT excitation energies ($\tilde{v}_{\text{TDDFT}}$, in 10^3 cm^{-1}) of the low-lying $^1(\pi,\pi^*)\leftarrow S_0$ transitions and oscillator strengths (f) for various forms of the studied **2-PPs** (the energies of the low lying $^1(n,\pi^*)\leftarrow S_0$ excitations are not included in the Table), as well as the locations of the experimental bands ($\tilde{v}_{\text{exp}}$, scatter of results: $\pm$ 150 cm^{-1}) and molar absorption coefficients (ε, in dm^3/mol cm, error ~5%) of the near-UV absorption band maxima in n-hexane.*

Compound	form		TD-DFT/B3LYP/6-31+G(d,p)			Experimental	
			$\tilde{\nu}_{\text{TDDFT}}$ [a]	f	μ [b]	$\tilde{\nu}_{\text{exp}}$	ε
PPP	*syn*	S_0			4.1		
		S_1	35.69	0.2769	3.5	34.78	10800
		S_2	37.94	0.2197	2.8	39.06	12770
		S_3	40.19	0.0203	4.4		
	anti1	S_0			1.6		
		S_1	38.63	0.2272	5.4		
		S_2	40.45	0.1990			
		S_3	42.59	0.0107			
MPP	*syn*	S_0			3.7		
		S_1	35.24	0.2859	5.8	34.60	10880
		S_2	37.21	0.0988		38.54	11160
		S_3	38.22	0.1592			
	anti1	S_0			2.0		
		S_1	38.31	0.2323	7.0		
		S_2	39.94	0.1971			
		S_3	40.83	0.0084			
BPP	*syn*	S_0			3.7		
		S_1	34.88	0.2879	4.7	34.66	12940
		S_2	37.95	0.0247		39.14	10770
		S_3	38.78	0.1615			
	anti1	S_0			2.6		
		S_1	37.49	0.2224	8.1		
		S_2	39.36	0.0225			
		S_3	41.32	0.1813			
NPP	*syn*	S_0			5.5		
		S_1	30.93	0.2238	10.3	33.11	10350
		S_2	37.24	0.1227		37.59	5920
		S_3				44.05	14500
	anti1 [c]	S_0			5.2		
		S_1	32.48	0.0476	12.8		
		S_2	39.57	0.0626			
	syn1 [c]	S_0			3.4		
		S_1	29.29	0.0175	6.5		
		S_2	31.62	0.0183			
		S_3	38.43	0.0593			
	anti [c]	S_0			6.8		
		S_1	34.51	0.0308	9.1		
		S_2	31.62	0.0183			
		S_3	38.43	0.0593			

[a] B3LYP/6-31+G(d,p) optimised ground-state conformations are used as input geometries. [b] Dipole moments in debyes, D. [c] Due to the lack of the planar structure of the *anti1*, *syn1*, and *anti* forms of **NPP** the strict distinction between $^1(\pi,\pi^*)$ states and $^1(n,\pi^*)$ states is not possible. Only transitions of significant intensity are shown.
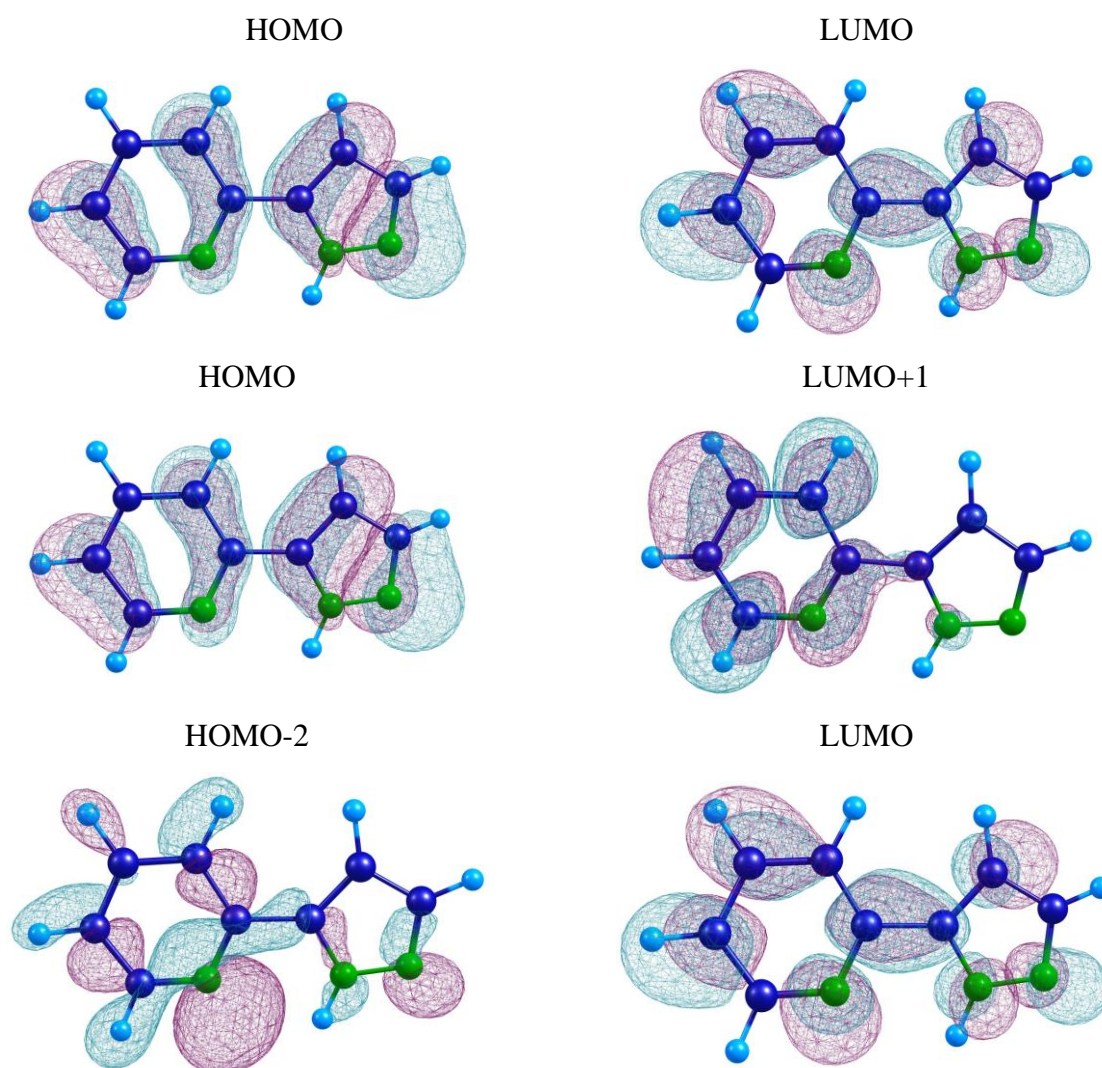
The TD-DFT/B3LYP/6-31+G(d,p) computed energies of transitions to the low-lying excited $^1(\pi,\pi^*)$ states of the *syn* tautomers of **PPP**, **MPP**, and **BPP** are in an excellent agreement with the experimentally measured absorption maxima (Table 4.4); the largest discrepancies do not exceed 1300 cm^{-1} for the $S_1 \leftarrow S_0$ and $S_i \leftarrow S_0$ transitions (i = 2 or 3 correspond to the computed transitions carrying higher oscillator strengths). The discrepancy for the lowest energy transition for **NPP** is about 2200 cm^{-1}. In agreement with experimental observations, the calculated spectral positions and oscillator strengths f_1, f_2, and f_3, of the three lowest $^1(\pi,\pi^*) \leftarrow S_0$ vertical transitions lead to the higher relative intensity of the first computed absorption band for the *syn* forms of **NPP** and **BPP** than for **PPP** and **MPP** (Fig. S.4.1, Chapter 7: Supporting Information).

The increase of solvent polarity and HB donor ability shifts the low-lying bands of **PPP**, **MPP**, and **BPP** to the blue part of the spectrum by about 1000 cm^{-1}. Moreover, the decrease of the relative intensity of the lowest absorption band with respect to the second one is observed (the most prominent effect is observed for **NPP**, Fig. 4.4. and Table 4.5).

Table 4.5. The ratios of the molar absorption coefficients $\varepsilon_1/\varepsilon_2$ of the two lowest absorption bands of ***2-PPs*** *(in brackets the values of $\varepsilon_1/\varepsilon_2$ which correspond to the lowest energy shoulders for* ***NPP****) and estimated (eq.2.8) absorption transition dipole moments (M_{abs}, in D) of the lowest absorption bands.[a]*

	HEX		ACN		1-PrOH	
	$\varepsilon_1/\varepsilon_2$	M_{abs}	$\varepsilon_1/\varepsilon_2$	M_{abs}	$\varepsilon_1/\varepsilon_2$	M_{abs}
PPP	0.8	2.3	0.6	2.3	0.7	2.7
MPP	1.0	2.6	0.8	2.8	0.8	2.4
BPP	1.2	3.1	1.0	2.4	1.0	2.5
NPP	1.7	2.6	(*ca.* 0.5)		(*ca.* 0.7)	

[a] Error is about 10%.

The latter finding is opposite to that expected on the basis of interactions between close lying $^1(\pi,\pi^*)$ and $^1(n,\pi^*)$ states (the "proximity effects").[70] The vertical transitions to the lowest $^1(n,\pi^*)$ states are computed to lie higher than those to the lowest $^1(\pi,\pi^*)$ states of about 2800 cm^{-1}, 3300 cm^{-1}, and 3300 cm^{-1} for the *syn* forms of **PPP** (Fig. 4.3), **MPP**, and **BPP**, respectively. The increase of solvent polarity and HB donor ability should destabilize the $^1(n,\pi^*)$ states (which carry a very low oscillator strength) with respect to the $^1(\pi,\pi^*)$ states. Thus, contrary to the experimental observations (Table 4.4), the considerable increase of the electronic transition dipole moments M_{abs} corresponding to the lowest absorption excitations in **2-PPs** is expected in polar and protic media. The most plausible explanation involves the

solvent-dependent co-existence of various tautomeric forms of **2-PPs** in the ground state. The DFT and TD-DFT computations at the B3LYP/6-31+G(d,p) level support this hypothesis. The increase of the solvent polarity should result in an appearance and rise of the fraction of the *anti1* tautomer of **PPP**, **MPP**, and **BPP** as well as the *anti*, *anti1*, and *syn1* forms of **NPP** (Table 4.2). The calculations predict, in agreement with the experimental findings, that the lowest absorption transitions for the *anti1* forms of **PPP**, **MPP**, and **BPP** should be considerably blue-shifted, by about 2600-3000 cm^{-1} with respect to those of the *syn* forms (Table 4.4). Figure 4.5 representatively demonstrates the comparison between the computed absorption spectra for the *syn* and *anti1* forms of **PPP** and the experimental spectrum.
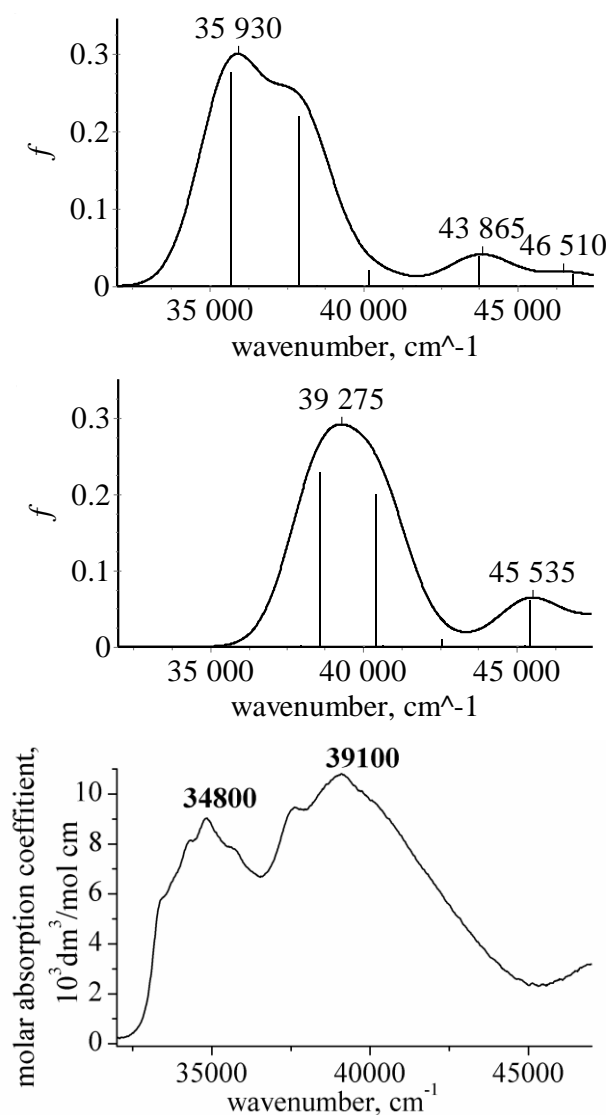
*Figure 4.5. Comparison of the electronic absorption spectra of syn (upper) and anti1 (middle) rotameric forms of **PPP** computed at the TD-DFT/B3LYP/6-31+G(d,p) level for the DFT/B3LYP/6-31+G(d,p) geometry (the spectral envelopes are obtained by convolution of the respective stick spectra with a Gaussian function of 2400 cm^{-1} FWHM) with the spectrum recorded in n-hexane (bottom).*

The computed spectrum of the *syn* form shows two broad bands at about 35900 cm^{-1} and 37800 cm^{-1} of similar intensity and a much weaker band at 43900 cm^{-1}. The computed spectrum of the *anti1* form reveals a strong band (corresponding to two vertical transitions) at *ca*. 39300 cm^{-1} and a weak band at *ca*. 45600 cm^{-1}. Thus, the hypothesis of the co-existence of both forms in the ground state is in a very good agreement with the observed solvent effects on the experimental spectrum; the increase of the fraction of the *anti1* tautomer is predicted to increase the relative intensity of the second absorption band with respect to the lowest one. For **NPP**, the oscillator strengths corresponding to the lowest $S_1 \leftarrow S_0$ transitions for the *anti*, *anti1*, and *syn1* forms are computed to be about one order of magnitude lower than that for the *syn* rotamer (Table 4.4). The appearance of these forms should lead to the dramatic decrease of the intensity of the lowest absorption band for **NPP**, which is indeed observed.

Moreover, the calculations for the *syn* forms predict that, upon excitation to the lowest $^1(\pi,\pi^*)$ state, the dipole moment decreases (**PPP**) or increases (**MPP, BPP**) (Table 4.1) and its direction is nearly reversed (Figs. 4.6 and S.4.2, Chapter 7: Supporting Information). Such a situation, in agreement with the experimental observations, should lead to a blue shift of the lowest absorption band of **PPP**, **MPP**, and **BPP** in polar solvents.
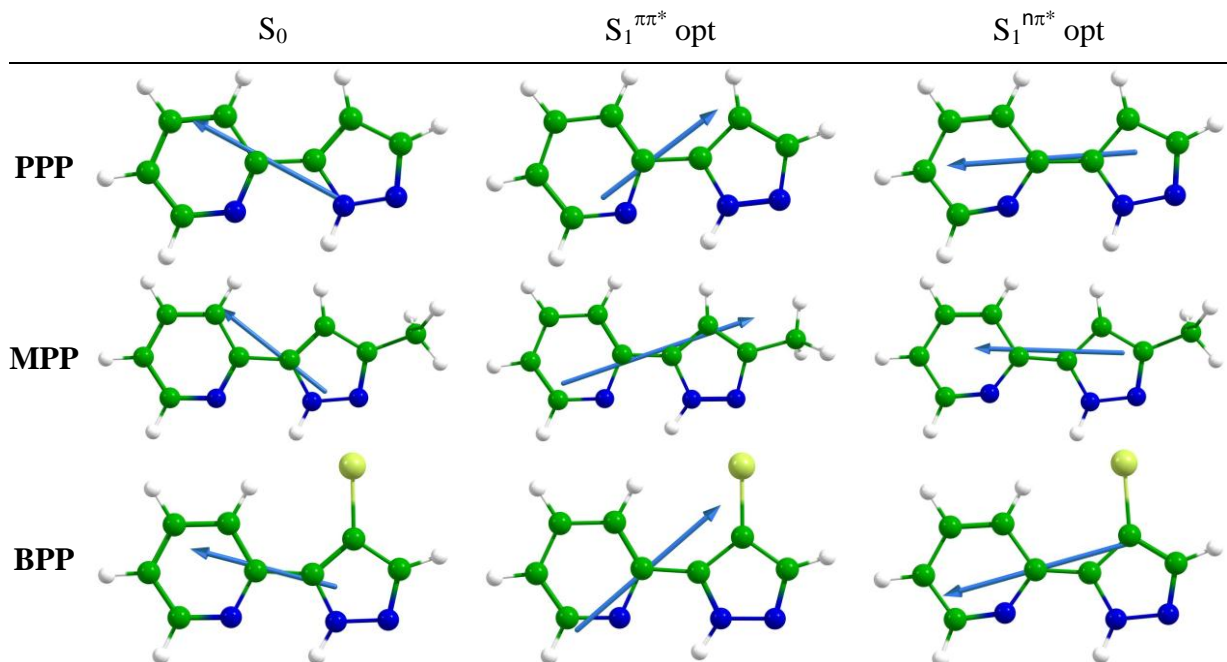
*Figure 4.6. DFT and TD-DFT computed (at the level B3LYP/6-31+G(d,p))[181] ground-state and the lowest $^1(\pi,\pi^*)$ and $^1(n,\pi^*)$ excited-state dipole moments of the syn forms of **PPP, MPP,** and **BPP**.*

4.3. Emission, excitation, and spectrophotometric titration

Room temperature fluorescence spectra of **PPP**, **MPP**, and **BPP** recorded in nonpolar (*n*-hexane), medium polar aprotic (ethyl acetate), strongly polar aprotic (acetonitrile) and polar protic (1-propanol, water) solutions are presented in Figure 4.7. The compounds show dual luminescence in *n*-hexane, 1-PrOH, and water: the dominant short-wave fluorescence is accompanied by a second band (or a long tail in aqueous solutions) of a very weak intensity, which appears at much lower energies. The short-wave emission band is located at about 31500 cm^{-1} (**PPP** and **BPP**) and 31100 cm^{-1} (**MPP**) in *n*-hexane and shows a red shift in polar (*ca.* 500-900 cm^{-1}) and protic (*ca.* 1000-2000 cm^{-1}) solvents. On the other hand, the shifts between the maxima of the two emissions vary from about 10000-11000 cm^{-1} for **PPP** and **BPP** to about 12000-14000 cm^{-1} for **MPP** in *n*-hexane and 1-PrOH, respectively. In highly polar aprotic media, such as ACN, only a trace of the low-energy band is observed.

The short-wave fluorescences of **MPP** and **PPP** exhibit similar responses to a change from aprotic to protic solvents: the values of the quantum yields Φ_f significantly increase in alcohols and water (Table 4.6). The emission quantum yields of studied compounds are quite low indicating the high efficiency of non-radiative processes (Table 4.9). Interestingly, the emission intensity for **PPP** and **MPP** increases with the increase of HB donor ability of a surrounding medium (the most efficient fluorescence is observed in aqueous solutions). The Φ_f values of the dominant emission for **MPP** (varying with the solvent from $8 \cdot 10^{-3}$ in ACN to $4.5 \cdot 10^{-2}$ in H$_2$O) and **PPP** ($3 \cdot 10^{-3}$ in ACN and $3.5 \cdot 10^{-2}$ in H$_2$O) are higher than those determined for **BPP**, which reveals a very weak fluorescence with a quantum yield close to 10^{-3} in various media. The emission of **NPP**, if any, is below the detection limit of our spectrofluorimeters (a trace of the emission is observed only in water). This finding is in agreement with the results of TD-DFT computations which predicts that the energy of the vertical transition to the lowest ^{1}(n,π*) state of the *syn* form of **NPP** is lower by about 1170 cm^{-1} than that of the lowest ^{1}(π,π*) state.

91
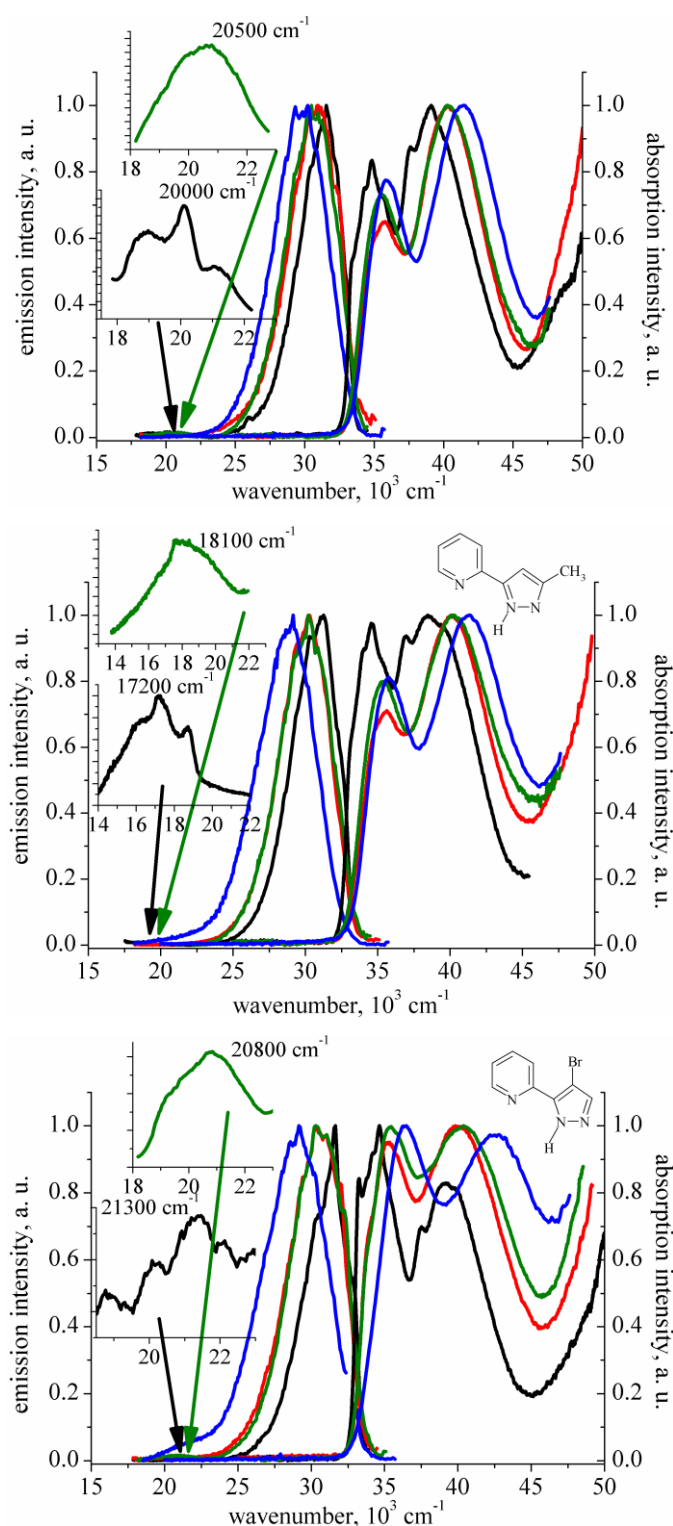
*Figure 4.7. Room-temperature, normalized absorption and fluorescence spectra of **PPP** (top), **MPP** (middle), and **BPP** (bottom) in n-hexane (black), acetonitrile (red), 1-propanol (green), and in aqueous solutions (blue). The spectra in ethyl acetate are similar to those in acetonitrile. The insets show the low-energy emission bands observed for the compounds in n-hexane (lower panel) and 1-propanol (higher panel). The latter spectra are smoothed using Savitzky-Golay method implemented in the Origin 8.0 software.*

Table 4.6 shows also the comparison of the spectral position of the short-wave fluorescence ($\tilde{\nu}_\mathrm{fl}$) in *n*-hexane with those predicted by TD-DFT computations ($\tilde{\nu}_\mathrm{TDDFT}$) for the *syn* and *anti1* forms of **PPP**, **MPP**, and **BPP**. An excellent agreement between the $\tilde{\nu}_\mathrm{fl}$ values and the $\tilde{\nu}_\mathrm{TDDFT}$ values calculated for the *syn* forms of **PPP** and **MPP** strongly suggests that the short-wave emission mainly originates from this form.

Table 4.6. Solvent effects on the spectral position of the short-wave fluorescence maxima ($\tilde{\nu}_\mathrm{fl}$, in cm^{-1}) and quantum yields (Φ_f). $\tilde{\nu}_\mathrm{TDDFT}$ denotes TD-DFT/B3LYP/6-31+G(d,p) energies of the $^1(\pi,\pi^*)\leftarrow S_0$ emission of the syn and anti1 forms for the TD-DFT/B3LYP/6-31+G(d,p) equilibrium geometry under vacuum isolation conditions.[181] The calculations were carried out for the excited state equilibrium geometries.

Compound	Solvent	$\tilde{\nu}_\mathrm{TDDFT}$		$\tilde{\nu}_\mathrm{fl}$ [a]	Φ_f
		syn	*anti1*		
PPP	HEX	31130	34710	31500	0.008 [b,c]
	EA			31000	~0.004
	ACN			31000	~0.003
	1-PrOH			30600	0.017 [b]
	H$_2$O			29800	0.035 [b]
MPP	HEX	29250	34200	31100	0.018 [b,c]
	EA			30200	0.012 [b]
	ACN			30200	0.008 [b]
	1-PrOH			30100	0.028 [b]
	H$_2$O			29100	0.045 [b]
BPP	HEX	30125	32190	31600	~0.003
	EA			30700	~0.003
	ACN			30700	~0.003
	1-PrOH			30700	~0.002
	H$_2$O			29200	~0.003

[a] Scatter of results: $\pm$ 150 cm^{-1}. [b] Error is about 10%. [c] Chou *et al.* very recently published values of quantum yields of 0.054 and 0.02 for **PPP** and **MPP** in cyclohexane, respectively.[236]

The spectral location of the low-energy fluorescence of **PPP**, **MPP**, and **BPP** in *n*-hexane, 1-propanol, and in aqueous solutions is similar to that previously observed for **MPP** in cyclohexane[237] and for 2-(2'-pyridyl)pyrrole (PP) in nonpolar and protic media.[134] Therefore, in accordance with previous investigations, this emission band can be assigned to a tautomeric species and the observed dual luminescence is most probably a manifestation of

photoreactions exemplified in *n*-hexane by the ESIPT process in the *syn* forms of the compounds and in protic media by the ESDPT process in hydrogen-bonded solute-solvent complexes.

To assure that the low-energy fluorescence bands in nonpolar solvent and in alcohol correspond to different individuals, titration experiments have been performed (Table 4.7). Upon adding 1-butanol (or 1-propanol), at concentrations low enough to prevent the formation of alcohol oligomers, to *n*-hexane solution of **PPP** (Fig. 4.8) an isosbestic point in the absorption spectra is observed. This fact demonstrates an equilibrium between two individuals in the ground state, probably between a monomer and its complex with alcohol. The absorption data yield (Chapter 2, eqs. 2.10 and 2.11) the 1:1 stoichiometry of the complex and the equilibrium constant $K \cong 35$ (± 3) dm^3 mol^{-1}. Very interesting result is provided by emission spectra: the intensity of the blue fluorescence band decreases with a simultaneous increase of the red, most probably tautomeric fluorescence. The relative intensities are drastically changed; the short-wave emission is recovered in the tautomeric fluorescence. When concentration of 1-butanol achieves 0.036 mol dm^{-3} both bands have comparable intensities in contrast to the situation in alcohol solutions, where the low-energy fluorescence band is very weak comparing to the short-wave one (Fig. 4.7). The relatively efficient fluorescence in mixed solvents with low concentration of alcohol can be explained by the preferable formation of the 1:1 complex with a structure capable of phototautomerization; most probably a hydrogen-bonded complex between *syn* tautomer of **PPP** and an alcohol molecule with a cyclic structure is formed under these conditions. In bulk alcohol solutions the existence of other complexes of various stoichiometries and structures which are unable to tautomerize leads to an extremely weak intensity of the low-energy emission.[132-134,238]

*Table 4.7. The stoichiometry and equilibrium constants of the complexes between **PPP**, **MPP**, and **BPP** and an alcohol molecule in mixed n-hexane/1-butanol solutions.*

	PPP	**MPP**	**BPP**
stoichiometry	1:1	1:1	1:1
K_{11}, dm^3 mol^{-1}	35±3	50±7	13±3

The titration of **MPP** and **BPP** in *n*-hexane with 1-butanol also reveals the formation of the 1:1 complexes; the respective equilibrium constants are $K \cong 50$ (± 7) dm^3 mol^{-1} and $K \cong 13$ (± 3) dm^3 mol^{-1}. However, the intensity of the low-energy emission is relatively weak.

Interestingly, the intensity of the tautomeric emission of **BPP** and **MPP** in aqueous solutions, contrary to that in alcohols, is higher than that of **PPP** (Fig. 4.7). **PPP** in water shows only a trace of the low-energy emission.
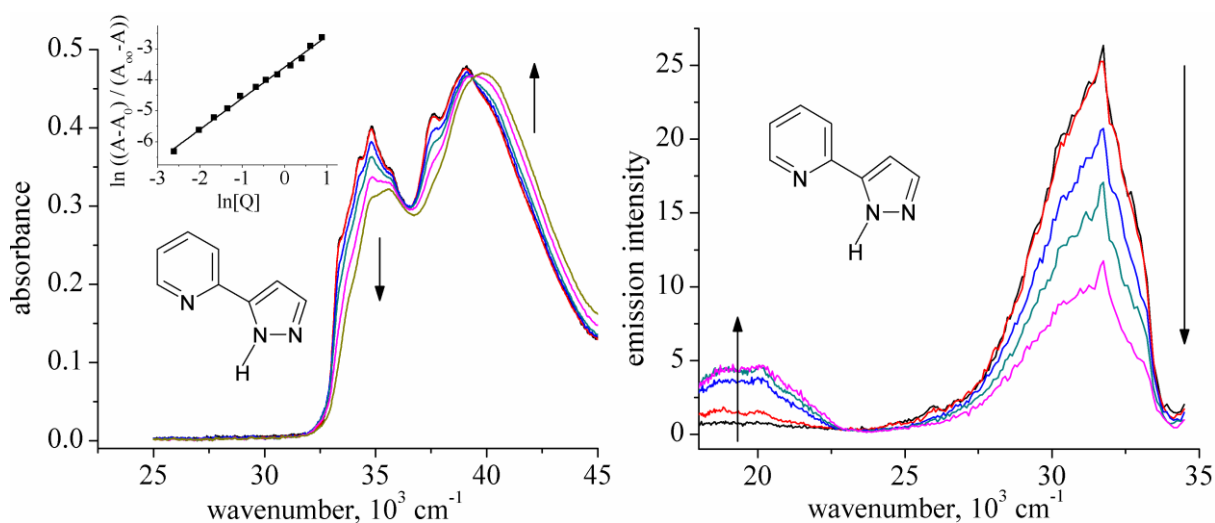
*Figure 4.8. Titration of **PPP** solution in n-hexane with 1-butanol at 293 K. Left: changes in absorption; right: evolution of both fluorescence bands. The arrows indicate the spectral changes accompanying the increase of alcohol concentration from 0.0036 to 0.072 mol/dm³. The inset in the absorption part shows the determination of the equilibrium constant and stoichiometry of the complex from the absorption data recorded at 37600 cm⁻¹; A_0 and A_∞ denote the optical density measured when only the bare or complexed forms are present, and A is the optical density measured at an alcohol concentration [Q] (see eqs. 2.10 and 2.11).*

The titration experiments in mixed *n*-hexane/alcohol solvents strongly suggest that the low-energy emission can be attributed to the tautomeric species which are formed in the ESDPT reaction. The driving force for the excited-state proton transfer is the electron density redistribution occurring upon excitation. This redistribution in similar compounds (such as 2-(2'-pyridyl)indoles[132,133] and 1*H*-pyrrolo[3,2-*h*]quinoline and related molecules[129]) leads to an increase in the excited-state pK_a^* of the proton acceptor and a decrease in the excited-state pK_a^* of the proton donor. The ground state acid-base equilibria for **PPP** and **MPP** have been very recently[236] determined using spectrophotometric titration. The reported pK_a^G values corresponding to the pyridine nitrogen atom, N_p (being the basicity center), and to the NH pyrazolic group (the center of acidity) for **PPP** and **MPP** are 5.15 and 5.17 or 11.6 and 12.1, respectively. To have more quantitative insight into the excited-state basicity, the changes in pK_a have been obtained from the absorption and fluorescence investigations of neutral molecules and protonated cations of all the studied **2-PPs** with the use of the "Förster cycle".[18,20] The estimated ΔpK_a values are huge (Table 4.8) and similar to that for PP ($\Delta pK_a \cong$ +11.0).[134] The pK_a^G and ΔpK_a values leave no doubts that the protonation center in the studied

2-PPs is the N_p atom[239]. It is interesting that the highest basicity increase is observed for **MPP**, a derivative substituted with an electron donating methyl group. Thus, a huge increase in basicity of the N_p atom upon excitation creates thermodynamically favorable conditions for excited state proton transfer processes such as ESIPT in the *syn* forms of the **2-PPs** molecules and ESDPT in alcohol complexes.

Table 4.8. The 0-0 transition energies ($\tilde{\nu}$, in cm^{-1}) obtained from the absorption and fluorescence maxima of the neutral ($\tilde{\nu}_B$, in ACN (PPP, MPP, BPP) and water (NPP)) and protonated ($\tilde{\nu}_{BH+}$)[a] forms and the resulting pK_a changes ($\Delta pK_a = pK_a^* - pK_a^G$) upon $S_1 \leftarrow S_0$ excitation.

	PPP	MPP	BPP	NPP
$\tilde{\nu}_B$	33120	32980	33000	~33700
$\tilde{\nu}_{BH+}$	29520	27600	29230	~30600
$\Delta pK_a(N_p)$	7.5[b]	11.3[b]	7.9[b]	~6.5[b]

[a] Protonation was achieved by adding about 0.1 mol dm^{-3} of $HClO_4$. [b] Estimated from eq. (2.12).

(Fig. 4.9) presents the fluorescence excitation spectra of **PPP** and **MPP**. The spectra were recorded by monitoring both emission bands. In *n*-hexane they match well the corresponding absorption spectra (with only a small discrepancy for **PPP** at the red edge of the excitation spectrum for the low-energy emission). On the other hand, in polar medium, such as ACN, the excitation spectra of the short-wave emission do not match the absorption ones. The intensity ratio of the two lowest bands in the excitation spectrum is reversed comparing to that of the absorption spectrum. Moreover, the excitation spectra are slightly shifted to the lower energies. A similar, but smaller effect is observed for **BPP**.

These results indicate that, in spite of the coexistence in the ground state of the *syn* and *anti1* forms of the compounds in the polar environment (Table 4.2), the short-wave fluorescence of **PPP**, **MPP**, and **BPP** originates mainly from the *syn* rotamer. This conclusion is made by taking into account the theoretical predictions that, contrary to the observed red shift of the excitation spectra, the lowest absorption transitions for the *anti1* forms of the **2-PPs** should be considerably blue-shifted, by about 2600-3000 cm^{-1}, with respect to those of the *syn* forms. Moreover, it suggests that the fluorescence rate constants for the *syn* rotamers are larger than those for the *anti1* forms (in agreement with the results obtained previously for 2-(2'-pyridyl)indole[133]).
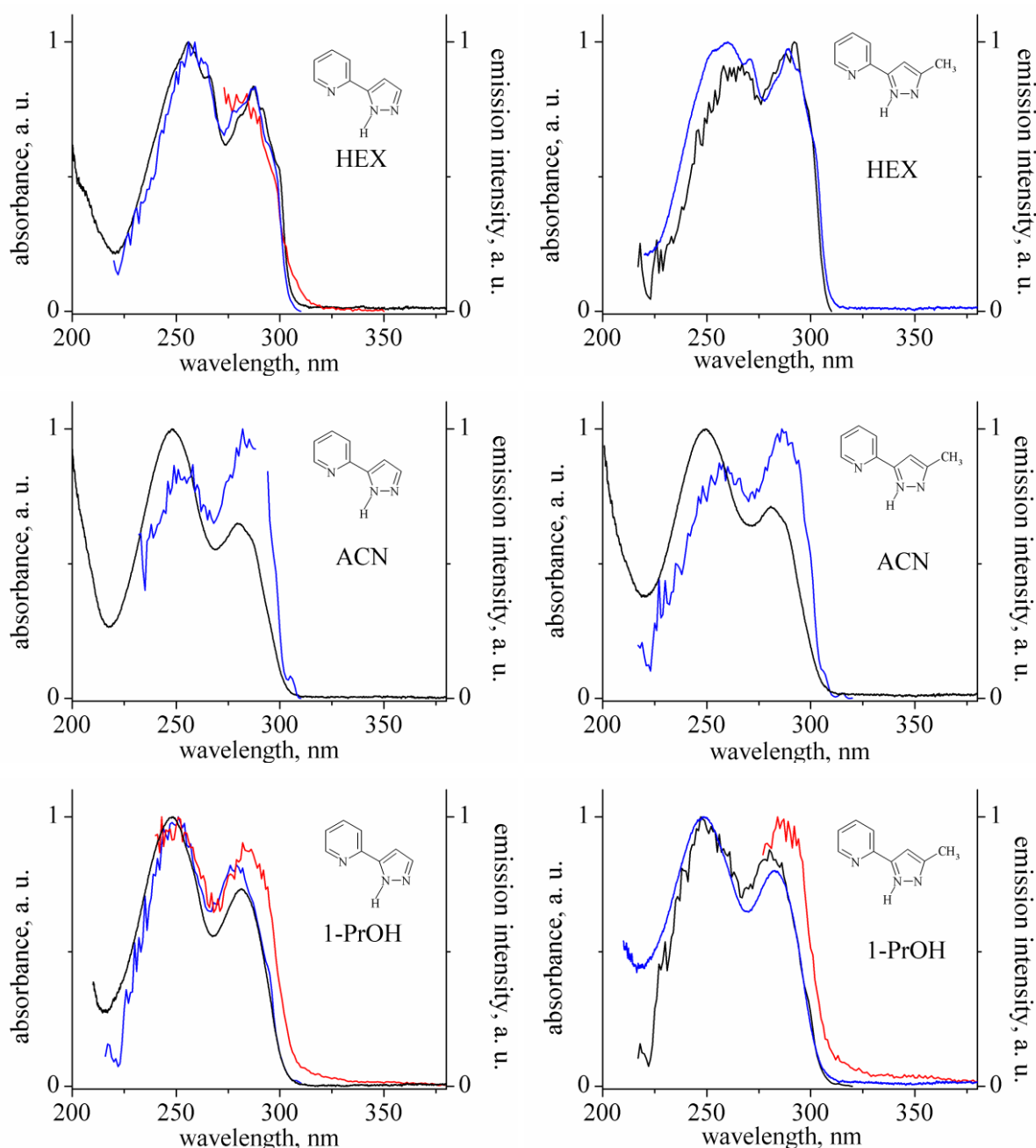
Figure 4.9. Normalized room-temperature absorption (black) and fluorescence excitation spectra of **PPP** *and* **MPP** *monitored at 330 nm (blue emission band) and at 500 nm (red emission band). Upper panel, n-hexane; middle panel, acetonitrile; lower panel, 1-propanol.*

The excitation spectra of the short-wave emission in 1-PrOH also show the relative increase of the low-energy excitation band with respect to that in absorption spectra. However, this effect is smaller comparing to that in ACN. Moreover, the maximum of the lowest excitation band is now slightly shifted to higher energies. Contrary to that, the lowest excitation band of the low-energy emission of **PPP** and **MPP** in 1-PrOH is markedly shifted to the red. According to the results of theoretical computations this effect is expected in all the studied **2-PPs** for the complex of the *syn* form with an alcohol molecule.

The assignment of the low-energy fluorescence band of **PPP**, **MPP**, and **BPP** in *n*-hexane is more ambiguous than that in alcohols. The calculations and the nuclear Overhauser effect spectroscopy (NOESY) investigations performed for 3,5-dimethyl-2-(2'-pyridyl)pyrrole[185] suggest the existence of hydrogen-bonded dimers of the *syn* forms in the ground state. Such dimers should be doubly hydrogen-bonded in a cyclic fashion. Our theoretical calculations predict a slightly higher stabilization energy for the ground-state dimers of **PPP** and **MPP** (6.8 kcal/mol and 6.6 kcal/mol, respectively) than for 2-(2'-pyridyl)pyrrole (5.8 kcal/mol). The calculated value for **BPP** is 5.5 kcal/mol.

4.4. Kinetics. The picosecond studies[181]

In order to gain more insight into the origin of both emissions, picosecond kinetic studies were performed. The fluorescence kinetic data obtained with nanosecond time resolution were not sufficient enough. The results for **PPP** in *n*-hexane showed a biexponential decay of the long-wave fluorescence band, with the longer component of about 1 ns. This component, however, was not detected in the decay of the short-wave fluorescence; the lifetimes of this emission of the studied compounds in various media appeared to be too short to be measured correctly with 0.5 ns resolution. Therefore, in order to check the anticipated bimodal kinetics of the irreversible excited-state tautomerization, picosecond kinetic studies in *n*-hexane, acetonitrile and in mixed *n*-hexane + 1-PrOH solvent at room temperature were carried out.[181]

The irreversible process including a primary excited species [P*] and a product of the excited-state tautomerization process [T*] is presented in Figure 4.10, which also explains the rate constants.
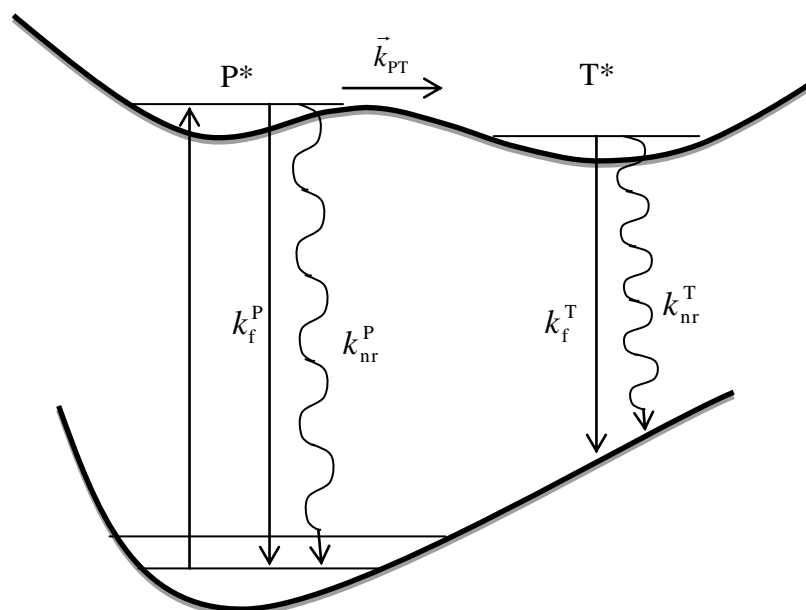
*Figure 4.10. Kinetic model of the excited-state tautomerization in **2-PP**s: schematic cross-section of the ground-state and lowest excited singlet state potential hypersurfaces along the reaction coordinate. **k** denotes the rate constants ($\vec{k}_{PT}$ – ESPT reaction, k_f^P and k_f^T – radiative deactivations of P* and T*, k_{nr}^P and k_{nr}^T – corresponding radiationless deactivations). Dual luminescence is related to the primary excited species P* (short-wave emission) and the product T* of the phototautomerization reaction (long-wave emission).*

At time $t > 0$ kinetic equations describing population and depopulation of both excited states are as follows:

$$\frac{d[P*]}{dt} = -[P*]\left(k_P + \vec{k}_{PT}\right)$$ (4.1)

$$\frac{d[T*]}{dt} = \vec{k}_{PT}[P*] - k_T[T*].$$ (4.2)

The concentrations of the primary excited species and the product of the excited-state tautomerization process can be expressed as

$$[P*] = [P*]_0 \exp[-(k_P + \vec{k}_{PT})]t$$ (4.3)

$$[T*] = A_{1,2}[\exp(-k_T t) - \exp(-(k_P + \vec{k}_{PT})t)],$$ (4.4)

where $[P*]_0$ is the initial concentration of the substrate of the photoreaction at $t = 0$ (the initial concentration of the product is $[T*]_0 = 0$). $A_{1,2}$ is a common amplitude of the decay and rise of the long-wave fluorescence

$$A_{1,2} = [P*]_0 \frac{\vec{k}_{PT}}{k_P + \vec{k}_{PT} - k_T}.$$ (4.4a)

The rate constants can be described as

$$k_P = k_{nr}^P + k_f^P$$ (4.5)

$$k_T = k_{nr}^T + k_f^T.$$ (4.6)

The quantum yields of the short-wave (Φ_P) and long-wave (Φ_T) fluorescence are given by

$$\Phi_P = \frac{k_f^P}{k_f^P + k_{nr}^P + \vec{k}_{PT}} = k_f^P \tau_P$$ (4.7)

$$\Phi_T = \frac{\vec{k}_{PT}}{k_f^P + k_{nr}^P + \vec{k}_{PT}} \frac{k_f^T}{k_f^T + k_{nr}^T}.$$ (4.8)

Assuming that $\vec{k}_{PT} >> k_f^P + k_{nr}^P$, the equation 4.8 giving the quantum yield of the tautomeric emission is simplified to

$$\Phi_T = \frac{k_f^T}{k_f^T + k_{nr}^T} = k_f^T \tau_T.$$ (4.8a)

The kinetics of the short-wave fluorescence, excited at 35700 cm^{-1} and monitored at 30800 cm^{-1}, of **MPP** and **PPP** in *n*-hexane and of **PPP** in ACN at 293 K could be satisfactorily fitted to monoexponential decay (Table 4.9). Variations of the excitation within the first absorption band (between 33300 cm^{-1} and 35700 cm^{-1}) and of the monitoring

emission spectral region within the main fluorescence band (between 27750 cm^{-1} and 31250 cm^{-1}) did not change the results. However, minor (less than 7%) very short-lived components (~10 (±5) ps) appear for **PPP** and **MPP** in *n*-hexane, as well as for **MPP** in ACN ($\tau_1 \cong 68$ ps and $\tau_2 \cong 18$ ps with contributions of about 91% and 9%, respectively). If not taking into account these insignificant very short components, the obtained lifetimes for the dominant forms of **MPP** and **PPP** in *n*-hexane and **MPP** and **PPP** in ACN lead to large values of the fluorescence rate constants $k_f^P > 10^8$ s^{-1}. This result is similar to the k_f^P values experimentally determined for the *syn* rotamers of 2-(2'-pyridyl)indole[133] and related compounds,[240] and 2-(2'-pyridyl)pyrrole.[240] For these molecules the fluorescence lifetimes attributed to the *anti* rotamers were much longer. For example, while for the *syn* form of 2-(2'-pyridyl)indole the decay time was found to be $\tau_{syn} \cong 33$ ps in *n*-hexane,[240] for the *anti* one it was more than 100 times longer ($\tau_{anti} \cong 4.6$ ns in ACN[134]). Thus, the results of kinetic studies are in agreement with the results of the photostationary investigations. They indicate that the short-wave fluorescence of **PPP** and **MPP** in aprotic media originates from the *syn* forms. The lack of the emission from the *anti1* form is in agreement with the results of calculations which predict that the lowest S$_1$ state of this form is of n,π* character.

Table 4.9. Solvent effects on the decay times (τ, with respective contributions, F_i) and quantum yields (Φ_f, see Table 4.6) of the short-wave fluorescence band, and resulting radiationless ($k_{nr} = k_{nr}^P + \vec{k}_{PT}$) and radiative ($k_f^P$) rate constants, and electronic transition dipole moments (M_{fl}).

Compound	Solvent	Φ_f	τ_{decay} (325 nm), ps	F_i, %	k_{nr}, 10^{10} s^{-1}	k_f^P, 10^8 s^{-1}	M_{fl}, D
PPP	HEX	0.008	42 [a]	> 93	2.4	~1.9	~2.7
	ACN	~0.003	19(±5)		~5.2	~1.6	~2.7
MPP	HEX	0.018	84 [a,*]	> 93	1.2	2.1	2.9
	ACN	0.008	68 [a]	91	1.5	1.2	2.4
BPP	HEX	~0.003	16(±5)	60			
			45 [a]	40			
	ACN	~0.003	16(±5)		~6.2	~1.9	~2.9

[a] Error is about 10%. Thus, the maximum error is about 20% for the rate constants k_{nr} and k_f^P, and about 10% for the transition moment M_{fl}. * 115 ps in Ref. [240].

The decay of the short-wave fluorescence of **BPP** in *n*-hexane, contrary to that in ACN (Table 4.9), involves two components: $\tau_1 \cong 16$ (±5) ps and $\tau_2 \cong 45$ (±5) ps with

comparable contributions of about 60% and 40%, respectively. This finding can hardly be explained in terms of the coexistence of the two rotameric forms *syn* and *anti1* as it is excluded by the results of the photostationary investigations and theoretical predictions. The concentration-dependence experiments do not show any significant changes of the relative contributions. The experiments performed in *n*-hexane containing very small contamination of water cannot exclude definitively that one of the decay components is connected with the complexes between **BPP** and water impurities in *n*-hexane. The relatively high intensity of the long-wave tautomeric emission of **BPP** in aqueous solutions (Fig. 4.7) with respect to those of **PPP** and **MPP** seems to support this hypothesis.

Table 4.10. Dual fluorescence kinetics: characteristic decay (τ_{decay}, in ps) and rise (τ_{rise}, in ps) times for the short-wave (monitored at 325 nm) and long-wave fluorescence (monitored at 540 nm) of PPP and MPP* in n-hexane and in a mixed solvent (n-hexane + 1-propanol, concentration of alcohol $c \cong 8.8 \cdot 10^{-2}$ mol dm^{-3}). F_i – corresponding relative contributions of decay times.

Compound	Solvent	325 nm		540 nm	540 nm	540 nm
		τ_{decay}	F_i	τ_{rise}	τ_{decay}	τ_{decay}
PPP**	*n*-hexane	42[a]		16($\pm$5)[b]	1400[a,***]	380[***]
	n-hexane + 1-PrOH	~21	40%	18($\pm$5)	630[a]	
		~55	37.5%	(-0.99)[c]	(1.0)[c]	
		~213	22.5%			
MPP**	*n*-hexane	84[a]		84[a]	105[a]	
				(-0.92)[c]	(1.0)[c]	
	n-hexane + 1-PrOH	~18	22%	16($\pm$5)	280[a]	~990
		~76	50%	(-1.0)[c]	(0.92)[c]	(0.02)[c]
		~200	28%			

[a] Error is about 10%. [b] The contribution of this component is very small for the small concentration of the solute of about $1 \cdot 10^{-5}$ mol/dm^3. [c] In the brackets are the amplitudes (in arbitrary units) of the corresponding rise and decay times. * The results of the kinetic studies of **BPP** are not collected in the Table, see text for explanation. **The intensity of the long-wave fluorescence band of **PPP** and **MPP** in acetonitrile was too weak to measure this fluorescence decay. *** See text for explanation.

The picosecond kinetic studies of the dual luminescence of **MPP** in *n*-hexane confirm the previously published[237] bimodal irreversible kinetic coupling of the both fluorescence bands (although decay values are slightly lower). The 84 ps decay time of the high-energy fluorescence is recovered in the rise of the low-energy emission, which decays in 105 ps (Table 4.10). The ratio of the amplitudes of the both kinetic components of the low-energy emission is about −1.0. This observation proves that the short-wave and the long-wave

fluorescence have the same precursor in the ground state. The kinetic studies do not reveal any concentration dependence. Thus, high- and low-energy emission bands are assigned to the *syn* and *taut* forms of the bare **MPP** molecule, respectively (Scheme 4.3). Radiative rate constants of both forms resulting from the fluorescence quantum yields and fluorescence decay times are compared in Table 4.11.

*Table 4.11. Quantum yields (Φ_f), decay times (τ), and resulting radiative (k_f) rate constants of primary excited (eq.4.7) and tautomeric (eq. 4.8a) forms of **MPP**. * Error is about 10%. Quantum yield of tautomeric species was estimated from the ratio of short-wave to long-wave emission intensities.*

	Φ_f	τ, ps	k_f, s^{-1}
Primary excited (the *syn* form)	0.018	84	$2.1 \cdot 10^8$
Tautomer	0.00036	105	$3.4 \cdot 10^6$

* Chou *et al.* very recently published[236] the results of photophysical studies of **MPP**. He obtained the quantum yield and lifetimes values corresponding to the primary excited and tautomer forms of 0.02 and 120 ps, and of 0.001 and 240 ps, respectively. These data results in radiative rate constants of the short-wave and long-wave emissions of $1.7 \cdot 10^8$ s^{-1} and $4.2 \cdot 10^6$ s^{-1}, respectively.

Contrary to **MPP**, the 42 ps decay of the short-wave fluorescence of **PPP** in *n*-hexane is not recovered in the rise time of the long-wave band (Table 4.10). Moreover, the decay of the long-wave band is biexponential; the longer component is of 1.4 ($\pm$0.15) ns and the shorter one of 380 ($\pm$40) ps. The relative contributions of these lifetimes depend on the concentration of the solute. The experiments show that the growth of concentration from $1.2 \cdot 10^{-5}$ mol/dm^3 to $5 \cdot 10^{-4}$ mol/dm^3 leads to the increase of the relative contribution of the longer component from 25% to 87% (Fig. 4.11). Therefore, it is no doubt that two emission bands of **PPP** in *n*-hexane originate from different species. The dominant short-wave emission characterized by the decay time of 42 ($\pm$4) ps corresponds to the *syn* form of the bare molecule. The long-wave band characterized by the long decaying component of about 1.4 ns seems to be related to the photoproduct of the ESDPT reaction in the doubly hydrogen-bonded dimer (Scheme 4.3). The formation of ground-state dimers, however, is not observed in the stationary absorption spectra. Theoretical calculations predict that the spectral position of the absorption maximum of the dimer of the *syn* forms of **PPP** is similar to that of the cyclic hydrogen-bonded complexes with methanol and the corresponding red shift with respect to that of the *syn* form of the bare molecule is about 1500 cm^{-1}. However, the absorption spectra of **PPP** in *n*-hexane (Fig. 4.4) do not show any significant changes with the increase of the concentration between $1.2 \cdot 10^{-5}$ mol/dm^3 and $1 \cdot 10^{-3}$ mol/dm^3. The most probable reason is that the relative fraction of

the dimers (with respect to the monomer) of **PPP** is too small to be observed in the absorption spectra. The appearance of the long-wave fluorescence band could be explained by the high quantum yield of the tautomeric emission (as corresponding to the long lifetime of 1.4 ns). It should be noted, that the shift to lower energies with respect to the absorption spectrum is observed at the red edge of the excitation spectrum of the long-wave emission (Fig. 4.9).

The origin of the long-wave fluorescence characterized by the 380 ps decay is not clear enough. It may be due to the monomeric phototautomer or to the tautomeric form of the complex with residual water. Chou *et al.*[236] very recently claimed that experiments at very low concentrations of about 10^{-6}-10^{-5} mol/dm^3 of **PPP** in cyclohexane results in the 98 ps decay of the short-wave fluorescence and the 100 ps rise and ~500 ps decay of the long-wave fluorescence. This finding supports the former explanation.
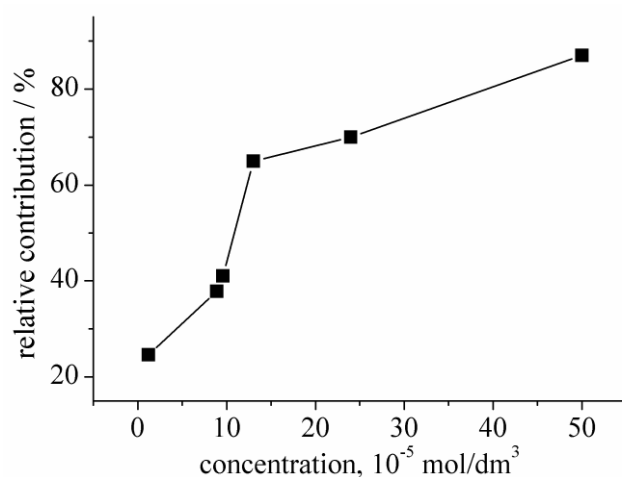
*Figure 4.11. The dependence of the contribution of the 1.4 ns decay component of the low-energy emission of **PPP** in n-hexane on the concentration of the solute.*

The kinetic investigations of dual luminescence of **PPP**, **MPP**, and **BPP** in mixed *n*-hexane/1-PrOH solvents have also been performed (the concentration of alcohol was varied from $c \cong 1.3 \cdot 10^{-2}$ mol/dm^3 to $c \cong 8.8 \cdot 10^{-2}$ mol/dm^3). As it was already shown (Fig. 4.8), the relative intensities of the both emission bands depend on the concentration of alcohol. The data collected in Table 4.10 corresponds, however, to the highest concentration of alcohol; for this concentration the decay curves do not show any components corresponding to the bare molecules. The dual luminescence can hardly be explained in terms of the bimodal irreversible kinetic model containing only single ground-state species. The decays of the short-wave fluorescences (excited at 35700 cm^{-1} and monitored at 30800 cm^{-1}) of **PPP** and **MPP** could be satisfactorily fitted to the three-exponential decays of comparable contributions while the kinetics of the long-wave emissions (monitored at 18500 cm^{-1}) contain the rise and decay components. For **PPP** the best fit of the decay of the blue emission

involves the decay times of ~21 ps (with the relative contribution of ~40%), ~55 ps (~37.5%), and ~213 ps (~22.5%). The kinetics of the long-wave emission is very well described by the rise time of 18 (±5) ps and the decay time of 630 (±50) ps. Within the experimental error the shortest decay time of the blue emission is recovered in the rise of the red emission. The ratio of the amplitudes $A_{\text{rise}}/A_{\text{decay}} = -1.0$ (± 0.03) indicates that the long-wave emission is not formed by direct excitation from the ground-state species. The results suggest that only one hydrogen-bonded complex of **PPP** with 1-propanol, among several other possible complexes of different structures, undergoes the excited state proton transfer reaction. The analysis of the photostationary absorption and fluorescence experiments in the mixed solvents (Fig. 4.8) indicate that the observed process can be attributed to the 1:1 cyclic doubly hydrogen bonded complex between **PPP** and the alcohol partner.

Similar results of kinetics investigations have been obtained for **MPP** in mixed *n*-hexane/1-PrOH solvents. The best three-exponential fit obtained for the alcohol concentration of $8.8 \cdot 10^{-2}$ mol/dm^3 involves the decay times of ~18 ps (with the relative contribution ~22%), ~76 ps (~50%), and ~200 ps (~28%). In spite of the very low intensity of the low-energy band, the kinetics of the low-energy emission could be satisfactorily fitted to the rise time of 16 (±5) ps and the decay time of 280 (±30) ps (with contribution of about 94%). Similarly to **PPP**, the 18 ps decay of the short-wave emission is recovered in the rise of the long-wave emission with the ratio of the amplitudes $A_{\text{rise}}/A_{\text{decay}} = -1.0$.

The results of the kinetic studies of **BPP** are not collected in Table 4.10. The investigations of **BPP** in the mixed solvent show even more complex kinetics than that observed for **PPP** and **MPP**. The decays of both fluorescence bands are multiexponential. The kinetic curves corresponding to the low-energy and to the high-energy fluorescence cannot be satisfactorily fitted either to a two-exponential model or to the three-exponential approximation. On the other hand, **BPP** in *n*-hexane, contrary to **PPP** and **MPP**, under conditions of picosecond kinetic studies (*i.e.* under the pulsed 280 nm irradiation) undergoes a photochemical reaction. The appearance of the photochemical product significantly increases the intensity of the low-energy fluorescence, but does not lead to any significant changes in the photostationary absorption and short-wave fluorescence spectra, as well as in the short-fluorescence kinetics.

4.5. Summary

The results of stationary and time-resolved photophysical studies, and quantum chemical computations for a family of four azaaromatic compounds based on pyrazole and pyridine chromophores are presented in this chapter. The aim of the work, *i.e.* the quantitative characterization of: (i) the photophysical parameters, (ii) the solvent-dependent rotamerization, and (iii) the photoinduced tautomerization reactions, was successfully realized.

The investigations show that all the **2-PPs** preferentially exist in the *syn* forms both in nonpolar and polar environments in the ground state. The *syn-anti1* rotamerization, however, is promoted by the increase of polarity and proticity of the surrounding medium due to the relative stabilization of the *anti1* species. The increase of the fraction of the *anti1* form in acetonitrile is especially considerable for **PPP** and **MPP**, being smaller for **BPP**. The absorption bands corresponding to the *anti1* forms are markedly blue-shifted with respect to those of the *syn* forms. For **NPP** in highly polar medium the appearance of the more or less equal ground-state fractions of the *anti*, *anti1*, and *syn1* forms are responsible for the dramatic change of the absorption spectrum with respect to that in *n*-hexane. Contrary to the other members of the family, **NPP** does not show any detectable fluorescence (a trace of the emission is observed only in water). This effect, at least in part, seems to be related to the interactions between close lying $^1(\pi,\pi^*)$ and $^1(n,\pi^*)$ states in the *syn* rotamer of **NPP**.

PPP, **MPP**, and **BPP** in *n*-hexane, 1-propanol, and in aqueous solutions show dual luminescence. The dominant short-wave band originates mainly from the *syn* rotameric form of the compounds. The long-wave band of very low intensity reveals a huge Stokes shift. The picosecond kinetic studies and spectrophotometric and spectrofluorimetric titration experiments in mixed *n*-hexane/alcohol solvents prove that this band originates from the product of the excited state proton transfer reactions (Scheme 4.3).

It is noteworthy, that this class of compounds provides a rare example of molecules that exhibit three types of photoreactions:

(1) the excited state intramolecular proton transfer (ESIPT) in the *syn* form of **MPP** in nonpolar media (Scheme 4.3a). Our studies in *n*-hexane are in agreement with previous investigations of **MPP** performed in cyclohexane by Chou and coworkers,[237] the excited state process in the monomeric form is strongly suggested by a lack of any concentration dependence of bimodal irreversible kinetic coupling of the two fluorescence bands. To prove

it, the investigations of **MPP** isolated under supersonic jet conditions should be performed (as it has been done for PP[135]),

(2) the solvent-assisted excited-state double proton transfer (ESDPT) in hydrogen-bonded complexes of **PPP** (Scheme 4.3b), **MPP**, and **BPP** with protic partners of 1:1 stoichiometry and most probably of cyclic structure (similarly to PP,[134] 1*H*-pyrrolo[3,2-*h*]quinoline and related compounds[129]). This process is especially pronounced in the 1:1 complexes of **PPP** which are preferentially formed in mixed *n*-hexane solutions containing a small concentration of alcohol,

(3) the ESDPT in the cyclic, hydrogen-bonded dimers of **PPP** in nonpolar media (Scheme 4.3c is similar to that describing this type of photoreaction in the dimers of 7-azaindole[107,109,110,241,242]). This process is suggested by the concentration dependence of the contribution of the 1.4 ns decay component of the low-energy emission of **PPP** in *n*-hexane (Fig. 4.11). Our hypothesis is supported by the formation of ground-state dimers in 2-(2'-pyridyl)pyrroles.[185] Very recently, in agreement with our interpretation, Chou and co-authors[236] postulated the ESDPT process in the dimers of 2-(3-trifluoromethyl-1H-pyrazol-5-yl)-pyridine.
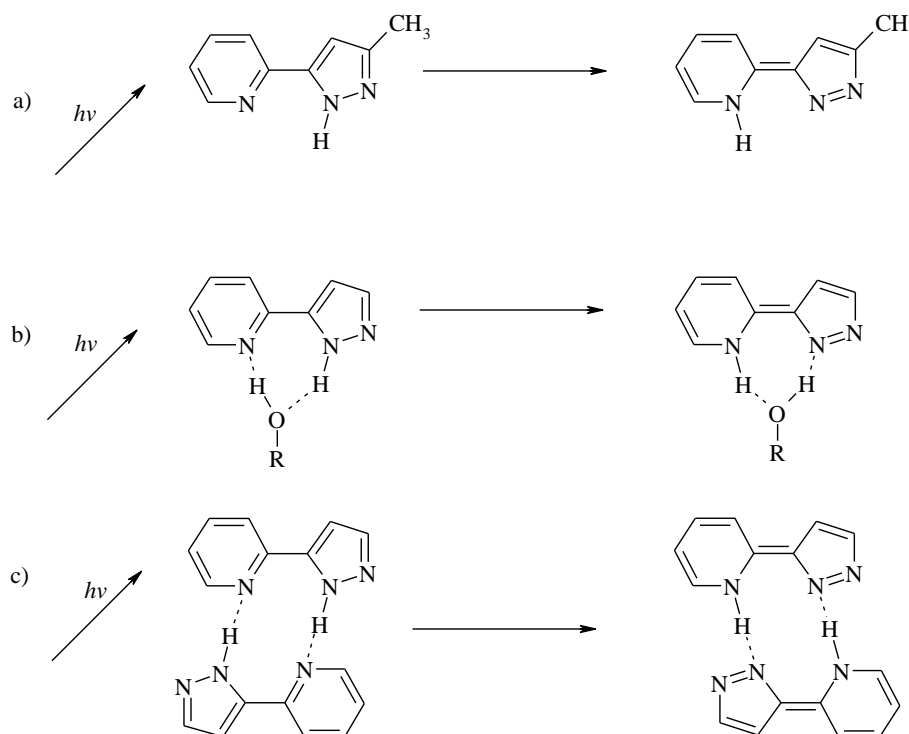
*Scheme 4.3. Scheme of proposed phototautomerization processes for **PPP**, **MPP**, and **BPP**: excited state intramolecular proton transfer (ESIPT) in the syn rotamer of **MPP** in n-hexane (a) and excited state double proton transfer (ESDPT) in 1:1 complexes of **PPP**, **MPP**, and **BPP** with protic partners (b) and in **PPP** dimer in n-hexane (c).*

Chapter 5: Spectroscopy and photophysics of bifunctional proton donor-acceptor indole derivatives

5.1. Introduction. Rotameric/tautomeric forms of compounds

This chapter describes the study of selected bifunctional indole derivatives for which the hydrogen bond donor (the indole NH group) and acceptor centers are located in separate moieties, covalently linked by a single bond (Scheme 5.1). The aim of the work is to compare spectroscopy and photophysics of the compounds which can form *syn* (with the donor and the acceptor on the same side) and *anti* (with the two groups on the opposite sides) conformers *via* internal rotation around a single bond (such as 2-thiophen-2-yl-1*H*-indole (**THOIN**), 2-thiazol-2-yl-1*H*-indole (**THAIN**), and 2-furan-2-yl-1*H*-indole, **FURIN**), with the compounds which either have not any acceptor center, *e.g.*, 2-(1*H*-pyrrol-2-yl)-1*H*-indole (**PYRIN**), or due to the topology can not exist in two rotameric forms, *e.g.*, 3-pyridin-4-yl-1*H*-indole (**3-PI**)[182]. Due to the fact that only the *syn* rotamers of bifunctional molecules are able to form cyclic, doubly hydrogen bonded dimers or complexes with protic partners, it was expected that the former three molecules, contrary to the latter two compounds, should show solvent dependent photophysics. This group of compounds was especially synthesized to study the effects of electronegativity of the hydrogen bond acceptor centers (such as oxygen, nitrogen, or sulphur atoms) on their photophysical properties.

FURIN   **THAIN**   **THOIN**

PYRIN   **3-PI**
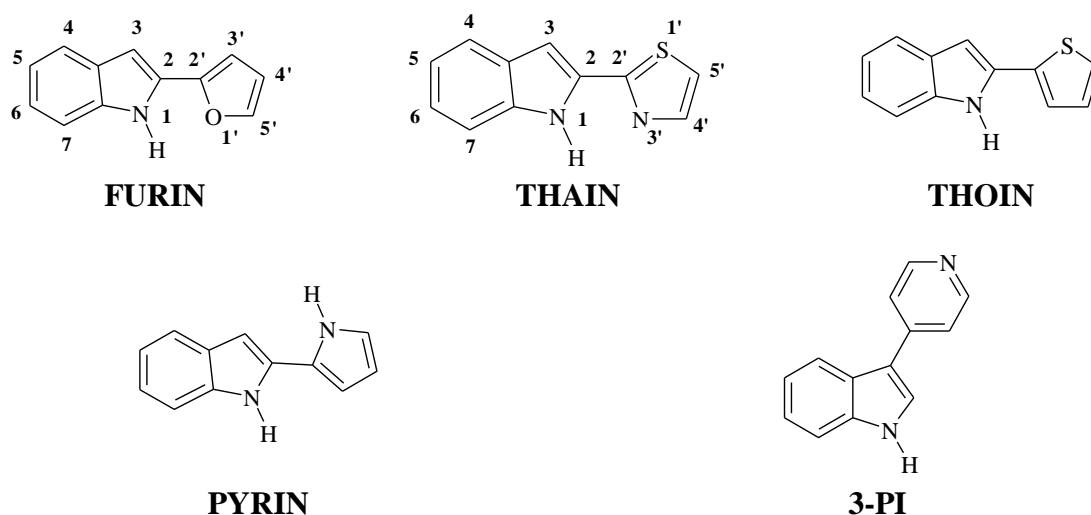
Scheme 5.1. Structures and acronyms of studied indole derivatives. The compounds are shown in the most stable ground state conformations.

In order to estimate the relative ground state energies of the rotameric forms the theoretical calculations at the DFT/B3LYP/3-61+G(d,p) level were performed (Table 5.1). The predicted low energy ground state species of **THAIN** and **FURIN** under vacuum isolation conditions correspond to the planar *syn* forms due to their stabilization by intramolecular hydrogen bond. For **PYRIN** and **THOIN** the low energy species are *anti* tautomeric forms with dihedral angles of 22.5° and 24º, correspondingly. Their *syn* conformers are also nonplanar. The nonplanar structure of **PYRIN** can be explained by strong repulsive interactions of the NH hydrogen atoms that do not allow the compound to become planar. The computed energy gaps between *syn* and *anti* conformers, however, are small; the values change from 0.1 kcal/mol for **THOIN** to -3.2 kcal/mol for **THAIN**. Additional calculations were performed for tautomeric form of **THAIN** which show relatively large destabilization energy of 23.1 kcal/mol of this form with respect to the *syn* rotamer (noteworthy, **FURIN** and **THOIN** are not able to form the tautomeric species, in which the proton is shifted from the indole nitrogen atom onto the furan oxygen atom or onto the thiophene sulphur atom, respectively). The computed ground state dipole moments values μ_g of the *syn* and *anti* forms are in the range from 1.4 D to 2.7 D; the value for **3-PI** is significantly higher. The directions of μ_g are shown in Figure 5.1.

Table 5.1. Ground state data: relative energies (computed at the DFT/B3LYP/3-61+G(d,p) level) of the various rotameric and tautomeric forms (ΔE), dipole moments (μ_g) and dihedral angles between proton donating and accepting moieties.

	ΔE, kcal/mol			μ_g, D			geometry (dihedral angle)		
	syn	*anti*	*taut*	*syn*	*anti*	*taut*	*syn*	*anti*	*taut*
FURIN	-	1.2		2.0	2.5		planar	planar	
THAIN	-	3.2	23.1	1.4	2.5	6.6	planar	planar	planar
THOIN	0.1	-		1.8	2.2		28°	24°	
PYRIN	1.6	-		2.7	1.7		32°	22.5°	
3-PI				4.7			35°		

The *ab initio* computations at the CIS/B3LYP/3-61+G(d,p) level predict that in the excited state the *syn* rotamer is relatively stabilized for all the compounds under study. The stabilization energy, however, which is significant (*ca.* 3.1 kcal/mol) for **FURIN** and

THAIN, seems to be negligibly small for **PYRIN** and **THOIN**. All the compounds (including **3-PI**) have tendency to flatten upon excitation.

Table 5.2. Excited state data: relative energies (ΔE), computed at the TD-DFT/B3LYP/3-61+G(d,p) and CIS/B3LYP/3-61+G(d,p) levels, of the various rotameric and tautomeric forms, dipole moments (μ_e) and dihedral angles between proton donating and accepting moieties.

		ΔE, kcal/mol			μ_e, D			geometry (dihedral angle)		
		syn	*anti*	*taut*	*syn*	*anti*	*taut*	*syn*	*anti*	*taut*
FURIN	CIS	-	2.7		1.3	1.9		planar	planar	
	TDDFT	-	2.1		0.8	1.9				
THAIN	CIS	-	3.5	9.2	0.9	2.2	2.6	planar	planar	planar
	TDDFT	-	4.0		3.4	3.6				
THOIN	CIS	-	0.6		0.8	2.1		planar	planar	
PYRIN	CIS	-	0.003		2.6	1.8		1.4°	5.2°	
3-PI	CIS				6.5[a]			10º		

[a] 11.0 D (TD-B3LYP/TZVP)[182]

Let us compare the computed relative stability under vacuum isolation conditions of the *syn* and *anti* forms of the indole derivatives with the results obtained for 2-(1*H*-pyrazol-5-yl)pyridines, **2-PPs** (Fig. 4.1). In the ground state the dominant species of **2-PPs**, similarly to **FURIN** and **THAIN**, correspond to the planar *syn* form. Relative energies between the *syn* and *anti1* forms of **PPP**, **MPP**, and **BPP** are similar to those computed for the *syn* and *anti* forms of the indole derivatives. Moreover, the tautomeric forms of **2-PPs**, *taut* and *taut1*, similarly to that of the tautomeric form of **THAIN**, are strongly destabilized in the ground state. On the other hand, upon excitation, CIS computations predict a significant stabilization of the *taut* form for **2-PPs**, except for **NPP** (the energy gap between the *syn* and *taut* forms in the S$_1$ state for **PPP**, **MPP**, and **BPP** lowers to about 1.9 kcal/mol, 0.5 kcal/mol, and 1.0 kcal/mol, respectively). In contrast, tautomeric form of **THAIN** is predicted to be much less stabilized upon excitation (the destabilization energy value is still as high as 9.2 kcal/mol).

The dipole moments μ_e of **FURIN**, **THAIN**, and **THOIN** in the lowest excited singlet states S$_1$ of $^1(\pi,\pi^*)$ character are slightly lower than those in the ground state S$_0$. For **PYRIN** they remain practically the same. The increase of the μ_e value in comparison to μ_g for **3-PI** and the similar direction of the both dipole moments suggest a partial charge transfer process from the indole to the pyridyl moiety upon S$_1 \leftarrow$ S$_0$ excitation (see Fig. 5.3).
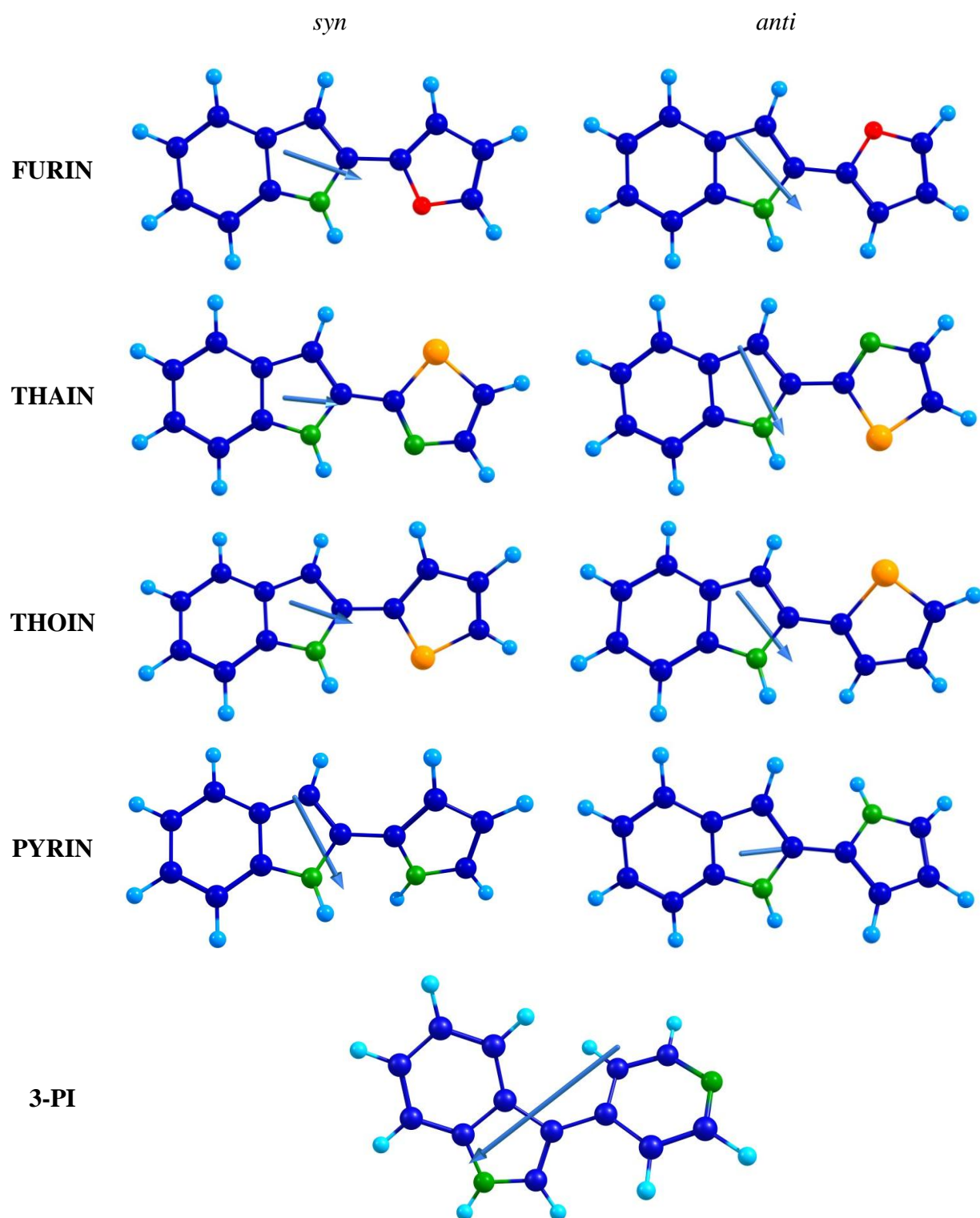
Figure 5.1. DFT/B3LYP/6-31+G(d,p) ground-state optimized molecular structures and corresponding dipole moments of the syn and anti rotameric forms of all the bifunctional indole derivatives under study.

5.2. UV-Vis spectroscopy and photophysics in solutions

Absorption and fluorescence spectra of the studied indole derivatives recorded in three solvents: *n*-hexane, acetonitrile, and 1-propanol, *i.e.* representing nonpolar, polar aprotic and protic media, respectively, are presented in Figure 5.2. The corresponding spectroscopic and photophysical data are collected in Tables 5.3 and 5.4.
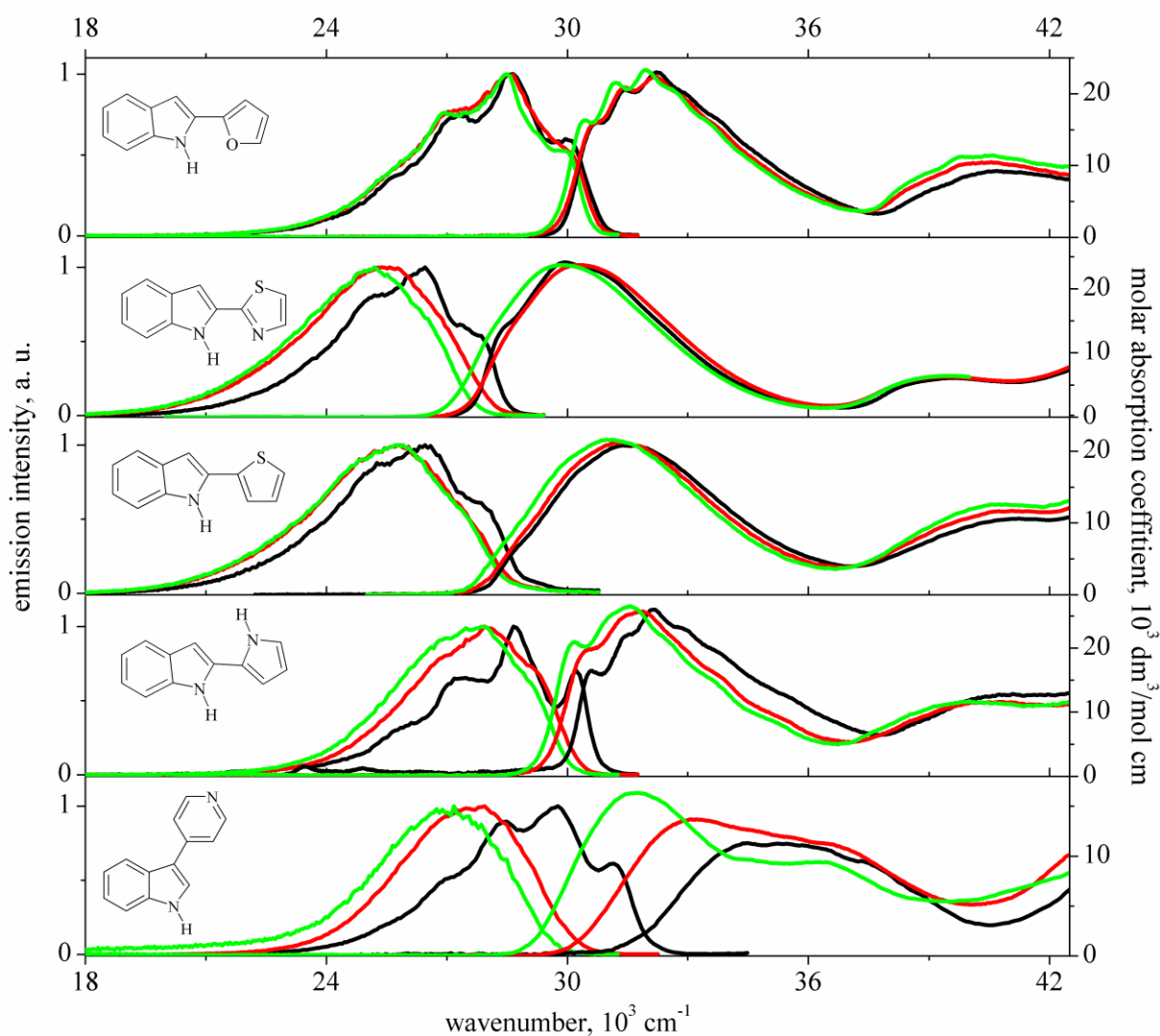
Figure 5.2. Room temperature absorption and corrected and normalized fluorescence spectra of **FURIN***,* **THAIN***,* **THOIN***,* **PYRIN***, and* **3-PI** *(from top to bottom). Black – n-hexane, red – acetonitrile, green – 1-propanol.*

The shape and spectral positions of the broad absorption and emission spectra of **PYRIN** and **FURIN** are very similar; two lowest absorption bands and the single emission spectra in various solvents are located at about 32000 cm^{-1}, 41000 cm^{-1}, and 28500 cm^{-1}, respectively. The spectra of sulfur containing compounds, **THAIN** and **THOIN**, are

considerably red shifted. The corresponding Stokes shift vary from *ca*. 3700 (±100) cm^{-1} for **FURIN** and **PYRIN** to about 5400 (±300) cm^{-1} for **THOIN**.

The TD-DFT computed spectral positions of transitions to the lowest excited $^1(\pi,\pi^*)$ states of **3-PI** and of the *syn* and *anti* tautomeric forms of the other compounds are in excellent agreement with the experimentally measured absorption maxima (Table 5.3).

Table 5.3. Comparison between TD-DFT/B3LYP/6-31+G(d,p) calculated energies ($\tilde{\nu}$, in cm^{-1}) and oscillator strengths (f) corresponding to the vertical transitions to low-lying $^1(\pi,\pi^*)$ states* of the syn and anti forms of the studied compounds, and locations of the experimental absorption band maxima ($\tilde{\nu}_{exp}$, in cm^{-1}) and molar absorption coefficients (ε, in dm^3/mol cm) in n-hexane.

Compound	State	$\tilde{\nu}$ syn	f syn	State	$\tilde{\nu}$ anti	f anti	$\tilde{\nu}_{exp}$ [a]	ε
FURIN	S_1	31650	0.676	S_1	31940	0.688	32300	*ca*. 23000
	S_2	34270	0.093	S_2	34390	0.087		
	S_4	38970	0.052	S_3	39150	0.059	41000	9240
	S_6	42060	0.129	S_6	41590	0.119		
THAIN	S_1	29130	0.392	S_1	29420	0.504	29900	24100
	S_2	31150	0.285	S_2	31400	0.208		
	S_6	40780	0.064	S_7	36650	0.035	39500	6400
THOIN	S_1	30500	0.512	S_1	30280	0.507	31550	20800
	S_2	33360	0.115	S_2	33200	0.126		
	S_6	41030	0.056	S_6	40700	0.091	41000	10500
PYRIN	S_1	33170	0.591	S_1	32800	0.665	32200	*ca*. 26000
	S_4	39400	0.101	S_5	39440	0.137	40500	12700
	S_5	39860	0.088	S_8	41200	0.061		
3-PI	S_1	33930	0.238				*ca*. 35300	
	S_4	37920	0.037					
	S_5	38200	0.066					

[a] Scatter of results: ± 150 cm^{-1}. * Only transitions of significant intensity are shown (f > 0.03). The computed energies of the $^1(n,\pi^*)$ states are higher than those of the $^1(\pi,\pi^*)$ states collected in the Table.

It should be stressed, however, that the computed energies and oscillator strengths of the low-lying vertical transitions of the both rotameric forms of each compound are very similar (the corresponding computed absorption spectra are shown in Fig. S.5.1 in Chapter 7: Supporting information). Therefore, the position and intensities of the near-UV experimental absorption bands do not allow us to distinguish which forms of the compounds exist in the ground state. The lowest computed transitions $S_1 \leftarrow S_0$ for all the compounds are dominated by a configuration corresponding to an electron jump from the highest occupied molecular orbital (HOMO) to the lowest unoccupied molecular orbital, LUMO (Fig. 5.3). These L_a-type

transitions carry high oscillator strength. For **3-PI**, contrary to the other compounds, the calculations predict that the transition involves electron density flow from an orbital localized mainly on the indole moiety into an orbital localized on the pyridyl unit. This result suggests a charge transfer character of the lowest excited singlet state. The $S_2 \leftarrow S_0$ transition carrying relatively low oscillator strength (except for **THAIN**) is of L_b–type. The comparison of calculations with the experimental absorption spectra of all the indole derivatives strongly suggests that both the $L_a \leftarrow S_0$ and $L_b \leftarrow S_0$ transitions are present in the spectral region of the lowest broad absorption band. It is noticeable that the computed energies of the lowest $^1(n,\pi^*)$ states are much higher than that to the $^1(\pi,\pi^*)$ states for all the compounds under study (Table 5.3).

HOMO   LUMO

FURIN

3-PI
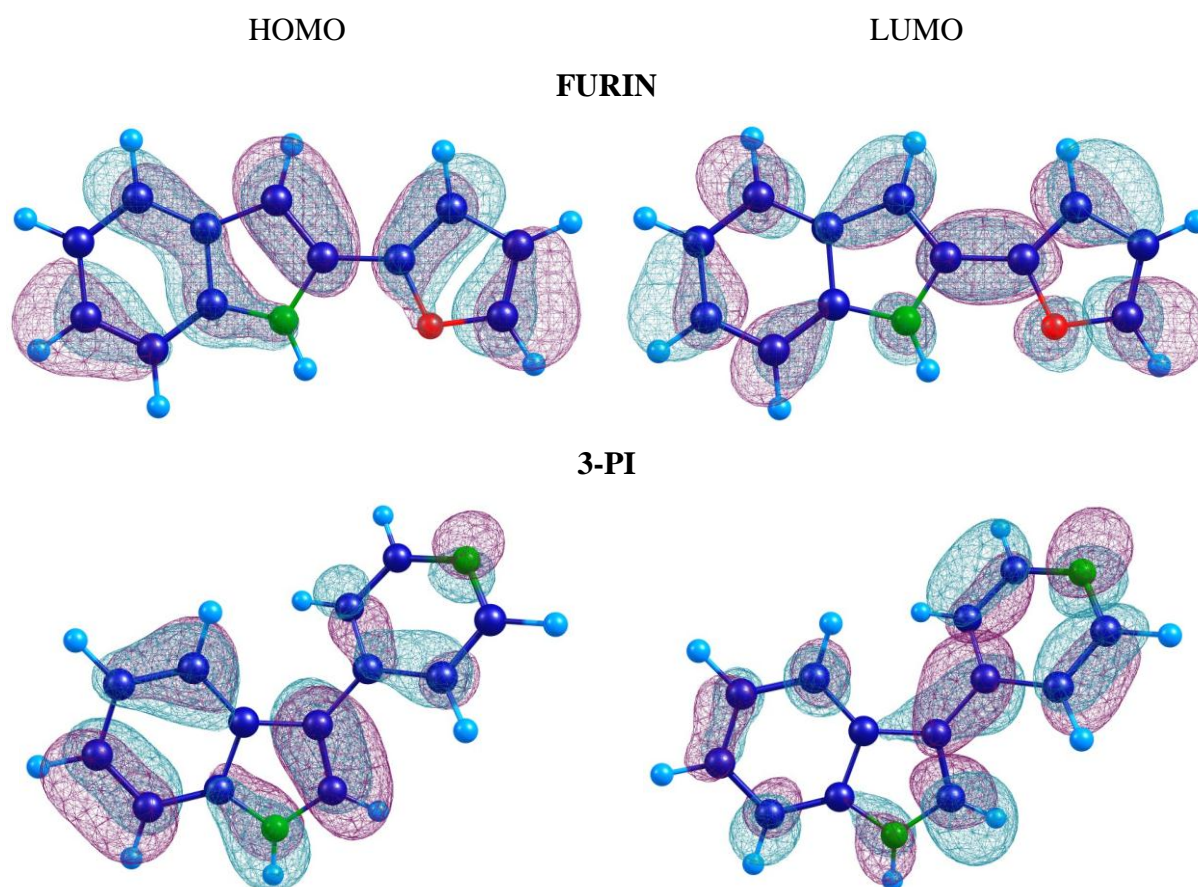
*Figure 5.3. Shapes of molecular orbitals of **3-PI** and the syn rotameric form of **FURIN** involved in the $S_1(L_a) \leftarrow S_0$ transitions.*

The fluorescence excitation spectra of **FURIN, THAIN**, **THOIN**, and **PYRIN** in *n*-hexane and 1-propanol, as well as in acetonitrile match well the corresponding absorption spectra (as an example, the spectra of **FURIN** are presented in Fig. 5.4). This finding indicates that the fluorescence originates from the same species which exist in the ground

state. Absorption and emission spectra of **FURIN, THAIN**, and **THOIN**, in agreement with the small values of the computed ground and excited state dipole moments (Tables 5.1 and 5.2), do not show any significant solvent dependence. On the other hand, for **3-PI** the lowest absorption band, as well as the fluorescence spectrum, reveal a significant shift to the red with increasing solvent polarity and hydrogen bond donor ability. Moreover, a red shift is observed upon passing from acetonitrile to a less polar 1-propanol (Table 5.3), indicating an important role of specific, hydrogen-bonding interactions in the ground and excited state stabilization of the molecule. The Stokes shifts are *ca*. 5500 cm^{-1} in aprotic solvents and about 5000 cm^{-1} in alcohols.
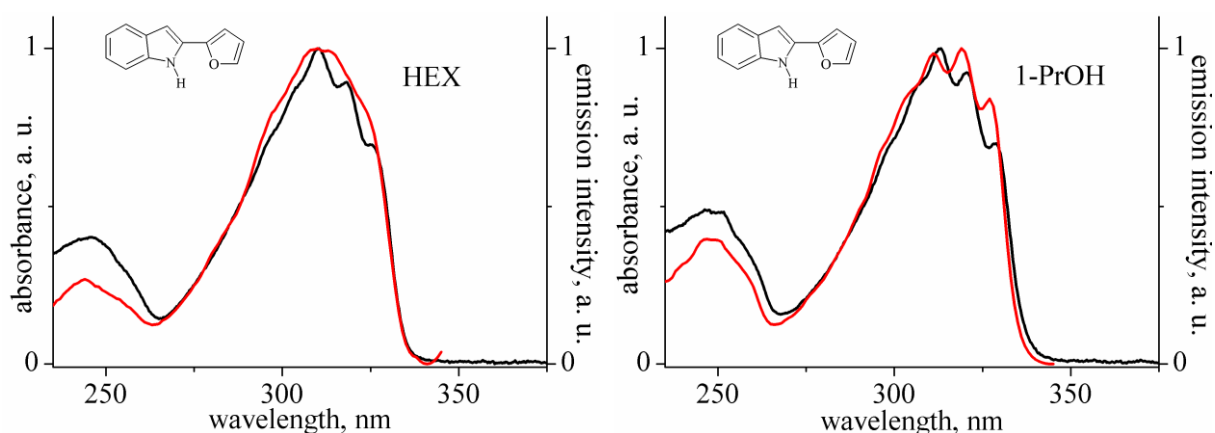
*Figure 5.4. Room-temperature absorption (black) and fluorescence excitation (red) spectra of **FURIN** (as the representative of the studied indole derivatives) in n-hexane and 1-propanol.*

Contrary to our expectation, the photophysical data of **FURIN**, **PYRIN**, **THAIN**, and **THOIN** do not show any solvent dependence (Table 5.4). The fluorescence quantum yields Φ_f are high (*ca*. 20% for the latter two compounds and *ca.* 80% for **FURIN** and **PYRIN**). The four times smaller Φ_f values for the sulfur containing compounds most probably manifest the increase of the efficiency of the intersystem crossing processes (leading to the increase of population of the triplet manifold) due to a "heavy atom effect".[243-246] Fluorescence decay times obtained on the nanosecond time scale can be well fitted to a monoexponential decay; the lifetime values τ are of about 0.5-1.0 ns for **THAIN** and **THOIN**, and about 1.2-1.7 ns for **FURIN** and **PYRIN**.

The obtained quantum yields and lifetimes lead to large values of the radiative k_f rate constants (eq. 2.5) as well as of the electronic transition dipole moments in fluorescence M_{fl} (eq. 2.8). The large k_f and M_{fl} values indicate that the radiative transitions in emission are fully allowed. Interestingly enough, the M_{fl} values are similar to the electronic transition dipole moments M_{abs} corresponding to absorption (eq. 2.8). This seems to reflect the similar

nature of the Franck-Condon excited states initially reached in absorption and the solvent equilibrated fluorescent states.

Table 5.4. Solvent effects on the spectral position of the absorption and fluorescence maxima ($\tilde{v}_{abs}$ and $\tilde{v}_{fl}$, correspondingly, in cm^{-1}), quantum yields (Φ_f), decay times (τ, in ns) and resulting radiationless (k_{nr}, in s^{-1}) and radiative (k_f, in s^{-1}) rate constants, and electronic transition dipole moments in absorption (M_{abs}, in D) and fluorescence (M_{fl}, in D).

Compound	Solvent	$\tilde{v}_{abs}$ [b]	$\tilde{v}_{fl}$ [b]	Φ_f [a]	τ [a]	$k_r 10^8$	$k_{nr} 10^8$	M_{fl}	M_{abs}
FURIN	HEX	32300	28600	0.78	1.4	5.6	1.6	5.4	4.3
	ACN	32250	28600	0.87	1.6	5.4	0.8	5.5	4.4
	1-PrOH	32000	28500	0.89	1.7	5.2	0.6	5.2	4.7
THAIN	HEX	29900	26400	0.23	~0.6	~3.8	~12.8	~5.0	4.9
	ACN	30300	25400	0.24	0.9	2.7	8.4	4.6	5.0
	1-PrOH	29800	25200	0.18	~0.6	~3.0	~13.7	~4.7	5.0
THOIN	HEX	31550	26400	0.22	~0.8	~2.8	~9.8	~4.3	4.7
	ACN	31400	25700	0.25	0.9	2.8	8.3	4.6	4.8
	1-PrOH	31100	25700	0.27	1.0	2.7	7.3	4.4	4.7
PYRIN	HEX	32200	28700	0.72	1.2	6.0	2.3	5.6	4.4
	ACN	31800	28000	0.84	1.6	5.3	1.0	5.6	4.5
	1-PrOH	31500	27800	0.89	1.6	5.6	0.7	5.6	4.2
3-PI	HEX	35000	29600	0.23	~0.5	~4.6	~15.4	~4.6	3.6
	ACN	33200	27500	0.75	2.2	3.4	1.1	4.7	4.5
	DMSO	32200	26750	0.88	2.3	3.8	0.5	4.4	4.7
	1-BuOH	31700	26750	0.2	0.8	2.5	10.0	3.9	
	1-PrOH	31700	26800	0.12	~0.5	~2.4	~17.6	3.9	4.9
	EtOH	31900	26750	0.80 [c] / 0.05	2.0	4.0	10.0		
				0.81 [c]	1.7 [c]	4.8 [c]	1.1		
	MeOH	31800	26750	0.013					
				0.07 [d]	$\approx$0.2 [d]	$\approx$3.5 [d]	$\approx$46.5		

[a] Error is about 10%. Thus, the maximum error is about 20% for the rate constants k_{nr} and k_f and about 10% for the transition moment M_{fl}. [b] Scatter of results: ± 150 cm^{-1}. [c] Measured at 173 K; [d] measured at 193 K.

It should be stressed that **FURIN**, **THAIN**, and **THOIN**, contrary to the other bifunctional molecules for which the proton donor and acceptor groups are located in separate moieties linked by a single bond (such as 2-(2'-pyridyl)indole,[132] 2-(2'-pyridyl)pyrroles,[134,135,185,186] and 2-pyridylpyrazoles[181,237]), do not show any spectral and

kinetic evidence of the rotamerization (for all the compounds) and/or photoinduced tautomerization (for **THAIN**) processes. The lack of the efficient deactivation of the lowest excited singlet states S_1 in protic media *via* internal conversion (IC) and/or ESDPT processes suggests that the studied compounds do not form cyclic, doubly hydrogen-bonded complexes. In order to gain more insight into the formation of the complexes, titration experiments have been performed (Fig. 5.5). Upon adding 1-butanol, at concentrations low enough to prevent the formation of alcohol oligomers,[132] to *n*-hexane solution of **THAIN** and **PYRIN** an isosbestic point in the absorption spectra is observed. This fact demonstrates an equilibrium between two individua in the ground state, most probably between the uncomplexed and complexed forms. The absorption data yield (eqs. 2.10 and 2.11) the 1:1 stoichiometry of the complex of **PYRIN** and the equilibrium constant of 30 ($\pm$5) dm^3 mol^{-1}. On the other hand, the analysis of the absorption of **THAIN** complexes does not lead to the equivocal results. The analysis performed in the red corner of the absorption spectra (at 366 nm) results in the 1:1 stoichiometry, the determination of stoichiometry from the absorption data at 328 nm and 350 nm lead to the values of 1:1.4 and 1:1.6, respectively. The latter findings can hardly be explained in terms of the model assuming a reaction involving one chromophore molecule and *n* alcohol molecules,[132] but it is most probably related to the faults caused by small absorption changes upon adding alcohol. For **THOIN** and **FURIN** no measurable changes in absorption were observed in a wide range of alcohol concentrations. The fluorescence spectra of **THAIN**, **THOIN**, and **PYRIN** show a small shift to lower energies with the increase of 1-BuOH concentration; the emission intensities, however, do not change significantly.

The topology of **3-PI** excludes a possibility of forming cyclic 1:1 solvates with water or alcohol, and therefore, of excited state proton transfer *via* a solvent bridge. The probability of forming cyclic 1:2 species should also be reduced. Formation of ground state complexes with 1-butanol is illustrated in Figure 5.5. In contrast to our previous studies of 2-(2'-pyridyl)indole and 2-(3'-pyridyl)indole,[132,133] where the 1:1 or 1:2 stoichiometries could readily be determined, the spectral changes accompanying titrations are quite complicated. This is manifested by not well-defined isosbestic points, present only in a small concentration range, if at all, and by continuous red shifts and intensity changes in both absorption and emission. This behavior suggests that various types of complexes are formed, with one or more molecules of alcohol attached either to the NH group or to the pyridine nitrogen atom.
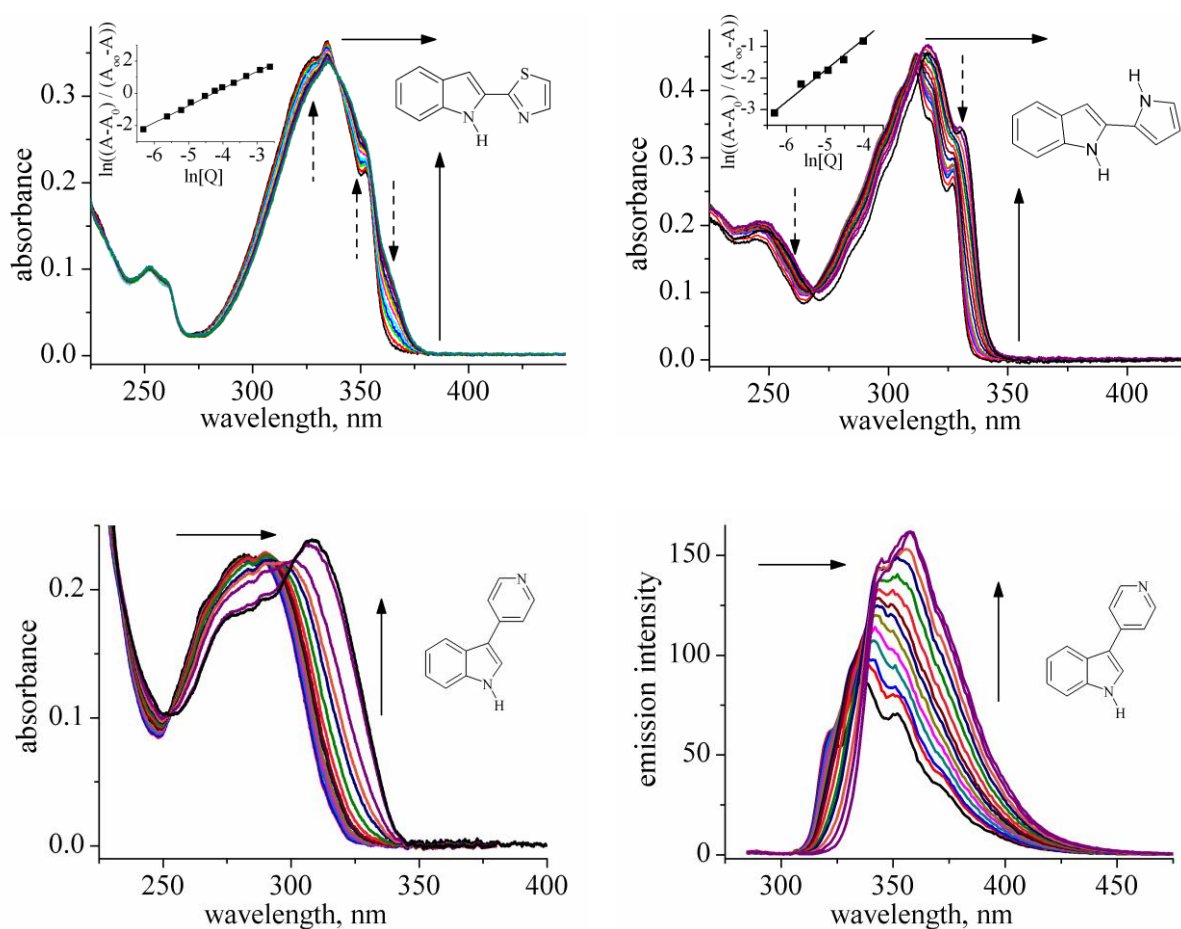
*Figure 5.5. Changes in absorption of **THAIN** and **PYRIN** (top panels) and absorption and emission of **3-PI** observed upon titrating n-hexane solutions with 1-butanol. The full arrows show the spectral evolution with increasing 1-butanol concentration, from 0 to 0.35 mol dm^{-3}. Because of the lack of clear isosbestic points for **3-PI**, fluorescence intensities reflect changes in quantum yield only in an approximate fashion. The insets in the top panels show the determination of the equilibrium constant and stoichiometry of the complex from the absorption data recorded at 366 nm and 333 nm for **THAIN** and **PYRIN**, respectively; the dashed arrows show the positions of the analysis; A_0 and A_∞ denote the absorbance measured when only the bare or complexed forms are present, and A is the absorbance measured at an alcohol concentration [Q] (see eqs. 2.10 and 2.11).*

Fluorescence quantum yields Φ_f of **3-PI** are as large as 0.75 and 0.88 in strongly polar aprotic solvents, such as acetonitrile and dimethyl sulfoxide (Table 5.4). The parallel decrease of the Φ_f and τ values observed in *n*-hexane solutions can hardly be explained in terms of the interactions between close lying $^1(\pi,\pi^*)$ and $^1(n,\pi^*)$ states, which can decrease the electronic transition dipole moments in nonpolar media (the "proximity effects"),[70] because: (i) the TD-DFT calculations predict that the vertical transition to the lowest $^1(n,\pi^*)$ state lies much higher in energy than that to the lowest $^1(\pi,\pi^*)$ state (Table 5.3), and (ii) the radiative rate constant in *n*-hexane $k_f \cong 4.6 \cdot 10^8$ s^{-1} is similar (or even slightly higher) than that in ACN and DMSO. The plausible explanation of this interesting finding involves the solvent-dependent

twisting of the pyridyl unit with respect to the indole moiety in the excited state.[182] Calculations (performed by Michał Kijak) of transition intensities as a function of α, the angle between the planes of pyridine and indole units, reveal a decrease of the oscillator strength practically to zero for $\alpha = 90^o$. Another observation which supports this hypothesis is that the values of the radiative rate constants are larger at lower temperatures in glassy solvents ($k_f \cong 4 \cdot 10^8$ s^{-1}) than those at room temperature alcoholic solutions ($k_f \cong 2.5 \cdot 10^8$ s^{-1}). This can be explained by a hindrance to twisting caused by increasing solvent viscosity.

The data collected in Table 5.4 indicate that an efficient nonradiative deactivation channel is switched on in protic environments. Only solvents acting as hydrogen bond donors cause this effect; no enhanced deactivation is observed for DMSO, a hydrogen bond acceptor. A systematic study of the room temperature fluorescence quantum yields of **3-PI** in a number of proton donating solvents such as various alcohols and water show that the decrease of the fluorescence efficiency is correlated with their solution phase acidity (as it is described by the Taft's parameter α;[180,247] this parameter increases from 0.78-0.79 for 1-PrOH and 1-BuOH to 1.17 for water solutions, Table 2.1). Another factor which seems to be responsible for quenching is solvent viscosity. The importance of this factor is revealed by the finding that no quenching is observed in rigid alcohol glasses. On the other hand, the solvent viscosity is not the only parameter which determines the decrease of the emission quantum yields. At room temperature, fluorescence quantum yield in water ($\Phi_f = 0.009$) is lower than that in methanol ($\Phi_f = 0.013$). The latter is less viscous, but also less acidic than water. Noticeably, the increase of the strength of the hydrogen bond between an alcohol molecule and the pyridyl nitrogen atom is expected upon electronic excitation due to the huge increase of basicity of this hydrogen bond acceptor center. The changes in pK_a have been obtained from the absorption and fluorescence investigations of neutral molecules and protonated cations in acetonitrile and aqueous solutions of all the studied indole derivatives with the use of the "Förster cycle".[18,20] **3-PI**, similarly to the other compounds, reveals a dramatic increase of the pK_a value (Table 5.5).

Table 5.5. pK$_a$ changes upon S$_1 \leftarrow$ S$_0$ excitation obtained with the use of eq. 2.12.

	FURIN[b]	THAIN[b]	THOIN[a]	3-PI[b]
$\Delta pK_a = pK_a{}^* - pK_a{}^G$	12.7	8.9	$\approx$9.7	~8.3

[a] The cation does not show any trace of fluorescence. Changes in pK_a are estimated from the absorption maxima.
[b] The protonated cations reveal very low intense fluorescence (about two orders of magnitude less intense than the emission of neutral molecules).

In order to test a behavior of the relatively well defined strongly hydrogen-bonded complexes upon excitation, the titration experiments in *n*-hexane solutions of **3-PI** by 1,1,13,3,3-hexafluoro-2-propanol (HFP) were performed (Fig. 5.6). HFP is the most acidic hydrogen bonding donor of all used in this work and an extremely weak base.[247] An isosbestic point in absorption and an increase of the fluorescence intensity was observed at very small HFP concentrations of about 10^{-3} mol dm^{-3} (curves a-c). The increase of the alcohol concentrations results in formation of various complexes of higher stoichiometry (no clear isosbestic point was detected) and in fluorescence quenching (curves d-e). Finally, absorption of the cation appeared (lowest energy band in curve e). The fluorescence of the cation was of extremely low intensity.
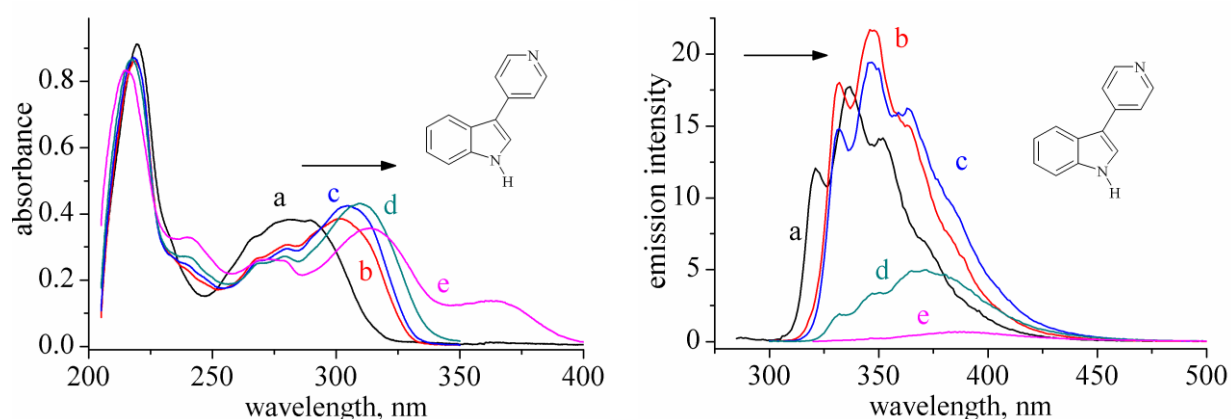
*Figure 5.6. Evolution of absorption and emission observed upon adding 1,1,1,3,3,3-hexafluoro-2-propanol (HFP) to n-hexane solutions of **3-PI** (a, no alcohol, b-e, alcohol concentrations: $7.9 \cdot 10^{-4}$, $7.1 \cdot 10^{-3}$, $7.9 \cdot 10^{-2}$, 0.31 mol dm^{-3}, respectively). The emission intensities reflect the relative fluorescence quantum yields.*

These observations suggest a model for the fluorescence quenching involving the changes of the intermolecular OH….N hydrogen bond.[182] As a result of electron density flow onto the pyridine moiety upon excitation (Fig. 5.3), the hydrogen bond becomes much stronger in the lowest excited singlet state S_1 than that in S_0. The increase of basicity can enable proton transfer from water or alcohol to the pyridyl nitrogen atom followed by twisting of the protonated pyridyl unit with respect to the indole moiety (both TD-DFT and CIS excited state geometry optimizations, performed by Michał Kijak, yield a perpendicular geometry in the lowest excited state S_1 for the protonated cation). Moreover, the calculations predict a very low S_1–S_0 energy gap of about 0.5-1.0 eV for this twisted cation. According to the "energy gap law",[248] the S_1 state of the cation should be efficiently depopulated, what is observed indeed.
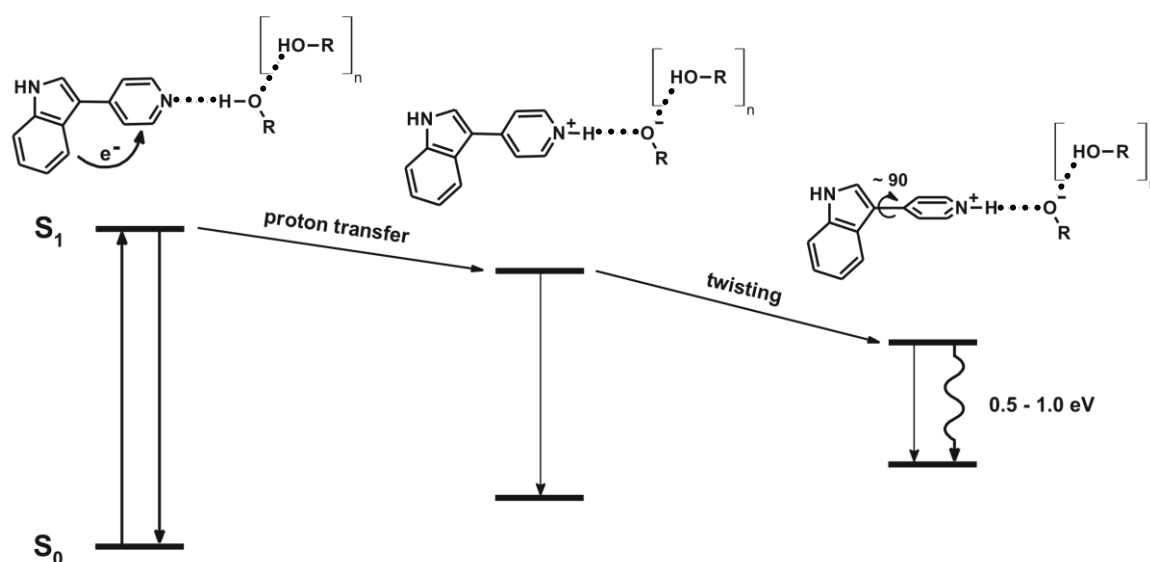
*Figure 5.7. Sequence of excited state processes leading to fluorescence quenching of **3-PI** in a hydroxylic solvent.*[182]

The electron density flow from the indole moiety onto the pyridine ring of **3-PI** upon electronic excitation should result in the increase of the dipole moment in S_1 (as it is predicted by DFT and TD-DFT computations (Tables 5.1 and 5.2). In order to verify the CT character of the lowest excited Franck-Condon state obtained directly upon excitation and the solvent equilibrated fluorescent state of **3-PI**, the corresponding dipole moments were estimated by the solvatochromic shift method with the use of simplified Lippert-Mataga relations[210-214] (Chapter 2.2.1.5). The solvatochromic plot (Fig. 5.8) corresponding to the absorption maxima in aprotic solvents of varying polarity yields the value of the dipole moment of 8.6 D in the Franck-Condon excited state (eq. 2.13 was used with an assumption that the Onsager cavity radius is 3.77 Å as estimated from the molecular dimensions of **3-PI** corresponding to the DFT/B3LYP/6-31+G(d,p) optimized geometry). Similar results were obtained (eqs. 2.14, 2.16 and 2.17) for the fluorescent state (as estimated from the solvatochromic shift of the emission maxima, 7.7 D) and from the solvatochromic dependence of the Stokes shifts (8.0 D) and the sum of the absorption and fluorescence maxima (8.2 D).
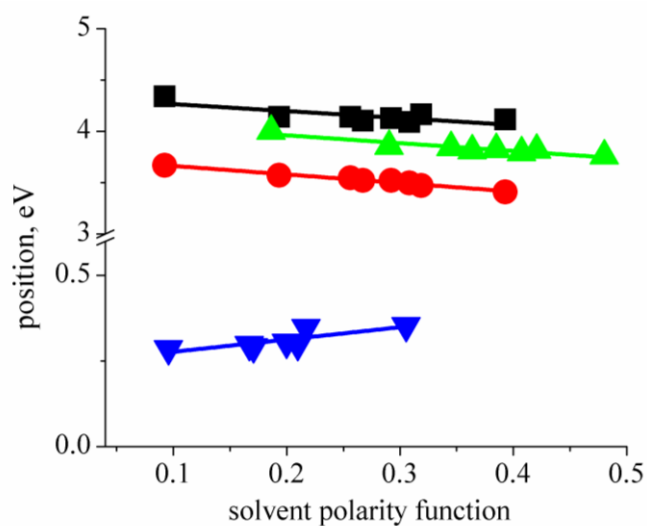
*Figure 5.8. Solvatochromic shift of energies related to absorption (black squares), fluorescence (red circles), sum of the absorption and fluorescence maxima (green triangles) and Stokes shifts (blue triangles) of **3-PI** in HEX, BE, EE, BA, EA, THF, DCM, DMSO, and ACN (from left to right).*

5.3. Supersonic jet studies

In this chapter the results of highly resolved spectroscopic investigations of **FURIN** and **THAIN** (as representatives of the studied indole derivatives) isolated under supersonic jet conditions are reported as a preliminary attempt to identify their rotameric forms and to gain more insight into the geometrical changes accompanying electronic excitation. The experimental laser-induced fluorescence (LIF) excitation (which provides an information about vibrational frequencies in the lowest excited singlet state S_1) and dispersed fluorescence (DF) spectra of bare molecules are compared with the results of theoretical DFT, TD-DFT, and CIS computations at the B3LYP 6-31+G(d,p) level. The 0-0 regions of the LIF and DF spectra of **FURIN** (Fig. 5.9) and **THAIN** (Fig. 5.12), similarly to 2-(2'-pyridyl)indole (2-PI),[137,216] show a rich pattern of low-frequency vibrations. The origins of the $S_1 \leftarrow S_0$ transitions are assigned to the lowest energy bands of the LIF spectra which are observed at 31612 ($\pm$ 1) cm^{-1} and 29350 ($\pm$ 1) cm^{-1}, respectively. The 0-0 bands of the LIF spectra of both compounds are found to be relatively strong, which suggests that only not dramatic structural changes in **FURIN** and **THAIN** take place upon 0-0 excitation to the S_1 state. Vibrationally resolved DF spectra of the compounds, obtained for excitation into specific vibronic levels (SVLF) are shown in Figures 5.11 and 5.13, respectively. These spectra give information about equivalent vibrational modes in the ground and S_1 electronic states. The precise nature of the vibrations optically active in the studied compounds cannot be established without a detailed analysis of the IR, Raman, and UV/VIS spectra of the isotope-substituted samples combined with quantum-chemical calculations. Nevertheless, on the basis of theoretical computations and a comparison with the results reported for 2-PI[137,216] the tentative assignment of the vibrational structure is proposed in Table 5.6 (the results of theoretical computations are shown in Table S.5.1 (**FURIN**) and Table S.5.2 (**THAIN**) in Chapter 7: Supporting information). The calculations predict that the compounds should be planar in both S_0 and S_1 states. **FURIN** exhibits 63 fundamental transitions, 43 of those are due to in-plane polarized (a') transitions, whereas 20 corresponds to out-of-plane (a") vibrations. **THAIN** has 60 normal modes (41 of a', and 19 of a" symmetry). Due to the fact that the lowest excited singlet states of the compounds are of $^1(\pi,\pi^*)$ character (the $^1(n,\pi^*)$ states are expected to lie higher than 37500 cm^{-1}, see Table 5.6) only totally symmetric, in-plane a' vibrations are expected to appear in the LIF and SVLF spectra. The transitions involving odd quanta of out-of-plane vibrations are non-totally symmetric and thus symmetry forbidden.
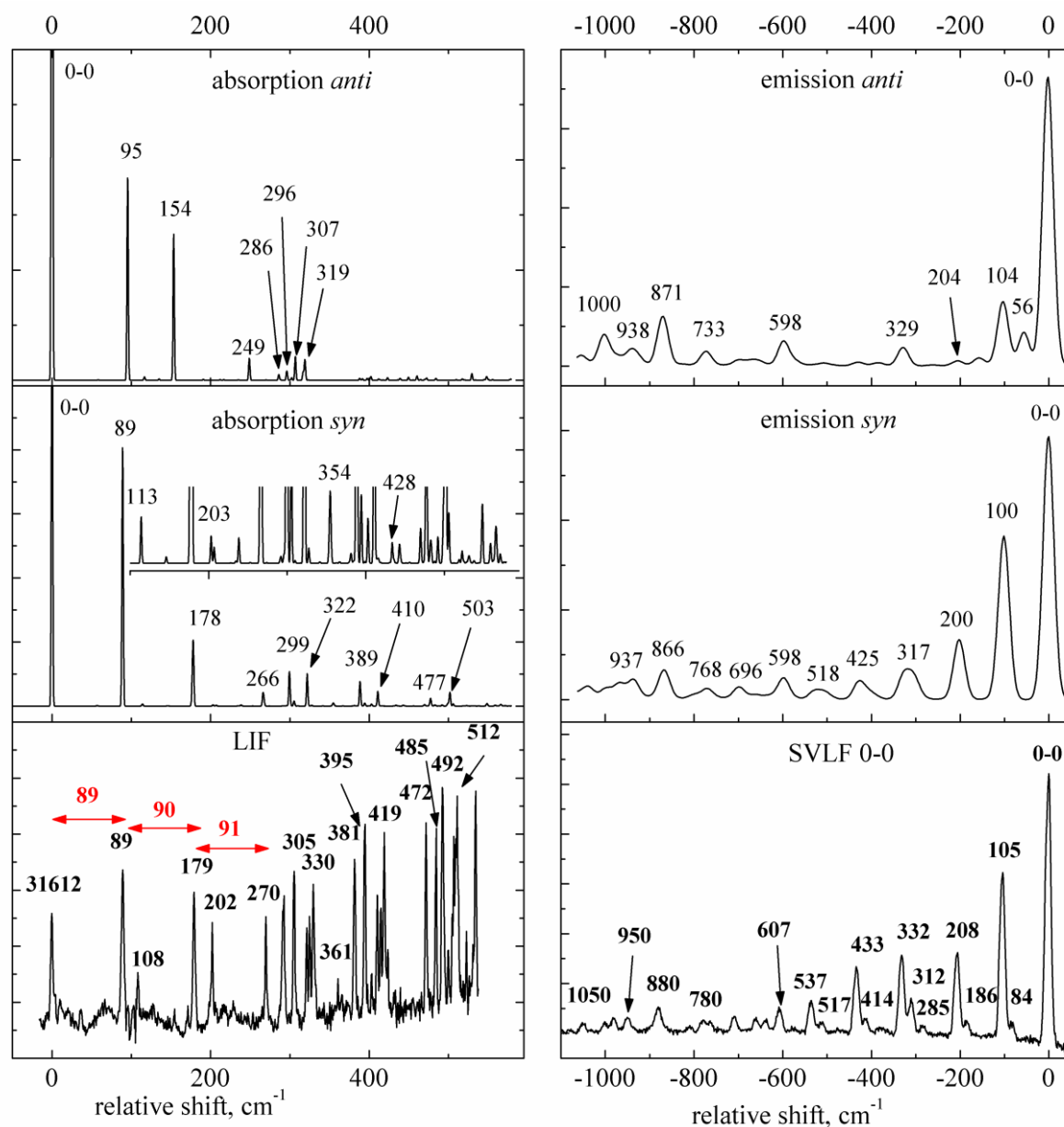
*Figure 5.9. LIF excitation (bottom left), SVLF recorded for excitation to the origin (bottom right) and calculated absorption (middle left – syn, top left – anti) and emission (middle right – syn, top right – anti) spectra of **FURIN** at the DFT/TD-DFT/B3LYP/6-31+G(d,p) and TD-DFT/DFT/B3LYP/6-31+G(d,p) levels, respectively. Scaling factor 0.9648. The inset presents the enlarged spectrum (intensity *100).*

Figure 5.9 shows the comparison of the LIF excitation and SVLF (excitation at the origin) spectra of **FURIN** with the TD-DFT computed spectra obtained for the both *syn* and *anti* rotamer. The origin of the $S_1 \leftarrow S_0$ transition is strong and located at 31612 cm^{-1}. The high relative intensity of this band suggests a considerable overlap of the vibrational eigenfunctions of the electronic states involved in the transition (Franck-Condon factor) and thus a similar geometrical structure. TD-DFT calculations predict the position of the 0-0 transition at 31645 cm^{-1} for the *syn* tautomeric form and 31940 cm^{-1} for the *anti* one; the

computed values are very similar and both are in a very good agreement with the experimental value. This finding does not allow us to distinguish between both rotameric forms.

There are several intense transitions in the LIF excitation spectrum. The analysis, however, could be performed only for the lowest 600 cm^{-1}; above 32800 cm^{-1} the spectrum becomes congested and difficult for analysis. The comparison of the experimental LIF spectrum with the DFT/TD-DFT/B3LYP/6-31+G(d,p) computed absorption spectra suggest that the LIF spectrum of **FURIN** monomer corresponds to the *syn* form. For example, the spectral positions of the bands observed at 89 cm^{-1}, 179 cm^{-1}, and 270 cm^{-1} are in a very good agreement with the bands at 89 cm^{-1}, 178 cm^{-1}, and 266 cm^{-1} theoretically predicted for the *syn* form. The spectral positions of the other bands observed in computed absorption fit satisfactorily to the LIF spectrum. The TD-DFT and CIS calculations at the B3LYP/6-31+G(d,p) level (Table S.5.1 in Chapter 7: Supporting information) of the excited-state vibrational frequencies allow us to assign tentatively the observed bands to fundamental vibrational transitions, their overtones and combinations (Table 5.6). The transitions observed at 89 cm^{-1} (A$_1$), 305 cm^{-1} (D$_1$), 330 cm^{-1} (E$_1$), and 512 cm^{-1} (F$_1$) most probably correspond to the in-plane modes which are visualized in Figure 5.10; the spectrum shows also their overtones (at 89 cm^{-1}, 179 cm^{-1}, 270 cm^{-1}, 361 cm^{-1} a most prominent progression built on the 0-0 transition by the in-plane C2-C2' rocking vibration is observed) and combinations (the bands at 395 cm^{-1}, 485 cm^{-1} as well as 419 cm^{-1} and ~508 cm^{-1} are assigned to the progressions of the 89 cm^{-1} vibration built on the 305 cm^{-1} and 330 cm^{-1} fundamental transitions, respectively). Under assumption that even overtones of out-of-plane vibrations are optically active, the band observed at 108 cm^{-1} (B$_2$) is assigned to the active overtone of the vibration predicted at 50 cm^{-1} or 56 cm^{-1} (CIS method) and at 57 cm^{-1} or 58 cm^{-1} (TD-DFT method) for the *syn* or *anti* forms, respectively. Noticeably, the origin of the band recorded at 202 cm^{-1} is not clear. On one hand, it can be assigned to the combination of the 89 cm^{-1} and 108 cm^{-1} vibrations (A$_1$B$_2$). On the other hand, it corresponds well to the even overtone (C$_2$) of the vibration computed by CIS method at 98 cm^{-1} for the *syn* rotamer (the TD-DFT computed frequency does not fit perfectly to this assignment, Fig. 5.10). The even overtone of similar out-of-plane mode is observed for 2-PI at 163 cm^{-1} (Table 5.6). Several observed transitions (*e.g.*, at 293 cm^{-1}, 321 cm^{-1}, 381 cm^{-1}, 413 cm^{-1}, 439 cm^{-1}, and 472 cm^{-1}) can be satisfactorily described by combinations of the B$_2$ and/or C$_2$ overtones. It is interesting to note that the most active in the LIF spectrum are the vibrations related to the C2-C2' single bond which links the indole ring with furan or thiazole moiety, *i.e.* the in-plane rocking (average

value ~94 cm^{-1}) as well as out-of-plane rocking (average value 2×~55 cm^{-1}) and/or torsion (average value 2×~94 cm^{-1} for the *syn* form) (Table S.5.1 in Chapter 7: Supporting information).
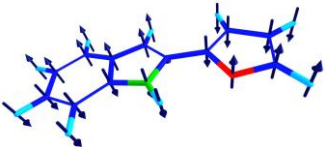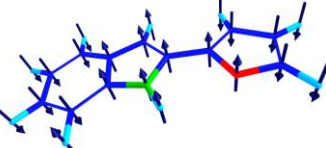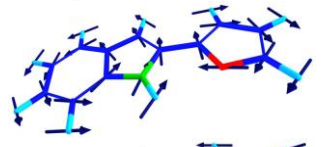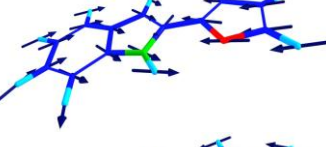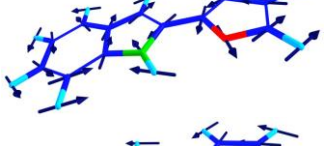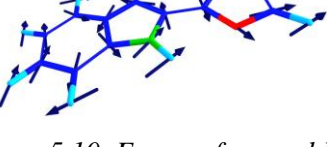
			S_0					S_1		
		syn	*anti*	exp.			*syn*	*anti*	exp.
	out-of-plane torsion	46	31	**84**	CIS TD-DFT		98 89	83 77	**202**
	out-of-plane rocking	68	68	-	CIS TD-DFT		50 57	56 58	**108**
	in-plane rocking	101	103	**105**	CIS TD-DFT		94 89	98 96	**89**
	in-plane stretching	309	306	**312**	CIS TD-DFT		312 299	315 302	**305**
	in-plane skeleton deformation	327	327	**332**	CIS TD-DFT		333 322	337 319	**330**
	in-plane skeleton deformation	506	505		CIS TD-DFT		522 502	523 505	**512**

*Figure 5.10. Forms of several low-frequency normal modes of **FURIN** with DFT/B3LYP/6-31+G(d,p) (S_0) or TD-DFT and CIS/B3LYP/6-31+G(d,p) (S_1) computed (for the syn and anti forms) and experimental (in bold) frequency values (in cm^{-1}) for the ground (S_0) and fluorescent (S_1) state. The experimental frequency values of the out-of-plane vibrations correspond to the first even overtones.*

A series of SVLF spectra of **FURIN** recorded for excitation to the origin (Fig. 5.9) and to various vibronic levels (Fig. 5.11) show a rich pattern of low frequency vibrations. The analysis of excitation-emission patterns allows mapping of correlations between vibrational modes in the ground and excited electronic states (Table 5.7). Excitation to the origin and to the vibronic bands corresponding to the fundamental (89 cm^{-1}) and overtones (179 cm^{-1} and 269 cm^{-1}) of the C2-C2' in-plane vibration leads to the SVLF spectra showing the prominent progression of this vibration at the 105 cm^{-1}, ~208 cm^{-1}, and ~310 cm^{-1} (the last one can also originate from long-axis in-plane stretch vibration). Thus, most probably the vibrations 89 cm^{-1} and 105 cm^{-1} represent the same mode in the S_1 and S_0 states, respectively. On the other

126

hand, the SVLF spectrum recorded upon excitation to the overtone of the out-of-plane vibrational band at 202 cm^{-1} shows a different pattern of the low frequency vibrations. The spectrum shows the clear overtones of the 84 cm^{-1} vibrational mode (*e.g.*, observed at 165 cm^{-1}) and combinations with the 105 cm^{-1} mode and its overtones (observed at 185 cm^{-1}, 268 cm^{-1}, 283 cm^{-1} and ~380 cm^{-1}). This indicates that this mode, which probably corresponds to the even overtone of the out-of-plane C2-C2' torsion, increases its energy from about 42 cm^{-1} to about 101 cm^{-1} upon $S_1 \leftarrow S_0$ excitation. This hypothesis is supported by the analysis of charges on the furan nitrogen and indole oxygen atoms. In the ground state both they both are negatively charged. Upon electronic excitation the charge on the nitrogen atom becomes positive. This effect forces them to attract, which, in turn, leads to the increase of frequency of the respective out-of-plane C2-C2' torsion mode.
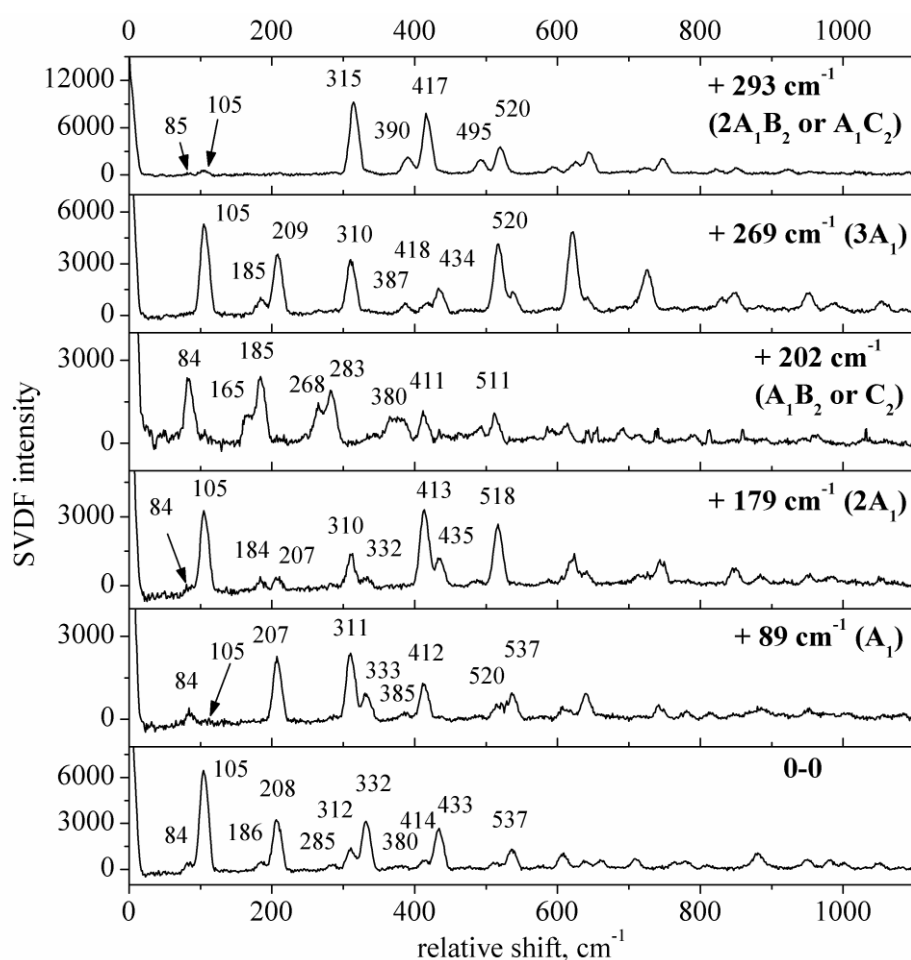
*Figure 5.11. SVLF spectra of jet-cooled **FURIN** obtained for excitation to the origin (0-0) and to different vibronic bands corresponding to the fundamental (89 cm^{-1}) and overtones (179 cm^{-1}, 269 cm^{-1}) of the in-plane C2-C2' rocking vibration as well as to the even overtone of the out-plane C2-C2' torsion vibration (202 cm^{-1}) and its combination with the in-plane 89 cm^{-1} mode (293 cm^{-1}) or, depending on the interpretation, to the combinations of 89 cm^{-1} and 108 cm^{-1} vibrations.*

*Table 5.6. Transition energies (in cm^{-1}) and tentative assignment ($\Delta\nu_{calc}$ computed at the TD-DFT (in brackets) and CIS/B3LYP/6-31+G(d,p) levels) of the vibronic transitions ($\Delta\nu_{exp}$) in the low-energy part of the LIF excitation spectra^a of **FURIN** and **THAIN**. The assignment of the main vibronic transitions of 2-PI ($\Delta\nu_{calc}$ computed at the CIS/B3LYP/6-31(d,p) level) is shown for comparison.[137,216] See text for explanation.*

2-PI			FURIN				THAIN			
$\Delta\nu_{exp}$	assign.	$\Delta\nu_{calc}$	$\Delta\nu_{exp}$	assign.	$\Delta\nu_{calc}$ ^{b}		$\Delta\nu_{exp}$	assign.	$\Delta\nu_{calc}$ ^{b}	
					syn	anti			syn	anti
30308 cm^{-1}	0-0		31612 cm^{-1}	0-0	31645	31940	29350 cm^{-1}	0-0	29130	29415
98	**A$_1$**	**101**	**89**	**A$_1$**	**94 (89)**	**98 (96)**	**78**	**A$_1$**	**88 (80)**	**93 (90)**
107	B$_2$	50*2	108	B$_2$	50 (57)*2	56 (58)*2	93	B$_2$	50 (48)*2	46 (49)*2
163	C$_2$	83*2	179	2A$_1$			156	2A$_1$		
196	A$_2$		202	A$_1$B$_2$ or C$_2$	98 (89)*2	83 (77)*2	171	A$_1$B$_2$?		
261	A$_1$C$_2$		216	2B$_2$			178	A$_1$B$_2$ or C$_2$	87 (72)*2	68 (43)*2
273	**D$_1$**	**280**	270	3A$_1$			236	3A$_1$		
320	**E$_1$**	**320**	293	2A$_1$B$_2$ or A$_1$C$_2$			255	2A$_1$B$_2$ or A$_1$C$_2$		
329	F$_1$?		**305**	**D$_1$**	**312 (299)**	**315 (302)**	**263**	**D$_1$**	**270 (259)**	**270 (254)**
357	2A$_1$C$_2$		321	A$_1$2B$_2$?			277	-		
371	A$_1$D$_1$		325	3B$_2$			**307**	**E$_1$**	**318 (308)**	**319 (308)**
418	A$_1$E$_1$		**330**	**E$_1$**	**333 (322)**	**337 (319)**	335	3A$_1$B$_2$ or 2A$_1$C$_2$		
433	G$_1$	221*2	361	4A$_1$			342	A$_1$D$_1$		
470	2A$_1$D$_1$		381	3A$_1$B$_2$ or 2A$_1$C$_2$			355	B$_2$D$_1$		
483	C$_2$E$_1$		395	A$_1$D$_1$			386	A$_1$E$_1$		
491	-		413	B$_2$D$_1$			396	B$_2$E$_1$		
499	**H$_1$**	**507**	419	A$_1$E$_1$			421	2A$_1$D$_1$		
531	A$_1$B$_2$2C$_2$		439	B$_2$E$_1$			465	2A$_1$E$_1$		
534	**I$_1$**	**544**	472	4A$_1$B$_2$ or 3A$_1$C$_2$			**485**	**F$_1$**	**488 (470)**	**489 (465)**

536	J_1		485	$2A_1D_1$			522	-		
551	-		492	-			**545**	**G_1**	**560 (536)**	**558 (538)**
			~508	$2A_1E_1$			**571**	**H_1**	**595 (581)**	**592 (580)**
579	**K_1**	**579**	**512**	**F_1**	**522 (502)**	**523 (505)**	**596**	**I_1**	**623 (606)**	**622 (596)**

[a] estimated error about 17 cm^{-1}.[240] [b] A scaling coefficient is 0.9648 (DFT) and 0.92 (CIS).[225,226]

Table 5.7. Transition energies (in cm^{-1}) and tentative assignment (Δv_{calc} computed at the DFT/B3LYP/6-31+G(d,p) level) of the vibronic transitions (Δv_{exp}) in the low-energy part of the SVLF spectra ^{a} of **FURIN** *and* **THAIN**.

						FURIN								THAIN	
	excitation to the origin (0-0)			excitation to C_2 ? (202 cm^{-1})						excitation to the origin (0-0)					
Δv_{exp}	assign.		Δv_{exp}	assign.		Δv_{calc} ^{b}			Δv_{exp}	assign.			Δv_{calc} ^{b}	
						syn	*anti*						*syn*	*anti*
0	0-0								0	0-0				
84	C_2'		83	C_2'		46*2	31*2		**94**	**A_1'**			**96**	**96**
105	**A_1'**					**101**	**103**		190	$2A_1$'				
			165	$2C_2$'					**270**	**D_1'**			**262**	**267**
186	A_1'C_2'		185	A_1'C_2'					319	-				
208	$2A_1$'		268	A_1'$2C_2$'					363	A_1'D_1'				
~285	$2A_1$'C_2'		283	$2A_1$'C_2'					407	-				
312	3A_1' or **D_1'**					**309**	**306**		461	$2A_1$'D_1'				
332	**E_1'**					**327**	**327**		**564**	**G_1'**			**560**	**560**
~380	$2A_1$'$2C_2$'		~380	$2A_1$'$2C_2$'					**609**	**H_1'**			**595**	**594**
414	C_2'E_1' or A_1'D_1'		411	C_2'E_1'					642	-				
433	A_1'E_1'													
517	$2A_1$'D_1'													
537	$2A_1$'E_1'													
607	**H_1'**					**596**	**596**							

[a] estimated error 3-6 cm^{-1}.[240] [b] A scaling coefficient is 0.9648.

The presented assignment of the equivalent vibrational modes in the ground and S_1 electronic states is supported by the vibrational structure of the SVLF spectrum obtained for the simultaneous excitation of the in-plane and out-of-plane modes at 292 cm^{-1} (both 84 cm^{-1} and 105 cm^{-1} bands of similar intensity are observed in the spectrum). The computed ground and excited state vibrations of **FURIN** (Table S.5.1 in Chapter 7: Supporting information) are in agreement with the proposed correlations. The analysis of the vibrational structure of the LIF and SVLF spectra indicates that the most considerable geometry change following electronic excitation to the fluorescent state takes place along the in-plane and out-of-plane low frequency modes connected with the C2-C2' single bond.

The LIF excitation and SVLF spectra of **THAIN** are similar to those recorded for **FURIN**. The 0-0 transition in the LIF excitation spectrum appears at 29350 cm^{-1} (Fig. 5.12), while TD-DFT calculations predict the origin of the lowest singlet state at 29130 cm^{-1} for the *syn* rotamer and at 29415 cm^{-1} for the *anti* form. Thus, similarly to **FURIN**, both computed values are in a very good agreement with the experimental observation. The intense bands observed at 78 cm^{-1} (A$_1$), 263 cm^{-1} (D$_1$), 307 cm^{-1} (E$_1$), 485 cm^{-1} (F$_1$), 545 cm^{-1} (G$_1$), 571 cm^{-1} (H$_1$), and 596 cm^{-1} (I$_1$) are assigned to fundamentals of the various in-plane vibrations (Fig. 5.12, Table 5.6). The spectrum shows a progression (observed at 156 cm^{-1} and 236 cm^{-1}) of the lowest vibrational mode corresponding to the in-plane C2-C2' rocking vibration and its combination with the other in-plane modes (the bands at 342 cm^{-1} and 421 cm^{-1}, as well as at 386 cm^{-1} and 465 cm^{-1} are assigned to the progressions of the 78 cm^{-1} vibration built on the 263 cm^{-1} and 307 cm^{-1} fundamental transitions, respectively). The band of lower intensity recorded at 93 cm^{-1} is assigned to the even overtone of the out-of-plane C2-C2' rocking vibrations (B$_2$) computed at 50 cm^{-1} and 46 cm^{-1} (CIS), and 48 cm^{-1} and 49 cm^{-1} (TD-DFT) for the *syn* and *anti* forms, respectively. The band at 178 cm^{-1}, similarly to **FURIN**, can be assigned either to the combination of the 78 cm^{-1} and 93 cm^{-1} vibrations (A$_1$B$_2$) or to the even overtone (C$_2$) of the C2-C2' torsion (which is theoretically predicted at 87 cm^{-1} (CIS) or 72 cm^{-1} (TD-DFT) for the *syn* rotameric form). Several optically active bands represent combinations of these transitions (B$_2$ and A$_1$B$_2$/or C$_2$) with various in-plane vibrations (*e.g.*, observed at 255 cm^{-1}, 335 cm^{-1}, 355 cm^{-1}, and 396 cm^{-1}). Noticeably, the progression of the 78 cm^{-1} vibration observed in the LIF spectrum of **THAIN** is in a very good agreement with theoretically predicted spectral positions of the vibronic bands at 79 cm^{-1}, 159 cm^{-1}, 238 cm^{-1} for the *syn* rotamer; the computed absorption spectrum of the *anti* form does not show these bands (Fig. 5.12). This finding suggests that the *syn* form of **THAIN**, similarly to **FURIN**, is dominant in the ground state.
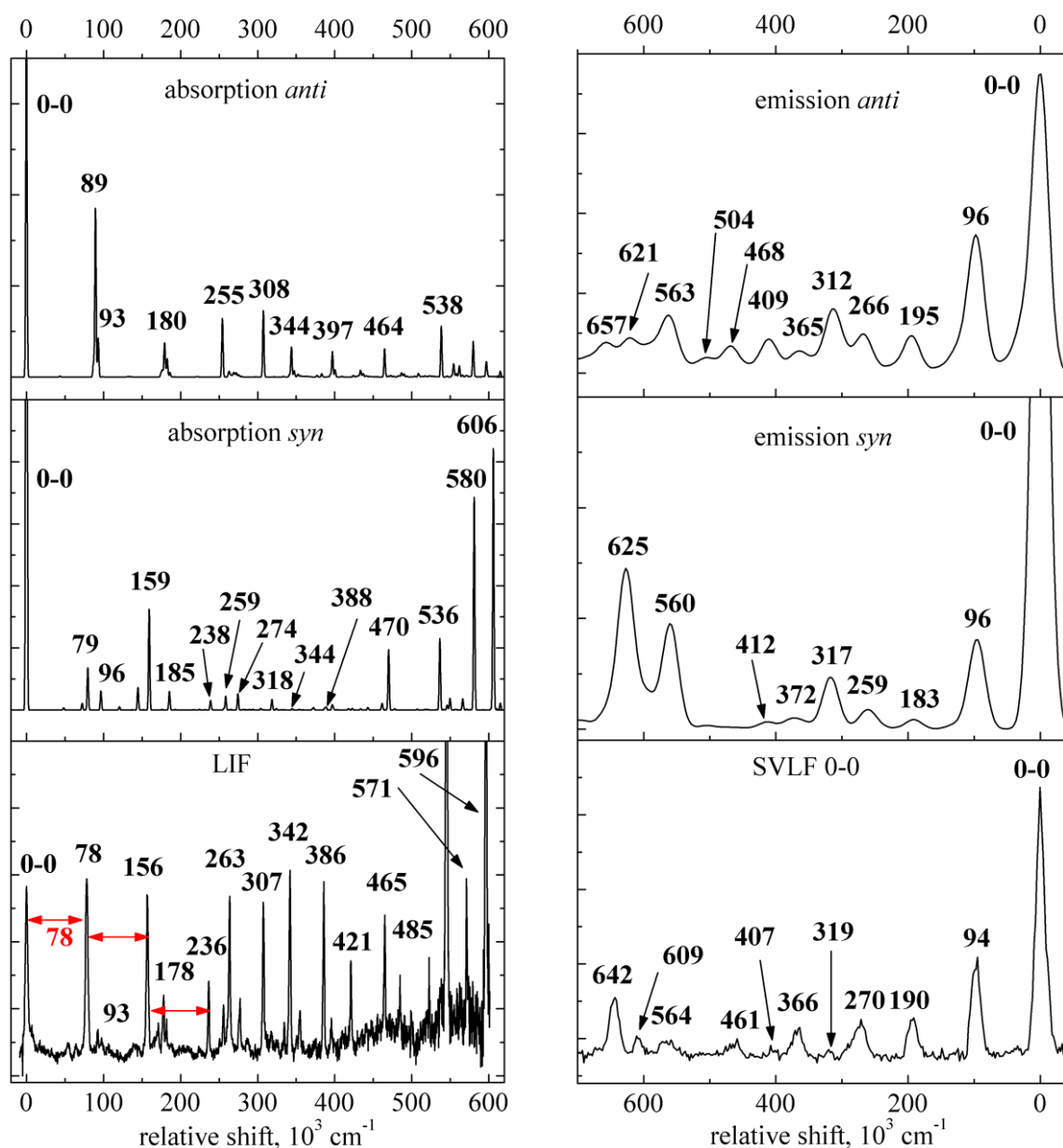
Figure 5.12. LIF excitation (bottom left), SVLF recorded for excitation to the origin (bottom right) and calculated absorption (middle left – syn, top left – anti) and emission (middle right – syn, top right – anti) spectra of **THAIN** *at the DFT/TD-DFT/B3LYP/6-31+G(d,p) and TD-DFT/DFT/B3LYP/6-31+G(d,p) levels, respectively. Scaling factor 0.9648.*

SVLF spectra of **THAIN** recorded for excitation to the origin and to the two other vibronic levels (corresponding to the in-plane C2-C2' rocking vibration and its overtone) are presented in Figs. 5.12 and 5.13. The bands observed at 94 cm⁻¹, 270 cm⁻¹, 564 cm⁻¹, and 609 cm⁻¹ are assigned to fundamentals of the various in-plane modes (Tables 5.7 and S.5.2 in Chapter 7: Supporting information). The spectra show an overtone of the in-plane C2-C2' rocking vibration (at 190 cm⁻¹) and several combinations at 363 and 461 cm⁻¹. Contrary to **FURIN**, the spectra do not show any sign of the optical activity of the out-of-plane C2-C2' vibrations, which are predicted to be observed at about 96 cm⁻¹ or 28 cm⁻¹ (the first even

131

overtone of the torsion vibration for the *syn* and *anti* forms, respectively) and at about 132 cm^{-1} (the overtone of the rocking vibration for both rotamers).

The analysis of the LIF and SVLF spectra of **THAIN** suggests that the change of its geometry takes place along the in-plane C2-C2' rocking vibration. The frequency value of this particular mode decreases from 94 cm^{-1} to 78 cm^{-1} upon electronic excitation.
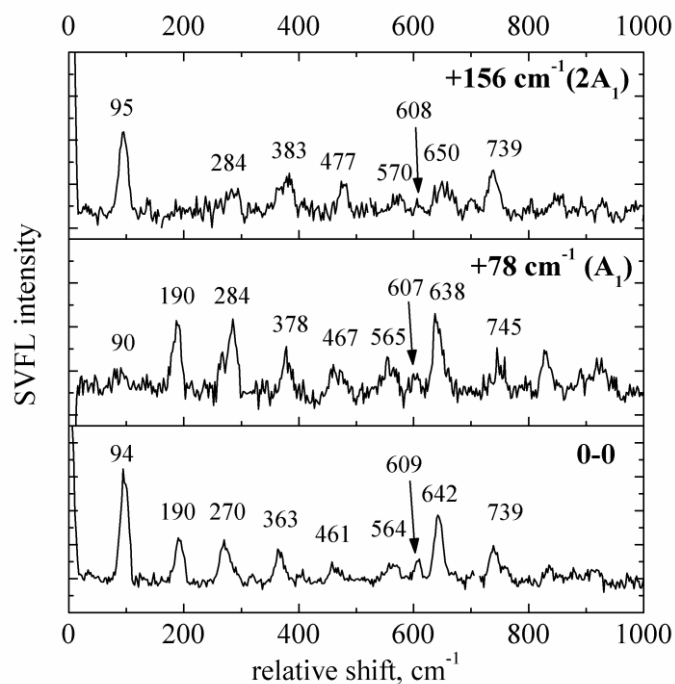
*Figure 5.13. SVLF spectra of jet-cooled **THAIN** obtained for excitation to the origin (0-0) and to two vibronic bands corresponding to the fundamental (78 cm^{-1}) and overtone (156 cm^{-1}) of the in-plane C2-C2' rocking vibration.*

Finally, it should be stressed that the preliminary investigations of complexes of **FURIN** and **THAIN** with acetonitrile, methanol, and water under supersonic jet conditions were also performed. The obtained LIF excitation spectra (not shown), however, are difficult to analyze without parallel investigations by resonant two-photon ionization (R2PI) and IR/R2PI ion depletion spectroscopy combining the structurally sensitive infrared (IR) vibrational predisociation spectroscopy with the mass selective R2PI spectrometry. These laser spectroscopy experiments combined with supersonic jet technique are in progress in our laboratory.

5.3. Summary

Spectroscopic and photophysical studies of the family of bifunctional proton-donor-acceptor indole derivatives which can form *syn* and *anti* conformers *via* internal rotation around a single bond (**THOIN**, **THAIN**, and **FURIN**) and of the compounds which either have not any acceptor center (**PYRIN**), or due to the topology, can not exist in two rotameric forms (**3-PI**) are presented in this chapter.

The investigations in solutions show that the shape and spectral positions of the broad absorption and emission spectra of **PYRIN** and **FURIN** are very similar; the spectra of **THAIN** and **THOIN** are markedly red shifted. The compounds emit fully allowed and efficient fluorescence of high quantum yield values (about 20% for sulfur containing compounds, and about 80% for **PYRIN** and **FURIN**). Photophysical data do not show any solvent dependence. The fluorescence excitation spectra of these compounds indicate that the fluorescence originates from the same species which exist in the ground state. Contrary to the other similar bifunctional molecules, these indole derivatives do not show any spectral and kinetic evidence of the rotamerization and/or photoinduced tautomerization processes. The lack of the efficient deactivation of the lowest excited singlet states S_1 in protic media *via* internal conversion (IC) and/or ESDPT processes suggests that the studied compounds do not form cyclic, doubly hydrogen-bonded complexes. The TD-DFT computed energies and oscillator strengths of the low-lying vertical transitions of the both *syn* and *anti* rotameric forms of the compounds are in excellent agreement with the experimental absorption maxima. Thus, it is difficult to distinguish from the solutions studies which form exists in the ground state. In order to resolve this problem, **THAIN** and **FURIN** were studied under isolated conditions in supersonic jets. The obtained LIF and SVLF spectra seem to correspond to one of the rotamers, *syn* or *anti*. The detailed analysis of the vibrational structure based on the DFT, TD-DFT, and CIS calculations suggests that the *syn* rotamer is a dominant form of the compounds. The compounds are planar both in the ground and fluorescent states. The changes of geometry following electronic excitation are connected with the in-plane and out-of-plane rocking and torsion motions along C2-C2' single bond which links the indole ring with the furan or thiazole moiety.

For **3-PI**, contrary to the other compounds, the calculations predict that the $S_1 \leftarrow S_0$ transition involves electron density flow from an orbital localized mainly on the indole moiety into an orbital localized on the pyridyl unit. This result is confirmed by the solvatochromic

effects on the absorption and fluorescence spectra; the estimated excited state dipole moment value is about two times higher than that in the ground state. The photophysical data indicate that an efficient nonradiative deactivation channel is switched on in protic media; the fluorescence quantum yield of about 80% in highly polar aprotic solvents (ACN, DMSO) decreases dramatically, by about one (1-PrOH, EtOH) or even two (MeOH, water) orders of magnitude in protic solvents. The proposed model (Fig. 5.7) for the fluorescence quenching involves a sequence of such excited-state processes as: (i) protonation at the pyridine nitrogen atom, (ii) mutual twist of the indole and protonated pyridyl moieties to obtain a perpendicular conformation, (iii) efficient radiationless depopulation of the excited state due to a small S_0-S_1 energy gap.[182]

Chapter 6: Summary and Outlook

Three series of bifunctional and trifunctional molecular systems having both a proton donor and acceptor centers were selected to study their spectroscopic properties, photophysical processes and photochemical reactions by means of steady-state and nanosecond and picosecond time-resolved UV-Vis spectroscopic methods, ^{1}H NMR spectrometry, and quantum chemical computations. The goal of the work was related to the qualitative and quantitative characterization of: (i) the photophysical parameters, (ii) the solvent-dependent rotamerization, and (iii) the ground and excited state tautomerization connected with proton transfer processes. In order to study the influence of the environment on the photophysical and photochemical processes the experiments were performed in various solvents selected to cover a wide range of their polarity and/or hydrogen bond donor ability (Table 2.1) as well as under supersonic jet conditions.

Chapter 3 provides a comparative study of the spectroscopy and photophysics of the series of 7-hydroxyquinoline-8-carbaldehydes (**7-HQCs**) and 7-hydroxyquinolines (**7-HQs**), and their prototropic reactions directed to the understanding of the solvent-dependent mechanism of the ground and excited-state long-range prototropic tautomerization.

The 7-quinolinol (**OH**) forms of all the studied 7-hydroquinolines (**7-HQs**), similarly to **7-HQ**, are dominant in the ground state both in aprotic solvents and in alcohols. Upon excitation, the compounds show a single short-wave fluorescence band in aprotic solvents and two emission bands in alcohols. The long-wave band corresponds to the 7(1H)-quinolinone (**NH**) tautomer created by the excited-state triple proton transfer in the hydrogen-bonded complexes of 1:2 stoichiometry. The appearance of the low-energy electronic absorption band located about 25000 cm^{-1} in aqueous solutions at pH = 7 proves the ground-state existence of the **NH** form for all the **7-HQs**, except for **HMMQ**. The investigations of the prototropic reactions in acidic and basic acetonitrile and water solutions reveal the ground-state formation of the protonated cations (**C**) and deprotonated anions (**A**). On the contrary, the fluorescence of the **C** and **A** ionic forms of the studied derivatives of **7-HQ** is observed only in very strong acids (60% HClO$_4$) or bases (c_{NaOH} = 8.6 mol/dm^3); in the range of pH between 1 and 13 only the emission of the **NH** form is observed. The electronic excitation leads to the deprotonation of the cations and protonation of the anions to yield a zwitterionic form **Z** (its resonance hybrid is the tautomeric form **NH**, Scheme 3.3) due to a simultaneous increase of acidity and basicity of the proton donor and acceptor centers, respectively.

The parallel ^{1}H NMR and electronic absorption investigations prove the presence of the **OH** and **NH** tautomers in the ground state for all the studied **7-HQCs**, except for **HMMQC** (it exists dominantly as the **OH** form). The fraction of the **NH** form (specifically characterized by the absorption band at about 25000 cm^{-1}) increases with the increase of polarity and hydrogen bond donor ability of the surrounding environment.

For all the studied **7-HQCs**, except for **HPQC**, the dominant fluorescence in aprotic media and in alcohols can be attributed to the $^1(\pi,\pi^*)$ excited state of the **NH** tautomer. This is confirmed by direct excitation of this tautomer and by the comparison with the emission of the protonated cations and deprotonated anions. The fluorescence of **HQC** and its methyl derivatives, **H2MQC**, **H4MQC**, and **HDMQC**, in nonpolar and low polarity media show two emission bands assigned to the **OH** tautomer (~24000-24500 cm^{-1}) and to the **NH** tautomer (~20500-21000 cm^{-1}). The single emission band of **HMMQC**, observed about 19800-20900 cm^{-1} is attributed to the **NH** tautomer which is formed *via* ESIPT process. The multiple, solvent and excitation dependent, fluorescence of **HPQC** most probably originate from three forms: **OH**, **IIa** or **IIb** (a transient product of the ESIPT reaction, Scheme 1.14), and **NH** (which in part originates from the ground state and in part is formed in the excited state *via* intramolecular proton transfer processes).

The mechanism of the excited state tautomerization of **7-HQCs** in aprotic media at room temperature seems to be similar to that proposed by Varma and coworkers,[164-166] *i.e.* can be interpreted in terms of the irreversible, adiabatic proton transfer processes connected with a torsional motion of a carbaldehyde group (Scheme 1.14). This interpretation is corroborated by the results of the excitation dependence of the quantum yield investigations of **H2MQC**. However, the time-resolved nanosecond fluorescence investigations of **HMMQC** in such a strongly viscous medium as paraffin do not show any measurable rise of the **NH** fluorescence. Most probably, the excited state process is too short to be measured with nanosecond resolution. The very efficient radiationless depopulation of the fluorescent states of **7-HQCs** is in agreement with the theoretical *ab initio* computations predicting the conical intersection on the route of the ESIPT process under vacuum conditions,[164-166] although, contrary to the results obtained for **H4MQC** in low temperature Ar matrices,[164-166] the reversible **OH** $\leftrightarrow$ **NH** transformation upon selective electronic excitation is not observed in solutions.

In water and alcohol solutions, however, the mechanism of ESIPT reaction seems to involve additional reactions producing various hydrates or hemiacetals, respectively, which are in dynamic equilibria with the **OH** and **NH** tautomers (Scheme 3.4). Similarly to **7-HQs**, the results of investigations of the prototropic reactions in acidic and basic acetonitrile and

water solutions of **7-HQCs** indicate a shift towards the **NH** form upon excitation and prove the opposite pK_a tendencies of the acidic and basic centers of the compounds.

The studied **7-HQCs**, except **HMMQC**, are not photostable. The UV irradiation of these compounds results in the photoproducts which emit short-wave fluorescence. In order to understand the mechanism of the photoreactions further studies have to be performed.

Chapter 4 is devoted to rotamerization and photoinduced tautomerization in the series of 2-(1*H*-pyrazol-5-yl)pyridines (**2-PPs**). Quantum chemical calculations show that all the studied **2-PPs** preferentially exist in the *syn* forms, both in nonpolar and polar environments in the ground state. The increase of polarity and hydrogen bond donor ability of the surrounding medium prompts *syn-anti1* rotamerization. This process is manifested by the change of the mutual intensity of the two low-energy **2-PPs** absorption bands with the change of solvent polarity.

PPP, **MPP**, and **BPP** in *n*-hexane, 1-propanol, and aqueous solutions show dual fluorescence (a trace of the emission of **NPP** was detected only in water). The dominant short-wave band was assigned mainly to the *syn* rotameric forms of the compounds. In order to understand the nature of the long-wave band (of very low intensity and strongly Stokes shifted) the picosecond kinetic studies and spectrophotometric and spectrofluorimetric titration experiments in mixed *n*-hexane/alcohol solvents were provided. The results indicate that the compounds exhibit three types of photoreactions and the long-wave band originates from the product of the following excited state proton transfer (ESPT) reactions:

(1) Intramolecular process (ESIPT) takes place in the *syn* form of **MPP** in nonpolar media (Scheme 4.3a). The picosecond kinetic studies of the dual luminescence of **MPP** in *n*-hexane reveal a concentration-independent bimodal irreversible kinetic coupling of both fluorescence bands. To prove it, resonant two-photon ionization (R2PI) and laser induced fluorescence excitation and dispersed fluorescence (LIF/DF) investigations of **MPP** isolated under supersonic jet conditions are planned;

(2) Titration experiments in mixed *n*-hexane/1-butanol solvents indicate solvent-assisted excited-state double proton transfer (ESDPT) in hydrogen-bonded complexes of **PPP** (Scheme 4.3b), **MPP**, and **BPP** with protic partners of 1:1 stoichiometry and most probably of cyclic structure. In order to verify the proposed structure of the complexes investigations with the double-resonance laser technique termed IR/R2PI ion depletion spectroscopy,[249-257] which combines the structurally sensitive infrared (IR) vibrational predisociation spectroscopy with the mass-selective R2PI spectroscopy, are needed. The characterization of the size and structure of the molecular clusters is based on a comparison of the IR/R2PI

vibrational spectra (*e.g.*, corresponding to the O-H stretching vibrations of the alcohol or water in the particular hydrogen-bonded complex) recorded under supersonic jet isolation conditions with theoretical calculations;

(3) Intermolecular ESDPT in the cyclic, hydrogen-bonded dimers of **PPP** in nonpolar media (Scheme 4.3c) is suggested by the concentration dependence of the contribution of the 1.4 ns decay component of the low-energy emission of **PPP** in *n*-hexane (Fig. 4.11). The evidence can be provided by the R2PI investigations performed under supersonic jet conditions.

Chapter 5 presents spectroscopic and photophysical investigations and quantum chemical calculations for a series of bifunctional indole derivatives which can form *syn* and *anti* conformers *via* internal rotation around a single bond (**THOIN**, **THAIN**, and **FURIN**) and their comparison with the compounds which either have not acceptor center (**PYRIN**), or, due to the topology, can not exist in two rotameric forms (**3-PI**). The study of the solvent effects on the photophysical properties of **FURIN**, **THAIN**, and **THOIN** does not show any spectral and kinetic evidence of rotamerization (for all the compounds) and/or photoinduced tautomerization (for **THAIN**) processes. The compounds show strongly allowed and efficient fluorescence; the lack of the efficient deactivation of the lowest excited singlet states S_1 in protic media *via* internal conversion (IC) and/or ESDPT (for **THAIN**) processes suggests that the studied compounds do not form cyclic, doubly hydrogen-bonded complexes. The use of a supersonic jet technique combined with laser spectroscopy and TD-DFT calculations leads to the results which suggest that the *syn* rotamer is a dominant form of **THAIN** and **FURIN**. The analysis of the LIF and SVLF spectra suggests that the deviations from planar structure following electronic excitation are connected with the out-of-plane rocking and torsion motions along C2-C2' single bond which links the indole ring with the furan or thiazole moiety.

3-PI reveals strong fluorescence in aprotic solvents, both polar and nonpolar. However, the emission, contrary to the other studied indole derivatives, is strongly quenched in alcohols and water although the topology of **3-PI** excludes a possibility of forming cyclic 1:1 or 1:2 solvates and therefore, of excited state proton transfer *via* a solvent bridge. The excited-state nonradiative deactivation becomes faster for more acidic media and is slowed down with increasing solvent viscosity. The experiments in mixed *n*-hexane/1-butanol solvents suggest that even for low concentration of alcohol various types of complexes are formed. Some of these complexes should be attached to the pyridine nitrogen atom. Theoretical calculations predict that the electronic excitation involves electron density flow

from an orbital localized mainly on the indole moiety into an orbital localized on the pyridyl unit. These observations suggest a model for the fluorescence quenching (Fig. 5.7) involving the increase of the strength of the intermolecular OH….N hydrogen bond upon electronic excitation, followed by the excited state protonation of the pyridine nitrogen atom and mutual twisting of the indole and pyridyl units. This leads to a protonated cation of a perpendicular geometry and characterized by the low energy gap between the S_1 and S_0 states. According to the energy gap law, this S_1 state of the protonated cation is efficiently depopulated *via* internal conversion.

References

1. Watson J. D., Crick F. H. C., *Nature (London)*, **1953**, *171*, 964.
2. Goodman M. F., *Nature*, **1995**, *378*, 237.
3. Pauling L., Corey R., *Proc. Natl. Acad. Sci. USA*, **1953**, *39*, 84.
4. Whewell C. S., *J. Soc. Cosmet. Chem.*, **1960**, 207.
5. Arnaut L. G., Formosinho S. J., *J. Photochem. Photobiol. A: Chemistry*, **1993**, *75*, 1.
6. Formosinho S. J., Arnaut L. G., *J. Photochem. Photobiol. A: Chemistry*, **1993**, *75*, 21.
7. Lakowicz J. R., *Priciples of Fluorescence Spectroscopy*. Second Edition, ed. **1999**, New York: Kluwer Academic/Plenum Publisher.
8. Turro N. J., *Modern Molecular Photochemistry*. **1978**, San Francisco, California, U.S.A.: Benjamin/Cummings Publishing Company.
9. Chattopadhyay N., *J. Photochem. Photobiol. A: Chemistry*, **1995**, *88*, 1.
10. Llano J., Eriksson L. A., *Phys. Chem. Chem. Phys.*, **2004**, *6*, 2426.
11. Perun S., Sobolewski A. L., Domcke W., *J. Phys. Chem. A*, **2006**, *110*, 9031.
12. Sobolewski A. L., Domcke W., *Chem. Phys. Chem.*, **2006**, *7*, 561.
13. Belevich I., Verkhovsky M. I., Wikstroem M., *Nature*, **2006**, *440*, 829.
14. Faxen K., Gilderson G., Aedelroth P., Brzezinski P., *Nature*, **2005**, *437*, 286.
15. Crofts A. R., *Biochim. Biophys. Acta*, **2004**, *1655*, 77.
16. Chowdhury P., Pania S., Chakravorti S., *J. Phys. Chem. A*, **2003**, *107*, 83.
17. Wan P., Shukla D., *Chem. Rev.*, **1993**, *93*, 571.
18. Förster T., *Z. Elektrochem., Ber. Bunsenges. Physik. Chem.*, **1950**, *54*, 42.
19. Förster T., *Naturwissenschaften*, **1949**, *36*, 186.
20. Grabowski Z. R., Grabowska A., *Z. Phys. Chem. N.F.*, **1976**, *101*, 197.
21. Weber K., *Z. Phys. Chem.*, **1931**, *B15*, 18.
22. Weller A., *Z. Elektrochem.*, **1952**, *56*, 662.
23. Weller A., *Z. Elektrochem.*, **1956**, *60*, 1144.
24. Weller A., *Z. Elektrochem.*, **1957**, *61*, 956.
25. Weller A., *Progr. Reaction Kinetics*, **1961**, *1*, 189.
26. Weller A., *Fast Reactions of Excited Molecules*, in *Reaction Kinetics*, Porter G., Stevens B., Phil D., **1961**, Pergamon Press: Oxford, London, New York, Paris.
27. Dick B., Earnsting N.P. , *J. Phys. Chem.*, **1987**, *91*, 4261.
28. Das K., English D. S., Petrich J. W., *J. Phys. Chem. A*, **1997**, *101*, 3241.
29. Barroso M., Arnaut L.G., Formosinho S. J., *J. Phys. Chem. A*, **2007**, *111*, 591.
30. van Benthem M. H., Gillespie G. D., *J. Phys. Chem.*, **1984**, *88*, 2954.
31. Ernsting N. P., Mordzinski A., Dick B., *J. Phys. Chem.*, **1987**, *91*, 1404.
32. Das K., English D. S., Petrich J. W., *J. Am. Chem. Soc. *, **1997**, *119*, 2763.
33. Das K., Ashby K. D., Petrich J. W., *J. Phys. Chem. B* **1999**, *103*, 1581.
34. Nayek M. K., Dogra S. K., *J. Photochem. Photobiol. A: Chemistry*, **2005**, *169*, 79.
35. Nachliel E., Ophir Z., Gutman M., *J. Am. Chem. Soc.*, **1987**, *109*, 1342.
36. Clark J. H., Shapiro S. L., Campillo A. J., Winn K. R., *J. Am. Chem. Soc.*, **1979**, *101*, 746.
37. Huppert D., Kolodney E., *Chem. Phys.*, **1981**, *63*, 401.
38. Robinson G. W., Thistlethwaite P. J., Lee J., *J. Phys. Chem.*, **1986**, *90*, 4224.
39. Mallick A., Chattopadhyay N., *Photochem. Photobiol.*, **2005**, *81*, 419.
40. Sengupta B. , Sengupta P.K., *Biopolymer*, **2003**, *72*, 427.
41. Guharay G., Sengupta B., Sengupta P.K., *Proteins Struct. Funct. Genet.*, **2001**, *43*, 75.
42. Mallick A., Chattopadhyay N., *Biophys. Chem.*, **2004**, *109*, 261.

43. Chattopadhyay N., Dutta R., Chowdhury M., *J. Photochem. Photobiol. A: Chemistry*, **1989**, *47*, 249.
44. Wang X., Wang J., Wang Y., Yan H., Li P., Thomas R.K., *Langmuir* **2004**, *20*, 53.
45. Varela A. P., Miguel M. G., Mac¸anita A. L., Becker R. S., Burrows H. D., *J. Phys. Chem. Chem. Phys.*, **1995**, *99*, 16093.
46. Kelker D. A., Chattopadhyay N. , *J. Phys. Chem. B*, **2004**, *108*, 12151.
47. Panja S., Chakravorti S., *Chem. Phys. Lett.*, **2003**, *367*, 330.
48. Mallick A., Haldar B., Chattopadhyay N., *J. Photochem. Photobiol. B: Biology*, **2005**, *78*, 215.
49. Hansen J. E., Pines E., Fleming G.R., *J. Am. Chem. Soc.*, **1992**, *96*, 6904.
50. Chattopadhyay N., *J. Photochem. Photobiol. A: Chemistry*, **1991**, *58*, 31.
51. Valeur B., Bardez E., Goguillon B.-T., Keh E., *J. Phys. Chem.*, **1984**, *88*, 1909.
52. Huppert D., Gutman M., Nachliel E., *J. Biochem.*, **1982**, *125*, 175.
53. Fendler J. H., Politi M. J., Brantd O., *J. Phys. Chem.*, **1985**, *89*, 2345.
54. Lee J., *J. Am. Chem. Soc*, **1989**, *111*, 427.
55. Sunamoto J., Kondo H. ,Miwa I. , *J. Phys. Chem.*, **1982**, *86*, 4826.
56. Tolbert L. M., Linares-Samaniego S., *J. Am. Chem. Soc*, **1996**, *118*, 9974.
57. Gutman M., Nachlieil E., *Biochemistry*, **1985**, *24*, 1941.
58. Iwanck W., Mattay J., *J. Photochem. Photobiol. A: Chemistry*, **1992**, *67*, 209.
59. Catalan J., Fabero F., Guijarro M. S., Claramunt R. M., Santa Maria M. D., Foces-Foces M. C., Cano F. H., Elguero J., Sastre R., *J. Am. Chem. Soc*, **1991**, *113*, 4046.
60. Smith T. P., Zaklika K. A., Thakur K., Walker G. C., Tominaga K., Barabara P. F., *J. Photochem. Photobiol. A: Chemistry*, **1992**, *65*, 165.
61. Chou P., McMorrow D., Aartsma T. J., Kasha M., *J. Phys. Chem.*, **1984**, *88*, 4596.
62. Nishiya T., Yamauchi S., Hitora N., Baba M., Hanazaki I., *J. Phys. Chem.*, **1986**, *90*, 5730.
63. Harrah L. A., Renschler C. L., *Nucl. Inst. Methods Phys. Rev.*, **1985**, *A235*, 41.
64. Kasha M., *J. Chem. Soc. Faraday Trans. 2*, **1986**, *82*, 2379.
65. Heldt J., Gormin D., Kasha M., *Chem. Phys. *, **1989**, *136*, 321.
66. Rossetti R., Haddon R. C., Brus L. E., *J. Am. Chem. Soc*, **1980**, *102*, 6913.
67. Ernsting N. P., Dick B., *Chem. Phys.*, **1989**, *136*, 181.
68. Chou P., Aartsma T. J., *J. Phys. Chem.*, **1986**, *90*, 721.
69. Mahanta S., Singh R. B., Kar S., Guchhait N., *Chem. Phys.*, **2006**, *324*, 742.
70. Lim E., *J. Phys. Chem.*, **1986**, *90*, 6770.
71. Acuna A. U., Amat-Guerri F., Catalan J., Gonzalez-Tablas F., *J. Phys. Chem.*, **1980**, *84*, 629.
72. Acuna A. U., Amat-Guerri F., Toribio F., Catalan J., *J. Photochem.*, **1985**, *30*, 330.
73. Herek J. L. , Pedersen S., Bañares L., Zewail A. H., *J. Chem. Phys. *, **1992**, *97*, 9046.
74. Laermer F., Elsaesser T., Kaiser W., *Chem. Phys. Lett.*, **1988**, *148*, 119.
75. Lochbrunner S., Wurzer A. J., Riedle E., *J. Phys. Chem. A*, **2003**, *107*, 10580.
76. Arthen-Engeland T., Bultmann T., Ernsting N. P., Rodriguez M. A., Thiel W., *Chem. Phys.*, **1992**, *163*, 43.
77. Stock K., Bizjak T., Lochbrunner S., *Chem. Phys. Lett.*, **2002**, *354*, 409.
78. Mordzinski A., Grellmann K. H., *J. Phys. Chem.*, **1986**, *90*, 5503.
79. Rodriguez Prieto M. F., Nickel B., Grellmann K. H., Mordzinski A., *Chem. Phys. Lett.*, **1988**, *146*, 387.
80. Elsaesser T., Kaiser W., *Chem. Phys. Lett.*, **1986**, *128*, 231.
81. Rini M., Kummrow A., Dreyer J., Nibbering E. T. J., Elsaesser T., *Faraday Discuss.*, **2002**, *122*, 27.
82. Lochbrunner S., Stock K., Riedle E., *J. Mol. Structure*, **2004**, *700*, 13.

141

83. Grabowska A., Borowicz P., Martire D. O., Braslavsky S. E., *Chem. Phys. Lett.*, **1991**, *185*, 206.
84. Langkilde F. W., Mordzinski A., Wilbrandt R., *Chem. Phys. Lett.*, **1992**, *190*, 305.
85. Borowicz P., Grabowska A., Wortmann R., Liptay W., *J. Lumnescence*, **1992**, *52*, 265.
86. Borowicz P., Waluk J., *J. Mol. Structure*, **1995**, *349*, 277.
87. Borowicz P., Grabowska A., Kaczmarek L., Les A., Adamowicz L., *Chem. Phys. Lett.*, **1995**, *239*, 282.
88. Sobolewski A. L., Adamowicz L., *Chem. Phys. Lett.*, **1996**, *252*, 33.
89. Marks D., Zhang H., Glasbeek M., Borowicz P., Grabowska A., *Chem. Phys. Lett.*, **1997**, *275*, 370.
90. Borowicz P., Grabowska A., Les A., Kaczmarek L., Zagrodzki L., *Chem. Phys. Lett.*, **1998**, *291*, 351.
91. Mordzinski A., Grabowska A., Kuhnle W., Krowczynski A., *Chem. Phys. Lett.*, **1983**, *101*, 291.
92. Mordzinski A., Grabowska A., Teuchner K., *Chem. Phys. Lett.*, **1984**, *111*, 383.
93. Mordzinski A., Kuhnle W., *J. Phys. Chem.*, **1986**, *90*, 1455.
94. Grabowska A., Mordzinski A., Tamai N., Yoshihara K., *Chem. Phys. Lett.*, **1990**, *169*, 450.
95. Vdovin A., Sepiol J., Jasny J., Kauffman J. M., Mordzinski A., *Chem. Phys. Lett.*, **1998**, *296*, 557.
96. Luzina E., Sepiol J., Svartsov Y. N., Grabowska A., *J. Chem. Phys.*, **2007**, *126*, 194308.
97. Gai F., Chen Y., Petrich J. W., *J. Am. Chem. Soc.*, **1992**, *114*, 8343.
98. Catalan J., Perez P., Del Valle J. C., De Paz J. L. G., Kasha M., *Proc. Natl. Acad. Sci. USA*, **2004**, *101*, 419.
99. Catalan J., Perez P., del Valle J. C., de Paz J. L. G., Kasha M., *Proc. Natl. Acad. Sci. USA*, **2002**, *99*, 5793.
100. Chen Y., Gai F., Petrich J. W., *J. Am. Chem. Soc.*, **1993**, *115*, 10158.
101. Catalan J., Kasha M., *J. Phys. Chem. A*, **2000**, *104*, 10812.
102. Waluk J., Grabowska A., Pakula B., Sepiol J., *J. Phys. Chem.*, **1984**, *88*, 1160.
103. Waluk J., Herbich J., Oelkrug D., Uhl S., *J. Phys. Chem.*, **1986**, *90*, 3866.
104. Chang C., Shabestary N., El-Bayoumi M. A., *Chem. Phys. Lett.*, **1980**, *75*, 107.
105. Waluk J., Komorowski S. J., Herbich J., *J. Phys. Chem.*, **1986**, *90*, 3868.
106. Sepiol J., Wild U. P. , *Chem. Phys. Lett.*, **1983**, *93*, 204.
107. Taylor C. A., El-Bayoumi M. A., Kasha M., *Proc. Natl. Acad. Sci. USA*, **1969**, *63*, 253.
108. Sekiya H., Sakota K., *J. Photochem. Photobiol. C: Photochemistry Reviews*, **2008**, *9*, 81.
109. Ingham K. C., Abu-Elgheit M., El-Bayoumi M. A., *J. Am. Chem. Soc.*, **1971**, *93*, 5023.
110. Ingham K. C., El-Bayoumi M. A., *J. Am. Chem. Soc.*, **1974**, *96*, 1974.
111. Catalan J., del Valle J. C., Kasha M., *Proc. Natl. Acad. Sci. USA*, **1999**, *96*, 8338.
112. Folmer D. E., Poth L., Wisniewski E. S., Castleman Jr. A. W., *Chem. Phys. Lett.*, **1998**, *287*, 1.
113. Folmer D. E., Wisniewski E. S., Castleman Jr. A. W., *Proc. Natl. Acad. Sci. USA*, **1999**, *96*, 12980.
114. Nakajima A., Negishi Y., Hasumi R., Kaya K., *Eur. Phys. J. D*, **2000**, *9*, 303.
115. Smedarchina Z., Siebrand W., Fernandez-Ramos A., Gorb L., Leszczynski J., *J. Chem. Phys.*, **2000**, *112*, 566.

116. Chen Y., Rich R. L., Gai F., Petrich J. W., *J. Phys. Chem.*, **1993**, *97*, 1770.
117. Smirnov A. V., English D. S., Rich R. L., Lane J., Teyton, L., Schwabacher A. W., Luo S. Thornburg R. W., Petrich J. W., *J. Phys. Chem. B*, **1997**, *101*, 2758.
118. Chou P. T., Martinez M. L., Cooper W. C., McMorrow D., Collin S. T., Kasha M., *J. Phys. Chem.*, **1992**, *96*, 5203.
119. Karthikeyan B., *Spectrochimica Acta Part A* **2006**, *64*, 1083.
120. Chaban G. M., Gordon M. S., *J. Phys. Chem. A*, **1999**, *103*, 185.
121. Fernandez-Ramos A., Smedarchina Z., Siebrand W., Zgierski M. Z., Rios M. A. , *J. Am. Chem. Soc.*, **1999**, *121*, 6280.
122. Kijak M., Zielińska A., Thummel R. P., Herbich J., Waluk J., *Chem. Phys. Lett.*, **2002**, *366*, 329.
123. Herbich J., Kijak M., Luboradzki R., Gil M., Zielinska A., Hu Y. Z., Thummel R. P., Waluk J., *J. Photochem. Photobiol. A: Chemistry*, **2002**, *154*, 61.
124. Kyrychenko A., Waluk J., *J. Phys. Chem. A*, **2006**, *110*, 11958.
125. Nosenko Y., Kunitski M., Thummel R. P., Kyrychenko A., Herbich J., Waluk J., Riehn C., Brutschy B., *J. Am. Chem. Soc.*, **2006**, *128*, 10000.
126. Nosenko Y., Kyrychenko A., Thummel R. P., Waluk J., Brutschy B., Herbich J., *Phys. Chem. Chem. Phys.*, **2007**, *9*, 3276.
127. Nosenko Y., Kunitski M., Riehn C., Thummel R. P., Kyrychenko A., Herbich J., Waluk J., Brutschy B., *J. Phys. Chem. A* **2008**, *112*, 1150.
128. Herbich J., Dobkowski J., Thummel R. P., Hegde V., Waluk J., *J. Phys. Chem. A* **1997**, *101*, 5839.
129. Kyrychenko A., Herbich J., Izydorzak M., Wu F., Thummel R. P., Waluk J., *J. Am. Chem. Soc.*, **1999**, *121*, 11179.
130. Herbich J., Rettig W., Thummel R. P., Waluk J., *Chem. Phys. Lett.*, **1992**, *195*, 556.
131. Herbich J., Waluk J., Thummel R. P., Hung C. Y., *J. Photochem. Photobiol. A: Chemistry* **1994**, *80*, 157.
132. Herbich J., Hung C. Y., Thummel R. P., Waluk J., *J. Am. Chem. Soc.*, **1996**, *118*, 3508.
133. Kyrychenko A., Herbich J., Wu F., Thummel R. P., Waluk J., *J. Am. Chem. Soc.*, **2000**, *122*, 2818.
134. Kijak M., Zielinska A., Chamchoumis C., Herbich J., Thummel R. P., Waluk J., *Chem. Phys. Lett.*, **2004**, *400*, 279.
135. Kijak M., Nosenko Y., Singh A., Thummel R. P., Waluk J., *J. Am. Chem. Soc.*, **2007**, *129*, 2738.
136. Waluk J., *Acc. Chem. Res.*, **2003**, *36*, 832.
137. Nosenko Y., Stepanenko Y., Wu F., Thummel R. P., Mordzinski A., *Chem. Phys. Lett.*, **1999**, *315*, 87.
138. Kijak M., Petkova I., Toczek M., Wiosna-Salyga G., Zielinska A., Herbich J., Thummel R. P., Waluk J., *Acta Physica Polonica A*, **2007**, *112*, S-105.
139. Marks D., Zhang H., Borowicz P., Waluk J., Glasbeek M., *J. Phys. Chem. A*, **2000**, *104*, 7167.
140. Ewing G. W., Steck E. A., *J. Am. Chem. Soc.*, **1946**, *68*, 2181.
141. Albert A., Phillips J. N. , *Chem. Soc.*, **1956**, 1294.
142. Mason S. F., *Chem. Soc.*, **1957**, 5010.
143. Mason S. F., *Chem. Soc.*, **1957**, 4874.
144. Mason S. F., *Chem. Soc.*, **1958**, 674.
145. Mason S. F., Philp J., Smith B. E., *J. Chem. Soc. A*, **1968**, 3051.
146. Schulman S., Fernando Q., *Tetrahedron*, **1968**, *24*, 1777.
147. Lee S. I., Jang D. J., *J. Phys. Chem.*, **1995**, *99*, 7537.

148. Senda N., Momotake A., Arai T., *Bull. Chem. Soc. Jpn.*, **2010**, *83*, 1272.
149. Thistlethwaite P. J., Corkill P. J., *Chem. Phys. Lett.*, **1982**, *85*, 317.
150. Thistlethwaite P. J., Corkill P. J., *Chem. Phys. Lett.*, **1983**, *96*, 509.
151. Itoh M., Adachi T., Tokumura K., *J. Am. Chem. Soc.*, **1983**, *105*, 4828.
152. Tokumura K., Itoh M., *J. Phys. Chem.*, **1984**, *88*, 3921.
153. Itoh M., Adachi T., Tokumura K., *J. Am. Chem. Soc.*, **1984**, *106*, 850.
154. Konijnenberg J., Huizer A. H., Varma C. A. G. 0., *J. Chem. Soc. Faraday Trans. 2*, **1989**, *85*, 39.
155. Lahmani F., Douhal A., Breheret E., Zehnacker-Rentien A., *Chem. Phys. Lett.*, **1994**, *220*, 235.
156. Bach A., Leutwyler S., *Chem. Phys. Lett.*, **1999**, *299*, 381.
157. Fang W. H., *J. Phys. Chem. A*, **1999**, *103*, 5567.
158. Kohtani S., Tagami A., Nakagaki R., *Chem. Phys. Lett.*, **2000**, *316*, 88.
159. Garcia-Ochoa I., Bisht P. B., Sanchez F., Martinez-Ataz E., Santos L., Tripathi H. B., Douhal A., *J. Phys. Chem. A*, **1998**, *102*, 8871.
160. Chou P. T., Wei C. Y., Wang C. R. C., Hung F. T., Chang C. P., *J. Phys. Chem. A*, **1999**, *103*, 1939.
161. Lavin A., Collins S., *Chem. Phys. Lett.*, **1993**, *204*, 96.
162. Fang W. H., *J. Am. Chem. Soc*, **1998**, *120*, 7568.
163. Jalink C. J., van Ingen W. M., Huizer A. H., Varma C. A. G. O., *J. Chem. Soc. Faraday Trans.*, **1991**, *97*, 1103.
164. Sobolewski A. L., *Phys. Chem. Chem. Phys.*, **2008**, *10*, 1243.
165. Lapinski L., Nowak M. J., Nowacki J., Rode M. F., Sobolewski A. L., *Chem. Phys. Chem.*, **2009**, *10*, 2290.
166. Rode M. F., Sobolewski A. L. , *J. Phys. Chem. A*, **2010**, *114*, 11879.
167. Pati R., McClain M., Bandyopadhyay A., *Phys. Rev. Lett.*, **2008**, *100*, 246801.
168. Mendes P. M., Flood A. H., Stoddart J. F., *Appl. Phys. A: Mater. Sci. Process.*, **2005**, *80*, 1197.
169. Liljeroth P., Repp J., Meyer J., *Science*, **2007**, *317*, 1203.
170. Benesch C., Rode M. F., Cizek M., Hartle R., Rubio-Pons O., Thoss M., Sobolewski A. L., *J. Phys. Chem. C*, **2009**, *113*, 10315.
171. Sigurdson C. J., Nilsson K. P. R., Hornemann S., Manco G., Fernandez-Borges N., Schwarz P., Castilla J., Wuthrich K., Aguzzi A., *The Journal of Clinical Investigation*, **2010**, *120*, 2590.
172. Warzecha C. C., Sato T. K., Nabet B., Hogenesch J. B., Carstens R. P., *Molecular Cell* **2009**, *33*, 591.
173. Khaled M., Levy C., Fisher D. E., *Genes Dev.*, **2010**, *24*, 2276.
174. Altoe P., Bernardi F., Conti, Garavelli M., Negri V., Orlandi G., *Theor. Chem. Acc.*, **2007**, *117*, 1041.
175. Otterstedt J.-E. A., *J. Chem. Phys.*, **1973**, *58*, 5716.
176. Sobolewski A. L., Domcke W., Hattig C., *J. Phys. Chem. A* **2006**, *110*, 6301.
177. Sobolewski A. L., Domcke W., *Phys. Chem. Chem. Phys.*, **2006**, *8*, 3410.
178. Douhal A., Lahmani F., Zewail A. H., *Chem. Phys.*, **1996**, *207*, 477.
179. Reichardt C., *Solvent Effects in Organic Chemistry*. Monographs in Modern Chemistry, ed. Ebel H. F., Vol. 3, **1979**, New York: Verlag Chemie Weinheim.
180. Kamlet M. J., Abboud J. L. M., Taft R. W., *Progr. Phys. Org. Chem.*, **1981**, *13*, 485.
181. Vetokhina V., Dobek K., Kijak M., Kaminska I. I., Muller K., Thiel W. R., Waluk J., Herbich J., *Chem. Phys. Chem.*, DOI: 10.1002/cphc.20120602.
182. Vetokhina V., Kijak M., Wiosna-Salyga G., Thummel R. P., Herbich J., Waluk J., *Photochem. Photobiol. Sci.*, **2010**, *9*, 923.

183. Nosenko Y., Wiosna-Salyga G., Kunitski M., Petkova I., Singh A., Buma W. J., Thummel R. P., Brutschy B., Waluk J., *Angew. Chem., Int. Ed.*, **2008**, *47*, 6037.
184. Wiosna-Salyga G., N.Y., Kijak M., Thummel R. P., Brutschy B., Waluk J., *J. Phys. Chem. A*, **2010**, *114*, 3270.
185. Schmidtke S. J., MacManus-Spencer L. A., Klappa J. L., Mobley T. A., McNeill K., Blank D. A., *Phys. Chem. Chem. Phys.*, **2004**, *6*, 3938.
186. MacManus-Spencer L. A., Schmidtke S. J., Blank D. A., McNeill K., *Phys. Chem. Chem. Phys.*, **2004**, *6*, 3948.
187. Thiel W. R., Eppinger J., *Chem. Eur. J.*, **1997**, *3*, 676.
188. Lipinska T. M., Czarnocki S. J., *Org. Lett.*, **2005**, *8*, 367.
189. Lipinska T. M., *Tetrahedron*, **2006**, *62*, 5736.
190. Bergman J., *J. Heterocycl. Chem.*, **1970**, *7*, 1071.
191. Vetokhina V., Nowacki J., Pietrzak M., Rode M. F., Sobolewski A. L., Waluk J., Herbich J., *submitted*,
192. Jasny J., *J. Lumnescence*, **1978**, *17*, 1720.
193. Velapoldi R. A., Tonnesen H. H., *J. of Fluorescence*, **2004**, *14*, 465.
194. Szydlowska I., Kyrychenko A., Nowacki J., Herbich J., *Phys. Chem. Chem. Phys.*, **2003**, *5*, 1032.
195. Demas J. N., Crosby G. A., *J. Phys. Chem.*, **1971**, *75*, 991.
196. Crosby G. A., Demas J. N., Callis J. B. in *Natl. Bur. Stand. U.S. Spec. Publ. 378, Proc. Conf. NBS*. **1972**; Gaithersburg.
197. Melhuish W. H. in *Natl. Bur. Stand. U.S. Spec. Publ. 378, Proc. Conf. NBS*. **1972**; Gaithersburg.
198. Velapoldi R. A. in *Natl. Bur. Stand. U.S. Spec. Publ. 378, Proc. Conf. NBS*. **1972**; Gaithersburg.
199. Karolczak J., Komar D., Kubicki J., Wrozowa T., Dobek K., Ciesielska B., Maciejewski A., *Chem. Phys. Lett.*, **2001**, *344*, 154.
200. Marquardt D. W., *J. Soc. Indust. Appl. Math.*, **1963**, *11*, 431.
201. Nelder J. A., Mead R., *Comput. J.*, **1965**, *7*, 308.
202. Walters F. W., Parker Jr. L. R., *Sequential Simplex Optimization*. **1992**, CRC Press LLC.
203. Förster T., *Fluorescenz Organischer Verbindungen*. **1951**, Göttingen: Vandenhoeck and Ruprecht.
204. Birks J. B., *Photophysics of Aromatic Molecules*, Wiley, **1978**: New York.
205. Michl J., Thulstrup E. W., *Spectroscopy with Polarized Light*, VCH, **1986**: New York. p. 28 and 75.
206. Mulliken R. S., *J. Am. Chem. Soc.*, **1952**, *74*, 811.
207. Mulliken R. S., Person W. B., *Molecular Complexes: A Lecture and Reprint Volume*. **1969**, New York: Wiley.
208. Miyasaka H., Tabata A., Ojima S., Ikeda M., Mataga N., *J. Phys. Chem.*, **1993**, *97*, 8222.
209. Paszyc S., *Podstawy fotochemii*. 51, **1992**, Warszawa: PWN.
210. Böttcher C. J. F., *Theory of Electric Polarization*. P.B. O. C. Van Belle, A. Rip, Vol. 1, **1973**, Amsterdam: Elsevier.
211. Mataga N., Kaifu Y., Koizumi M., *Bull. Chem. Soc. Jpn.*, **1955**, *28*, 690.
212. Onsager L., *J. Am. Chem. Soc.*, **1936**, *58*, 1486.
213. Bayliss N. S., McRae E. G., *J. Phys. Chem.*, **1954**, *58*, 1002.
214. Lippert E., *Z. Naturforsch. Teil A*, **1955**, *10*, 541.
215. Nosenko Y., Jasny J., Pietraszkiewicz M., Mordzinski A., *Chem. Phys. Lett.*, **2004**, *399*, 331.

216. Nosenko Y., *Laser-jet spectroscopy of donor-acceptor H-bonding compounds and their molecular clusters*. PhD Thesis, **2004**, Institute of Physical Chemistry PAS Place, Published.

217. *EXCITON information bulletin*, **1992**

218. Foresman J. B., Frish A., *Exploring Chemistry with Electronic Structure Methods*. Second ed, **1996**, Pittsburgh, PA: Gaussian Inc.

219. Frisch M. J., Trucks G. W., Schlegel H. B., Scuseria G. E., Robb M. A., Cheeseman J. R., Montgomery Jr. J. A., Vreven T., Kudin K. N., Burant J. C., Millam J. M., Iyengar S. S., Tomasi J., Barone V., Mennucci B., Cossi M., Scalmani G., Rega N., Petersson G. A., Nakatsuji H., Hada M., Ehara M., Toyota K., Fukuda R., Hasegawa J., Ishida M., Nakajima T., Honda Y., Kitao O., Nakai H., Klene M., Li X., Knox J. E., Hratchian H. P., Cross J. B., Adamo C., Jaramillo J., Gomperts R., Stratmann R. E., Yazyev O., Austin A. J., Cammi R., Pomelli C., Ochterski J. W., Ayala P. Y., Morokuma K., Voth G. A., Salvador P., Dannenberg J. J., Zakrzewski V. G., Dapprich S., Daniels A. D., Strain M. C., Farkas O., Malick D. K., Rabuck A. D., Raghavachari K., Foresman J. B., Ortiz J. V., Cui Q., Baboul A. G., Clifford S., Cioslowski J., Stefanov B. B., Liu G., Liashenko A., Piskorz P., Komaromi I., Martin R. L., Fox D. J., Keith T., Al-Laham M. A., Peng C. Y., Nanayakkara A., Challacombe M., Gill P. M. W., Johnson B. G., Chen W., Wong M. W., Gonzalez C., Pople J. A., *Gaussian 03, Revision B.03*. **2003**, Pittsburgh PA: Gaussian, Inc.

220. Frisch M. J., Trucks G. W., Schlegel H. B., Scuseria G. E., Robb M. A., Cheeseman J. R., Scalmani G., Barone V., Mennucci B., Petersson G. A., Nakatsuji H., Caricato M., Li X., Hratchian H. P., Izmaylov A. F., Bloino J., Zheng G., Sonnenberg J. L., Hada M., Ehara M., Toyota K., Fukuda R., Hasegawa J., Ishida M., Nakajima T., Honda Y., Kitao O., Nakai H., Vreven T., Montgomery Jr. J. A., Peralta J. E., Ogliaro F., Bearpark M., Heyd J. J., Brothers E., Kudin K. N., Staroverov V. N., Kobayashi R., Normand J., Raghavachari K., Rendell A., Burant J. C., Iyengar S. S., Tomasi J., Cossi M., Rega N., Millam J. M., Klene M., Knox J. E., Cross J. B., Bakken V., Adamo C., Jaramillo J., Gomperts R., Stratmann R. E., Yazyev O., Austin A. J., Cammi R., Pomelli C., Ochterski J. W., Martin R. L., Morokuma K., Zakrzewski V. G., Voth G. A., Salvador P., Dannenberg J. J., Dapprich S., Daniels A. D., Farkas Ö., Foresman J. B., Ortiz J. V., Cioslowski J., Fox D. J., *Gaussian 09, Revision A.1.* **2009**, Wallingford CT: Gaussian, Inc.

221. Stratmann R. E., Scuseria G. E., Frisch M. J., *J. Chem. Phys.*, **1998**, *109*, 8218.

222. Lee C., Yang W., Parr R. G., *Phys. Rev. B*, **1988**, *37*, 785.

223. Becke A. D., *J. Chem. Phys.*, **1993**, *98*, 5648.

224. Becke A. D., *Phys. Rev. A*, **1988**, *38*, 3098.

225. Merrick J. P., Moran D., Radom L., *J. Phys. Chem. A*, **2007**, *111*, 11683.

226. http://cccbdb.nist.gov/vsf.asp *Vibrational frequency scaling factors*.

227. Cossi M., Barone V., Cammi R., Tomassi J., *Chem. Phys. Lett.*, **1996**, *255*, 327.

228. Tomasi J., Mennuci B., Cammi R., *Chem. Rev.*, **2005**, *105*, 2999.

229. Pietrzak M., *Private Information*,

230. Geerlings J. D., Huizer A. H., Varma C. A. G. O., *J. Chem. Soc. Faraday Trans.*, **1997**, *93*, 237.

231. Stickel F., Fischer E. W., Richert R., *J. Chem. Phys.*, **1996**, *104*, 2043.

232. Würflinger A., *Ber. Bunsenges. Phys. Chem.*, **1980**, *84*, 653.

233. Dobek K., *Private information*,

234. Berger M., Goldblatt I. L., Steel C., *J. Am. Chem. Soc.*, **1973**, *95*, 1717.

235. Feenstra J. S., Parks S. T., Zewail A. H., *J. Chem. Phys.*, **2005**, *123*, 221104.

236. Lin T. Y., Tang K. C., Yang S. H., Shen J. Y., Cheng Y. M., Pan H. A., Chi Y., Chou P. T., *J. Phys. Chem. A*, **2012**, *116*, 4438.

237. Yu W. S., Cheng C. C., Cheng Y. M., Wu P. C., Song Y. H., Chi Y., Chou P. T., *J. Am. Chem. Soc.*, **2003**, *125*, 10800.

238. Kyrychenko A., Herbich J., Izydorzak M., Gil M., Dobkowski J., Wu F., Thummel R. P., Waluk J., *Isr. J. Chem.*, **1999**, *39*, 309.

239. Perrin D. D., *Dissociation Constants of Organic Bases in Aqueous Solutions: Supplement*. **1972**, London: Butterworth.

240. Kijak M., Nosenko Y., Singh A., Thumel R. P., Brutschy B., Waluk J., *J. Mol. Structure*, **2007**, *844-845*, 286.

241. Douhal A., Kim S. K., Zewail A. H., *Nature*, **1995**, *378*, 260.

242. Avouris P., Yang L. L., El-Bayoumi M. A., *Photochem. Photobiol.*, **1976**, *24*, 211.

243. McGlynn S. P., Azumi, T., Kinoshita M., *Molecular Spectroscopy of the Triplet State*. **1969**, New Jersey: Prentice-Hall Inc., Englewood Cliffs.

244. Jarzeba W., Najbar J., Cioslowski J., *J. Mol. Structure*, **1986**, *141*, 469.

245. Berberan Santos M. N., *Phys. Chem. Comm.*, **2000**, *3*, 18.

246. Najbar J., Jarzeba W., Urbanek Z. H., *Chem. Phys.*, **1983**, *79*, 245.

247. Kamlet M. J., Abboud J. L. M., Abraham M. H., Taft R. W., *J. Org. Chem.*, **1983**, *48*, 2877.

248. Sinclair W. E., Yu H., Phillips D., Hollas J. M., *J. Chem. Phys.*, **1997**, *106*, 5797.

249. Boesl U., *J. Phys. Chem.*, **1991**, *95*, 2949.

250. Brutschy B., *Chem. Rev.*, **2000**, *100*, 3891.

251. Page R. H., Shen Y. R., Lee Y. T., *J. Chem. Phys.*, **1988**, *88*, 4621.

252. Riehn C., Lahmann C., Wasserman B., Brutschy B., *Chem. Phys. Lett.*, **1992**, *197*, 433.

253. Tanabe S., Ebata T., Fujii M., Mikami T., *Chem. Phys. Lett.*, **1993**, *215*, 347.

254. Pribble R. N., Zwier T. S., *Science*, **1994**, *265*, 75.

255. Mons M., Robertson E. G., Snoek L. G., Simons J. P., *Chem. Phys. Lett.*, **1999**, *310*, 423.

256. Wu R., Nachtigall P., Brutschy B., *Phys. Chem. Chem. Phys.*, **2004**, *6*, 515.

257. Szydlowska I., Nosenko Y., Brutschy B., Tarakeshwar P., Herbich J., *Phys. Chem. Chem. Phys.*, **2007**, *9*, 4981.

GLOSSARY OF ACRONYMS

A, **A**	deprotonated anion or acceptor
1AC	1-azacarbazole
ACN	acetonitrile
7AI	7-azaindole
B3LYP	Becke's three parameter hybrid functional and the correlation functional of Lee, Yang and Parr
BA	butyl acetate
BBHQ	bis-2,5-2(2-benzoxazolyl)hydroquinone
BE	dibutyl ether
BN	butyronitrile
BP(OH)$_2$	2,2'-bipyridyl-3,3'-diol
BPP	2-(4-bromo-1H-pyrazol-5-yl)pyridine
BSSE	basis set superposition error
1-BuOH	1-butanol
C	protonated cation
CC2	coupled-cluster rank 2 [hybrid model]
CFD	constant fraction discriminator
CI	conical intersection
CIS	configuration interaction singles (singly excited configurations)
COSY	COrrelation SpectroscopY (1D and 2D NMR technique)
CT	charge transfer
D	donor
DCE	1,2-dichloroethane
DCM	dichloromethane
DF	dispersed fluorescence
DFT	density functional theory
DMAP	4-dimethylaminopyridine
DMF	N,N-dimethylformamide
DMSO	dimethyl sulfoxide
DNA	deoxyribonucleic acid
DPC	dipyrido[2,3-a:3',2'-i]carbazole
EA	ethyl acetate
EE	diethyl ether
ESDPT	excited state double proton transfer
ESIPT	excited state intramolecular proton transfer
ESPT	excited state proton transfer
EtOH	ethanol
FURIN	2-furan-2-yl-1H-indole
FWHM	full width at half-maximum
HAN	1-hydroxy-2-acetonaphthone
HB	hydrogen bond
HBO	2-(2'-hydroxyphenyl)benzoxazole

148

HBT	2-(2'-hydroxyphenyl)benzothiazole
HEX	*n*-hexane
3-HF	3-hydroxyflavone
HFP	1,1,13,3,3-hexafluoro-2-propanol
2HMMN	2-hydroxy-1-(N-morpholinomethyl)naphthalene
7HMMQ	7-hydroxy-8-(N-morpholinomethyl)quinoline
HN32	3-hydroxy-2-naphthaldehyde
HOMO	highest occupied molecular orbital
9-HP	9-hydroxyphenalenone
2HPMN	2-hydroxy-1-(N-piperidinomethyl)naphthalene
H2MQ	7-hydroxy-2-methylquinoline
H2MQC	7-hydroxy-2-methylquinoline-8-carbaldehyde
H4MQ	7-hydroxy-4-methylquinoline
H4MQC	7-hydroxy-4-methylquinoline-8-carbaldehyde
HDMQ	7-hydroxy-2,4-dimethylquinoline
HDMQC	7-hydroxy-2,4-dimethylquinoline-8-carbaldehyde
HMMQ	7-hydroxy-2-methoxy-4-methylquinoline
HMMQC	7-hydroxy-2-methoxy-4-methylquinoline-8-carbaldehyde
HMPQ	7-hydroxy--2-(2'-methylphenyl)quinoline
HMPQC	7-hydroxy-2-(2'-methylphenyl)quinoline-8-carbaldehyde
HPQ	7-hydroxy-2-phenylquinoline
HPQC	7-hydroxy-2-phenylquinoline-8-carbaldehyde
7-HMMQ	7-hydroxy-8-(N-morpholinomethyl)quinoline
7-HQ	7-hydroxyquinoline
7-HQs	7-hydroxyquinolines
7-HQCs	7-hydroxyquinoline-8-carbaldehydes
HQC	7-hydroxyquinoline-8-carbaldehyde
IC	internal conversion
IR	infrared
IRF	instrument response function
ISC	intersystem crossing
^1L_a, ^1L_b	orbital configuration of states in Platt's notation
^1LE	locally excited singlet state
LCAO	linear combination of atomic orbitals
LIF	laser induced fluorescence
LUMO	lowest unoccupied molecular orbital
MCA	multichannel analyser
MCD	magnetic circular dichroism
MCH	methylcyclohexane
MCP	microchannel plate
MEC	main electronic configuration
MeOH	methanol
MPP	2-(3-methyl-1*H*-pyrazol-5-yl)pyridine
MP2	second order Møller-Plesset level
MS	mass spectroscopy
MTHF	2-methyltetrahydrofuran

NH	tautomeric form of **7-HQs** and **7-HQCs** (7-(1*H*)quinolinone)
NMR	nuclear magnetic resonance
NOESY	nuclear Overhauser effect spectroscopy
NPP	2-(4-nitro-1*H*-pyrazol-5-yl)pyridine
OH	tautomeric form of **7-HQs** and **7-HQCs** (7-quinolinol)
OHBA	o-hydroxybenzaldehyde
OPO	optical parametric oscillator
P*	primary excited state
PA	proton-accepting
PAS	Polish Academy of Sciences
PCM	Polarizable Continuum Model
PDA	proton-donating/accepting
PES	potential energy surface
2-PI	2-(2'-pyridyl)indole
2-PIs	2-(2'-pyridyl)indoles
3-PI	3-pyridyn-4-yl-1*H*-indole
PP	2-(2'-pyridyl)pyrrole
2PPs	2-(1*H*-pyrazol-5-yl)pyridines
PPP	2-(1*H*-pyrazol-5-yl)pyridine
PQ	1*H*-pyrrolo[2,3-*h*]quinoline
1-PrOH	1-propanol
PT	proton transfer
PYRIN	2-(1*H*-pyrrol-2-yl)-1*H*-indole
R2PI, IR/R2PI	resonant two-photon ionization, infrared ion depletion R2PI
S_0	ground singlet state
S_1	lowest excited singlet state
STM	scanning tunneling microscopy
SVLF	single vibronic level fluorescence
T*	product of excited state tautomerization reaction
TAC	time-to amplitude converter
TD-DFT	time-dependent density functional response theory
THAIN	2-thiazol-2-yl-1*H*-indole
THF	tetrahydrofuran
THOIN	2-thiophen-2-yl-1*H*-indole
T/R	tautomeric/rotameric
UV	ultraviolet
Vis	visible
Z, **Z**	zwitterion
ZPE	zero-point energy
π	orbital

GLOSSARY OF MATHEMATICAL TERMS

a_0	effective radius of the Onsager cavity
A	absorbance or optical density
A_0, A_∞	absorbance, optical density measured when only the uncomplexed or complexed forms are present
c	speed of light or concentration of solution
f	oscillator strength
$f(\varepsilon, n)$	solvent polarity function
h	Planck constant
K^G	equilibrium constant of the ground state process
K^*	equilibrium constant of the excited state process
k_{IC}	internal conversion rate constant
k_{ISC}	intersystem crossing rate constant
k_{nr}	nonradiative rate constant
k_f	radiative rate constant in fluorescence
k_f^P	rate constant of the radiative deactivation of the primary excited state
k_f^T	rate constant of the radiative deactivation of the product of the phototautomerization reaction
$\vec{k}$	rate constant of excited-state reaction
$\vec{k}_{PT}$	rate constant of excited-state proton transfer (ESPT) reaction
M_{abs}	electronic transition dipole moment related to absorption
M_{fl}	electronic transition dipole moment related to fluorescence
n	refractive index
N_A	Avogadro number
p_0	high-pressure in the reservoir
pK_a	acid dissociation constant, negative logarithm
pK_a^G, pK_a^*	ground- and excited-state acid dissociation constant
Q	quencher concentration
T	temperature
S, S_0	areas under the fluorescence spectra of the studied compound and the standard, respectively
ΔE	energy gap
ΔH_0	enthalpy of the
ε	static dielectric constant or molar extinction coefficient
$\varepsilon(\tilde{v})$	molar extinction coefficient (in dm^3/mol cm) at wavenumber $\tilde{v}$
Φ_f	fluorescence quantum yield
Φ_0	fluorescence quantum yield of the standard
η	viscosity
λ	wavelength (in nm)
$\lambda_{em}, \lambda_{exc}$	emission and excitation wavelength
μ_g, μ_e	ground- and excited-state dipole moment value
$\tilde{v}$	wavenumber (in cm^{-1})
$\tilde{v}_{abs}$	spectral position of absorption maximum
$\tilde{v}_{fl}$	spectral position of fluorescence maximum
τ	lifetime

151